

N72-28664

APOLLO

GUIDANCE, NAVIGATION AND CONTROL

CASE FILE COPY

PREPARED UNDER
CONTRACT NAS 9-4065, TASK ORDER 42
FOR NASA MANNED SPACECRAFT CENTER
HOUSTON, TEXAS
UNDER TECHNICAL DIRECTION OF
NASA GODDARD SPACE FLIGHT CENTER
GREENBELT, MARYLAND

E-2651

INTERIM TECHNICAL REPORT No. 3
CANDIDATE CONFIGURATION TRADE
STUDY, STELLAR-INERTIAL MEASUREMENT
SYSTEM (SIMS) FOR AN EARTH OBSERVATION
SATELLITE (EOS)

by

G. Ogletree, J. Coccoli, R. McKern
M. Smith and R. White

15 June 1972

MIT

**CHARLES STARK DRAPER
LABORATORY**

CAMBRIDGE MASSACHUSETTS 02139

APOLLO

GUIDANCE, NAVIGATION AND CONTROL

Approved: G. Ogletree Date: 6/30/72
G. OGLETREE, DEPUTY ASSOCIATE DIRECTOR
SIMS Trade Study Project Leader

Approved: N. E. Sears Date: 30 June 72
N. E. SEARS, ASSOCIATE DIRECTOR
Director, Apollo G&N Systems

Approved: D. G. Hoag Date: 30 June 72
D. G. HOAG, ASSOCIATE DIRECTOR
Director, Apollo Project

Approved: R. R. Ragan Date: 30 June 72
R. R. RAGAN, DEPUTY DIRECTOR
Director, NASA Programs

E-2651

INTERIM TECHNICAL REPORT No. 3
CANDIDATE CONFIGURATION TRADE
STUDY, STELLAR-INERTIAL MEASUREMENT
SYSTEM (SIMS) FOR AN EARTH OBSERVATION
SATELLITE (EOS)

by

G. Ogletree, J. Coccoli, R. McKern
M. Smith and R. White

15 June 1972

MIT

CAMBRIDGE, MASSACHUSETTS, 02139

**CHARLES STARK DRAPER
LABORATORY**

ACKNOWLEDGEMENT

This report was prepared under DSR Project 55-39200, sponsored by the Manned Spacecraft Center of the National Aeronautics and Space Administration through Task Order No. 42 of Contract NAS 9-4065 with the Massachusetts Institute of Technology. Technical Direction of the effort was provided by Mr. John W. Kelly and Dr. Arun K. Guha of NASA Goddard Space Flight Center.

Authorship of the technical sections was as follows: Section Three - Richard A. McKern, IARU Studies Task Leader; Section Four - Joseph D. Coccoli, Star Sensor Studies Task Leader; Section Five - Robert L. White, Star Availability Studies and Error Analysis and Simulation Studies Task Leader, and Section Six - Mark A. Smith, Technical Advisor.

Technical assistance or supporting authorship in these sections included: Section Three: Harry McOuat and Roscoe Cooper - General Writing and Editorial Assistance; George L. Suntheimer and Arthur J. Boyce - SIMS-D IARU Mechanical Design Study; Raymond J. Cushing - SIMS-D Electronics, including Readout Electronics; Charles Lory - Electronics Consultation on Pulse Width Modulated Loops; and Howard Musoff - IARU Reliability Considerations. Section Four: Lawrence Yorgy - Star Tracker Investigations; George Karthas - Optics Consultation. Section Five: Frederick D. Grant - Assistance in Preparation of Subsections 5.3 and 5.4; Peter C. Vernam - Star Availability Studies; Katherine Tompkins - Assistance in Preparation of Subsection 5.4.

Glenn Ogletree wrote Sections One and Two and prepared and edited the overall report for publication. The report was typed by Gladys Grover and Elaine DeSimone. Illustrations were prepared by William Eng and David Farrar. Publication was accomplished by the MIT/CSDL Publications Department.

The publication of this report does not constitute approval by the National Aeronautics and Space Administration of the findings or the conclusions contained therein. It is published only for the exchange and stimulation of ideas.

INTERIM TECHNICAL REPORT NO. 3 --
CANDIDATE CONFIGURATION TRADE STUDY,
STELLAR-INERTIAL MEASUREMENT SYSTEM (SIMS)
FOR AN EARTH OBSERVATION SATELLITE (EOS)

ABSTRACT

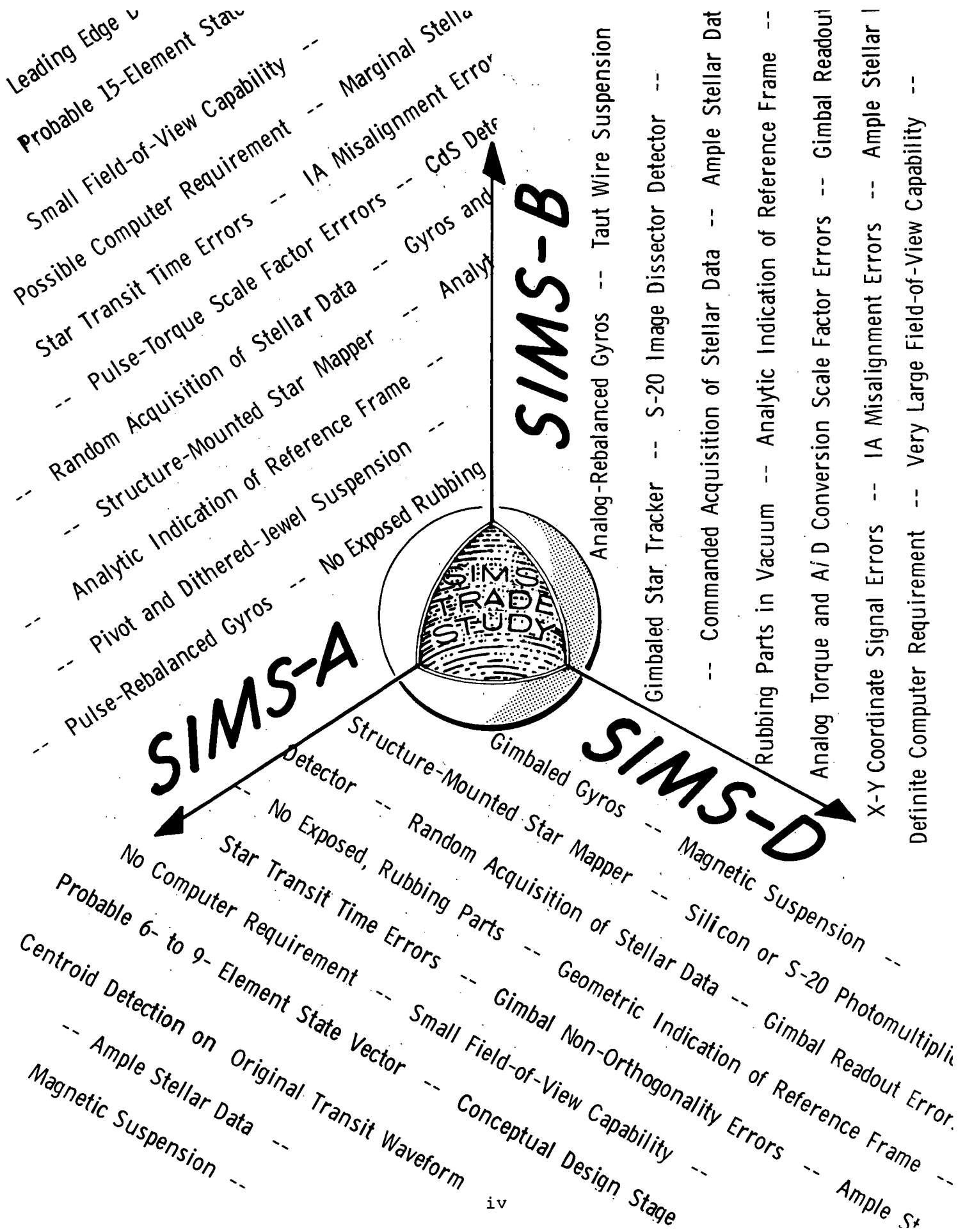
A fifteen month trade study for the NASA Manned Spacecraft Center by the Charles Stark Draper Laboratory Division of the Massachusetts Institute of Technology, under the technical direction of the NASA Goddard Space Flight Center, is reported on at the middle of the twelfth month.

The ten candidate SIMS configurations were defined in the first interim report in November 1971 and reduced to three in the second such report in February 1972. The latter three have been studied in the prior reports - and in greater depth in this report - in terms of their cost, accuracy, weight, power, telemetry requirement, and field-of-view needed, and also from the standpoints of simplicity and reliability, modularity and growth potential, GSE cost, complexity of ground control/command/data processing operations, and availability. Further, specialized studies are planned for two of the three candidates prior to the final report, planned for 29 September 1972, in which they will be documented. The four reports are intended to facilitate NASA/GSFC decisions pertaining to gimballed versus structure-mounted gyros and star sensors, and combinations thereof, suitable for the EOS and similar applications.

This third report emphasizes the results of analytical and simulation studies at subsystem and system levels and the estimates of candidate accuracies and sensitivities based thereon. Also, some significant additional subsystem design analyses and sensor design trades are reported on, such as definition and evaluation of additional inertial and stellar subsystems relevant to the trade study. Finally, a major discussion of trade considerations and their import is offered, to aid NASA personnel in their own evaluation of the implications of this study. Material presented thus constitutes a technical comparison of the three candidates (SIMS-A: structure-mounted gyros with structure-mounted star mapper; SIMS-B: structure-mounted gyros with gimballed star tracker; and SIMS-D: gimballed gyros with structure-mounted star mapper), with supporting technical discussions, on the basis of which NASA can proceed to the SIMS configuration selection, using program- and spacecraft-related weighting factors.

by G. Ogletree, J. Coccoli, R. McKern
M. Smith and R. White

Charles Stark Draper Laboratory
a Division of the Massachusetts Institute of Technology
Cambridge, Massachusetts 02142



PREFACE

Tasks originally undertaken have now been completed to the extent time and resources permitted. This is not to say the tasks are complete; they are not. In many cases, tasks tended to expand and defy documentation (e.g., development of firm math models adequately describing sensor and subsystem errors and error rates).

If initial cost or availability is overriding, the SIMS-D candidate suffers, and SIMS-A appears to be the beneficiary. If telemetry requirement, accuracy, and growth potential are given strong relative weights, SIMS-D emerges as the preferred approach. SIMS-B offers high accuracy and shortest settling time but loses strength in the physical trades - weight, power, field-of-view required. Thus each SIMS configuration has significant advantages and disadvantages.

A major aim of this and the two previous Interim Technical Reports is to provide NASA with an objective technical comparison of the candidates. It was assumed that NASA will determine the proper weighting factors to apply to the several SIMS configuration selection criteria, so a configuration selection can be made. Clearly, weighting factors applied can determine the outcome of the choice, since the trade study shows that the three final candidates each has merit with respect to some of the SIMS trade criteria.

CONTENTS

<u>Section</u>	<u>Page</u>
ACKNOWLEDGMENT	ii
ABSTRACT	iii
PREFACE	v
ILLUSTRATIONS	xiii
TABLES	xvii
1. INTRODUCTION AND SUMMARY	1-1
1.1 INTRODUCTION	1-1
1.1.1 Background	1-2
1.1.2 Project Activities	1-3
1.2 SUMMARY	1-9
1.2.1 Summary Description of the Candidates	1-9
1.2.2 Technical Approach to the Trade Study	1-12
1.2.3 Summary of Contents of This Report	1-15
2. SIMS CONFIGURATION	2-1
2.1 INTRODUCTION	2-1
2.2 SIMS-A	2-2
2.3 SIMS-B	2-3
2.4 SIMS-D	2-4

CONTENTS (Cont.)

<u>Section</u>	<u>Page</u>
3. INERTIAL ATTITUDE REFERENCE UNITS	3-1
3.0 INTRODUCTION.	3-1
3.0.1 EOS-SIMS IARU Requirements.	3-1
3.0.1.1 Statement of Work Requirements.	3-1
3.0.1.2 Mission-Related Requirements.	3-2
3.1 SIMS-A (SPARS-LIKE) IARU.	3-2
3.1.1 Review of Honeywell/St. Petersburg Discussions	3-2
3.2 SIMS-B (PPCS/PADS IARU)	3-4
3.2.1 Description of Northrup Electronics T/B Loop Design	3-4
3.2.2 Review of TRW Information	3-6
3.3 SIMS-D.	3-7
3.3.1 Implementation of IARU.	3-7
3.3.2 SIMS-D Design (TGG Instruments)	3-8
3.3.3 SIMS-D Design (13-IRIG Instruments)	3-8
3.3.3.1 Detailed Layout of IARU	3-8
3.3.3.2 Interface Requirements.	3-10
3.3.3.3 IARU Characteristics.	3-10
3.3.3.4 Gyro Description (13-IRIG).	3-10
3.4 IARU RELIABILITY CONSIDERATIONS	3-15
3.5 IARU SUMMARY.	3-22

CONTENTS (Cont.)

<u>Section</u>	<u>Page</u>
3.6 PROPOSED FUTURE TASKS	3-25
3.6.1 13-IRIG	3-25
3.6.2 Torque Loop Evaluation	3-25
3.6.3 Computer Requirements Study	3-25
4. STAR SENSOR STUDIES	4-1
4.1 INTRODUCTION	4-1
4.2 STAR MAPPERS	4-3
4.2.0 Star Mapper Performance Characteristics	4-3
4.2.0.1 Stellar Interval Evaluation	4-3
4.2.0.2 Signal and Noise	4-4
4.2.0.3 Signal Shape Effects	4-10
4.2.0.4 Probability of Detection and False Alarm Rates	4-29
4.2.1 General Description of Star Mapper Subsections	4-35
4.2.2 SIMS-A Star Mappers	4-35
4.2.2.1 SIMS-A-C Star Mapper Functional Description	4-36
4.2.2.2 SIMS-A-HR Star Mapper Functional Description	4-43
4.2.2.3 SIMS-A-KI Star Mapper Functional Description	4-50
4.2.3 SIMS-D-HR Star Mapper	4-58
4.3 SIMS-B STAR TRACKER	4-58

CONTENTS (Cont.)

<u>Section</u>	<u>Page</u>
4.4 SIMS-B STAR TRACKER, RANDOM ACQUISITION FEASIBILITY	4-59
5. ERROR STUDIES	5-1
5.1 INTRODUCTION.	5-1
5.2 STAR AVAILABILITY STUDIES	5-7
5.2.1 Introduction	5-7
5.2.2 Update of General Star Catalog and Detector Catalogs	5-8
5.2.3 Star Mapper Distribution Plots	5-8
5.2.4 Star Tracker Distribution Plots.	5-10
5.2.5 Star Distribution Cases Selected for Error Studies	5-10
5.3 SYSTEM EQUATIONS.	5-12
5.3.1 Introduction	5-12
5.3.2 System Equations for SIMS-A.	5-14
5.3.2.1 State Equation for SIMS-A.	5-14
5.3.2.2 Measurement Equations for SIMS-A	5-16
5.3.3 System Equations for SIMS-B.	5-25
5.3.3.1 State Equation for SIMS-B.	5-25
5.3.3.2 Measurement Equations for SIMS-B	5-25
5.3.4 System Equations for SIMS-D.	5-28
5.3.4.1 State Equation for SIMS-D.	5-31
5.3.4.2 Measurement Equations for SIMS-D	5-33

CONTENTS (Cont.)

<u>Section</u>	<u>Page</u>
5.4 ERROR STUDY RESULTS.	5-41
5.4.1 Introduction.	5-41
5.4.2 Error Study Results for SIMS-A.	5-43
5.4.3 Error Study Results for SIMS-B.	5-62
5.4.4 Error Study Results for SIMS-D.	5-78
5.5 CONSIDERATION OF ADDITIONAL ERROR SOURCES.	5-96
5.5.1 Introduction.	5-96
5.5.2 Gyro Scale Factor Error	5-98
5.5.3 Gyro Input Axis Misalignment.	5-104
5.5.4 Other Error Sources	5-108
6. CONFIGURATION TRADES	6-1
6.1 HIGHLIGHTS OF THE SIMS TRADE STUDY	6-1
6.2 TRADES	6-6
6.2.1 Criterion 1 - Cost.	6-6
6.2.2 Criterion 2 - Accuracy.	6-10
6.2.3 Criterion 3 - Weight.	6-13
6.2.4 Criterion 4 - Power	6-15
6.2.5 Criterion 5 - Telemetry Requirement	6-18
6.2.5.1 SIMS-A.	6-18
6.2.5.2 SIMS-B.	6-21
6.2.5.3 SIMS-D.	6-22
6.2.6 Criterion 6 - Total Unobstructed FOV Required.	6-25

CONTENTS (Cont.)

<u>Section</u>	<u>Page</u>
6.2.7 Criterion 7 - Simplicity of Design, and Reliability	6-29
6.2.8 Criterion 8 - Modularity of Design, and Growth Potential . . .	6-45
6.2.9 Criterion 9 - Cost of GSE	6-68
6.2.10 Criterion 10 - Complexity of Ground Control/Command/Data Processing Operations	6-69
6.2.11 Criterion 11 - Availability	6-71
6.3 RECOMMENDATIONS	6-73

APPENDICES

A	TRADE CRITERION INFORMATION SUMMARY	A-1
B	REVISED CATALOG OF STARS OF MAGNITUDE 4.0 OR BRIGHTER AS SEEN BY ONE OR MORE DETECTORS	B-1
C	STAR DISTRIBUTION RESULTS	C-1
D	COMPARISON OF MIT/CSDL AND HONEYWELL TECHNIQUES OF STAR MAPPER MEASUREMENT . . .	D-1
E	EXCERPTS FROM THE TECHNICAL PROPOSAL COVERING EXPANSIONS OF TASKS 4 AND 6 OF THE ORIGINAL STATEMENT OF WORK . . .	E-1
F	POST SCRIPT	F-1
7.	REFERENCES	7-1
8.	DISTRIBUTION	8-1

ILLUSTRATIONS

<u>Figure</u>		<u>Page</u>
3-1	K7G Torque to Rebalance Loop (Block Diagram)	3-5
3-2	13-IRIG Three-Gimbal Layout.	3-9
3-3	IARU External Electronics.	3-11
3-4	IARU Interface	3-12
3-5	Mission Success Probability (Gyro Loop MTBF = 10,000 Hrs).	3-17
3-6	Mission Success Probability (Gyro Loop MTBF = 50,000 Hrs).	3-18
3-7	Mission Success Probability (Gyro Loop MTBF = 100,000 Hrs)	3-19
3-8	Mission Success Probability.	3-23
3-9	Mission Success Probability.	3-24
4-1	Detector Response as a Function of Stellar Magnitude With AO Type Stars . . .	4-5
4-2	S/N Versus Equivalent AO Stellar Magni- tude for Specific SIMS SSAs	4-8
4-3a	Input Signal Modification for Square- Toothed Edge Roughness and a Masking Ratio, $M = 0$ at Both the Leading and Trailing Edges	4-20
4-3b	(Same as 4-3a except) $M = -M$ at the Leading Edge, and $M = +M$ at the Trailing Edge	4-20
4-4	Limiting Modifications of the Input Signal Due to Edge Waviness of Both Slit Edges .	4-26

ILLUSTRATIONS (Cont.)

<u>Figure</u>		<u>Page</u>
4-5	Probability of Detection, $P_D(V_T)$, for a Typical $\sigma_R = 0.05V_P$ Starmapper, and False Alarm Probability, $P_F(V_T)$	4-33
4-6	Probability of Detection, $P_D(V_T)$, for a Typical Cadmium Sulfide Starmapper, and False Alarm Probability, $P_F(V_T)$	4-34
4-7	Speculative Functional Block Diagram of SIMS-A-HR Star Mapper.	4-44
4-8	Symmetry Error as a Function of Threshold Indicated on a Typical Silicon Star Mapper Filtered Output, where Both Leading and Trailing Edge Detection is Used.	4-47
4-9	SIMS-A-KI Star Mapper Waveform Center Detection Principle.	4-53
4-10	Simplified Block Diagram of the SIMS-A-KI Star Mapper Electronics.	4-54
4-11	SIMS-A-KI Star Mapper Detection Electronics. .	4-55
4-12	Symmetry Error for the SIMS-A-KI Star Mapper	4-57
5-1	Slit Pattern of Star Mapper.	5-17
5-2	Platform and Orbital Inertial Coordinate Systems.	5-30
5-3	Body-Fixed and Platform Coordinate Systems . .	5-30

ILLUSTRATIONS (Cont.)

<u>Figure</u>		<u>Page</u>
5-4	SIMS-A Performance Versus Data Processing Interval Size Using SIL Mapper.	5-45
5-5	SIMS-A Performance Versus Data Processing Interval Size Using CDS Mapper.	5-46
5-6	SIMS-A Sensitivity to SIL Mapper Measurement Error	5-54
5-7	SIMS-A Sensitivity to CDS Mapper Measurement Error	5-55
5-8	SIMS-A Sensitivity to FOV of SIL Mapper.	5-56
5-9	SIMS-A Sensitivity to FOV of CDS Mapper	5-57
5-10	SIMS-A Sensitivity to Detector Magnitude Threshold of SIL Mapper	5-60
5-11	SIMS-A Sensitivity to Detector Magnitude Threshold of CDS Mapper	5-61
5-12	SIMS-A Sensitivity to Gyro Random Drift . . .	5-63
5-13	SIMS-A Sensitivity to Gyro Constant Angle Noise.	5-64
5-14	SIMS-B Performance Versus Data Processing Interval Size.	5-67
5-15	SIMS-B Sensitivity to Star Tracker Measurement Error.	5-71
5-16	SIMS-B Sensitivity to Star Tracker Outer Gimbal Limit	5-74

ILLUSTRATIONS (Cont.)

<u>Figure</u>		<u>Page</u>
5-17	SIMS-B Sensitivity to Gyro Random Drift . . .	5-76
5-18	SIMS-B Sensitivity to Gyro Constant Angle Noise.	5-77
5-19	SIMS-D Performance Versus Data Processing Interval Size.	5-82
5-20	SIMS-D Sensitivity to SIL Mapper Measurement Error.	5-86
5-21	SIMS-D Sensitivity to FOV of SIL Mapper . . .	5-87
5-22	SIMS-D Sensitivity to Detector Magnitude Threshold of SIL Mapper.	5-88
5-23	SIMS-D Sensitivity to IARU Gimbal Errors. . .	5-90
5-24	SIMS-D Sensitivity to Gyro Random Drift as Modeled for the TGG Gyro.	5-92
5-25	SIMS-D Sensitivity to Gyro Random Drift Rate Modeled as White Noise.	5-93
5-26	SIMS-D Sensitivity to Gyro Constant Angle Noise.	5-94
5-27	Rate Error Introduced by Scale Factor Bias Error When the Vehicle Attitude Departs from Nominal	5-103
A-1	Index to Contents of Appendix A	A-3

TABLES

<u>Table</u>	<u>Page</u>
3-1	Summary of Pulse Torquing Parameters. 3-6
3-2	Electronics Characteristics 3-13
4-1	Usable Stars for SIMS Star Mappers. 4-4
4-2	Noise-Equivalent Inputs Affecting Transit Time Detection Accuracy 4-7
5-1	Number of Stars Brighter Than or Equal To a Given Detector Magnitude 5-9
5-2	Stellar Magnitude Ranges Denoted by Various Symbols 5-9
5-3	Star Mapper Distributions Selected for Error Studies 5-11
5-4	SIMS-A Sensitivity to SIL Mapper Pointing Direction 5-48
5-5	SIMS-A Sensitivity to CDS Mapper Pointing Direction 5-49
5-6	SIMS-A Sensitivity to Initial State Uncertainties 5-50
5-7	SIMS-A Performance at Various Points in 8-Orbit Data Processing Interval-Using CDS Mapper 5-52
5-8	SIMS-A Sensitivity to Star Mapper FOV 5-58
5-9	SIMS-A Performance for Two Techniques of Star Measurement 5-65
5-10	SIMS-B Performance Versus Star Update Interval Size 5-69

TABLES (Cont.)

<u>Table</u>		<u>Page</u>
5-11	SIMS-B Sensitivity to Initial State Uncertainties	5-70
5-12	SIMS-B Sensitivity to Star Tracker Measurement Errors	5-72
5-13	SIMS-B Sensitivity to Star Tracker Outer Gimbal Limit	5-75
5-14	SIMS-B Performance Using Star Field of SIL Mapper and SIMS-A Gyro	5-79
5-15	SIMS-D Sensitivity to Initial State Uncertainties	5-83
5-16	SIMS-D Performance at Various Points in 8 Orbit Data Processing Interval	5-85
5-17	SIMS-D Sensitivity to IARU Gimbal Errors	5-91
5-18	SIMS-D Performance for Two Techniques of Star Measurement	5-95
6-1	Comparison of SIMS Candidates	6-5
6-2	Evaluation of Reliability Formulas for the SIMS-A IARU	6-39

SECTION 1

INTRODUCTION AND SUMMARY

1.1 INTRODUCTION

This report has been prepared as the Third Interim Technical Report covering work from 22 January 1972, through 15 June 1972, performed by the Charles Stark Draper Laboratory Division of the Massachusetts Institute of Technology (MIT/CSDL), on the "Candidate Configuration Trade Study--Stellar-Inertial Measurement System (SIMS) for a Proposed Earth Observation Satellite (EOS)" for the NASA Goddard Space Flight Center (GSFC).

Two prior Interim Technical Reports^{85,141*} and eleven Monthly Letter Reports^{58-60, 86-88, 142-146} have been published. Four additional Monthly Letter Reports and a Final Report are planned. Excerpts from MIT/CSDL Technical Proposal No. 71-173, dated June 1971, including the statement of work for the first eleven months of this effort and CSDL comments thereon, were provided as Appendix A of ref 85. Excerpts from MIT/CSDL Technical Proposal No. 72-176, dated 16 May 1972 (reference 147), including the statement of work for the final four months of the effort, are provided as Appendix E hereof.

The first interim technical report⁸⁵ documented the reference data assimilation and candidate configuration definition

* Superscripts refer to similarly-numbered references in Section 7, REFERENCES. Note that reference numbers 1 through 84 called out on the first interim report (reference 85) and reference numbers 85 through 140 called out in the second interim report (reference 141) are continued herein.

phases of the study. The second such report¹⁴¹ presented the results of configuration and subsystem design studies and of star availability and error analysis studies. Both of the prior interim reports provided a limited discussion of the Configuration Trades aspects of the study. The treatment of that subject is essentially completed in this third interim report, which also provides an overview of the candidate configuration trade study (first eleven month) portion of the overall task order effort and presents certain MIT/CSDL recommendations pertaining thereto. It is planned that the Final Report will be devoted principally to the documentation of the special study tasks of the final four months of the overall effort (see Appendix E), and secondarily to a final, retrospective summary of highlights, results, conclusions and recommendations arising from the accomplishment of the Task Order as a whole.

1.1.1 BACKGROUND

Section 1.1.1 of ref. 85 provided a brief description of the NASA EOS program and described the relevance of the SIMS Trade Study at MIT to that program. As footnoted on p. 1-11 thereof, certain EOS program and Thematic Mapper data presented was then (and continues to be) in need of review and revision. For example (ref. 89), an image surface-scanning thematic mapper design was tentatively selected by NASA at one point to eliminate the need for a massive plane mirror nodding with extreme precision over an appreciable angle at 10 Hz. Also, further NASA work is currently in progress to more completely define and specify the thematic mapper to be developed for EOS. Such points of possible

non-relevance as these in the background descriptions of ref. 85 have not seriously impacted the design or other decision processes in the SIMS Trade Study at MIT. Hence, no effort was expended in reference 141, nor will be expended here, to update the prior material. Interested readers are referred to NASA EOS Program documents for more current descriptions of the evolving definition of EOS and its payloads and subsystems.

In view of certain EOS program delays such as those associated with the thematic mapper studies, NASA/GSFC was able to grant MIT requests for a one month extension of the original contract period to improve the content and scope of reference 141 and the second technical review meeting presentation, and for an additional two month extension to similarly improve this report. A final, four-month extension has been implemented to support new studies (see Appendix E hereof).

1.1.2 PROJECT ACTIVITIES

The SIMS Study Team has continued to function in the organizational manner indicated in Fig. 1-4 of ref. 85 through the publication of the present report. (During the remaining months of the Task Order, figure 2 of Appendix E applies.)

Efforts in the second reporting period (documented in ref. 141) were concentrated in preliminary studies of each of the configurations using data previously acquired and assimilated (refs. 8 through 57) and the internal SIMS-related documents prepared from those and other sources (refs. 62-76, 78, 83). This work led to the convergence in ref. 141 on a single generic type

of SIMS-D candidate: fully-gimbaled gyros and a body-fixed star mapper (as in SIMS-D1-A, ref. 85). With the elimination of SIMS-C in ref. 85 as well as the MIT introduction and elimination of SIMS-E therein, the candidates were reduced to three in ref. 141, as work in preparation of the present report began:

SIMS-A	Strapped Down Gyros and Strapped Down Star Mapper	Derived from Honeywell SPARS
SIMS-B	Strapped Down Gyros and Gimbaled Star Tracker	Derived from TRW PPCS/PADS
SIMS-D	3-Axis Gimbaled Gyro Plat- form and Strapped Down Star Mapper	Subsystems being Defined by MIT

The detailed work of the Task Leaders was reported on in ref. 141 and is amended and further amplified as necessary in this report. In both ref. 85 and ref. 141, the Technical Advisor has provided an overview section dealing with configuration trade considerations. For the present report, he has compiled the trade tabulation data from his own and the cognizant engineers' efforts. With the Project Leader, he and the Consultants and Task Leaders have attempted to ensure that the accomplishment and the presentation of final trade comparisons is as adequately, accurately and objectively done in the present report as can be accomplished within available time and resources.

Five monthly letter reports, ref's 142 through 146, provided NASA with an account of technical and financial activities and status during this reporting period. The Second Technical Review Meeting was held at NASA/GSFC on 18 February 1972, one month later than originally planned, continuing the one month slip in

schedule noted in ref. 85, p. 1-12. That meeting was documented in ref. 143. Some of the GSFC inputs to MIT, then and since, have been treated explicitly or implicitly in ref. 143, in other documents, and/or in this report. Specifically, the following tabulation of inputs by GSFC personnel, on 18 February and subsequently, are discussed in the tabulation, or references and/or the indicated sections of this report:

<u>GSFC Input</u>	<u>Comments, or References</u>
1. Scattered light should be taken into account in star mapper studies. GSFC flight experience has shown it to be a severe problem.	(Not included in simulations due to time limitations. Need empirical data to formulate model.)
2. Star tracker error is greater at limits of gimbal angular freedom.	(Sensitivity to magnitude of outer gimbal angle limit studied, but not to variation in error model with gimbal angle magnitude. See subsection 5.4.3, pp. 5-68 to 75, and subsection 5.5.4.)
3. Imposition of the constraint of a 90 minute update interval on SIMS-D cannot be justified as a "Mission-Related Requirement."*	See p. 4 of ref. 143. Also, subsections 3.0.1.2 and 3.3.1 hereof.

* See p. 3-2 of ref. 141.

- | | |
|--|---|
| 4. Dimensional stability of an inductosyn gimbal angle readout after exposure to launch environment needs to be determined. | (Needs further study. Note multi-speed resolvers specified in subsection 3.3.3.1 of this report.) |
| 5. Shutters add complexity and reduce reliability. Need to know why it is needed with CdS. | See p. 5 of ref. 143. No further information available. |
| 6. MIT opinion sought on CdS as a star mapper detector candidate. | See p. 5 of ref. 143. CdS is a major contender, but has some major technical problems; see subsections 4.2.0 and 4.2.2.1. |
| 7. Need to force SIMS candidates with biases varying at orbital frequency to test for sensitivity to same. (Insert varying biases into state transition matrix, as one approach in the MIT covariance analysis.) | Insufficient time in current study segment to pursue this suggestion. |
| 8. Desire to see cost presented as function of the trade parameters. Cost may well be the key factor in program-level SIMS decisions. | It was not practical to attempt this sort of presentation. However, limited cost information is included in subsection 6.2.1 and in Appendix A. |
| 9. Need to know how choice of configuration is impacted by reliability goals assumed. | See p. 6 of ref. 143. Also, see subsections 3.4 and 6.2.7 hereof. |

- | | |
|---|--|
| 10. Desire to determine applicability of the MIT-designed OAO IRU to the EOS/SIMS problem, and the associated cost factors. | See pp. 6,7 of ref. 144. See pp. 7,8 of ref. 145. See also ref. 148. No details available on associated cost trades. |
|---|--|

The star availability studies reported on in subsection 5.3 of ref. 141 and in subsection 5.2 herein generally correspond to similar studies that were accomplished independently by GSFC personnel, using star catalogs in common use at GSFC. This was to increase mutual confidence in the results obtained. All MIT information pertaining to the study was made available to GSFC (as reported on in refs. 87 and 88). The GSFC results were formatted similarly to MIT's for ease of comparison. No significant discrepancies were observed.

There were several technical communications of interest during this reporting period. Dr. Guha of NASA/GSFC, in reference 149, commented on the MIT/DL SIMS-A starmapper measurement equations (referred to in subsection 5.3.2.2 of this report as the "Original Technique of Measurement"); he posed several questions regarding their validity, and suggested an alternative method of star-mapper data utilization. The questions were responded to in reference 150 and are treated in subsection 5.3.2.2 and Appendix D of this report, and a second alternative measurement method (referred to as the "Alternate Technique of Measurement" in subsection 5.3.2.2 of this report) was introduced and evaluated. A further response to Dr. Guha's letter was contained in reference 151.

Letters were also received from the manufacturers of the original SIMS Study Candidates A, B and C, in response to information contained in references 85 and 141 and other communications. In reference 152, Messrs. Klestadt and Telle of Hughes Aircraft Company agreed with the MIT recommendation to drop the SIMS-C candidate (see reference 141), under the ground rules of the EOS spacecraft attitude control system performance stated in reference 85. They asserted, however, that if the spacecraft attitude were permitted to be more precisely controlled, with the Hughes STARS system included in the EOS attitude control system, "the STARS approach"... (to the EOS payload sensor attitude determination problem)... "would not only be a viable one but a very strong contender." Time has not permitted a careful response to the Hughes suggestion, nor to the brief first order analysis submitted in reference 152 to support it. The Hughes letter was forwarded to NASA/GSFC as Attachment C to reference 144.

Mr. D. Paulson of Honeywell Aerospace Division, in reference 153, described — and furnished cost and trade parameter information on — the specific variation of the original SPARS hardware designs that Honeywell proposes for the SIMS-A candidate in this study. The data in reference 153 and in later communications from Honeywell are utilized extensively in this report. A copy was furnished to Mr. J. Kelly of NASA/GSFC by Honeywell.

Mr. D. Kirby of TRW Systems Group, in reference 154, presented a review of reference 141 as it pertained to SIMS-B, as had been requested by Mr. T. Huber of NASA/GSFC. The TRW information, supplemented by later discussions, is also referred to in the technical sections of this report. (A specific example is contained in subsection 6.2.6).

The completion and documentation of studies in the three primary task areas (see Sections 3, 4 and 5), the team effort in compiling the parametric trade tabulation (see Appendix A), and the larger-than-originally-planned effort by the Technical Advisor in documenting and discussing the trade considerations for convenient use by NASA, (see Section 6), were the dominant project activities of this reporting period.

1.2 SUMMARY

(The material in this subsection supersedes the similar material in subsection 1.2 of ref. 141; it reflects the updating permitted by the viewpoint near the midpoint of the twelfth month of the study. This repetition of prior material, as in ref. 141, is for convenience.)

1.2.1 SUMMARY DESCRIPTION OF THE CANDIDATES

Four categories of candidate SIMS configurations were originally required to be evaluated and compared in this study:

<u>Category</u>	<u>Chief Characteristics</u>
A	Strapped Down Gyros and Star Mapper(s)
B	Strapped Down Gyros; Gimbaled Star Tracker
C	No Gyros; Gimbaled Cluster of Star Trackers
D	Gimbaled Gyros; Gimbaled or Strapped Down Star Sensor(s)

An additional category, Category E, was defined in ref. 85 as one of potential interest, as follows:

E	No Gyros; Three Individual, Separately-Gimbaled Star Trackers
---	---

and Category D was subdivided in ref. 85 as follows:

D1-A	Gyros Fully Gimbaled; Strapped Down Star Mapper(s)
D1-B	Gyros Fully Gimbaled; Gimbaled Star Tracker
D2-A	Gyros Gimbaled in One Axis; Strapped Down Star Mapper(s)
D2-B	Gyros Gimbaled in One Axis; Gimbaled Star Tracker

D1-B and D2-B were further subdivided in ref. 85 according to star sensor moding, as follows:

D1-B1	Gyros Fully Gimbaled; Gimbaled Star Tracker; Star Tracker Pro- grammed in Roll to Acquire Known Stars.
-------	---

D1-B2	Gyros Fully Gimbaled; Gimbaled Star Tracker; Star Tracker Executes Roll Scan, Acquires and Tracks Stars At Random
D2-B1	Gyros Gimbaled in One Axis; Gimbaled Star Tracker; Star Tracker Programmed in Roll to Acquire Known Stars
D2-B2	Gyros Gimbaled in One Axis; Gimbaled Star Tracker; Star Tracker Executes Roll Scan, Acquires and Tracks Stars at Random

Thus, ten candidate categories (A,B,C,D1-A,D1-B1,D1-B2, D2-A,D2-B1,D2-B2,E) were defined as potential SIMS design approaches at the time of the First Interim Technical Report, ref. 85. Of these, Categories C and E were recommended therein to be dropped from further study, as discussed in subsec's. 2.4, and 2.6 of ref. 85. NASA accepted the recommendation. Categories D1-B2 and D2-B2 were given reduced emphasis in the earlier report, due to the unavailability of a suitable star sensor candidate for them, as indicated in subsec's. 2.5.3 and 2.5.6 of ref. 85. The remaining six (A,B,D1-A,D1-B1,D2-A,D2-B1) were retained as primary candidates as the study continued. (Note, however, that the effort to define a -B2 type star tracker was continued and has led to new, encouraging information as reported in subsection 4.4 of this report.)*

* Also, see subsection 6.2.8, 3), under "Random Acquisition with a SIMS-B Tracker"

In the study segment reported on in ref. 141, the candidates were, as mentioned in subsection 1.1.2 thereof, further reduced in number to three (A,B, and D1-A) as a result of selection of the -D1 (rather than the -D2) type of SIMS-D gyro configuration, and because of the determination that not only a gimbaleed star tracker but also a star mapper would meet the SIMS-D star sensor requirements, regardless of choice of gyro configuration. (See Sections 3. and 4. of ref. 141, and subsection 3.3.1 hereof where the fully-gimbaleed IARU and star mapper selections for SIMS-D are documented.) In the portion of the study effort covered by this report, the three final candidates are designated simply as SIMS-A, SIMS-B, and SIMS-D, as was indicated in subsection 1.1.2.

1.1.2 TECHNICAL APPROACH TO THE TRADE STUDY

As noted in subsec. 1.1.1 of ref. 85, the aim of the present study is to provide "adequate data which may be used (by NASA) to select an 'optimum' configuration (of a SIMS) for a particular (the EOS-C or similar) application".* The need is for MIT to define the several configurations, to establish appropriate figures of merit for each, at least in terms of trade factors established by NASA, and to present these findings in a tabular or other appropriate manner,** supported by narrative discussion as required to clarify the points of comparison.***

* See Appendix A, para. II.1, of ref. 85.

** See Appendix A of ref. 85, Section 6 of ref. 141, and Appendix A of this report. Also, see Section 6 hereof, e.g., p. 6-5.

*** The narrative discussion is contained in sections 3, 4, 5, and 6 of ref. 141, and of this report. It is highlighted and summarized in Section 6 hereof.

The actual NASA trade study to select an optimum approach will require knowledge of the proper weight for each of the several trade parameters. The weights are not yet established by NASA, and in any case are not likely to be available to MIT during even the remaining extension of the original contract period. Therefore, it would be relatively meaningless for MIT to conduct such a final trade study using only the results of this work and to produce a specifically-recommended approach. However, in the course of studying the various candidates and preparing figures of merit, etc., there have been some trade comparisons that are general in nature and that can lead to some fairly strong, if not specific, recommendations for NASA to consider. An example was the recommendation to discontinue investigations pertaining to SIMS-C (see subsec's. 1.2.1 and 2.3 of ref. 85.)

The outline below indicates the elements of the step-by-step approach shown in ref. 85, subsection 1.2.2, for achieving the objectives of this study, and thus established the goals of the various task areas. In view of time and personnel-availability limitations, not all of the indicated steps were fully accomplished. A major effort was made by the study team to fulfill all essential contract objectives. The outline follows:

- I. Define stellar data requirements and availability
 - A. Define fields of view and moding of star sensors
 - B. Define stellar update requirements
 - C. Conduct star availability studies
 - 1. Establish star catalog for each detector
 - 2. Impose field-of-view, moding constraints

3. Include representatives of all orbits
4. Select "typical" and "average" cases
 - a. Repeat for several limiting magnitudes
5. Prepare data inputs for simulations

II. Define SIMS candidate configurations

- A. Prepare functional block diagrams
 1. Identify major subsystems, components
 2. Include signal flow
 3. Include operating modes
 4. Include switching logic
 5. Include any necessary modifications to existing design work
- B. Prepare interface specifications
 1. Electrical
 2. Mechanical
 3. Thermal
 4. Data-handling
- C. Define ground control/command operations
- D. Define data-processing requirements
- E. Perform preliminary design
 1. Define specifications for major components
 2. Specify
 - a. Performance
 - b. Weight
 - c. Power
 - d. Telemetry-requirement
 - e. Field-of-view requirement
 3. Specify modifications to existing candidate configurations

F. Develop error models

1. Emphasize error components that increase with time

III. Perform error analyses

A. Simulate realistic environment

1. Spacecraft rotational dynamics
2. Typical and average case stellar updates

IV. Perform sensitivity analyses

A. Determine effect on SIMS performance, power, reliability, etc.

1. Field-of-view available
2. Gyro performance variation
3. Star sensor performance variation
4. Other expected parametric variations

V. Prepare Candidate Configuration Comparisons

A. Tabulate and/or otherwise present:

1. Cost (development and production)
2. Accuracy
3. Weight
4. Power requirement
5. Telemetry requirement
6. Total unobstructed field-of-view required
7. Simplicity of design and reliability
8. Modularity of design and growth potential
9. Cost of ground support equipment
10. Complexity of ground control/command/data processing
11. System availability

- B. Provide supporting engineering discussions
- VI. Conduct limited trade study
 - A. Emphasize potential for achieving performance goals
 - B. Discuss availability and development risks
- VII. Develop and present any MIT recommendations

- - - - -

In Section 2, the configuration candidates are discussed briefly, and references to locations of more detailed definitions and descriptions are provided.

Sections 3, 4, and 5 comprise an updating and completion of similar sections of the Second Interim Technical Report¹⁴¹, and thus finish the descriptions by the Primary Task Leaders of investigations in their task areas during the course of the study.

Section 3 hereof includes: documentation of a visit to Honeywell Aerospace Division; a description of the electronics employed by Northrup Nortronics Division in its GI-K7G gyro torque-to-balance loop design; exposition of a SIMS-D (3-axis gimbale) IARU candidate using 13-IRIG gyros, (similar to that presented in ref. 141 for the TGG version); a further discussion of IARU reliability from the standpoint of gyro reliability estimates only, including the introduction of a particular four gyro (tetrad) IARU concept, both for strapdown and for gimbale application; and recommendations concerning proposed future IARU-related tasks.

In Section 4, a detailed updating of the star mapper information contained in ref. 141 is presented, including changes, corrections, clarifications (with some derivations) and the addition of material not contained in or adequately dealt with or completed in the prior report. In addition, an investigation of the feasibility of using a SIMS-B (TRW-PADS)⁸⁵ star tracker in a random acquisition mode (see category D1-B2 in subsection 1.2.1 hereof) is reported and is shown to provide optimism that the TRW tracker can indeed meet the D1-B2 scan and acquisition requirements.

Section 5 provides an updating and expansion of reportage of the earlier¹⁴¹ star availability studies and of the system, state and measurement equations for the three candidates. Results of the extensive error analysis and sensitivity studies are then presented in subsection 5.4, in graphical and tabular formats. The section ends with a consideration of those error sources that were not taken into account in the performance results of subsection 5.4

Section 6 contains a summary of highlights of the SIMS Trade Study, including (p. 6-5) a simplified tabular comparison of the three primary SIMS candidates. It then presents a criterion-by-criterion discussion of the eleven technical trades summarized by the tabulation.

Appendix A was planned as a self-contained summary of all trade criterion information. Due to unforeseen time constraints it is, instead, a supplement to (or is supplemented by) information contained in Sections 3, 4, 5 and 6. (See subsection A.1 on p. A-1)

Appendix B is a revised catalog of stars of magnitude 4.0 or brighter (as seen by one or more of the detectors considered in this study.) The tabulation includes the influence of the additional photometric data recently received, and supersedes the similarly-numbered Appendix of ref. 141.

In Appendix C, the results of the studies of star availability as influenced by variations in the minimum usable detector magnitude (for star mappers) and by reductions in the maximum allowable out-of-orbital-plane angle (for the SIMS-B star tracker) are presented. Appendix C plots of star availability supplement those found in Appendix C of ref. 141.

Appendix D presents a brief comparison of the techniques of star mapper measurement employed by MIT/CSDL in SIMS-A studies and by Honeywell Aerospace Division in SPARS studies (see ref. 16). This is in response to questions raised¹⁴⁹ concerning the equivalence of the two techniques.

The special study tasks of the final four months of the overall effort are indicated in Appendix E, which provides excerpts from the technical proposal submitted in connection with those tasks.

The provision for including last-minute-before-publication information was accomplished through Appendix F, in view of unresolved decisions pertinent to selection of the star mapper for SIMS-A and -D.

Sections 7 and 8 list the References and Distribution, respectively, of this report.

SECTION 2

SIMS CONFIGURATIONS

2.1 INTRODUCTION

Descriptions of the SIMS configuration candidates considered in this study, which are listed in subsection 1.2.1 of this report for easy reference, have been presented in Section 2 of ref. 85. The selected primary candidates for the final comparison, SIMS-A, -B and -D (or -A, -B and -D1-A, as originally defined), were among those receiving further exposition in Section 3 of ref. 85, and were given detailed description and analysis throughout ref. 141.

Moreover, plans to have developed at least preliminary layout sketches of each SIMS candidate in a typical EOS sensor bay location, for presentation here, and perhaps to include isometric or artist's conception sketches as well, were thwarted by limitations of time and energy of certain team members - perhaps principally of the Project Leader. (The star sensor sketches of Appendix A would have been highly useful to this purpose.)

Accordingly, the candidate configuration description information that follows is of very limited scope, and is intended primarily to update or correct the earlier descriptions where appropriate.

2.2 SIMS-A

Refer to subsection 2.2, pages 2-5 through 2-11, of ref. 85. The SIMS-A configuration description presented therein is essentially valid. The functional diagram shown in Fig. 2-2 on p. 2-8 thereof is accurate except that the star mapper may use silicon, not cadmium sulfide, detectors (see Appendix F).

The telemetry requirements (see subsection 6.2.5 of this report) are now increased somewhat relative to those of ref. 85, particularly due to the need to recover data on a continuous basis* when the gyros are structure-mounted. Referring to subsections 6.2.3 and 6.2.4 herein, it is seen that prior weight and power estimates of 62 lb and 72 W are replaced by 22 lb and 39 W, respectively. The revision of the SIMS-A IARU definition to one based on 13-IRIG pulse-rebalanced gyros as opposed to GG334A gyros, and revisions to star sensor weight and power estimates, are among the bases for the improvements in these parameters. (Note that the predicted improvements to 31 lb and 37 W cited in ref. 85, p. 2-9, have been essentially accomplished or exceeded in current Honeywell estimates.)

A 10° field-of-view replaces the 4° of ref. 85, p. 2-9 (see subsection 6.2.6 in this report). Refer to Sections 5 of this report and the preceding report, ref. 141, and to Sections 4 and 6 of the same two reports, as appropriate, for a complete updating of the subjects of stellar data requirements and stellar data availability. (e.g., note the yaw sensitivity to size of the

* Assuming the attitude algorithm is updated on the ground.

star mapper's field-of-view on pages 5-56 and 5-57 hereof; note how the number of stars per orbit is influenced by FOV and by detector type, on p. 5-11.)

SIMS-A error model information is presented in pages A-10 through A-14 of Appendix A hereof.

2.3 SIMS-B

Refer to subsection 2.3, pages 2-11 through 2-16, of ref. 85. The six-gyro redundant configuration IARU referred to there would instead be a three-gyro orthogonal triad similar to that of SIMS-A (Ref. 154; also subsection 3.2.2 hereof).

Computer-controlled star acquisition, as described in ref. 85, p. 2-12, may well be replaceable by a random acquisition moding [see subsection 4.4, and subsection 6.2.8, item 3), "Random Acquisition...etc," in this report.] Elimination of the SIMS-B computer could be the highly-desirable result*.

Figure 2-3 of ref. 85 needs: to show "3", not "6" gyros; "three", not "three to six" words of gyro data in Note 1; and possibly to have Notes 3 and 4 deleted if the computer is eliminated*. At the top of p. 2-15 thereof, "hexad" would be "triad", the star tracker field-of-view might be reduced (see subsections 5.4.3 and 6.2.6 hereof), and reference to a computer might be deleted*.

Telemetry requirements stated in ref. 85 were overstated there, but are currently about the same as previously estimated,

* Assumes the attitude algorithm is updated on the ground.

due to the need for recovery of strapped down IARU data on a continuous basis if the attitude algorithm is updated on the ground. Refer to subsection 6.2.5 hereof for the current estimate.

Size, weight and power requirements still are not well-defined for SIMS-B, as can be seen in Appendix A of this report. (Refer to pages A-26, A-27 and A-32, and to subsections 6.2.3 and 6.2.4 hereof.) Note the choice of aluminum or beryllium construction in the star tracker gimbal assembly. Note also that a single-gimbal tracker is under consideration [see subsection 6.2.8, at 3), "Elimination of a Star Tracker Gimbal."] Stellar data requirements and availability are adequately treated in subsections 5.2 and 5.4.3 hereof and subsection 5.3 of ref. 141.

The SIMS-B error model information is tabulated on pages A-16, A-17 and A-18 hereof.

2.4 SIMS-D

The descriptions of SIMS-D in ref. 85 (pp. 2-24 through 2-49 thereof) are essentially valid to the extent that they refer to the sub-candidate defined as SIMS-D1-A (pp. 2-38 through 2-41 thereof). Estimates of telemetry requirements are currently somewhat lower (see subsection 6.2.5 of this report). Two 3-axis gyro platforms are currently being considered [see subsection 3.3.2 of ref. 141 and subsections 3.3.3 and 6.2.8, at 2), hereof], one employing the higher-performance Third Generation Gyros (TGGs) and the other the smaller, lighter, less-costly and lower-performance Size 13 (≈ 1.3 inch case diameter) Inertial Reference Integrating Gyros (13-IRIGs). The star mapper selected has a

10° field-of-view and employs silicon detectors (see subsection 4.2.3 hereof.) Subsection 5.4.4 of this report presents results of the SIMS-D error studies, and subsection 6.2 includes a relatively comprehensive summary of SIMS-D in terms of all the requisite trade criteria in this study. Pages A-19 through A-21 hereof present the available SIMS-D error model information.

SECTION 3

INERTIAL ATTITUDE REFERENCE UNITS

3.0 INTRODUCTION

3.0.1 EOS-SIMS IARU REQUIREMENTS

In order to evaluate the IARU for the EOS/SIMS application the following preliminary requirements have been tabulated.

3.0.1.1 Statement of Work Requirements

(a) Continuously determine SIMS attitude with respect to an inertial frame (within $0.001^\circ/\text{axis} - 1\sigma$)

(1) The IARU should be mechanized within an allotment of $0.00056^\circ/\text{axis} - 1\sigma$ (2 sec).

(b) Configuration selection to be based upon the following factors.

(1) Accuracy, cost, weight, power, telemetry requirements, reliability of components, simplicity of design, modularity and growth potential, cost of ground support equipment, complexity of ground control/command operation.

(c) - ~~Spacecraft attitude is to be maintained in all~~ axes to within $\pm 0.5^\circ + 0.2$ degrees (1σ) and rates shall be below 0.005 degrees/second (3σ). Acceleration at the time of attitude control jet firing is $2.9^\circ/\text{sec}^2$. *

* Jet firing occurs only when momentum wheel system is being unloaded, and this will be done in orbital segments during which high resolution payload is not required. SIMS accuracy requirement is relieved during jet firing and for a time interval to be determined afterward.

3.0.1.2 Mission-Related Requirements

(a) The expected input rate due to earth orbit is about 3.4°/min.

(b) The expected operating life is in excess of 3 years.

(c) The IARU pitch axis will require full circle readout capability; however, the system roll and yaw axes will require a maximum readout to ± 5 degrees at specified accuracy.

(d) Separate capability to return the gimbal system roll and yaw axes to a reference position is required at some interval to be determined from system simulations.

(e) Attitude reference celestial updates will be available for absolute attitude determination at periodic intervals determined by the optics subsystem star availability tradeoff.

3.1 SIMS-A (SPARS-LIKE IARU)

(Information on SIMS-A presented in subsection 3.1 of Interim Report No. 2, ref. 141, is applicable without revision; the following, also related to SIMS-A, supplements that information.)

3.1.1 REVIEW OF HONEYWELL/ST. PETERSBURG DISCUSSIONS

On January 20-21 a trip to Honeywell was made to review the SPARS technology hardware which has been reported by us in reference 141. The present SPARS technology performance requirements are outlined in Appendix A at page A-37. This technology was initiated by the Air Force to advance the state of the art for in-orbit attitude determination

capability. It is the desire of the Air Force (SAMSO) Project Office to make this technology study generally available to NASA as well as Air Force agencies.

It should be noted that the SPARS technology reporting made to date is based upon existing real hardware. The hardware status shown in this report and in Appendix A reflect the projections of the SPARS technology hardware development for the near future. This projection is based upon the use of a strapdown gyro package of 13-IRIG instruments.

Further discussions were held with Honeywell in the area of torque rebalance loops. The torque-to-balance loop mechanization of the GG2200 shows that an overall ternary loop is mechanized using a 9.6 KHZ torquing rate with a dual pulse weight having nominal fine loop quantization of 0.065 $\overline{\text{sec.}}$ per pulse⁹⁰. Because of this fine loop quantization a limit cycle frequency will be induced resembling a binary loop output. This resultant lower frequency limit cycle is expected to produce lower variance in the net pulse count distribution than is possible with a straight binary loop. This implementation will also be less sensitive to variations in the difference between positive and negative scale factor than the conventional binary loop. This loop has a voltage-to-pulse frequency converter which converts the instrument signal generator error voltage to an appropriate torque decision for the ternary rebalance loop electronics. This converter is a high gain integrator which develops a torquing decision based upon the signal generator error voltage. Immediately after a torquing decision is made the integrator input is reset to zero. This then requires a finite predetermined integration time regardless of the signal generator error signal magnitude and would prevent pulse bursting over a specified loop dynamic range depending upon the instrument float time constant,

pulse size, torque generator time constant, etc. Report from Honeywell¹⁵³ testing of SPARS with rates commensurate with the EOS orbit rate have shown no pulse bursting present using the standard GG2200 rebalance loops. It should be pointed out, however, that the method described may not provide pulse bursting protection over the complete instrument loop dynamic range. This implementation is also believed to desensitize the torquing decision process to signal generator noise.

3.2 SIMS-B (PPCS/PADS IARU)

(Information on SIMS-B presented in subsection 3.2 of ref. 141 is applicable without revision; the following, also related to SIMS-B, supplements that information.)

3.2.1 DESCRIPTION OF NORTHRUP ELECTRONICS T/B LOOP DESIGN

Information was received since the second interim report (ref. 141) from John Dieselman of Northrup regarding a proposed SAS/D torquing loop¹⁵⁵ for use with the GI-K7-G instrument. This implementation is a binary moded pulse-width modulated rebalance loop. The features of this type of loop are illustrated in Figure 3-1. Referring to the figure, the preamplified instrument signal generator error voltage is demodulated and the D.C. voltage level is amplified. A precision ramp voltage is now generated and summed with the D.C. error voltage within the analog-to-pulse width converter. The ramp voltage generator frequency is set at 1350 Hz. This then represents the torquing loop forced limit cycle. The resulting waveform (ramp plus signal) is applied to a zero crossing detector (also within the converter) which sets the binary control logic for the torquing current desired for that particular limit cycle. The digital readout in attitude pulses of the required rebalance torquing current is obtained using a

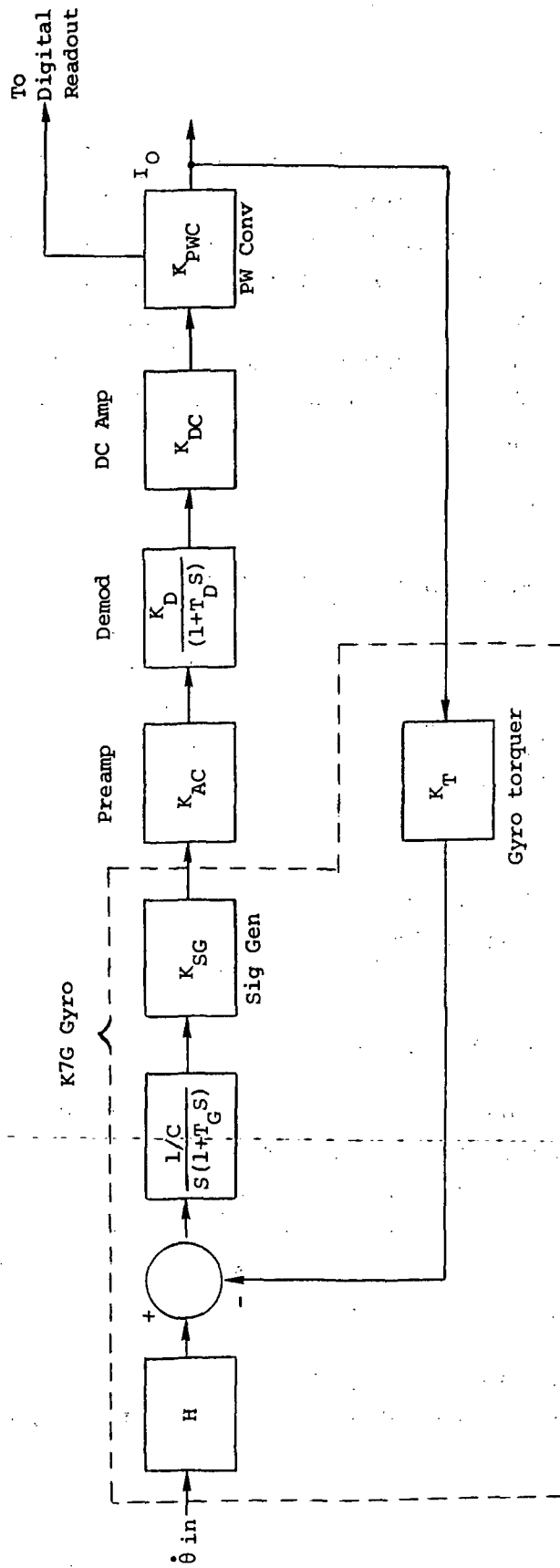


Figure 3-1 K7G Torque to Rebalance Loop (Block Diagram)

108 KHz clock frequency; two accumulators are mechanized to sum the $\Delta\theta$ pulses for positive and negative torquing intervals separately. It is expected that instrument bias will be removed by a known adjustment in the accumulator outputs. This method of instrument bias compensation within the torque-to-balance loop mechanization then becomes a part of the instrument loop calibration. Table 3-1 is a summary of the pulse torquing parameters received from Northrup.

Table 3-1

SUMMARY OF PULSE TORQUING PARAMETERS

Clock Frequency	108 KHz
Readout Pulse Frequency	108 KHz
Limit Cycle Frequency	1350 Hz
Readout Pulses/Limit Cycle	80
Current to Torquer	10 ma
Quantization	0.0082 arc-sec/pulse
(Counting both "positive" and "negative" readout pulses)	

3.2.2 REVIEW OF TRW INFORMATION¹⁵⁴

It was shown in subsection 3.2.1 of ref. 141 that the PPCS/PADS mechanization included a requirement of a six-gyroscope array. For the EOS/SIMS application the redundancy implementation should be commensurate with reliability analysis requirements and would be similar to that for all candidate systems as discussed in Section 3.4 of this report.

The IARU summary shown for System B in Appendix A includes all SIMS-B material available up to the time of publication of this report.

3.3 SIMS-D

3.3.1 IMPLEMENTATION OF IARU

In the past reporting period two separate gimbale implementations have been presented as possible SIMS-D candidates. The first system is a conventional three-axis gimbale system using very limited freedom on the outer two gimbals. The second is a single-axis platform mechanization in which two torque-to-balance loop gyros are mounted on the platform with input axes normal to the single, stabilized platform axis. Both of these MIT/DL systems were evaluated using the TGG instrument type.

It has become apparent during the study of all the candidate IARU mechanizations that the strongest candidates are the fully-strapdown and fully-gimbale configurations. The SAP/Hybrid system was proposed originally to eliminate the additional scale factor uncertainties which are propagated in a fully-strapdown mechanization because of variations in the constant orbital rate. If the fully-strapdown configuration uses the adaptive torque-to-balance loop suggested in Appendix A of ref. 141, the sensitivity of a strapdown system to scale factor uncertainty is greatly reduced. Further, it is believed that gimbal orthogonality errors can be held in calibration to 2 sec , which eliminates another principal reason for consideration of the SAP/Hybrid. For these reasons the SAP/Hybrid configuration was eliminated from further study.

Since the last reporting period, system studies have shown that gyroscope uncertainty levels do not have a direct effect upon the overall attitude accuracy. It was shown that short term performance levels in the $0.01^\circ/\text{hr}$ drift area appear satisfactory in the EOS mission simulations using most star mapper models. For this reason we are including a three-axis

gimbal system based upon the MIT 13 IRIG instrument technology.

3.3.2 SIMS-D DESIGN (TGG INSTRUMENTS)

(Information presented in subsection 3.3.2 of ref. 141, is applicable without revision; the following, relating to the SIMS-D IARU using 13-IRIG gyros, supplements that information.)

3.3.3 SIMS-D DESIGN (13 IRIG INSTRUMENTS)

3.3.3.1 Detailed Layout of IARU

3.3.3.1.1 Layout Drawing - A layout definition drawing of the IARU is shown in Figure 3-2. This three-axis gimbal assembly has unlimited motion about the inner axis (Pitch) and $\pm 5^\circ$ motion about the middle and outer axes. Mounted on the stable member are three MIT/DL 13-IRIG gyros.

The three-inter-gimbal readout devices shown are 1- and 128-speed resolver chains. Associated with this layout are fifty one cubic inches of stable member-mounted electronics including servo amplifiers, instrument temperature control, pre-amplifiers, wheel and suspension supplies, the readout excitation and a signal multiplexer.

Also attached to the stable member is an optical cube which will define the three gimbal axes for alignment and calibration purposes.

The stable member is supported in the middle gimbal through two sets of preloaded duplex pairs of bearings. The assembly at one end of the axis contains the readout device and a slip ring with up to 34 circuits*. The other end of the axis has a D.C. torque motor and a gyro error resolver.

* This number is expected to be reduced by multiplexing. See subsection 3.3.3.2.

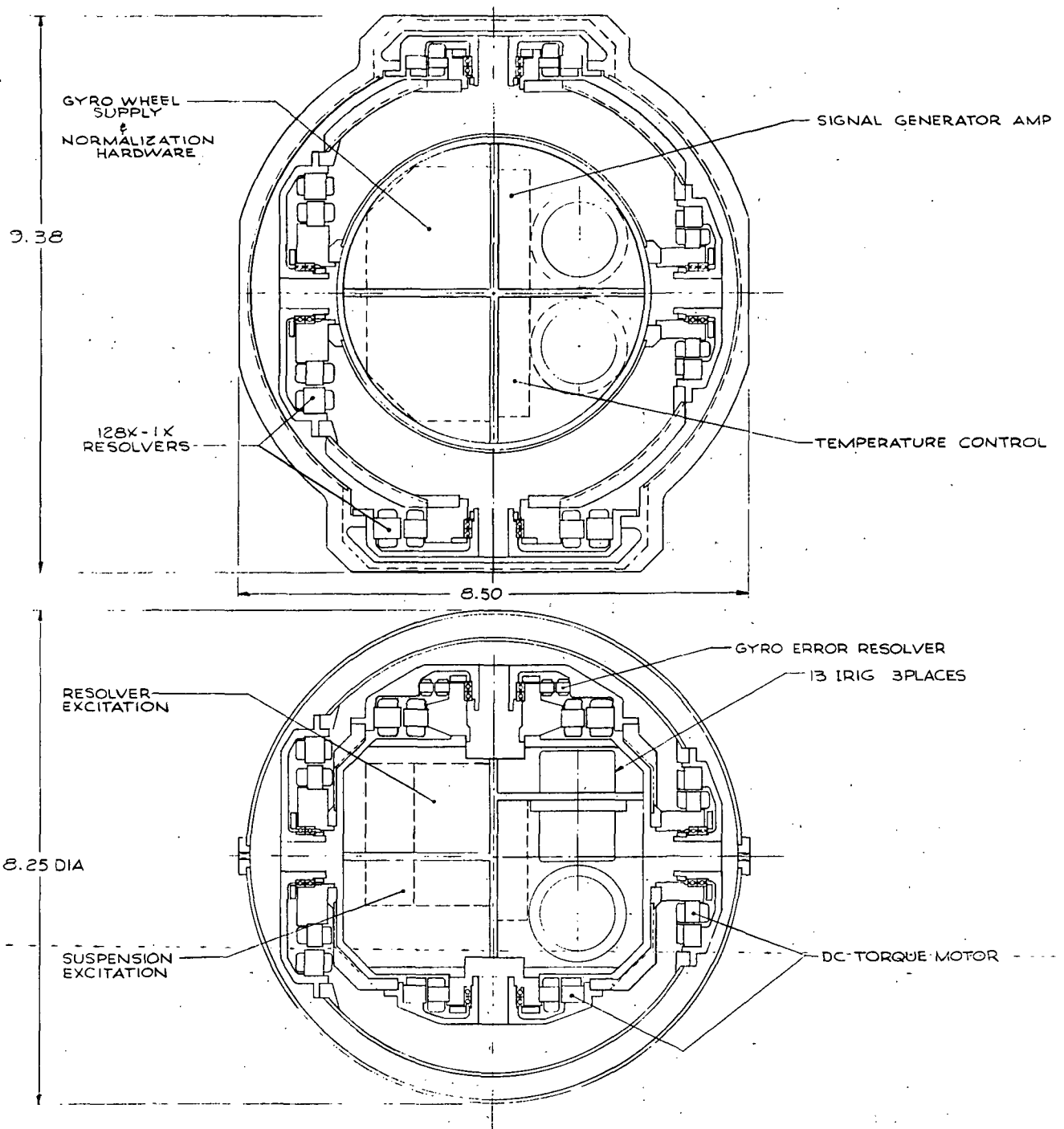


Figure 3-2 13 IRIG Three-Gimbal Layout

The middle gimbal is supported in the outer gimbal and the outer gimbal in the case through similar assemblies, except that no gyro error resolver is required and the slip-ring assembly is replaced by flexible wires.

3.3.3.2 Interface Requirements

The external electrical interface requirements for the three-gimbaled IARU are shown in Figure 3-3. The internal IARU interface is shown in Figure 3-4. It is presently estimated that, using the multiplexer capability, less than fifteen slip ring assignments or flexleads will be required along any gimbal axis.

3.3.3.3 IARU Characteristics

The overall weight, power and size estimates are:

Weight = 15 lbs.

Size = 9.4" x 8.5" x 8.25"

Power = 35 watts

A detailed breakdown of the electronics characteristics is shown in Table 3-2.

3.3.3.4 Gyro Description (13-IRIG)

The 13-IRIG is in the third generation instrument family of floated single-degree-of-freedom integrating inertial gyros developed by the MIT Charles Stark Draper Laboratory. The intent of the 13 IRIG design is to provide a simple, highly-reliable, easily produced, high performance gyroscope. This low angular momentum instrument is especially qualified for earth satellite application where high reliability and low power requirements are critical. The basic technology incorporated into the 13 IRIG design includes: (cont'd on p. 3-14)

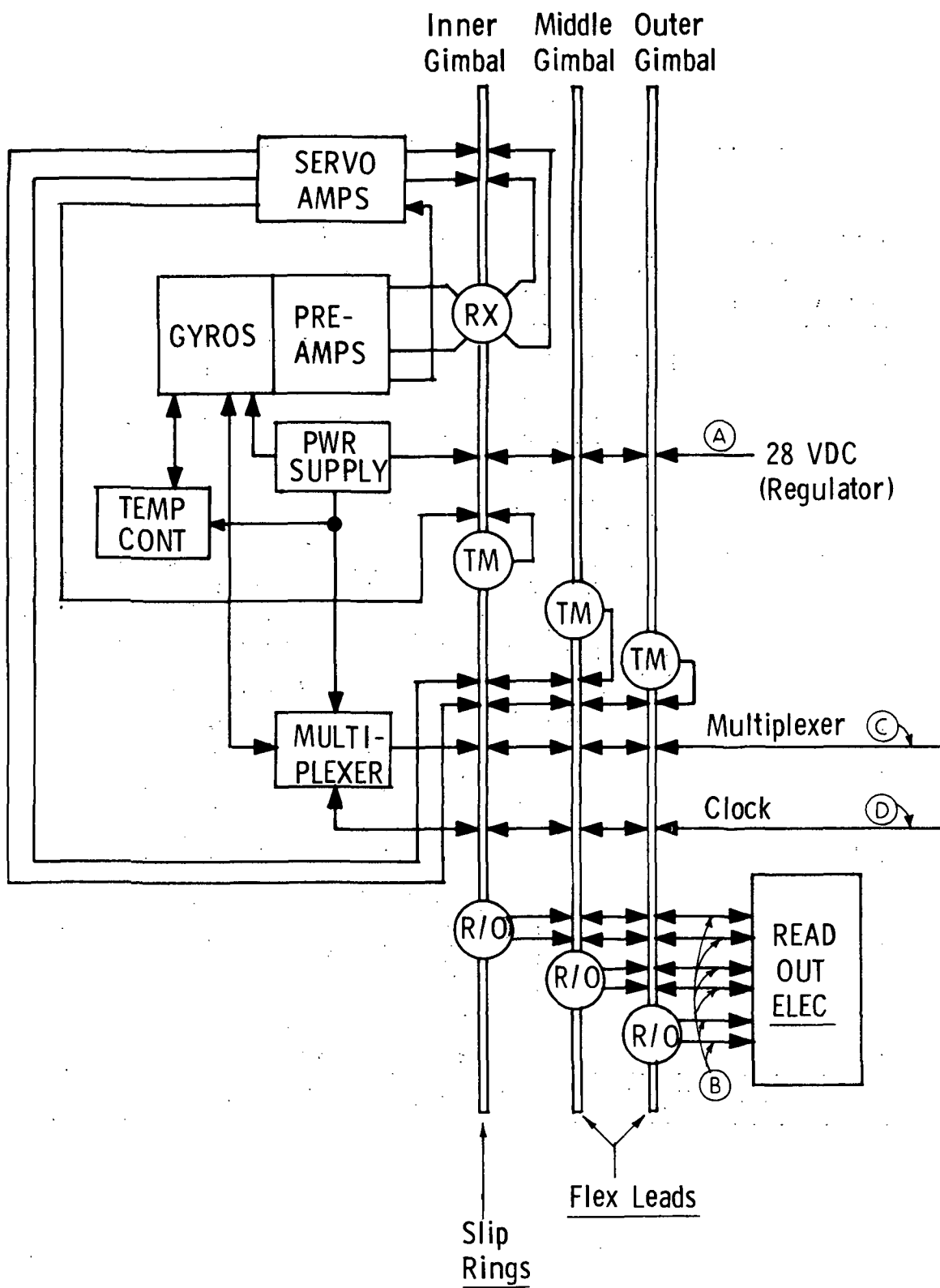


Figure 3-4 IARU Interface

Table 3-2

ELECTRONICS CHARACTERISTICS

<u>POWER SOURCE</u>	<u>POWER (W)</u>	<u>VOLUME (in³)</u>	<u>WEIGHT</u>
Gyro Wheel Supply	5.2 (Note 1)	10 (Note 2)	
Suspension Excitation	0.2	3 (Note 2)	
Normalization Hardware	0.1	1	
Sig Gen Amp	0.1	2	
Inductosyn Excitation	1.0	6 (Note 2)	
Temp Control	0.5	2 (Note 2)	
Servo Amp.	1.5	7	
RRS. R/O	3.0	6	
11.6 watts/axis		21 in ³ (Note 2)	1.2 lbs/axis
		+ 16 in ³ /axis	

Summary (Notes 2,3)

Weight: 3.6 lbs

Power: $11.6 \times 3 = 34.8$ watts

Volume: 69 in³ (51 in³ on SM)

Notes

1. The 13 IRIG gyros will use 3.1 watts for each wheel*. To provide 0.1% power supplies about 60% efficiency is achievable. The wheel supplies will be included on the stable member.
2. This estimate includes all three axes
3. This estimate is for all the electronics but does not include any mounting or support structure.

* 6 1/2 watts for 30 sec to START; 3.1 watts to RUN.

Boron Carbide Gas Bearing

The spool-type self-acting gas bearing incorporates a high-performance, computer-optimized design. The small rotating mass, which defines a large support area-to-volume ratio, allows the hydrodynamic support of large inputs. The specific grade of boron carbide has been developed for integrity and reliability as the critical operating surfaces of a gas bearing. No boundary lubricant is required.

Boron Carbide Float Structure

The excellent stability and low thermal expansion characteristics ensure a stable float structure.

Balancing Wafer

A meltable alloy, incorporated in the balancing wafer, allows fine balancing at the completed gyro level. The degree of fine balancing is controlled by accurate positioning in the gravitational field of the earth.

Adhesive Bonding

The float structure utilizes adhesive bonding throughout; in many cases thin capillary bonding is utilized. Several of the adhesive joints are hermetic seals as well.

Encapsulation

The electromagnetic components (motor stator, magnetic suspension stator, torque generator stator) are encapsulated with low-stress potting compounds.

Printed-Circuit Signal Generator Pickoff

The float angular displacement pickoff utilizes low-volume printed-circuit components.

Electromagnetic Suspension

The electromagnetic suspension ensures centered float operation within the fluid.

Electrical Connections

Electrical connections utilize welded joints wherever practical.

Heater/Sensor Assemblies

Dual heater/sensor assemblies control instrument operating temperature.

Center-Flange Mounting

Center-flange mounting allows a symmetric mechanical mounting interface to the system.

3.4 IARU RELIABILITY CONSIDERATIONS

Information in this subsection is used to address the 3 to 5 year expected operating life requirement identified for EOS/SIMS. Since little actual instrument reliability information has been available in this study, certain assumptions will be defined to introduce reliability requirements. The IARU reliability will be based upon expected gyroscope axis reliability estimates only, since the effect of the support electronics hardware or redundancy electronic mechanization requirements are presently unknown. It will be assumed here that the failure detection and isolation capability will be implemented on the ground, and that the ability to change status of the airborne redundant system configuration can be accomplished by uplink command with perfect reliability.

Previous reporting has included reliability estimates using both the multiple triad-standby and hexad instrument loop standby mechanizations. Figures 3-5 through 3-7 illustrate the predicted reliability of various standby configurations with expected gyro loop MTBF values of 10,000, 50,000 and 100,000 hours respectively. These curves assume the redundant triads or gyro axes (for the hexad) are on standby with infinite MTBF and are activated and processed using externally-derived failure detection, isolation and reconfiguration decisions. It is assumed the triad configurations are similar in reliability for either a strapdown or gimbaled IARU design. From Figure 3-5 it is apparent that regardless of the redundancy employed using gyro loop MTBF values of 10,000 hours the mission requirements are not satisfied. Figure 3-6 shows that a gyro loop MTBF value of 50,000 hours is marginal for this mission while all redundancy configurations shown in Figure 3-7 appear adequate. The MTBF values here are based on a gyro loop failure definition including all those failures which prevent attitude determination to specified accuracy, as determined by ground processing, and not simply wheel synch type of failures.

Another redundancy configuration which has not been previously considered in this study is the four gyro (tetrad) array. To apply this redundancy configuration with the ground detection capability of EOS/SIMS requires different techniques when considering strapdown and gimbaled system mechanization.

For continuous stabilization in a gimbaled system employing four gyros a detection, isolation, and reconfiguration method is necessary within the gimbaled system mechanization.

The strapdown doesn't require this capability because it is essentially an open loop monitoring device when complete ground processing is assumed. The single redundant instrument

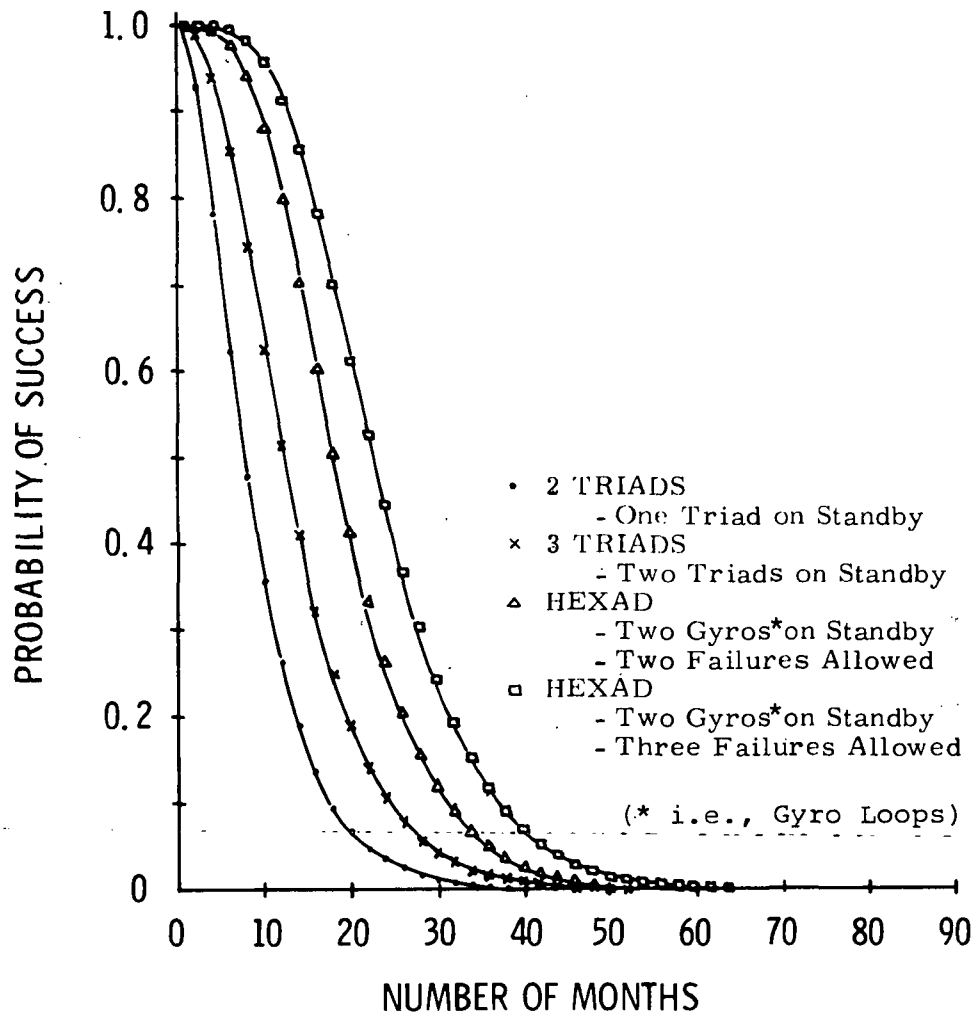


Figure 3-5 Mission Success Probability
(Gyro Loop MTBF = 10,000 Hrs.)

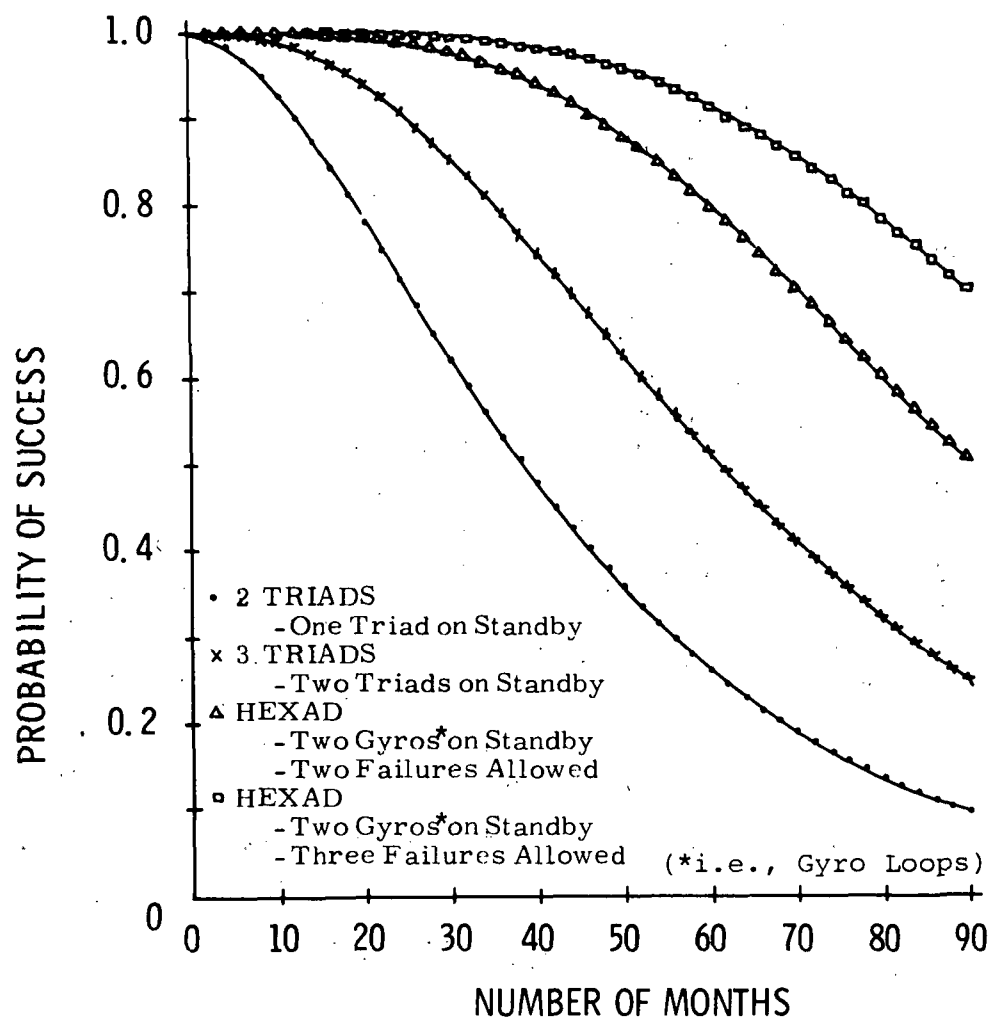


Figure 3-6 Mission Success Probability
(Gyro Loop MTBF = 50,000 Hrs.)

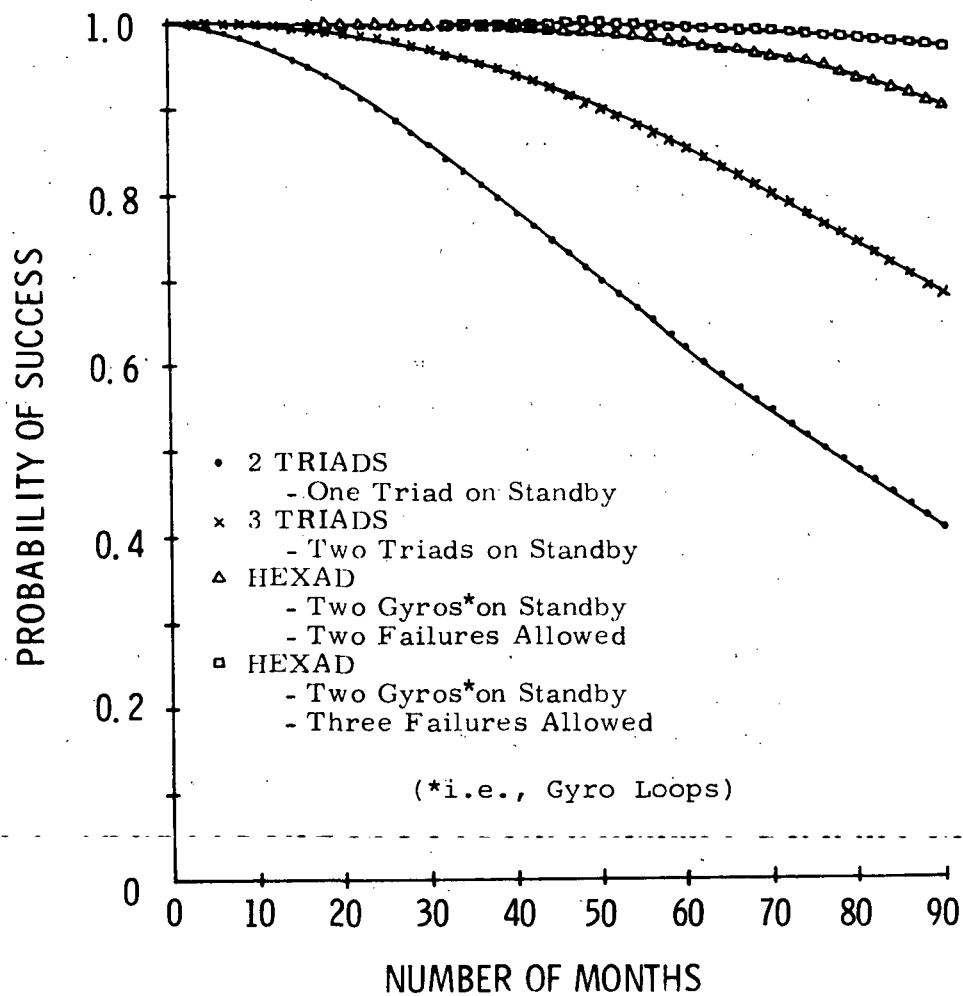


Figure 3-7. Mission Success Probability
(Gyro Loop MTBF = 100,000 Hrs.)

loop in a strapdown mechanization should then be placed in a known geometric orientation such that components of all three basic triad axes are adequately represented. This gyroscope loop can adequately replace any of the three triad axes for any single triad failure, while the fourth gyroscope loop failure itself is detected by the correctly operating triad.

The tetrad concept applied to a three-axis gimbaled system implementation may be visualized by considering the stable member conceptually as a cube.¹⁵⁶ Define the stable member computational axes as the orthogonal set of normals to the cube faces. The input axes of the four gyros are aligned to be respectively parallel to the four lines each of which passes through opposite pairs of vertices of the cube. The sense of each gyro's input axis is chosen such that the angular separation of the positive sense of any gyro's input axis from any other such axis is $\cos^{-1}(-1/3)$ (approx. 109.5°). In such an arrangement, each gyro's input axis will be angularly separated from each of the three stable member computational axes by $\cos^{-1}(\pm 1/\sqrt{3})$ (approx. 54.7° or 144.7°).

To circumvent the loss of gimbal servo stabilization in the event of failure of one of the four gyros, it will be necessary that the gyro signal generator outputs be preprocessed to allow automatic failure detection and reconfiguration.

The four gyro input axis unit vectors in the stable member computational frame (x,y,z) are defined as:

$$\begin{aligned}\underline{u}_1 &= 1/\sqrt{3} (1,1,1) \\ \underline{u}_2 &= 1/\sqrt{3} (-1,-1,1) \\ \underline{u}_3 &= 1/\sqrt{3} (-1,1,-1) \\ \underline{u}_4 &= 1/\sqrt{3} (1,-1,-1)\end{aligned}\tag{3-1}$$

Assume the measured angular velocity of the stable member is to be expressed in stable member axes as:

$$\underline{\omega}_m = (\omega_x, \omega_y, \omega_z) \quad (3-2)$$

The four gyros will each sense the component of the stable member angular velocity occurring about its own input axis. Thus:

$$\begin{aligned} \omega_1 &= \underline{u}_1 \cdot \underline{\omega}_m = 1/\sqrt{3} (\omega_x + \omega_y + \omega_z) \\ \omega_2 &= \underline{u}_2 \cdot \underline{\omega}_m = 1/\sqrt{3} (-\omega_x - \omega_y + \omega_z) \\ \omega_3 &= \underline{u}_3 \cdot \underline{\omega}_m = 1/\sqrt{3} (-\omega_x + \omega_y - \omega_z) \\ \omega_4 &= \underline{u}_4 \cdot \underline{\omega}_m = 1/\sqrt{3} (\omega_x - \omega_y - \omega_z) \end{aligned} \quad (3-3)$$

It can be seen from (3-3) that a properly operating system can be verified by the equation:

$$\sum_{i=1}^4 \omega_i \leq |\epsilon| \quad (3-4)$$

where ϵ represents the expected system noise level. A single failure detection parity is then available by observing equation (3-4). The remaining task is to identify and isolate any failed gyroscope. Using combinations of equations in (3-3), dual computational axis solutions can be identified as:

$$\begin{aligned} \omega_z &= \sqrt{3}/2 (\omega_1 + \omega_2) \\ \omega_y &= \sqrt{3}/2 (\omega_1 + \omega_3) \\ \omega_x &= \sqrt{3}/2 (\omega_1 + \omega_4) \\ \omega_x &= -\sqrt{3}/2 (\omega_2 + \omega_3) \\ \omega_y &= -\sqrt{3}/2 (\omega_2 + \omega_4) \\ \omega_z &= -\sqrt{3}/2 (\omega_3 + \omega_4) \end{aligned} \quad (3-5)$$

For failure of any single gyroscope of the four, three valid signals always remain available to provide the correct computational axis measurement. The technique for isolation of the failed instrument axis is now under study for the EOS/SIMS mission application.

Using an appropriate preprocessor on the four gyroscope signal generator outputs it may be possible to develop both the stable member stabilization signals and the ability to do fault detection and isolation. The expected tetrad gyroscope system reliability curves associated with gyroscope loop MTBF values of 50,000 and 100,000 hours are shown in figures 3-8 and 3-9 respectively. For similar gyroscope MTBF reliability the tetrad configuration is directly comparable to a two-triad standby configuration or is better than two triads if both triad systems are assumed operating throughout the mission.

Note that all the figures shown here are sized for IARU attitude determination reliability considerations under the constraints cited and must be justified as an IARU subsystem when considering the required overall spacecraft reliability.

3.5 IARU SUMMARY

From the IARU subsystem standpoint the EOS/SIMS reliability requirement of 3 - 5 years seems realizable. The use of redundancy from simplex systems doesn't appear as effective an approach to the satellite application as would a single simplex system using redundant components. With gyroscope reliability of MTBF of 100,000 hours a tetrad system appears desirable. MTBF gyroscope reliability calculations, however, must be viewed from the soft failure requirements of the EOS/SIMS mission and not just from wheel life or hard failure histories.

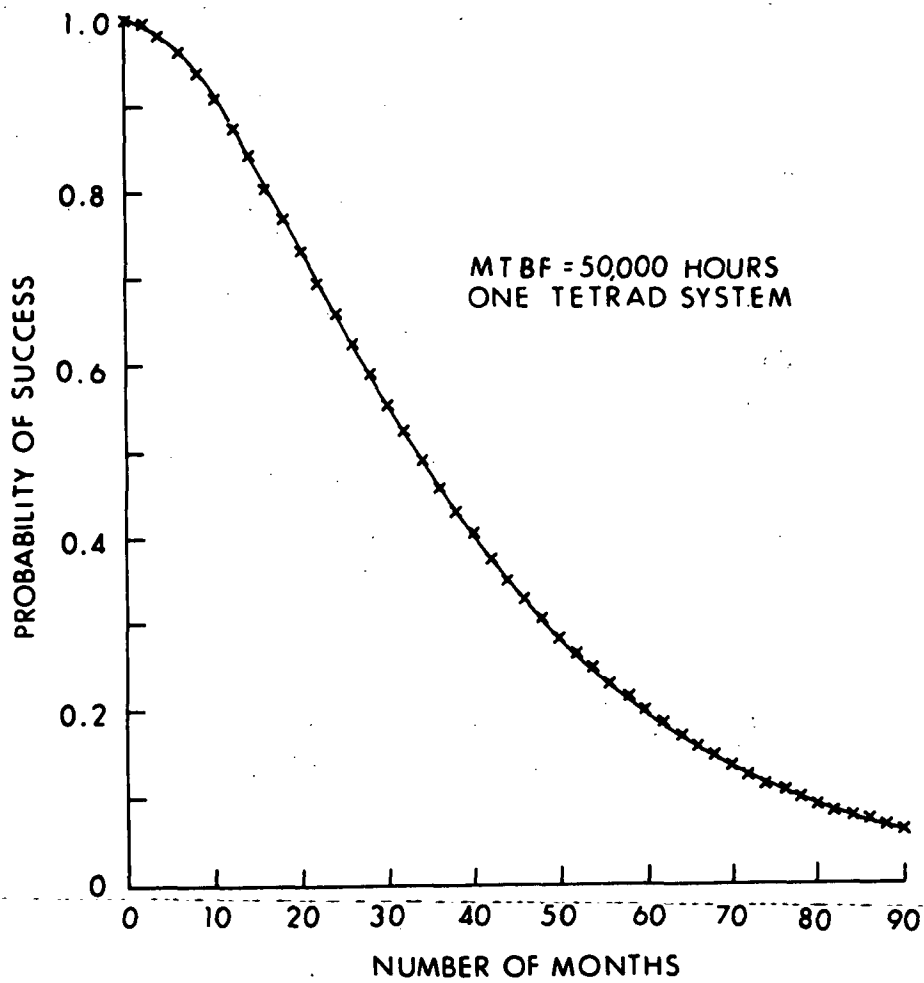


Figure 3-8 Mission Success Probability

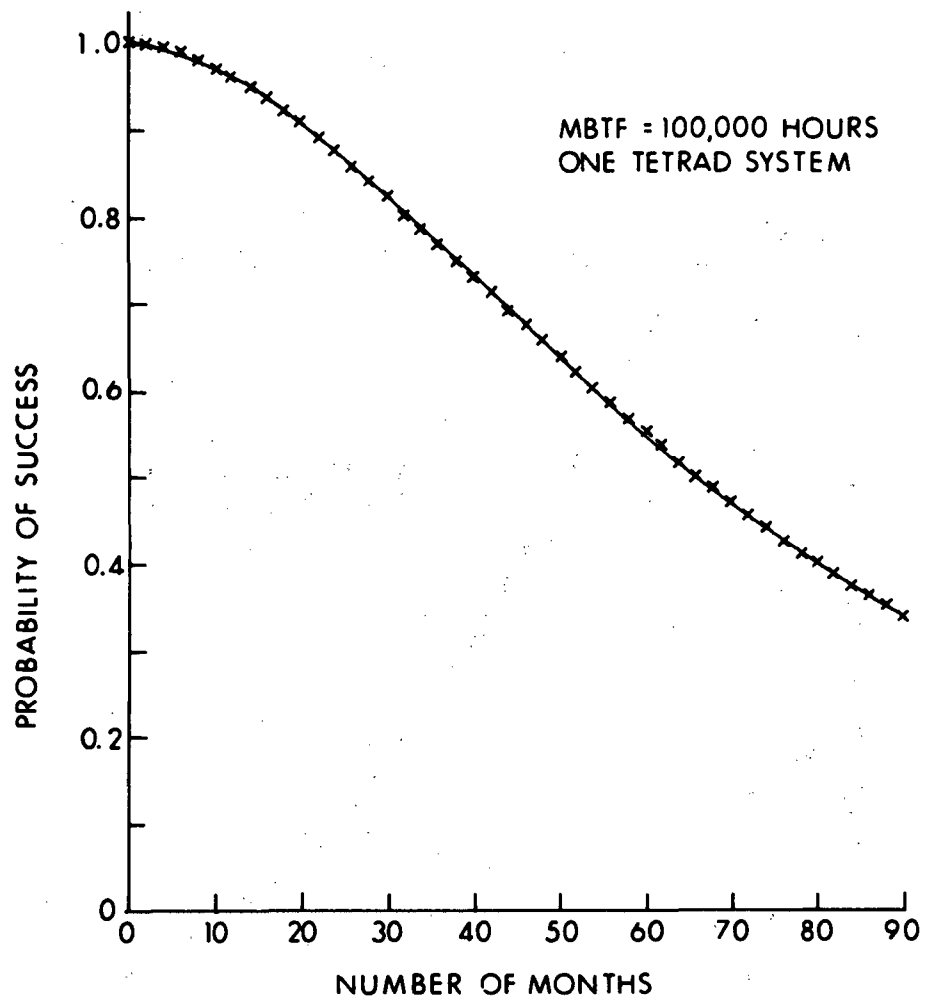


Figure 3-9 Mission Success Probability

It has been found that either the strapdown or gimbaled mechanization can satisfy the SIMS accuracy requirements with moderate-performance gyroscopes. Instrument reliability appears to be of primary importance. The assumption of no airborne computer has been used in this IARU study. The inclusion of a computer available to the overall system should be studied to evaluate the implications for the strapdown or gimbaled approach as well as for growth implications in areas of attitude control, ground data management, or fine attitude pointing requirements.

3.6 PROPOSED FUTURE TASKS

3.6.1 13 IRIG

MIT/DL would like to test a 13 IRIG for the following characteristics:

- a) Test instrument signal-to-noise levels
- b) Establish performance sensitivities to thermal control requirements

3.6.2 TORQUE LOOP EVALUATION

A strapdown version 13 IRIG instrument will be available for testing in June 1972. This instrument requires unconventional torque-to-balance electronic circuitry for strapdown loop sizing in a satellite application. It is proposed that a basic study be initiated to implement a torque loop design based upon the use of the strapdown 13 IRIG considering the satellite environment and the high attitude resolution requirements of EOS/SIMS.

3.6.3 COMPUTER REQUIREMENTS STUDY

When viewing the growth potential of the EOS/SIMS hardware the implications of computational availability is a

sideration in all subsystems. It is suggested a study be initiated to evaluate the additional capabilities available at the subsystem level, the data management implications, and the effect on the overall system reliability of adding an air-borne computer.

SECTION 4

STAR SENSOR STUDIES

4.1 INTRODUCTION

In this section the format for examination of Star Sensor configuration follows that established in Section 4 of Reference 141. Each item reported in Ref. 141 was reexamined for this report. The text of this report will include changes, corrections, clarifications (including some derivations), and the addition of material not contained in or adequately dealt with or completed in Ref. 141. However, a complete summary of error model and trade parameters will be included in this report, in this section and Appendix A, even where there are no changes from Ref. 141.

At the time of writing Ref. 141, the SIMS-A Star Mapper configuration, based upon the experience gained and technology developed from the USAF/Lockheed/Honeywell (HA) SPARS program was considered by the MIT/SIMS Study Team to consist of a concentric catadioptric optical system developed by Control Data Corporation (CDC) incorporating cadmium sulfide photoconducting "slit" cells. Presently, HA is closely examining the merits of two star mapper configurations for an advanced Precision Attitude Reference System (PARS) as well as for SPARS. These include a star sensor assembly (SSA) derived from the SPARS-Phase IB using silicon and a 10^0 FOV concentric optical system, and a silicon SSA developed to the engineering prototype stage by the Honeywell Radiation Center (HR) which is similar to the SIMS-DA-HR SSA described in subsec. 4.2.4 through 4.2.4.6 of Ref. 141. A silicon SSA developed by Kollsman Instrument Corporation (KI), which is similar (with several important modifications) to the SIMS-DA-KI SSA described in subsec. 4.2.3 through 4.2.3.6 of

Ref. 141 is examined in this report as another candidate SIMS-A SSA. There are also other activities at CDC and TRW Systems Group (TRW) involving the development of silicon SSAs, which we will not be able to examine in time for this report.

In view of the temporary uncertainties in the choice of a SSA in the SPARS and similar programs*, we will consider as potential SIMS-A SSAs all three SPARS-like SSAs, i.e., HA, HR and KI.

The SIMS-B SSA is represented by the gimbaled star tracker developed for PPCS/PADS by TRW.

The tentative choice by the MIT/SIMS Study Team of a SSA for the SIMS-D is the SIMS-DA-HR reported in Ref. 141, with some modifications. It has been generally recognized that the solid catadioptric optics employed by HR will, in theory, result in a smaller, lighter and mechanically more stable star mapper than the others considered. While the proof of these claims lies buried in the developmental stages at HR we expect its emergence soon. On the other hand the PARS CDC star mapper using concentric optics has met its performance goals in laboratory tests. Thus, our tentative choice of the HR SSA for SIMS-D is an expression of confidence in HR's ultimate ability, as yet unsubstantiated, to meet performance goals. We have seen some performance data, and design details of the HR SSA. However, we have not been given full design details by HR and have been constrained from public release of some information that has been made available to us, since HR is presently engaged in several competitive proposal efforts. HR has indicated that much supporting evidence could be available as early as July 1972 pending resolution of its present competitive issues.

Much new information on silicon and cadmium sulfide star mappers is just becoming available as a result of

* These issues may have been resolved before this report is issued. Check Appendix F.

evaluations taking place in the SPARS and PARS programs. Since we must meet a cutoff date in assembling this report, any additional new material acquired will be placed in an Appendix F of this report.

4.2 STAR MAPPERS

The common features of configuration, operational mode, and basic requirements for all star mappers considered for the SIMS-A and SIMS-D star sensors are described in subsec. 4.2 of Ref. 141.

4.2.0 STAR MAPPER PERFORMANCE CHARACTERISTICS

Three essential performance characteristics required of a SIMS/EOS SSA can be summarized as timing accuracy, FOV and stellar catalog. What constitutes reasonable values or trades is a system problem discussed more fully in Section 5. Generally it is found from system simulation that accuracy about one axis is considerably poorer than about the other two (comparable) axes when the FOV is less than (approximately) 6° . Third axis accuracy improves to a sufficient extent with FOVs of 8° to 10° . In fact the third axis accuracy sensitivity to change of FOV is much greater than to change in the number of detectable stars.

4.2.0.1 Stellar Interval Evaluation

The stellar interval evaluation presented in subsec. 4.2.0.1 of Ref. 141 is replaced by the much better criteria of simulated system performance found in Section 5 of the present report.

The number of usable stars is defined by us as the count of those achieving a S/N of greater than 20. The criteria used in the PARS program was that there should be 380 detectable

stars with a probability of detection greater than 90%. We calculate that this corresponds to an average S/N = 20 at a limiting magnitude of 3.9^M for the SIMS-A-C. We take an average S/N = 20 as the criterion for all SIMS SSAs in assembling Table 4-1.

Table 4-1

USABLE STARS FOR SIMS STAR MAPPERS

<u>SIMS SSA</u>	<u>USABLE STARS</u>	<u>FOV</u>	<u>LIMITING MAG.</u>
SIMS-A-C	380	10°	3.9^M
SIMS-A-HR	500	10°	3.5^M
SIMS-D-HR	500	8°	3.5^M
SIMS-A-KI	403	6°	$0.8-3.3^{M*}$

* KI calculation of S/N in Ref. 157 does not agree with (is less than) ours. KI assumed a peak response of 0.35 A/W, but Texas Instruments (TI) data (Ref. 158) shows 0.45 A/W is reasonable.

4.2.0.2 Signal and Noise

The responses of various photodetectors to stellar magnitude and spectral class were obtained from several sources and presented in Figure 4-5 of Ref. 141. Figure 4-1 of the present report summarizes the responses of silicon, cadmium sulfide, and S-20 photocathodes to A0 class stars of different magnitudes with three modifications not found in Fig. 4-5 of Ref. 141:

- Slit transit times of 46 and 115 milliseconds corresponding to $10^{\widehat{m}}$ (SPARS-Phase IB-like) and to

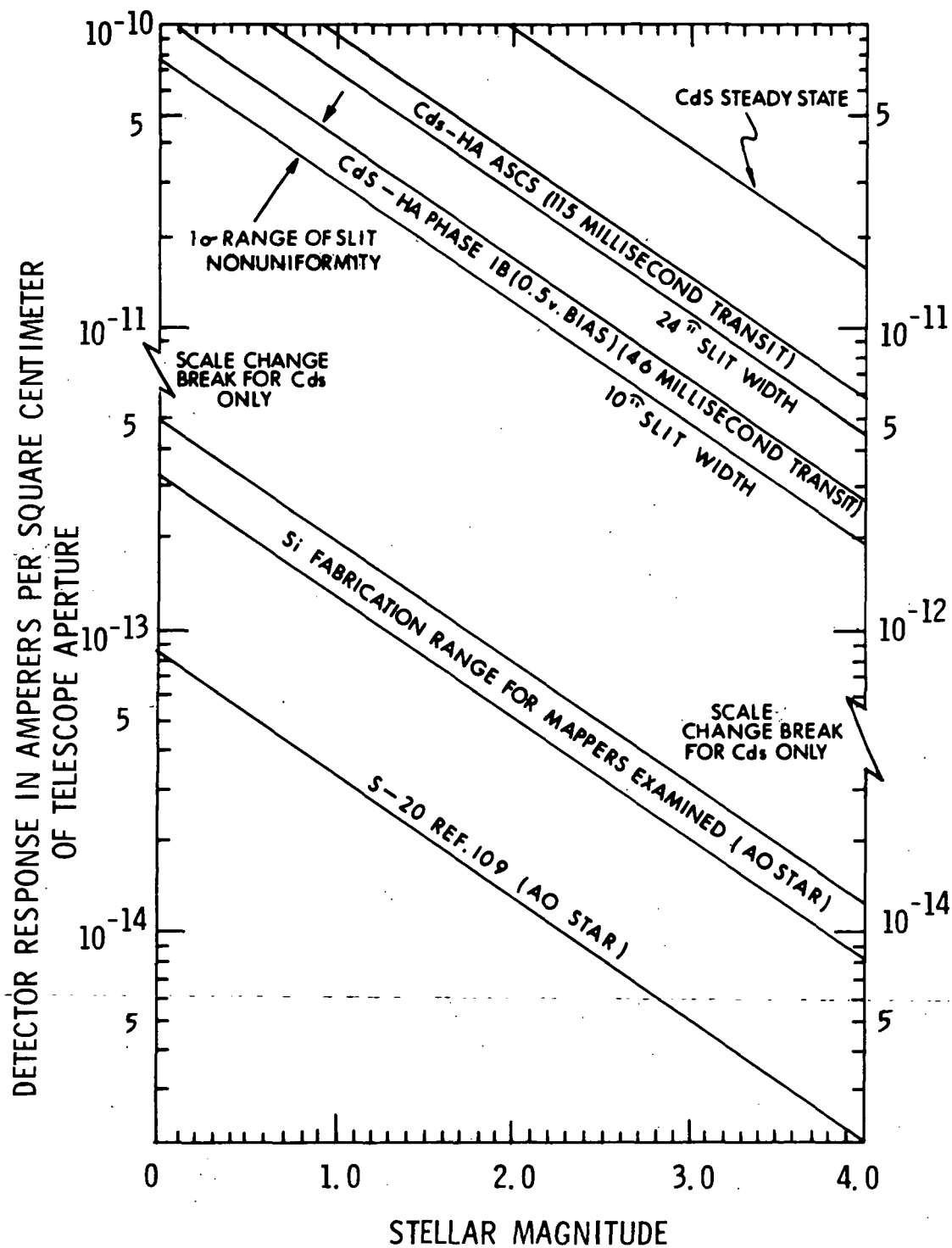


Figure 4-1 Detector Response as a Function of Stellar Magnitude with AO Type Stars

24" (PARS-like) slit widths, respectively, are used to calculate the response of the slow CdS photodetectors.

- A range of response is given for each of the two CdS transit times. This range corresponds to our estimate of an effective 1σ value of detector non-uniformity along the slit cell.
- A range of response is given for silicon corresponding to the range of data between LPL (Ref. 118), HR and KI/TI.

Only data for AO stars is shown in Fig. 4-1, since a handy color index is given in Fig. 5-8 of Ref. 141. For example, if we are interested in assigning an equivalent silicon AO response to a 3.6^M (visual) K7 star, we read a color index of +1 in Ref. 141, Fig. 5-8. Then, using $3.6^M - 1 = 2.6^M$ we read from Fig. 4-1, a nominal response of 3.6×10^{-14} amperes per square centimeter of effective telescope aperture.

Representative noise equivalent inputs affecting the transit time detection are given in Table 4-2.

The net estimate for CdS in Table 4-2 is larger for the 10° FOV PARS-like SSA because the cell slit length and physical width are greater, resulting in greater noise contributions from cell leakage current, bias lamp radiant power and maximum background radiant power.

Figure 4-2 presents a relationship between the star mapper S/N ratio present at the transit time detector and the magnitude of the equivalent AO star input. The dotted lines are labeled with the pertinent SIMS SSAs. This diagram is constructed and used in the same manner as Fig. 4-6 in Ref. 141.

Table 4-2

NOISE-EQUIVALENT INPUTS AFFECTING TRANSIT
TIME DETECTION ACCURACY

<u>Source of SSA</u>	<u>Photo- Detector</u>	<u>NEI amps/Hz^{1/2}</u>	<u>Detection Method</u>
KI	Si	1.3×10^{-14}	Leading and trailing edge times at a fixed threshold
HR	Si	0.4×10^{-14}	Leading and trailing* edge at a fixed frac- tion of peak amplitude
HA/CDC	Cds		Leading edge at a fixed fraction of peak ampli- tude
(PARS-Like)		1.6×10^{-12}	
(SPARS-Like)		1.0×10^{-12}	

However, there are several differences in detail in the present diagram. The limiting magnitudes in Fig. 4-6 of Ref. 141 represented the average behavior of the sensor for the total star catalog, containing stars of many spectral classes. The present Fig. 4-2 is specifically constructed for equivalent A0 stars. In order to determine the response to some other class of star, the color index, Figure 5-8 in Ref. 141, should be determined and applied as a magnitude shift to the limiting magnitudes of Fig. 4-2 of the present report. To use Fig. 4-2, draw a horizontal line from the color-corrected limiting magnitude of the specific SIMS SSA to the dotted line labeled by the same SIMS SSA. From this intersection with the dotted line, drop a vertical line and read the signal-to-noise ratio from the scale.

* See Appendix F for a correction.

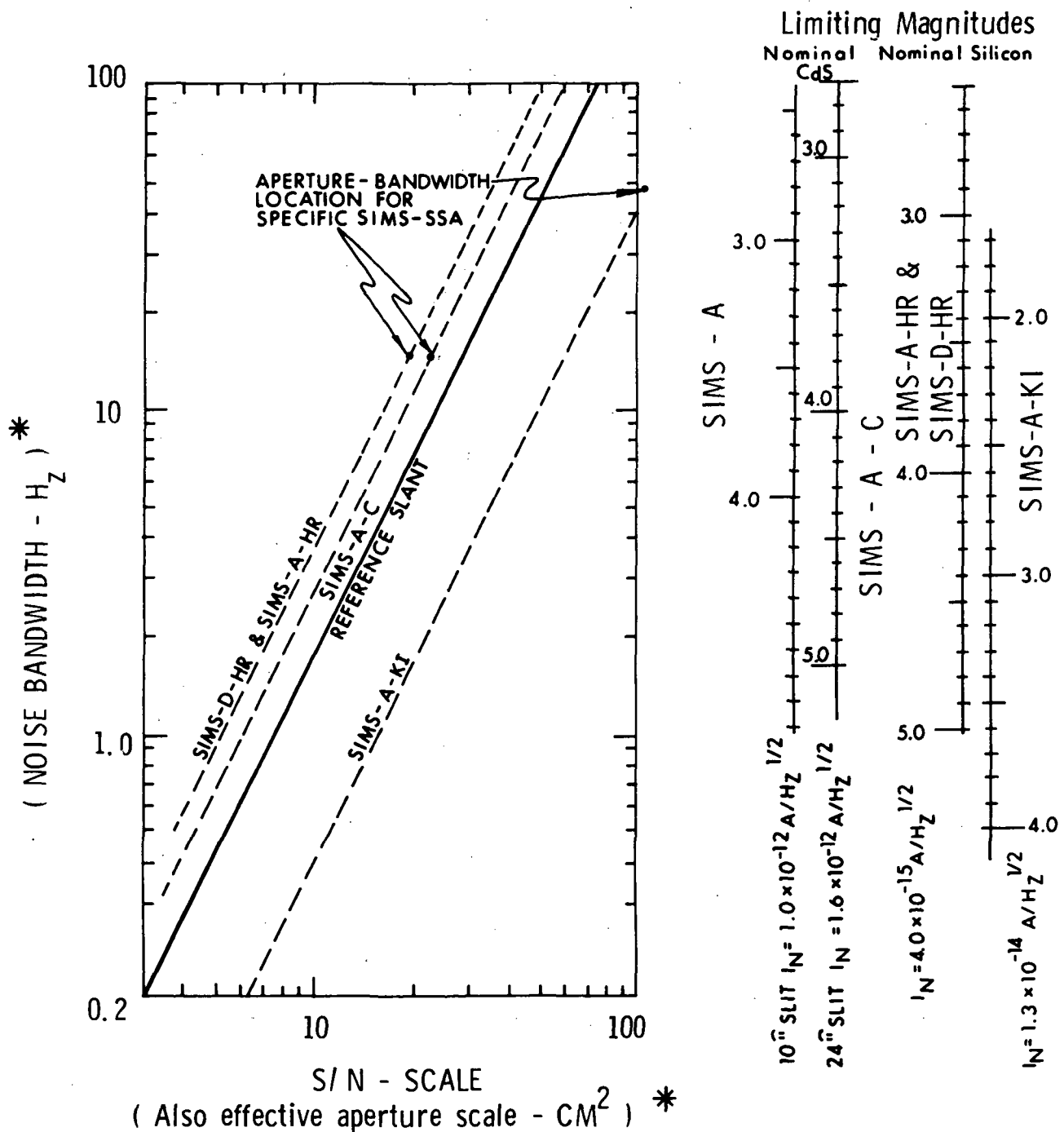


Figure 4-2 S/N vs Equivalent AO Stellar Magnitude for Specific SIMS SSAs

*See Figure 4-6 of Ref 141 for general use of this nomogram for values of bandwidth and aperture different than the specified SIMS SSAs

Example:

Determine S/N for a 3.6 visual magnitude
K8 star for SIMS-A-HR.

Steps

1. Color index from Fig. 5-8 of Ref. 141 for a K8 star with a silicon sensor is +1.0.
2. $3.6^M(\text{Vis}) - 1.0 = 2.6^M(\text{Si})$.
3. Draw horizontal line from the 2.6^M value of the SIMS-A-HR limiting magnitude scale to the SIMS-A-HR dotted slant line.
4. Drop a vertical line from the intersection point at the SIMS-A-HR dotted slant line to the S/N scale and read $S/N = 45$.

Only two significant figures are used in our estimates of NEI, reflecting our level of confidence in their validity. Contributions from excess (low frequency) noise are not important according to KI and HR. KI states in Appendix B of Ref. 157 that "by operating at an applied junction potential equal to zero, the $1/f$ noise due to shunt conductance is minimized. A forward bias can only serve to increase the shot and $1/f$ components and is a mode of operation that is avoided in low level light detection". In subsec. 4.1.8 of Ref. 157 KI states, "In our simulation (the diode DC leakage) currents were not sufficiently high and $V_r = 0.1\text{V}$ was relatively too low to perceive the excess noise in the presence of the predominant Johnson noise in the preamplifier". Data from the HR SCADS report (Ref. 111) indicates a breakpoint at about 1 Hz. No information on excess noise with CdS has been obtained.

4.2.0.3 Signal Shape Effects

The output of the star mapper preamplifier is applied to a narrow pass-band filter with a high frequency cutoff, f_H , (7.0 Hz for SIMS-A-HR and SIMS-A-C to 30 Hz for SIMS-A-KI) and a low frequency cut-on, f_L , (usually less than 1.0 Hz).

Presumably, the high frequency cutoff is chosen to optimize the compromise between reducing noise bandwidth and improving the signal's maximum slope, symmetry and amplitude. Since a simple, passive, one pole linear, first order filter introduces a significant amount of signal distortion and amplitude reduction, the filters employed in the star mappers of this study are multi-poled, active filters. A complete and independent analysis of the dynamic performance of the filters with realistic star transit input signals for each star mapper configuration is a major task beyond the scope (in level of activity and funding) of the present task. However, we attempted in subsec. 4.2.0.3 of Ref. 141 to ascertain in at least a qualitative sense the sensitivities of a star mapper to certain variables. We shall here spend some few pages in clarification of the assumptions and derivations used in subsec. 4.2.0.3 of Ref. 141, and some additional analysis of subjects inadequately treated in Ref. 141 due to time limitations.

4.2.0.3.1 Results of Analysis of a Simplified Filter Model - We assumed as a simplification, in Ref. 141, that the spatial distribution of stellar radiant power was uniform within a rectangular area on the focal plane of width in the optics tangential direction equal to the width of the slit detector, and of an extent in the sagittal direction that is arbitrary but small compared to the slit length.

The SPARS Phase IB SSA employed a concentric catadioptric optical system that eliminates off-axis aberrations, and that

results in a blur circle determined by spherical and chromatic aberrations that has little variation throughout the usable field-of-view (Fig. 4-11 of Ref. 141). The blur circle is somewhat smaller than a CdS slit diameter, and varies with stellar spectral class, being smaller for a KO star than for an AO star. The time evolution of radiant power for a star transiting the slit would be fairly well approximated by a triangular input signal for an AO star with a $10''$ slit width and the difference resulting from a KO star transit could be estimated by using a slightly trapezoidal pulse (relative to a triangle) for a KO star. When the slit width is opened to $24''$ without a corresponding increase in blur circle, the input signal will be a pronounced trapezoid for both star classes. The accuracy of transit detection for the SIMS-A-C type of star mapper relies upon the shape of the detector output leading edge being constant, i.e., signal pulses from stars of different magnitudes when normalized to their respective peak values should be indistinguishable. The response to the leading edge of a trapezoidal signal is the same as the response to the leading edge of a triangular signal of the same slope. However, in the case of a $10''$ slit width the peak response to the trapezoidal input will tend to be greater since the input slope is actually slightly greater and the peak value is the same as in the triangular input, but held for a short interval with the trapezoid. A compensating factor which tends to reduce the peak response is the shorter total transit time.

This source of error can be estimated in subsec. 4.2.0.3.4 from the similar analysis of the effect of slit widening at constant blur circle diameter due to edge roughness. From the calculated error due to a 10% signal widening, the transit time error resulting from the difference between an AO and KO star can be inferred to be less than $0.05''$, (since in subsec. 4.2.2.1 of Ref. 141, it was estimated that if an AO star fills the slit a KO will be 8% to 10% narrower). In the case of a $24''$ slit width

the error difference attributed to a variation in stellar spectral class will be even less.

Computer simulations of off-axis blur images from the optics employed by KI (Ref. 112) in the SIMS-A-KI star mapper show little significant tangential variation although considerable variation in sagittal aberration occurs. The internal distribution of irradiance of these blur images becomes quite complex off-axis although maintaining symmetry about a radial line from the optical center. Simulated sagittal knife edge scans by KI (Ref. 157) are pertinent if transiting real star signals are approximately Gaussian.

The off-axis simulated optical blur images of HR appear to maintain a width comparable to that of the slit with considerable geometric and chromatic sagittal aberration (no reference document made available at this time.)

In Reference 159 the output of a scanning slit is compared for various inputs such as a two-dimensional Gaussian intensity distribution and a uniform rectangle. The figures were chosen so that eighty percent of the radiant power is incident within the slit when the slit is centered on the intensity distribution. However, the general conclusion was reached that "if the intensity distribution is reasonably symmetric the input to a scanning slit can be thought of as coming from a two-dimensional Gaussian intensity distribution". (We have substituted the words input to for the words output from used in Ref. 159. The meaning in Ref. 159 of output from is the radiant power transmitted through a slit reticle, i.e., radiant power output from a slit reticle. However, we use input to to mean the radiant power incident on the slit detector cell and reserve the words output from to denote the electrical response of the slit detector cell). We liberally interpret this

conclusion to mean that we may approximate, without serious alteration of important functional dependencies, one reasonably symmetric intensity distribution by another and can therefore choose a uniform rectangle for simplicity of analysis.

Next, in subsec. 4.2.0.3 of Ref. 141, we examined the effect on the input of a filter characterized by a first order pole, $(1+\tau s)^{-1}$, with a time constant τ , for example, a parallel RC combination. Without any filtering the output from an infinitely fast detector would be a triangular signal of half-width T and amplitude A . The cadmium sulfide photoconducting detector is not a fast detector and the primary signal filtering responsible for signal shaping derives from the photoconducting mechanism itself. The electronic filters that follow the CdS preamplifier have only secondary effects on shaping the signal, and are primarily for the purpose of limiting the noise bandwidth and delaying the signal. The silicon photodiode is a fast detector for purposes of the star mapper and the primary filtering responsible for signal shaping is the electronic filter that follows the detector. These distinctions in the origins of τ for CdS and for Si should be kept in mind throughout Section 4.

The filtered signal output in the time domain can be derived either from taking the inverse Laplace transform of the frequency domain solution, or directly by solution of the differential equations, matching initial conditions at the input function breakpoints. The solution for the output response, \mathcal{R} , is

$$\mathcal{R}_1 = A \frac{\tau}{T} \left\{ e^{-t/\tau} + \frac{t}{\tau} - 1 \right\}, \quad 0 \leq t \leq T$$

$$\mathcal{R}_2 = A \frac{\tau}{T} \left\{ \left[1 - 2e^{T/\tau} \right] e^{-t/\tau} - \frac{t}{\tau} + \left[1 + \frac{2T}{\tau} \right] \right\},$$

$$T \leq t \leq 2T$$

$$\mathcal{R}_3 = A \frac{\tau}{T} \left[1 - e^{T/\tau} \right]^2 e^{-t/\tau}, \quad 2T \leq t \leq \infty.$$

The time of peak response can be derived in two ways. In the first method, the time that satisfies setting $d\mathcal{R}_2/dt = 0$, is the time of peak occurrence. In the second method, one realizes that the response is seeking the input level, so the peak occurs when the increasing output equals the decreasing input (see Fig. 4-7 in Ref. 141). By either method the time of peak response, t_p is found as

$$t_p = \tau \ln(2e^{T/\tau} - 1) \quad (4-1)$$

The time important for attitude determination is the time of coincidence of the slit optical center plane with the star line-of-sight, or, equivalently, the time at which $\vec{N} \cdot \vec{LOS} = 0$ where \vec{N} is the normal to the slit center plane, which occurs at $t=T$. Relative to this event, the peak signal occurs a little later at time difference t_{pc} , where

$$t_{pc} = \tau \ln(2e^{T/\tau} - 1) - T \quad (4-2)$$

The value of peak response at t_p is

$$\mathcal{R}_p = A \left\{ 2 - \frac{\tau}{T} \ln(2e^{T/\tau} - 1) \right\} \quad (4-3)$$

These results are applicable when the blur figure width is approximately that of the slit. For a $10''$ wide slit ($t=.046$ seconds) and a CdS photodetector with response time $\tau=0.3$ seconds,

$$\mathcal{R}_p = 0.14 A,$$

and the response is only a small fraction of the steady state value the detector is capable of attaining (as indicated in Fig. 4-1).

The above results are also applicable to the silicon star mapper configurations under study, where the blur dimension is approximately a slit width. For a $16''$ wide slit ($T \approx .074$ seconds) and a filter response time, $\tau = 0.1$ seconds,

$$\mathcal{R}_p = 0.43 A \quad .$$

The SIMS-A-C star mapper has a $24''$ slit width, but if the blur circle diameter is not correspondingly increased, i.e., remains $10''$, the proper input signal model would be a fairly pronounced trapezoid with the leading edge ramp achieving the amplitude A in a time $T = .046$ seconds. Thereafter the signal remains at amplitude A for an interval $T + \mathcal{T} = .064$ seconds, followed by a trailing edge ramp, returning the signal from amplitude A to zero in an interval $T = .046$ seconds. The CdS output response (before any additional electronic filtering) is

$$\begin{aligned} \mathcal{R}_a &= A \frac{\tau}{T} \left[e^{-t/\tau} + \frac{t}{\tau} - 1 \right] , & 0 \leq t \leq T \\ \mathcal{R}_b &= A \frac{\tau}{T} \left[e^{-t/\tau} \left(1 - e^{-T/\tau} \right) + \frac{T}{\tau} \right] , & T \leq t \leq 2T + \mathcal{T} \\ \mathcal{R}_c &= A \frac{\tau}{T} \left\{ e^{-t/\tau} \left[1 - e^{-T/\tau} \left(1 + e^{T+\mathcal{T}/\tau} \right) \right] - \frac{t}{\tau} + \frac{3T+\mathcal{T}}{T} + 1 \right\} , & 2T+\mathcal{T} \leq t \leq 3T+\mathcal{T} \end{aligned}$$

from which we may obtain

$$t_{pc} = \tau \ln \left[e^{T/\tau} \left(1 + e^{T+\mathcal{T}/\tau} \right) - 1 \right] - \frac{3T+\mathcal{T}}{\tau} , \quad (4-4)$$

and

$$\begin{aligned} \mathcal{R}_p &= A \left\{ \frac{3T+\mathcal{T}}{T} - \frac{\tau}{T} \ln \left[e^{T/\tau} \left(1 + e^{T+\mathcal{T}/\tau} \right) - 1 \right] \right\} . \quad (4-5) \\ &= 0.29 A \quad . \end{aligned}$$

4.2.0.3.2 Angular Error Velocity Effect - An angular velocity introduced into the spacecraft attitude rate will cause the centroid of the star image to transit the slit in a time differing from the nominal value of T (blur width \approx slit width) or $2T + \mathcal{L}$ (blur width $<$ slit width) by some Δt . This rate variation will not effect the geometrical relation between slit width and blur image. We must consider the effect of the variation in T or $2T + \mathcal{L}$ on the accuracy of CdS and the variation of T on the accuracy of silicon star mappers separately, since their attitude determination methods are different.

The CdS star mapper detects the half-amplitude point of the leading edge of the detector response. The time, $t_{1/2}$, at which this occurs (corrected for deliberate electronic delays) is found from a transcendental expression when the slit width equals the blur image width, (e.g., $\theta_w = 10''$),

$$e^{-\frac{t_{1/2}}{\tau}} - \frac{t_{1/2}}{\tau(1-2e^{T/\tau})} = F(T/\tau) \quad (4-6)$$

where

$$F(T, \tau) = \frac{\frac{T}{\tau} + 1 + \frac{1}{2} \ln(2e^{T/\tau} - 1)}{2e^{T/\tau} - 1}$$

With $T = .046$ seconds, $\tau = .30$ seconds,

$$t_{1/2} \approx 0.94 T. \quad (4-7)$$

From (4-6)

$$\delta t_{1/2} = \left[\begin{array}{cc} \frac{T-t_{1/2}}{\tau} & -\frac{e^{T/\tau}}{2e^{T/\tau}-1} - 1 \\ \frac{T-t_{1/2}}{\tau} & -t_{1/2}/\tau \end{array} \right] \delta T$$

and with (4-7) this produces

$$\delta t_{\frac{1}{2}} \approx 0.87 \delta T$$

The shift of $t_{\frac{1}{2}}$ with respect to $\vec{N} \cdot \vec{LOS} = 0$ is

$$\delta t_{\frac{1}{2}C} = \delta t_{\frac{1}{2}} - \delta T$$

If the angular error velocity is $.0017^\circ/\text{sec}$ (1σ) (see Ref. 85, subsection 1.1.1), and the nominal orbital rate is $.06^\circ/\text{sec}$, then $\delta T/T = .03$ and

$$\delta\theta = \theta_w \frac{\delta t_{\frac{1}{2}C}}{T} \approx .04''(1\sigma), \text{ for } \theta_w = 10''.$$

The anticipated angular error velocities in the EOS introduce negligible measurement error for this example.

The silicon star mappers establish a threshold and detect both leading and trailing edge crossings. The star mark is taken to be one half the interval between the leading and trailing edge times of detection. Since both KI and HR strive for signal symmetry we are in effect interested in the variation of t_{pc} with T for the silicon star mapper. From (4-2),

$$\delta t_{pc} = \frac{1}{2e^{T/\tau} - 1} \delta T$$

From the previously-used values of T and τ for the silicon star mapper,

$$\delta t_{pc} = 0.314 \delta T$$

With the same angular error velocity employed in the CdS example the attitude uncertainty is

$$\delta\theta = 16'' \times 0.03 \times 0.314 = 0.15'' \text{ (1}\sigma\text{)}$$

and the anticipated angular error velocities in the EOS introduce a small error contribution to the silicon star mapper measurement (perhaps not entirely negligible, since $\delta\theta = 0.45''$, 3σ).

Finally, we consider the CdS star mapper with a $24''$ slit width when the angular subtense of the blur image is not correspondingly increased, but remains at $10''$. An analytical expression can be found for $t_{\frac{1}{2}}$ in this case (i.e., with $T = .046$ seconds, $\tau = .018$ seconds, $\tau = .30$ seconds):

$$t_{\frac{1}{2}} = \tau \ln \left\{ \frac{e^{T/\tau} - 1}{\frac{1}{2} \left\{ \frac{3T+\tau}{\tau} - \ln \left[e^{T/\tau} \left(1 + e^{\frac{T+\tau}{\tau}} \right) - 1 \right] \right\} - \frac{T}{\tau}} \right\} \quad (4-8)$$

and

$$\delta t_{\frac{1}{2}C} = \delta t_{\frac{1}{2}} - \delta \left(\frac{3T+\tau}{2} \right)$$

or, after considerable algebraic manipulation and calculation,

$$\delta\theta = \theta_w \frac{\delta t_{\frac{1}{2}C}}{\frac{3T+\tau}{2}} \approx .106'' \text{ (1}\sigma\text{), (24'' slit width and 10'' blur dia.)}$$

[Interestingly enough, if we had just assumed a triangular input signal with $T = .115$ we would also obtain $\delta\theta = .10''$ (1 σ) for $\theta_w = 24''$.]

4.2.0.3.3 Slit Orientation Effects - In a SPARS-like slit array there are slits deployed at an angle of 30° with respect to the central slits. Stars nominally transit perpendicular to the central slit and at 60° to the centerline of the other slits.

Since the relationship between the blur size and slit width remains unaffected the analysis of the preceding section dealing with transit time variation can be applied here, where the transit time across a canted slit is $1 - (2/\sqrt{3}) \approx 0.15$ greater than across the central slits. Then, the biases of the canted slits, independent of forward or aft cant are

SIMS-A-SPARS MOD IB-like	0.2 ^μ lag
SIMS-A-C (24 ^μ slit width, 10 ^μ blur dia.)	0.5 ^μ lag
SIMS-A-HR.	0.8 ^μ lag
SIMS-A-KI.	0.2 ^μ lag

4.2.0.3.4 Slit Edge Roughness Effects - Let the edge of the slit be described by a square-toothed pattern. This model will allow us to estimate the degradation of accuracy when there is a predominant spatial frequency to the edge roughness. We assume that quoted values of edge roughness are characteristic of a predominant spatial wavelength sagittally (along the slit edge) as well as tangential (normal to the slit edge). This simple model is a starting point.

The zone of roughness will be defined as the 1σ dimension across the slit of the quoted roughness which in our simple model is twice the amplitude of the square-toothed edge pattern.

Figure 4-3a shows that if the sagittal extent of the rectangular blur image (i.e., along the slit edge) is an integral number of edge square-tooth wavelengths, the time history of radiant power amplitude through the slit will follow the same sawtooth signal input as the nominal slit with no edge roughness, except at the beginning, peak, and end. The signal begins at a time $\Delta T/2$ earlier and ends at a time $\Delta T/2$ later than it would for a smooth-edged slit, where

$$\frac{\Delta T}{T} = \frac{\epsilon}{W}$$

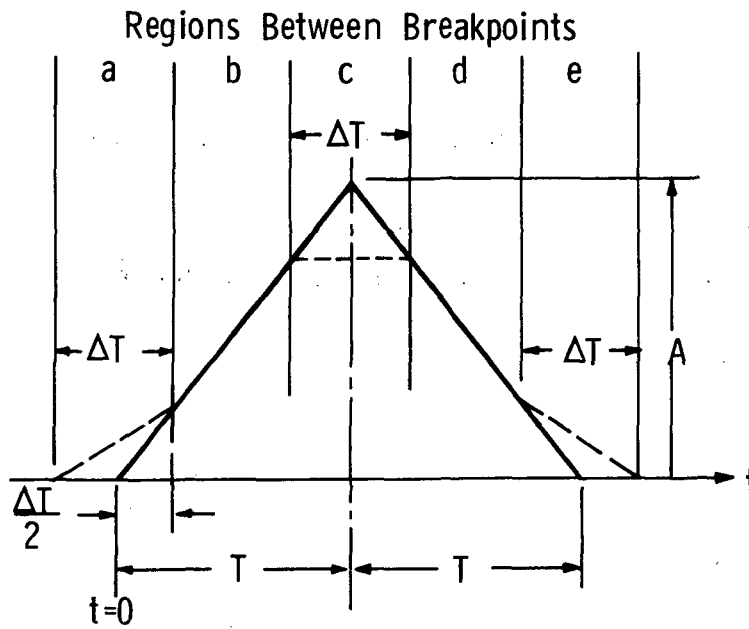


Figure 4-3a Input Signal Modification for Square-Toothed Edge Roughness and a Masking Ratio $M=0$ at Both the Leading and Trailing Edges.

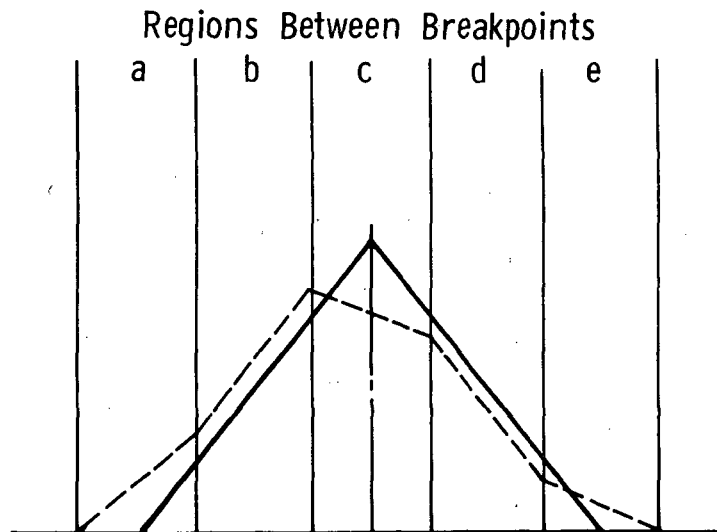


Figure 4-3b $M = -M_\ell$ at the Leading Edge, and $M = +M_\ell$ at the Trailing Edge.

and where

ϵ = slit roughness dimension (1σ)

W = nominal slit width

The magnitude of the slope at the beginning and end of the input signal is $\frac{1}{2}$ that of the unchanged portion of the input signal. We shall derive the response for the filter model employed in subsec. 4.2.0.3 and apply it to the CdS detector and the silicon detector. The shift in the half amplitude point and peak will indicate the error introduced for the respective detectors.

The response from $-\Delta T/2 \leq t \leq \Delta T/2$ is

$$\mathcal{R}_a = \frac{A\tau}{2T} \left\{ e^{-\frac{t+\frac{\Delta T}{2}}{\tau}} + \frac{t+\frac{\Delta T}{2}}{\tau} - 1 \right\}.$$

The response from $\Delta T/2 \leq t \leq T - \Delta T/2$ is

$$\mathcal{R}_b = \frac{A\tau}{2T} \left\{ e^{-\frac{T}{\tau}} \left[e^{-\frac{\Delta T}{2\tau}} + e^{\frac{\Delta T}{2\tau}} \right] + 2\frac{t}{\tau} - 2 \right\}.$$

The response from $T - \frac{\Delta T}{2} \leq t \leq T + \frac{\Delta T}{2}$ is

$$\mathcal{R}_c = \left\{ e^{-\frac{t}{\tau}} \left[e^{-\frac{\Delta T}{2\tau}} \left(1 - e^{\frac{T}{\tau}} \right) + e^{\frac{\Delta T}{2\tau}} \right] + \left[\frac{2T - \Delta T}{\tau} \right] \right\}.$$

The response from $T + \frac{\Delta T}{2} \leq t \leq 2T - \frac{\Delta T}{2}$ is

$$\mathcal{R}_d = \frac{A\tau}{2T} \left\{ e^{-\frac{t}{\tau}} \left[1 - 2e^{\frac{T}{\tau}} \right] \left[e^{-\frac{\Delta T}{2\tau}} + e^{\frac{\Delta T}{2\tau}} \right] - 2\frac{t}{\tau} + 4\frac{T}{\tau} + 2 \right\}.$$

A check on the correctness of the algebra at this point is the reduction of \mathcal{R}_d to \mathcal{R}_2 when $\Delta T \rightarrow 0$. The response from $2T - \frac{\Delta T}{2} \leq$

$t \leq 2T + \frac{\Delta T}{2}$ is

$$\mathcal{R}_e = \frac{A\tau}{2T} \left\{ e^{-\frac{t}{\tau}} \left[\left(1 - 2e^{-\frac{T}{\tau}} + e^{-\frac{2T}{\tau}} \right) e^{-\frac{\Delta T}{2\tau}} + \left(1 - 2e^{-\frac{T}{\tau}} \right) e^{\frac{\Delta T}{2\tau}} \right] - \frac{t}{\tau} + \left[\frac{4T + \Delta T + 2\tau}{2\tau} \right] \right\}$$

Depending on whether the peak value, \mathcal{R}_p , is greater or less than $A\Delta T/2T$, the time of peak, t_p , is found by setting \mathcal{R}_d or \mathcal{R}_e respectively equal to the value of the input and solving for t .

The solution when region d is the correct choice is

$$t_p = \tau \ln \left[\left(2e^{\frac{T}{\tau}} - 1 \right) \cosh \frac{\Delta T}{2\tau} \right] \quad (4-9)$$

The difference between (4-9) and (4-1) is

$$\Delta t_p = -\tau \ln \left(\cosh \frac{\Delta T}{2\tau} \right) \approx -\frac{(\Delta T)^2}{8\tau}$$

for the special case where the sagittal extent of the rectangular blur image is an integral number of edge square-tooth wavelengths. Consider the silicon mapper with $\varepsilon = 30 \mu$ inches (1σ):

$$\Delta\theta = \theta_w \frac{\Delta t_p}{T} = \theta_w \left(\frac{\Delta T}{T} \right)^2 \frac{T}{8\tau} = \varepsilon^2 \left(\frac{\theta_w}{W} \right)^2 \frac{1}{\delta\tau\dot{\theta}} = .003^{\circ} (1\sigma).$$

Since θ_w/W is a constant of the geometrical optics, the error (for constant nominal $\tau\dot{\theta}$) is only determined by the slit roughness and not by the slit width for a given optical system.

Since $\Delta t_{\frac{1}{2}}$ was of the order of $\frac{1}{2} \Delta t_p$ we anticipate an even smaller effect on the CdS star mapper.

This example, and the angular error velocity effect of the previous section, only serve to reinforce an earlier conclusion that accuracy is not sensitive to input signal shape on the condition that the input signal shape is symmetrical.

The input signal asymmetry shown in Fig. 4-3b will be examined for effect on accuracy of silicon star mappers, and the shift in input signal leading edge shown in Fig. 4-3b will be examined for effect on accuracy of CdS star mappers. This case can arise when the sagittal extent of the rectangular blur image is not an integral number of edge square-tooth wavelengths.

A masking ratio M is defined as the ratio of sagittal length covered by the excess square-tooth (or gap) in the zone of edge roughness to the spatial wavelength, λ_T . Therefore, when the sagittal extent is an integral number of square-tooth wavelengths, $\lambda_T = 2\epsilon$, the masking ratio, M , is zero. The masking ratio can never be outside the range from -0.5 to $+0.5$. Within this range for a given sagittal extent, the masking ratio, M , can have any value between two limits of the same magnitude but different sign, depending on the location of the blur rectangle along the slit. For example, if the sagittal extent is $(n + 1/4)\lambda_T$ where n is an integer, then $-0.25 \leq M \leq +0.25$. In Fig. 4-3b, we illustrate the case of the negative of the two limiting values of M , $-M_\ell$, at the leading edge of the slit and the positive value, $+M_\ell$, at the trailing edge of the slit. First, we must express the signal slope magnitudes, m , for the signal time intervals $-\Delta T/2 \leq t \leq \Delta T/2$, $T - \Delta T/2 \leq t \leq T + \Delta T/2$ and $2T - \Delta T/2 \leq t \leq 2T + \Delta T/2$ as a function of masking ratio, M . These are

$$m_a = \frac{\frac{1}{2} + \frac{M}{n} \frac{A}{T}}{1 + \frac{M}{n}} \quad , \quad -\Delta T/2 \leq t \leq +\Delta T/2$$

$$m_c = \frac{2 \frac{M}{n} \frac{A}{T}}{1 + \frac{M}{n}}, \quad T - \Delta T/2 \leq t \leq T + \Delta T/2$$

$$m_e = \frac{-\frac{1}{2} + \frac{M}{n} \frac{A}{T}}{1 + \frac{M}{n}}, \quad 2T - \Delta T/2 \leq t \leq 2T + \Delta T/2$$

The effect is greatest for the smallest n , so we will take as worst case a square blur image whose sagittal extent is equal to the nominal slit width. Then, $n = (W/2\varepsilon)^*$, where the star indicates we only use the digits to the left of the decimal point. Now $\varepsilon/W = \Delta T/T$, so

$$m_a = \frac{\frac{1}{2} + \left(\frac{2\Delta T}{T}\right)^{**} \frac{M}{T} \frac{A}{T}}{1 + \left(\frac{2\Delta T}{T}\right)^{**} \frac{M}{T} \frac{A}{T}}$$

$$m_c = -2 \frac{\left(\frac{2\Delta T}{T}\right)^{**} \frac{M}{T} \frac{A}{T}}{1 + \left(\frac{2\Delta T}{T}\right)^{**} \frac{M}{T} \frac{A}{T}}$$

$$m_e = \frac{-\frac{1}{2} + \left(\frac{2\Delta T}{T}\right)^{**} \frac{M}{T} \frac{A}{T}}{1 + \left(\frac{2\Delta T}{T}\right)^{**} \frac{M}{T} \frac{A}{T}}$$

where the double star indicates we take the reciprocal of $\left(\frac{T}{2\Delta T}\right)^*$ whose value is calculated from the digits to the left of the decimal point.

The magnitude of shift in time of the input signal in the region $\Delta T/2 \leq t \leq T - \Delta T/2$ is

$$\Delta t = \left(\frac{T m_a}{A} - \frac{1}{2} \right) \Delta T$$

If we assume that the peak and leading edge of the output response also shift by approximately Δt , then the resulting shift in $\vec{N} \cdot \vec{LOS}$ measurement is

$$\begin{aligned}\Delta\theta_A &\approx .034'' \quad (16'' \text{ slit width, } 16'' \text{ blur dia.}) \\ &.021'' \quad (10'' \text{ slit width, } 10'' \text{ blur dia.}) \\ &.071'' \quad (24'' \text{ slit width, } 10'' \text{ blur dia.}) \quad .\end{aligned}$$

Since the edge roughness is randomly located, these values of $\Delta\theta$ are effectively 3σ and the resulting 1σ expressions are

$$\begin{aligned}\Delta\theta &= .011'' \quad (1\sigma) \quad (16'' \text{ slit width, } 16'' \text{ blur dia.}) \\ &.007'' \quad (1\sigma) \quad (10'' \text{ slit width, } 10'' \text{ blur dia.}) \\ &.024'' \quad (1\sigma) \quad (24'' \text{ slit width, } 10'' \text{ blur dia.}) \quad .\end{aligned}$$

Next, the effect of a long wavelength edge roughness, or edge waviness, where the predominant wavelength is large compared to the sagittal extent of the assumed blur rectangle, is examined. A number of effects can result, such as slit narrowing, widening, or shifting, or any possible combinations, with the attendant signal effects shown in Fig. 4-4 representing limiting (3σ , worst) cases.

The signal widening and narrowing effects have been analytically found approximately equal for the blur image = slit width type of star mapper, where for widening,

$$t_p = \tau \ln \left[e^{\frac{T}{\tau}} \left(e^{\frac{\Delta T}{\tau}} + 1 \right) - 1 \right] - \frac{\Delta T}{2}$$

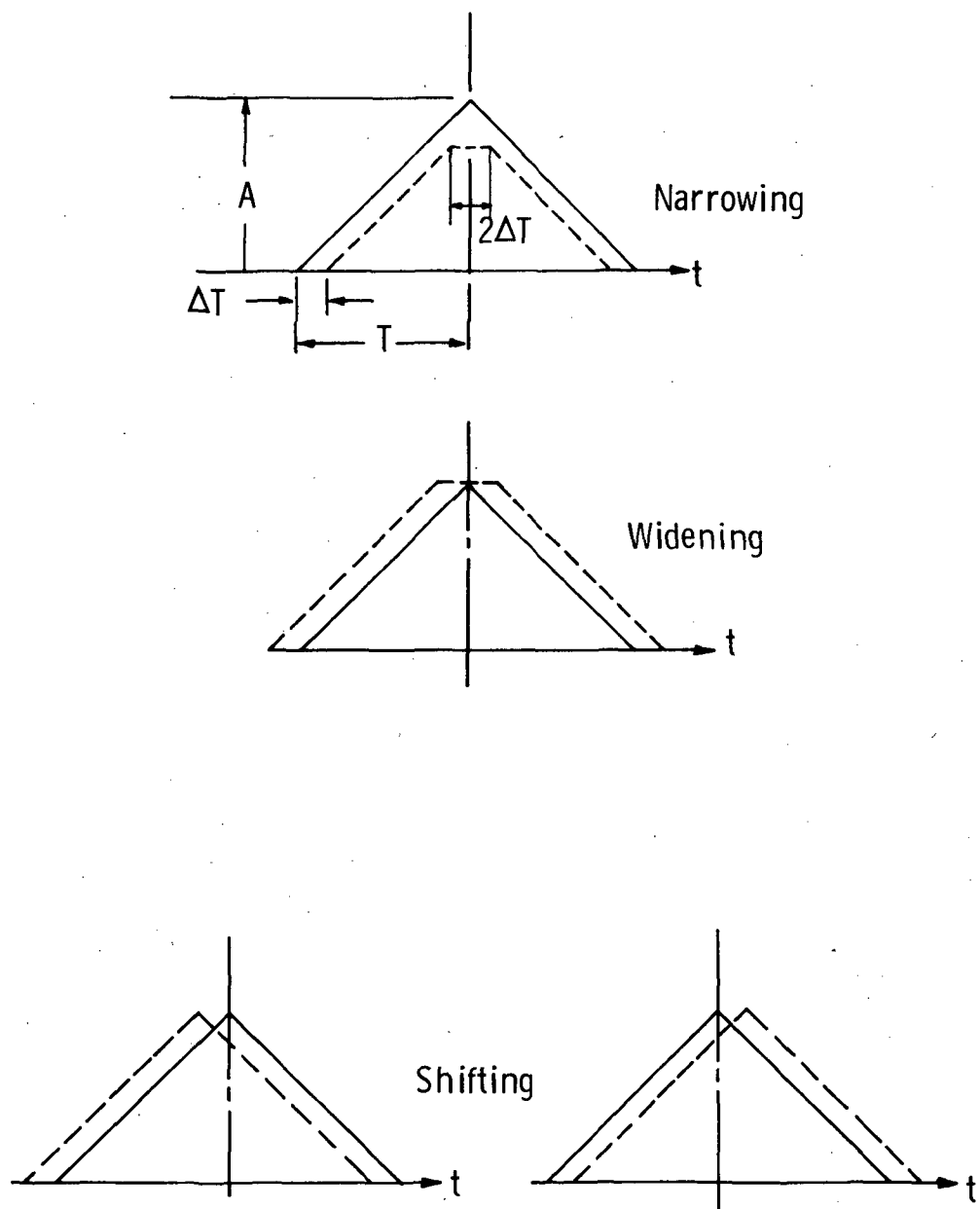


Figure 4-4 Limiting Modifications of the Input Signal Due to Edge Waviness of Both Slit Edges.

$$\mathcal{R}_p = \frac{A}{T - \frac{\Delta T}{2}} \left[2T - t_p \right] .$$

For the silicon star mapper,

$$\begin{aligned} \Delta t_p &= \tau \ln \left[\frac{e^{\frac{T}{\tau}} \left(e^{\frac{\Delta T}{\tau}} + 1 \right) - 1}{2e^{\frac{T}{\tau}} - 1} \right] - \frac{\Delta T}{2} \\ &= \tau \ln \left[1 + \left(\frac{e^{\frac{\Delta T}{\tau}} - 1}{2} \right) \left(\frac{2e^{\frac{T}{\tau}}}{2e^{\frac{T}{\tau}} - 1} \right) \right] - \frac{\Delta T}{2} \\ &\approx \tau \left(\frac{e^{\frac{\Delta T}{\tau}} - 1}{2} \right) \left(\frac{2e^{\frac{T}{\tau}}}{2e^{\frac{T}{\tau}} - 1} \right) - \frac{\Delta T}{2} \end{aligned}$$

or

$$\Delta \theta = \theta_w \frac{\Delta t_p}{T} \approx 0.19'' \text{ for a } 16'' \text{ slit width.}$$

Thus, since narrowing gives $\approx -0.19''$,

$$\Delta \theta_{E2} \approx 0.06'' \text{ (1}\sigma\text{) for a } 16'' \text{ slit width.}$$

Approximately the same degree of effect is found in calculating $\Delta t_{\frac{1}{2}C}$ for the $10''$ slit width with CdS [$\Delta \theta_{E2} \approx 0.05''$ (1 σ)], while for a $24''$ slit width and $10''$ blur diameter the actual blur image dimension is smaller in relation to the edge roughness, and $\Delta \theta_{E2} \approx 0.13''$ (1 σ). But if, as seems more likely, the physical dimension of the blur remains unchanged, then $\Delta \theta_{E2} \approx .05''$ (1 σ) again.

The signal shifting effect is a straightforward time shift, $\Delta t_{\frac{1}{2}} = \Delta t_p = \Delta T$ for both the silicon and CdS star mappers.

$$|\Delta\theta| = \theta \frac{\Delta T}{T} = \begin{cases} 0.67'', & \text{for } 10'' \text{ slit width} \\ 1.07'', & \text{for } 16'' \text{ slit width} \\ 1.61'', & \text{for } 24'' \text{ slit width} \end{cases}$$

or

$$(\Delta\theta_\epsilon)_s = \begin{cases} 0.22'' (1\sigma), & \text{for } 10'' \\ 0.36'' (1\sigma), & \text{for } 16'' \\ 0.54'' (1\sigma), & \text{for } 24'' \end{cases} .$$

4.2.0.3.5 Filter Time Constant Stability Effects - Another source of possible error is the stability of the filter time constant τ which can affect t_p and $t_{1/2}$, where

$$t_p = \tau \ln(2e^{T/\tau} - 1) ,$$

and

$$\left[1 - 2e^{-T/\tau}\right] e^{-t_{1/2}/\tau} - \frac{t_{1/2}}{\tau} = - \left[\frac{T}{\tau} + \frac{1}{2} \ln(2e^{T/\tau} - 1) + 1 \right] ,$$

for a triangle wave input.

The variation pertinent to the silicon star mapper is

$$\frac{\delta t_p}{T} = \left(\frac{t_p}{T} - \frac{2e^{T/\tau}}{2e^{T/\tau} - 1} \right) \frac{\delta \tau}{\tau} ,$$

and for the CdS star mapper, with slit width equal to blur diameter,

$$\frac{\delta t_{1/2}}{T} = \left\{ \frac{t_{1/2}}{T} - 1 + \frac{e^{-\frac{t_{1/2}}{\tau}} - \frac{e^{-T/\tau}}{2e^{T/\tau} - 1}}{e^{-\frac{t_{1/2}}{\tau}} (2e^{T/\tau} - 1) - 1} \right\} \frac{\delta \tau}{\tau} .$$

With the values of T , τ , θ_w and $t_{1/2}$ used previously,

$$\text{Silicon} \quad \text{---} \quad |\Delta\theta_\tau| = 4.05 \frac{\delta\tau}{\tau}, \quad (16'' \text{ slit width})$$

$$\text{CdS} \quad \text{---} \quad |\Delta\theta_\tau| = 1.19 \frac{\delta\tau}{\tau}, \quad (10'' \text{ slit width, } 10'' \text{ blur dia.}).$$

For the case of CdS with a $24''$ slit width and a $10''$ blur dia., we obtain from (4-8), the relation

$$\begin{aligned} \frac{\delta t_{1/2}}{T} = & \left\{ \frac{t_{1/2}}{T} + \frac{e^{T/\tau}}{1-e^{T/\tau}} \left[1 - \frac{1}{2} \frac{e^{\frac{t_{1/2}}{\tau}} \left(e^{\frac{T+x}{\tau}} + 1 + \frac{x}{T} \right)}{e^{T/\tau} \left(1 + e^{\frac{T+x}{\tau}} \right) - 1} \right] \right. \\ & \left. + \frac{1}{2} \frac{e^{t_{1/2}/\tau}}{1-e^{T/\tau}} \left[1 + \frac{x}{T} - \frac{1}{e^{T/\tau} \left(1 + e^{\frac{T+x}{\tau}} \right) - 1} \right] \right\} \frac{\delta\tau}{\tau} \end{aligned}$$

$$\text{CdS} \quad \text{---} \quad |\Delta\theta_\tau| = 29.8 \frac{\delta\tau}{\tau}, \quad (24'' \text{ slit width, } 10'' \text{ blur dia.})$$

4.2.0.4 Probability of Detection and False Alarms

The distribution $p_R(V)$ of output signal amplitudes obtained when a star or simulated star of a given magnitude and spectral class is caused to cross the slit many times at a given sagittal position R along the slit is approximately a Gaussian, when $1/f$ noise is negligible:

$$p_R(V) = \frac{1}{\sqrt{2\pi\sigma_N^2}} e^{-\frac{(V-V_{RP})^2}{2\sigma_N^2}}$$

where: V = value of output signal peak

$V_{RP} = \langle V \rangle$, where $\langle \rangle$ indicates the ensemble average at the position R along the slit.

σ_N = standard deviation of the distribution due to noise processes

The probability of detection $P_{DR}(V_T)$ at the position R along the slit when a threshold is set at V_T is

$$P_{DR}(V_T) = 1 - \int_{-\infty}^{V_T} p_R(V) dV .$$

The noise amplitude probability distribution $p_N(V)$ is

$$p_N(V) = \frac{1}{\sqrt{2\pi\sigma_N^2}} e^{-\left[\frac{V^2}{2\sigma_N^2}\right]} .$$

The probability of a false detection $P_F(V_T)$ (false alarm) in the absence of true signal is

$$P_F(V_T) = \int_{V_T}^{\infty} p_N(V) dV .$$

Expressions for the probabilities of detection and of false alarm are required to describe operation of the entire slit in the presence of slit non-uniformity. For simplicity of analysis we will approximate the distribution of V_{RP} of a slit by a Gaussian

$$p(V_R) = \frac{1}{\sqrt{2\pi\sigma_R^2}} e^{-\left[\frac{(V_{RP}-V_P)^2}{2\sigma_R^2}\right]}$$

where:

$$V_P = \langle\langle V \rangle\rangle_R, \text{ where } \langle \rangle_R \text{ denotes the average over the entire slit length.}$$

The distribution of responses for CdS which can be derived from data in Ref. 108 indicates that the Gaussian approximation is rather poor, the actual distribution being more skewed towards lower responses. There the actual probability of detection will be somewhat worse than that which we derived. From data in Ref. 108 we approximate $\sigma_R = 0.3 V_P$ for a CdS detector. From static detector test data of silicon detectors we approximate $\sigma_R = 0.05 V_P$ (silicon). Recent tests of a silicon SSA with simulated star transits indicated a variation in response comparable to that of CdS, but there is every indication that this is a correctible problem of the optics assembly alignment and/or tolerance.

The probability distribution, $p(V)$, of obtaining an output signal peak of amplitude V for a star transiting the slit at an arbitrary location is then

$$p(V) = \int_{-\infty}^{\infty} P_R(V) P(V_{RP}) dV_{RP}$$

$$= \frac{1}{\sqrt{2\pi(\sigma_N^2 + \sigma_R^2)}} e^{-\left[\frac{(V-V_P)^2}{2(\sigma_N^2 + \sigma_R^2)} \right]}$$

since the covariance is zero.

The probability of detection for a given threshold V_T is

$$P_D(V_T) = 1 - \int_{-\infty}^{V_T} p(V) dV$$

The probability of false detection is still

$$P_F(V_T) = \int_{V_T}^{\infty} p_N(V) dV$$

Figures 4-5 and 4-6 show the probability of detection, $P_D(V_T)$, as a function of a normalized gate threshold V_T/σ_N , for three different values of V_P/σ_N , i.e., $V_P/\sigma_N = 4, 10$, and 20 . The parameter V_P/σ_N is the slit-averaged signal-to-noise ratio for a stationary stochastic light source, such as a star or simulated star. As an example of the information in Figure 4-6, suppose that a 4th magnitude AO class star yields $V_P/\sigma_N = 20$ for this CdS (and possibly Si) star mapper. If the threshold is set at $V_T/\sigma_N = 18$, the probability of detecting a 4th magnitude star is 63%. From Figure 4-5 the probability of detection for a mapper with 5% slit non-uniformity would be 92%.

The effective stellar catalogs for star mappers represented by Fig. 4-6 will be significantly altered from those which might be predicted on the basis of star mapper average response. First, the effective number of detectable stars brighter than the threshold detector magnitude will be less than the stellar catalog number of stars brighter than that detector magnitude because of the spread in the $P_D(V_T)$ curve. Secondly, a large population of stars of greater magnitude (dimmer) than the threshold will have a finite probability of being detected. For example, if $V_T/\sigma_N = 18$ and a 4th magnitude star has an average $S/N = 20$, the probability of detecting a 4.75^M star is 1%. The stellar catalog of stars brighter than 4.75^M is about twice the size of the catalog of stars brighter than 4.0^M. Thus, because of the reduced effective number of stars brighter than magnitude 4.0^M and the finite probability of detecting stars dimmer than magnitude 4.0^M, the unwanted detections could amount to 10% to 20% of all detections (a rough estimate which should be calculated

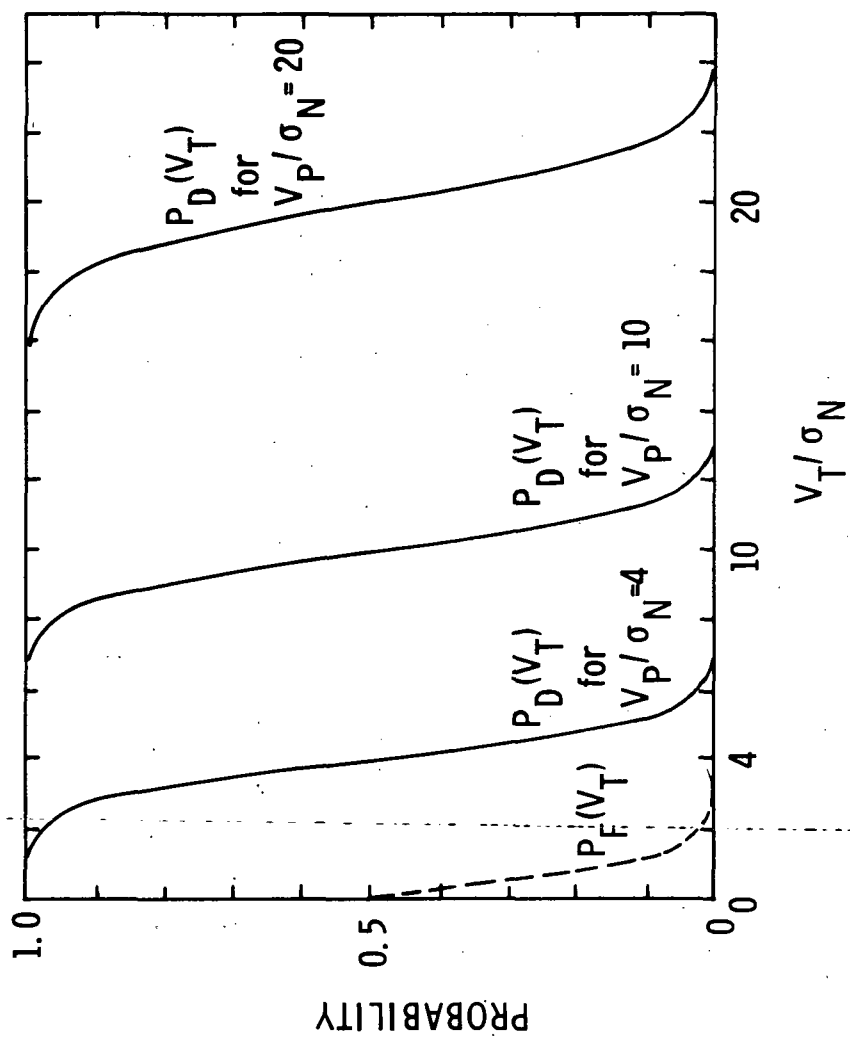


Figure 4-5 Probability of Detection, $P_D(V_T)$, for a Typical $\sigma_R = 0.05 V_P$ Starmapper, and False Alarm Probability, $P_F(V_T)$.

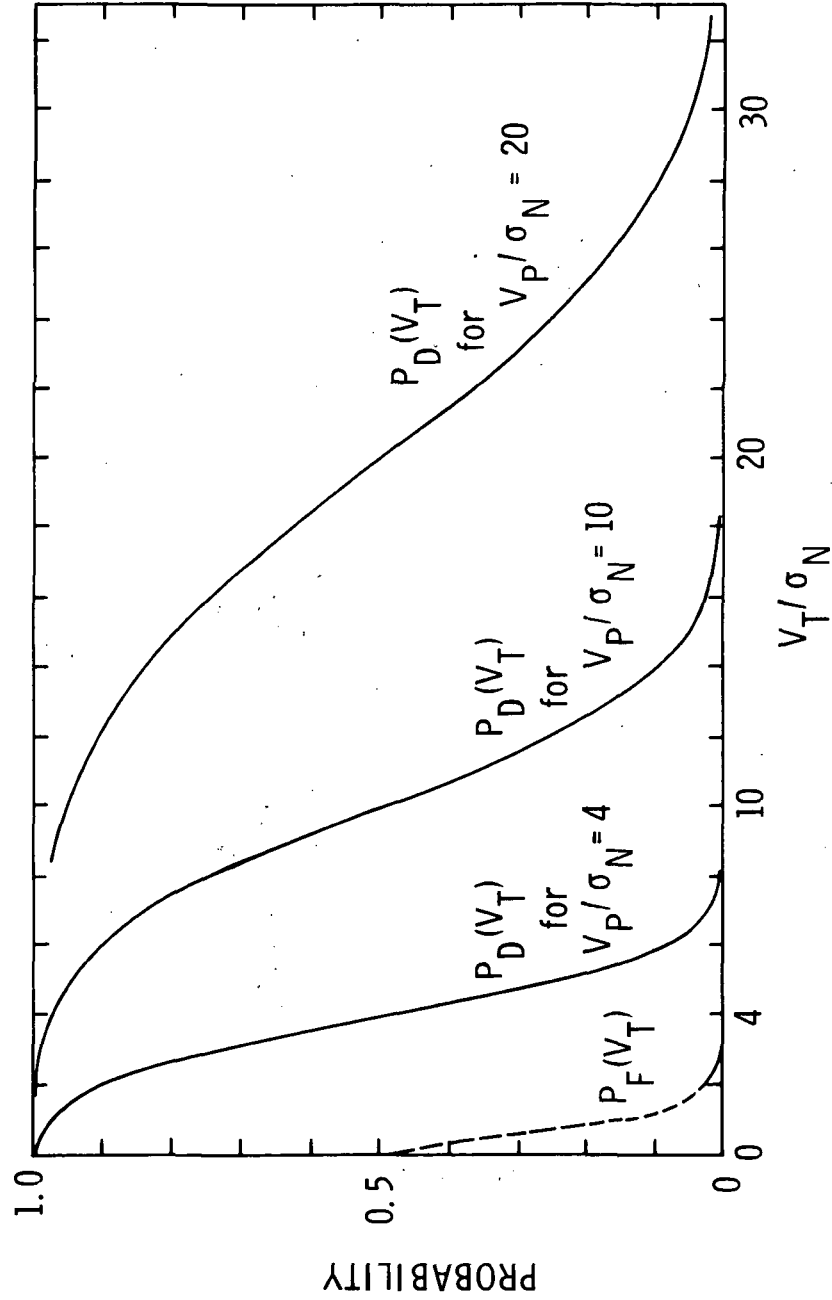


Figure 4-6 Probability of Detection, $P_D(V_T)$, for a Typical Cadmium Sulfide Star Mapper, and False Alarm Probability, $P_F(V_T)$.

more carefully by forming a ratio of integrals of the stellar magnitude distribution weighted by the detection probabilities for stars dimmer than 4.0^M to the integral of those brighter than 4.0^M .)

4.2.1 GENERAL DESCRIPTION OF STAR MAPPER SUBSECTIONS

Subsection 4.2.2 describes three alternative SIMS-A star mappers, and subsection 4.2.3 pertains to the star mapper selected for SIMS-D. Subsections 4.2.2.2 and 4.2.2.3 cover silicon detector approaches suggested by HR and KI respectively. They differ significantly in the optics and electronics implementations. Subsection 4.2.2.1 presents a modification of the SPARS star mapper, using CdS, that differs principally in FOV from the original SPARS Phase IB star mapper.

Each of the SIMS-A star mapper subsections, 4.2.2.1 to 4.2.2.3, are further divided into four subdivisions describing major components or functions and a fifth subdivision tabulating and summarizing the error model items identified in the first four subdivisions, in much the same manner as in Ref. 141 (see subsection 4.2.1 thereof.)

Note that summary descriptions of each star mapper candidate appear in Appendix A, including a display of the configurations and their dimensions. Reference is made to directly-applicable subsections of Ref. 141 wherever it is appropriate to do so.

4.2.2 SIMS-A STAR MAPPER

The SIMS-A star mapper, employing a CdS photodetector and concentric catoptric optics, derives from the experience and technology of the SPARS program and was functionally described in subsection 4.2.2 of Ref. 141. In addition, silicon-based

star sensors with alternate optical designs have lately become strong contenders for consideration in the SPARS and similar programs. Three possible SIMS-A star sensor configurations are identified in this report, with the following designations:

SIMS-A-C.....A 10° FOV star mapper using the concentric catadioptric optics and CdS detector developed by CDC for use in an HA precision attitude reference system.

SIMS-A-HR.....A 10° FOV star mapper using the solid catadioptric optics and silicon photo-detector developed by HR for use in an HA precision attitude reference system.

SIMS-A-KI.....A 4° to 6° FOV star mapper proposed by KI for consideration in the SPARS program.

4.2.2.1 SIMS-A-C Star Mapper, Functional Description

See subsection 4.2.2 of Ref. 141.

4.2.2.1.1 Sims-A-C Star Mapper, Optics - See subsection 4.2.2.1 of Ref. 141 for a general description. The FOV is changed to 10°. The effective aperture area is reduced to 23 cm².

SUMMARY

f/No.....	1.14
FOV.....	10°
Effective Aperture Area.....	23 cm ²
Sunshield Design Angle.....	30°
Sunshield Attenuation at 31°.....	10 ⁶
Approximate Size (See Appendix A).....	21.7" long × 8.7" dia (includes sunshield)

SUMMARY (Cont.)

Weight (See Appendix A).....7.7 lbs (includes sunshade)

Accuracy:

Stellar spectral class..... $<0.13''$ bias range

Temperature bias ($T - T_{\text{nom}} = 4^\circ\text{F}$)..... $0.20''$ bias

Temperature gradient

Meniscus mounting..... $0.34''/^{\circ}\text{F}$

Mirror mounting..... $0.07''/^{\circ}\text{F}$

4.2.2.1.2 SIMS-A-C Star Mapper, Photodetector- See subsection

4.2.2.2 of Ref. 141 for general comments.

The slit width is now $.00045'' (24'')$, and the slit length is $0.33'' (5^\circ)$.

Edge roughness and waviness were incorrectly labeled as (1σ) in Ref. 141 where they were actually 3σ . For a granular edge roughness,

$$\Delta\theta_{E_1} = \begin{cases} .007'' (1\sigma), (10'' \text{ slit width}) \\ .024'' (1\sigma), (24'' \text{ slit width, } 10'' \text{ blur dia.}), \end{cases}$$

and for a wavy edge variation,

$$\Delta\theta_{E_2} = \begin{cases} .23'' (1\sigma), (10'' \text{ slit width}) \\ .56'' (1\sigma), (24'' \text{ slit width, } 10'' \text{ blur dia.}). \end{cases}$$

Various values of time constants for CdS response have been quoted to us during the course of this study, ranging from 96 milliseconds to 300 milliseconds; it seems that some of this variability is between detectors and some within a detector and dependent on the light level, temperature and possibly stellar blur distribution. No documentation of the scale of these effects is known to us. If we assume the most likely value is 300 (just because this number has been mentioned in

our discussions with contractors and critics more frequently than any other) and that departure from 300 to the value of 96 is some kind of 3σ departure [$\Delta\tau = 300 - 96 = 204$ ms (3σ)], then $\Delta\tau(1\sigma)/\tau$ ($=68/300$) ≈ 0.23 , and from subsection 4.2.0.3.4

$$\Delta\theta_{\tau} = \begin{cases} 0.27'' (1\sigma), (10'' \text{ slit width}) \\ 6.90'' (1\sigma), (24'' \text{ slit width, } 10'' \text{ blur dia.}) \end{cases}$$

This is not to be construed as a documented error, but as a point of confusion requiring, for proper caution, further definitive investigation.

Finally, we expect that the increased slit perimeter and area due to increased slit length and width will increase the noise contributions of the bias lamp and maximum background irradiance and leakage current from 0.73×10^{-12} amps/Hz $^{1/2}$ (SPARS-like Mod Phase IB) to 1.6×10^{-12} amps/Hz $^{1/2}$.

SUMMARY

Material	CdS
Slit Width.....	.00045" (24'')
Slit Length.....	.33" (5°)
Slit Array.....	SPARS-like
Edge Roughness.....	$\begin{cases} 0.23'' (1\sigma) \text{ for } 10'' \text{ slit width} \\ 0.56'' (1\sigma) \text{ for } 24'' \text{ slit width} \end{cases}$
(waviness only)	
Possible Time Constnat Stability...	$\begin{cases} 0.27'' (1\sigma) \text{ for } 10'' \text{ slit width} \\ 6.90'' (1\sigma) \text{ for } 24'' \text{ slit width} \end{cases}$
Noise.....	
	1.6×10^{-12} amps/Hz $^{1/2}$

4.2.2.1.3 SIMS-A-C Star Mapper, Electronics - See subsection 4.2.2.3 of Ref. 141 for a block diagram and description of the electronics.

We note that the delay filter consists of two two-pole Butterworth active filter sections in tandem, each with a cutoff

of 7 Hz. One would expect to see a Pade Approximant employed for the delay (e.g., Truxal, Automatic Feedback Control System Synthesis, p. 550, McGraw-Hill, 1955). If the Pade Approximant was in fact considered it would be interesting to know why it was rejected.

The estimate of transit time uncertainty on page 4-45 of Ref. 141 contains several errors due to factors of two, slit width change, misplaced decimal point, and an addition where a root sum square is required. The estimate derivation and correct values are given below.

The half-amplitude time for a $10^{\widehat{n}}$ slit width and $10^{\widehat{n}}$ blur diameter with CdS is

$$t_{\frac{1}{2}} = 0.94 T$$

The response, in the region $0 \leq t \leq T$, derived in subsection 4.2.0.3.1 is

$$\mathcal{R}_1 = A \frac{T}{T} \left(e^{-t/T} + \frac{t}{T} - 1 \right),$$

and the slope at $t_{\frac{1}{2}}$ is

$$m_{\frac{1}{2}} = \frac{A}{T} \left(1 - e^{-0.94 \frac{T}{T}} \right) = 0.134 \frac{A}{T}.$$

The peak was found to be

$$\mathcal{R}_p = 0.14 A,$$

and, therefore,

$$m_{\frac{1}{2}} = 20.8 \mathcal{R}_p \text{ sec}^{-1} (10^{\widehat{n}} \text{ slit width, } 10^{\widehat{n}} \text{ blur dia.}).$$

The half-amplitude time for a $24''$ slit width and a $10''$ blur diameter with CdS is

$$t_{\frac{1}{2}} = 0.63(2T + \tau) \quad .$$

The response, in the region $T \leq t \leq 2T + \tau$, derived in subsection 4.2.0.3.1 is

$$\mathcal{R}_b = A \frac{\tau}{T} \left[e^{-\frac{t}{\tau}} \left(1 - e^{\frac{T}{\tau}} \right) + \frac{T}{\tau} \right]$$

and the slope at $t_{\frac{1}{2}}$ is

$$m_{\frac{1}{2}} = \frac{A}{T} \left[e^{-0.63 \frac{T+\tau}{\tau}} \left(e^{\frac{T}{\tau}} - 1 \right) \right] = 0.131 \frac{A}{T} \quad .$$

The peak was found to be

$$\mathcal{R}_p = 0.27 A$$

and, therefore,

$$m_{\frac{1}{2}} = 10.4 \mathcal{R}_p \text{ sec}^{-1} \text{ (} 24'' \text{ slit width, } 10'' \text{ blur dia.)} \quad .$$

The peak amplitude can be expressed in terms of the slit-averaged signal-to-noise ratio

$$\overline{S/N} = \mathcal{R}_p / \sigma_N \quad ,$$

and the timing error is

$$\Delta t = \sigma_N / m_{\frac{1}{2}} = .048 / (\overline{S/N}), \text{ (} 10'' \text{ slit width)} \\ .096 / (\overline{S/N}), \text{ (} 24'' \text{ slit width)}$$

yielding

$$\Delta\theta_{\frac{1}{2}} = \theta_w \frac{.048}{T} \bigg/ (\overline{S/N}) = 10.4 \bigg/ (\overline{S/N})^{\frac{1}{2}}, (1\sigma), (10'' \text{ slit width, } 10'' \text{ blur dia.})$$

or,

$$= \theta_w \frac{.096}{2T+8} \bigg/ (\overline{S/N}) = 21 \bigg/ (\overline{S/N})^{\frac{1}{2}}, (1\sigma), (24'' \text{ slit width, } 10'' \text{ blur dia.})$$

The above expressions are correct if:

1. The delayed signal has the same shape as the signal that is peak detected (e.g., through use of a Pade Approximant)
2. The peak is detected at the value \mathcal{R}_p .

Since the delay filter has only a finite number of elements it must provide only an approximation to a perfect delay line and decreases the signal slope at $t_{\frac{1}{2}}$ slightly. However, in the absence of detailed circuit analysis we will assume the slope decrease is not too significant. This is a point that requires future analysis.

With regard to the second point, the peak, in repeated measurements, is distributed about \mathcal{R}_p in the presence of noise. Therefore, the half-amplitude point is distributed in time about the ideal value $t_{\frac{1}{2}}$ by an amount

$$t_{\frac{1}{2}} = \frac{\sigma_N/2}{m_{\frac{1}{2}}}$$

contributing an additional error

$$\Delta\theta_p = 5.2 \bigg/ (\overline{S/N})^{\frac{1}{2}}, (1\sigma), (10'' \text{ slit width, } 10'' \text{ blur dia.})$$

or,

$$= 10.5 \bigg/ (\overline{S/N})^{\frac{1}{2}}, (1\sigma), (24'' \text{ slit width, } 10'' \text{ blur dia.}).$$

An approximation to the combined error is the root-sum-square (RSS)

$$\Delta\theta_{t_1} \geq (\Delta\theta_{\frac{1}{2}}^2 + \Delta\theta_p^2)^{\frac{1}{2}}$$

$$\approx 12/(\overline{S/N})^{\frac{1}{2}}, (1\sigma), (10'' \text{ slit width, } 10'' \text{ blur dia.})$$

or,

$$\approx 24/(\overline{S/N})^{\frac{1}{2}}, (1\sigma), (24'' \text{ slit width, } 10'' \text{ blur dia.})$$

The inequality in the above expression for $\Delta\theta_t$ reflects the fact that the covariance is not zero, but is determined by the action of the electronic filters and delays on the input noise, a matter for future investigation.

If we also include the effect of slit non-uniformity of response as a variation of S/N, then

$$\Delta\theta_t \approx 13/(\overline{S/N})^{\frac{1}{2}}, (1\sigma), (10'' \text{ slit width, } 10'' \text{ blur dia.})$$

or,

$$\approx 26/(\overline{S/N})^{\frac{1}{2}}, (1\sigma), (24'' \text{ slit width, } 10'' \text{ blur dia.})$$

Then, for a limiting magnitude of 3.9^M and a $S/N = 20$ for a SIMS-A-C SSA, the noise-equivalent angle is

$$\text{SIMS-A-C; } \Delta\theta_t \approx 1.3'', (1\sigma), (24'' \text{ slit width, } 10'' \text{ blur dia.}).$$

For a SPARS-Mod. IB-like SIMS-A SSA, at 3.9^M the S/N will be $(53/23)(.14/.27)(20) = 24$ to account for the effective aperture difference with respect to a SIMS-A-C and the peak response difference for the narrower slit ($10''$). Therefore, at 3.9^M , for a SIMS-A (Mod IB-like), the noise-equivalent-angle is

$$\Delta\theta_t = 0.54'', (1\sigma), (10'' \text{ slit width, } 10'' \text{ blur dia.}).$$

4.2.2.1.4 SIMS-A-C Star Mapper, GSE - No launch-pad GSE is anticipated, assuming the system is calibrated in the lab, shipped in a special container to preserve alignment, mounted in the vehicle and aligned by means of a theodolite.

4.2.2.1.5 SIMS-A-C Star Mapper, Error Model -

<u>Contributing Source</u>	<u>Error</u> *
Attitude rate error.....	$0.1''$ (1σ)
Edge roughness.....	$0.02''$ (1σ)
Edge waviness.....	$0.6''$ (1σ)
CdS time constant per 1% stability..	$0.3''$ (1σ)
Optics blur with spectral class.....	$0.2''$ (1σ)
Noise-equivalent angle (at 3.9^M)....	$1.3''$ (1σ) lacking 1/f noise information
Temperature per $\Delta T = 4^\circ\text{F}$	$0.2''$ (Bias)
Temperature gradient:	
Meniscus-mounting flange location...	$0.3''/\text{°F}$ (Bias)
Mirror-mounting flange location.....	$0.07''/\text{°F}$ (Bias)
RSS (of 1σ contributors, with $1\% \Delta\tau/\tau$) =	
$1.5''$ (1σ)	

Laboratory tests of a similar star mapper at the HA facility have yielded $2''$ (1σ). The contributions to this error from the SSA and the test equipment are comparable so that our estimate of $1.5''$ (1σ) has some limited confirmation.

4.2.2.2 SIMS-A-HR Star Mapper, Functional Description

See subsection 4.2.4 of Ref. 141. Figure 4-7 is a functional block diagram of the unsubstantiated probable SIMS-A-HR star mapper. No direct confirmation of the HR signal processing assumed in Fig. 4-7 has been given by HR. HR considers its signal processing detail proprietary during its present competitive phase.

* Only the first rounded-off digit to the right of the decimal point is retained in this summary.

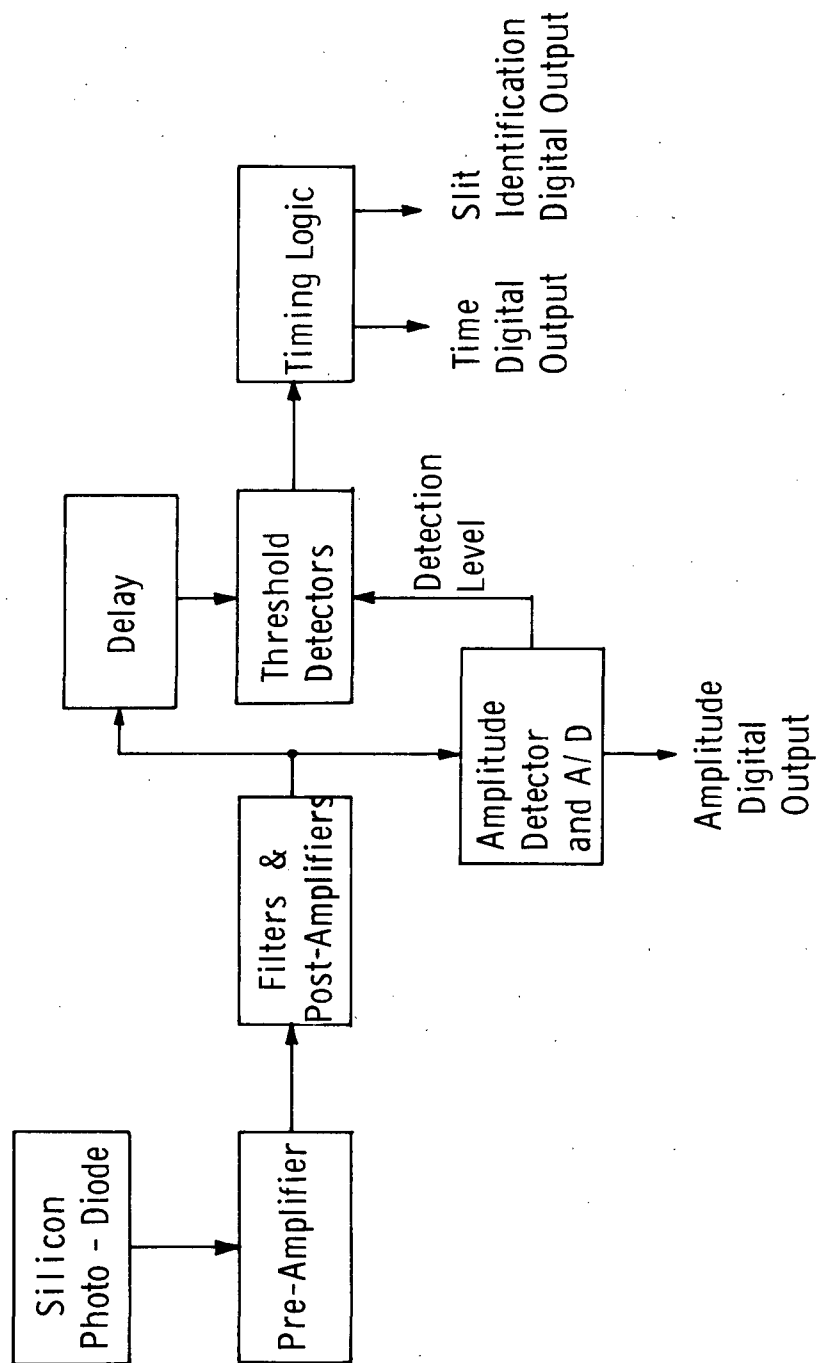


Figure 4-7 Speculative Functional Block Diagram of SIMS-A-HR Star Mapper.*

* See Appendix F for updated information.

4.2.2.2.1 SIMS-A-HR Star Mapper, Optics - See subsection 4.2.4.1 of Ref. 141 for a general description of the solid catadioptric optical assembly employed by HR. Specific parameters, which differ from those in subsection 4.2.4.1 of Ref. 141 are listed below.

SUMMARY

Weight (See Appendix A):

Optical/mechanical head.....	3.0 lbs
Sunshade.....	1.25 lbs
Overall dimensions (See Appendix A).....	22.5"Lx3.75" dia. (includes sunshield)
Physical aperture.....	2.5" dia.
Effective aperture area.....	19 cm ²
f/No.....	2.0
FOV.....	10° (swath width)
Accuracy.....	[unspecified; assign 0.5" (1σ)]
Sunshade design angle.....	30°
Sunshade attenuation.....	~10 ⁵

4.2.2.2.2 SIMS-A-HR Star Mapper, Photodetector - See subsection 4.2.4.2 of Ref. 141 for a description of the SPARS-like array of silicon slit detectors employed. Edge roughness estimate has been revised here in accordance with subsection 4.2.0.3.3.

SUMMARY

Material.....	Photovoltaic silicon
Slit width.....	0.00045 inch (16")
Slit length.....	0.500 inch (5°)
Edge roughness.....	0.01" (1σ)
Edge waviness.....	0.3" (1σ)
Peak responsivity.....	0.5 amp/watt
Degradation of responsivity.....	2%/year
Cell leakage noise spectral density.....	16x10 ⁻³⁰ amp ² /Hz

4.2.2.2.3 SIMS-A-HR Star Mapper, Electronics - See subsection 4.2.4.3 of Ref. 141.*

If, as we assume, the signal is delayed until the peak is detected and an optimum threshold set (i.e., at maximum signal slope), the analysis that follows is useful.

One possible reason for detecting the peak and setting a threshold thereafter is that there is a symmetry error (especially apparent in our simple analysis) which may be large and intolerably threshold-sensitive when the threshold is set too low relative to the peak (see Fig. 4-8). At a threshold near 63% of the peak response it is apparent in Fig. 4-8 that the symmetry error is not sensitive to small variations in threshold setting, i.e., $d\epsilon_s/dV_T = 0$, and can be removed by calibration in systems which always choose the same 60% threshold relative to peak.

In a system describable by this simple analysis a range in stellar magnitude of two is about all that could be tolerated with fixed threshold. With more sophistication in filter design greater signal symmetry can be attained, allowing an increased range of stellar magnitudes.

The slope of the response is maximum when

$$\frac{dm_1}{dt} = 0 \quad .$$

In the present analysis the inflection point always occurs at $t = T$,

$$m_{MAX} = \frac{A}{T} \left\{ 1 - e^{-\frac{T}{T}} \right\} \quad ,$$

* See Appendix F for updated information

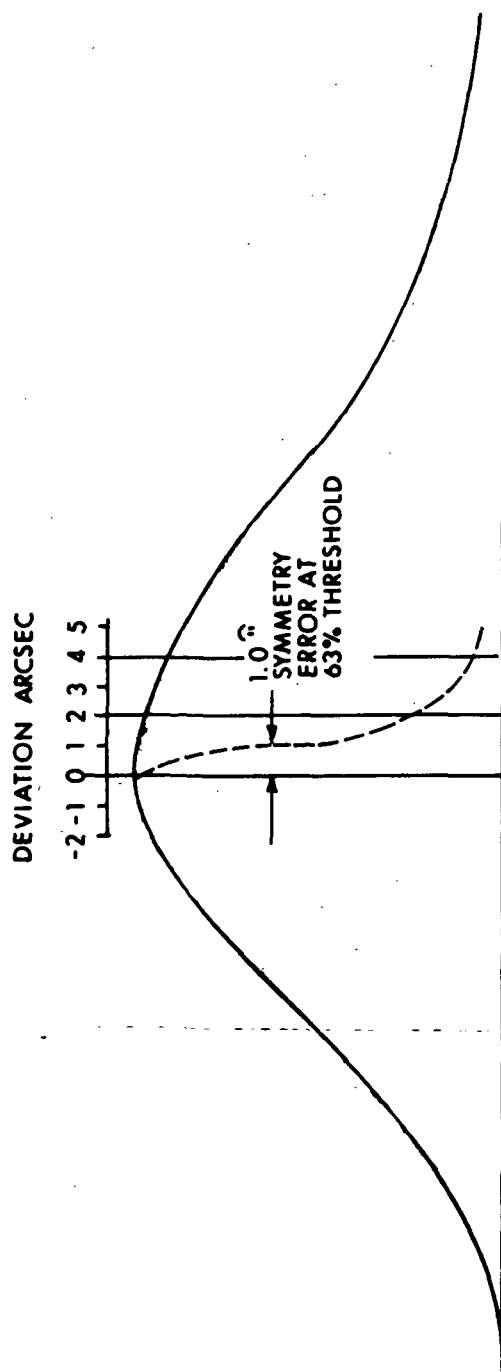


Figure 4-8 Symmetry Error as a Function of Threshold Indicated on a Typical Silicon Star Mapper Filtered Output, Where Both Leading and Trailing Edge Detection is Used.

$$\mathcal{R}_{1M} = A \frac{\tau}{T} \left\{ e^{-T/\tau} + \frac{T}{\tau} - 1 \right\} ,$$

and

$$\frac{\mathcal{R}_{1M}}{\mathcal{R}_p} = \frac{e^{-T/\tau} + \frac{T}{\tau} - 1}{2 \frac{T}{\tau} - \ln(2e^{T/\tau} - 1)} .$$

For typical values of T and τ for silicon star mappers, $T/\tau \approx 0.74$, and

$$\frac{\mathcal{R}_{1M}}{\mathcal{R}_p} = 0.678$$

where, from subsection 4.2.0.3.1, $p = 0.43$ A. Then

$$\frac{\Delta T}{T} = \frac{\sigma_N}{T_m} = \frac{0.43}{(S/N)(1 - e^{-T/\tau})} = \frac{0.82}{(S/N)} .$$

Then, taking into account the detection of both leading and trailing edges,

$$\Delta\theta_t = \frac{13.2}{\sqrt{2} (S/N)} \hat{n} = \frac{9.32}{(S/N)} \hat{n} (1\sigma) .$$

Since both the leading and trailing edges are detected, we divided by $\sqrt{2}$, and with $S/N = 20$ for a 3.5^M AO star,

$$\Delta\theta_{t_{MAX}} \approx 0.47 \hat{n} (1\sigma)$$

Power requirements are listed in Appendix A.

SUMMARY

Noise spectral density.....	$16 \times 10^{-30} \text{ amp}^2/\text{Hz}$
Noise bandwidth.....	15 Hz
Quantization error.....	$0.05''$ (1 σ)
NEA (at 3.5^M AO).....	$0.5''$ (1 σ)
Signal symmetry.....	$<1.0''$ fixed bias
Total power:	
Driving 3 low-powered TTL inputs.....	3 watts
Driving 1 high-powered TTL input.....	3.6 watts
Reliability.....	a 1% chance of one of four slits failing in 3 years

4.2.2.2.4 SIMS-A-HR Star Mapper, GSE - No launch-pad GSE is anticipated, assuming the system is calibrated in the lab, shipped in a special container to preserve alignment, mounted in the vehicle and aligned by means of a theodolite.

4.2.2.2.5 SIMS-A-HR Star Mapper, Error Model -

<u>Contributing Source</u>	<u>Error*</u>
Attitude rate error.....	$0.2''$ (1 σ)
Edge roughness.....	$0.01''$ (1 σ)
Edge waviness.....	$0.3''$ (1 σ)
Slit straightness.....	$1.5''$ (3 σ)
Electronic stability per 1% $\Delta\tau$	$0.01''$ (1 σ)
Optics.....	$<0.5''$ (unsupported)
Noise-equivalent angle (at 3.5^M).....	$0.5''$ (1 σ)
Temperature effects.....	$<0.01''/\Delta^\circ\text{F}$
Symmetry error.....	$<1.0''$ (fixed bias)

RSS (of 1 σ contributors with $\Delta\tau/\tau = 1\%$) $\leq 0.9''$ (1 σ)

* Only the first rounded-off digit to the right of the decimal point is retained in this summary.

4.2.2.3 SIMS-A-KI Star Mapper, Functional Description

See subsection 4.2.3 of Ref. 141 for a general description.

The SIMS-A-KI SSA candidate is fully discussed in Ref. 157. A copy of this document was forwarded to NASA/GSFC as supplementary material for the EOS/SIMS study.

The SIMS-A-KI SSA has many features of the SIMS-DA-KI described in subsections 4.2.3 through 4.2.3.6 of Ref. 141, and has eliminated the chief drawback of the SIMS-DA-KI by incorporating both leading and trailing edge detection.

The design range of stellar magnitude is from 0.8^M to 3.3^M (Si).

4.2.2.3.1 SIMS-A-KI Star Mapper, Optics - The SIMS-DA-KI star mapper optics (subsection 4.2.3.1 of Ref. 141) is similar in principle to the SIMS-A-KI star mapper optics (Ref. 157). The details presented here differ from those in Ref. 141 and are summarized below:

SUMMARY

f/No.....	1.67
FOV.....	4° - 6° (optional)
Physical aperture.....	6 inch Dia.
Effective aperture area.....	16.4 inches ² (106 cm ²)
Sunshade design angle.....	30°
Sunshade attenuation at 31°.....	10 ⁷
Approximate size (see Appendix A).....	16.3 inches × 7.5 inch Dia. (includes sunshade)

SUMMARY (Cont.)

Weight (see Appendix A):

Optical/Mechanical head.....	8.7 lbs
Sunshade.....	1.4 lbs
Accuracy.....	TBD (assign $0.5^{\hat{n}}$ see subsec. 4.2.3.1 of Ref. 141)

4.2.2.3.2 SIMS-A-KI Star Mapper, Photodetector - See subsection 4.2.3.2 of Ref. 141 for a description of the SPARS-like array of silicon slit detectors employed. Silicon detectors are supplied by TI (See Ref. 158 for typical spectral response curves.) Edge roughness estimates have been revised in accordance with subsection 4.2.0.3.3.

SUMMARY

Material.....	TI Photovoltaic Silicon
Slit width.....	.0005 inch ($10^{\hat{n}}$)
Slit length.....	as required for 2° - 3° /slit
Edge roughness.....	$0.01^{\hat{n}}$ (1σ)
Edge waviness.....	$0.2^{\hat{n}}$ (1σ)
Slit straightness*	$1.0^{\hat{n}}$ (1σ)
Peak responsivity.....	0.45 amp/watt
Degradation of responsivity.....	<2%/year
Cell leakage noise spectral density...	0.32×10^{-28} amp ² /Hz

* A slit straightness figure of $1.0^{\hat{n}}$ over the diameter of the mask is indicated by the tolerances on Fig. 4-4 of subsection 4.2.5 of Ref. 157, although they state $10^{\hat{n}}$ in the text (this must be a typographical error).

4.2.2.3.3 SIMS-A-KI Star Mapper, Electronics - There are several important additions in threshold detection and signal processing

not reported in subsection 4.2.3.3 of Ref. 141. We quote two paragraphs from page 6-1 of Ref. 157:

"The principle of operation of the system which generates the output time mark pulse with relation to the center of the star pulse is described with reference to (Figure 4-9). When the leading edge of the star (signal) crosses the threshold a counter begins counting at a rate of $f/2$ pulses per second. When the trailing edge crosses the threshold the counter ceases the $f/2$ count and begins counting at a rate of f pulses per second. After counting N pulses (the capacity of the counter) the counter 'spills over'....and an output time mark pulse is generated. During the time, (t') , that the star pulse is above the threshold level the total of counts accumulated is $(f/2)(2t')$ or $t'f$. The number of pulses counted after the star pulse is $N - t'f$ and the time period at count rate f is $(N - t'f)/f$. The total time between the star pulse center and the output time pulse (generated at counter spillover) is then:

$$T_t = t' + \frac{N - t'f}{f} = N/f$$

which is independent of the star pulse width.

The single-channel simplified block diagram of the electronic system which accomplishes the star pulse center measurement is shown in (Figure 4-10). The pre- and post-amplifiers provide the necessary signal gain and noise filtering. The threshold detector is a voltage comparator which interprets the amplitude of the star pulse and provides a compatible TTL logic drive output."

Quantization error is estimated at $<0.2\sigma$ (3σ).

Figure 4-11 updates the detection electronics diagram presented as Fig. 4-18 in subsection 4.2.3.3 of Ref. 141.

Power requirements are given in Appendix A.

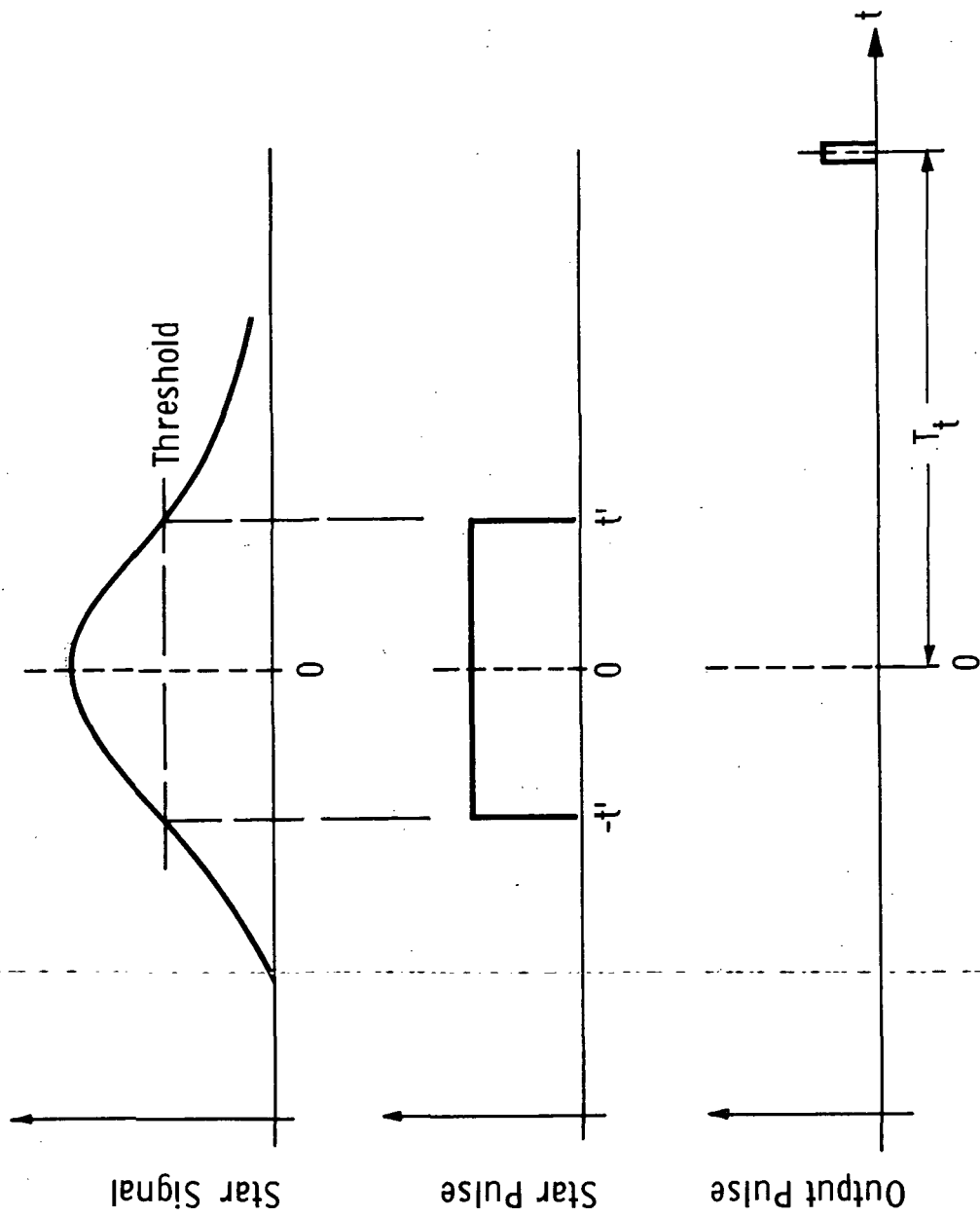


Figure 4-9 SIMS-A-KI Star Mapper Waveform Center Detection Principle.

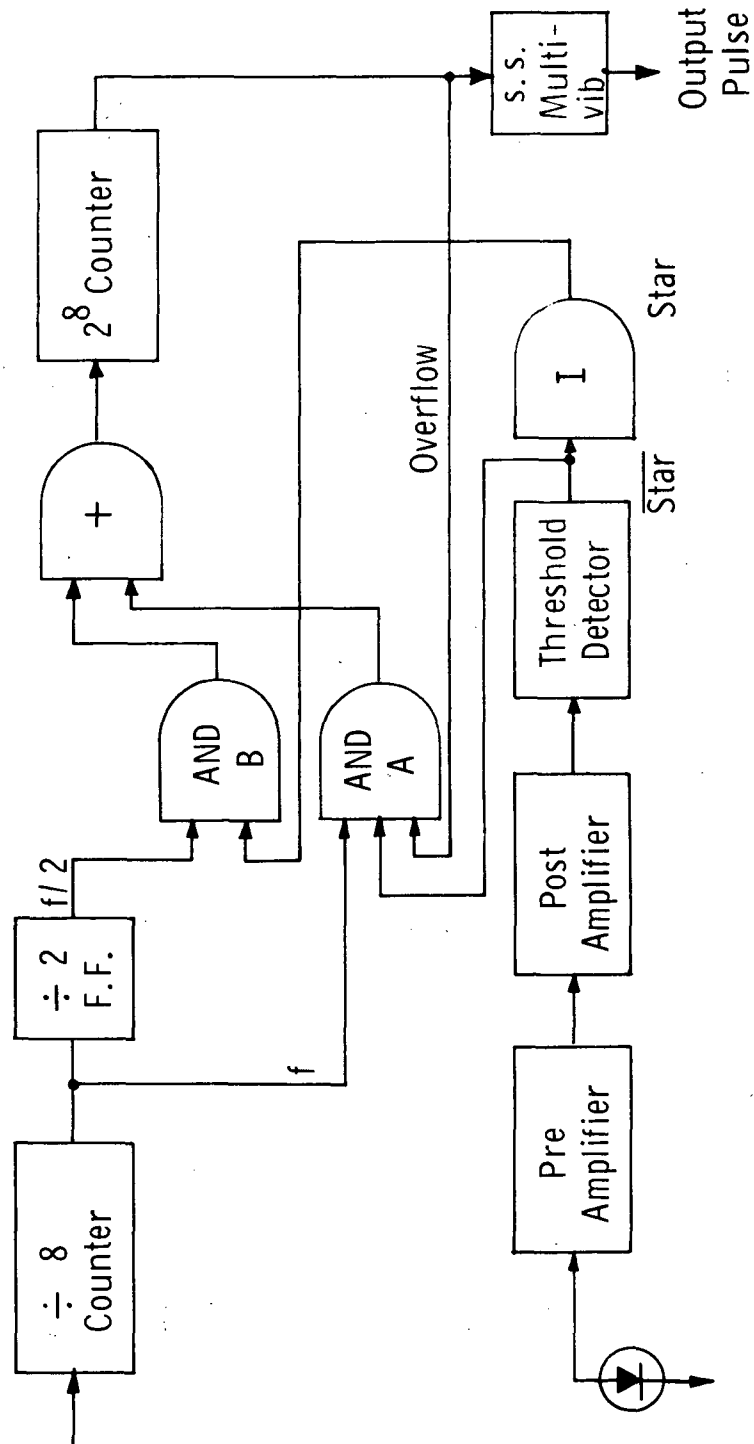


Figure 4-10 Simplified Block Diagram of the SIMS-A-KI Star Mapper Electronics.

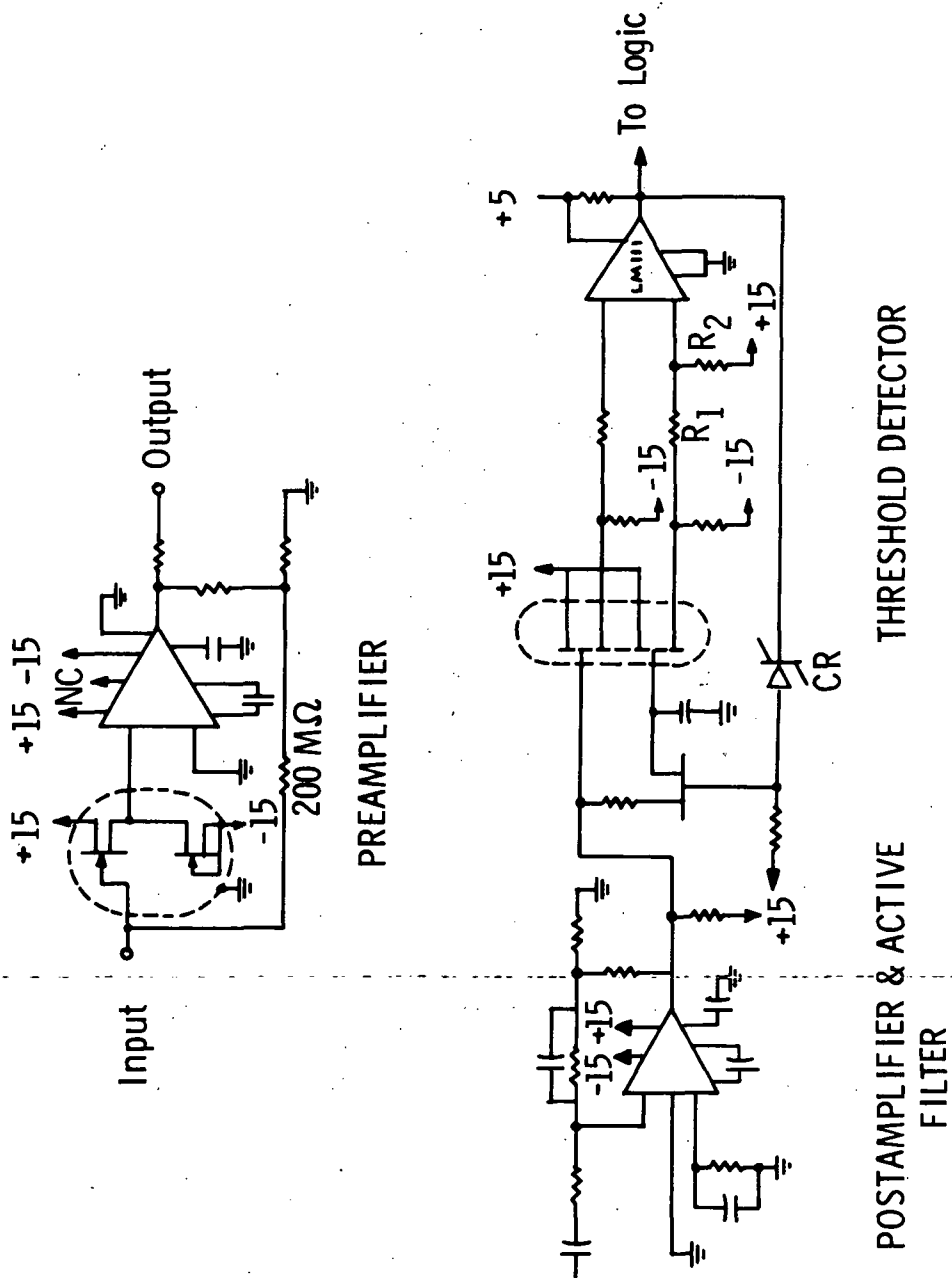


Figure 4-11 SIMS-A-KI Star Mapper Detection Electronics.

Since the threshold is set at 60% of the peak response of the minimum-brightness usable star,

$$\begin{aligned} \left(\frac{\delta t}{T} \right) &= \frac{\sigma_r}{m} = \frac{\mathcal{R}_p / (S/N)}{m} \\ &= \frac{2 \frac{T}{\tau} - \ln(2e^{T/\tau} - 1)}{(S/N) [1 - e^{-T/\tau}]} \tau/T \\ &= \frac{0.8}{(S/N)} \end{aligned}$$

with $T = .046$ seconds ($10''$ slit width) and $\tau = 0.033$ seconds (30 Hz signal bandwidth); and, with $S/N = 20$,

$$\Delta \theta_t = \frac{\theta_w}{\sqrt{2}} \frac{\delta t}{T} \approx 0.3'' \quad (1\sigma)$$

at $3.3^M(\text{Si})$.

Figure 4-12 shows a simulated response from Ref. 157 for the SIMS-A-KI star mapper along with an MIT-based estimate of the symmetry error excursion in the region from 5% to 80% of peak response.

SUMMARY

Noise spectral density.....	1.3×10^{-28} amp ² /Hz
Noise bandwidth.....	47 Hz
Quantization error.....	$< 0.06''$ (1σ)
NEA.....	$0.3''$ (1σ)
Signal symmetry error.....	$0.4''$ bias range with varying stellar mag- nitude.
Total power.....	3.0 watts

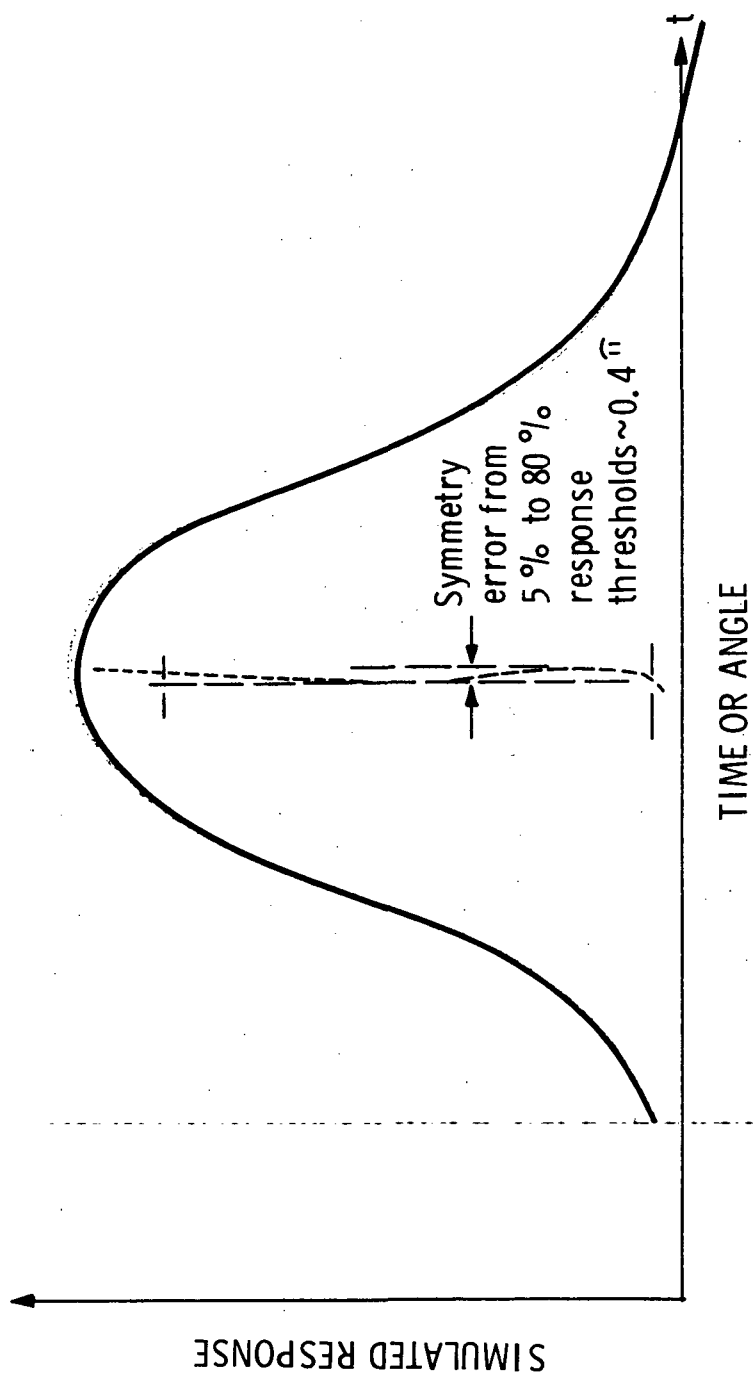


Figure 4-12 Symmetry Error for the SIMS-A-KI Star Mapper

4.2.2.3.4 SIMS-A-KI Star Mapper, GSE - No launch-pad GSE is anticipated, assuming the system is calibrated in the lab, shipped in a special container to preserve alignment, mounted in the vehicle and aligned by means of a theodolite.

4.2.2.3.5 SIMS-A-KI Star Mapper, Error Model -

<u>Contributing Source</u>	<u>Error</u> *
Attitude rate error.....	$0.2''$ (1σ)
Edge roughness.....	$0.01''$ (1σ)
Edge waviness.....	$0.2''$ (1σ)
Slit straightness.....	$1.0''$ (3σ)
Electronic stability per $1\% \Delta\tau$	$0.01''$ (1σ)
Optics.....	$<0.5''$ (1σ) (unsupported)
Noise-equivalent angle (at 3.3^M).....	$0.3''$ (1σ)
Symmetry error.....	$0.4''$ (bias, ranges with stellar magnitude)

RSS (of 1σ contributors and symmetry error with $\Delta\tau/\tau=1\%$) $\leq 0.8''$ (1σ)

* Only the first rounded-off digit to the right of the decimal point is retained in this summary.

4.2.3 SIMS-D-HR STAR MAPPER

The SIMS-D-HR SSA is an updated version of the SIMS-DA-HR reported in Section 4 of Ref. 141 and is now identical with the SIMS-A-HR discussed in subsections 4.2.2.2 through 4.2.2.2.6 of the present report.

4.3 SIMS-B STAR TRACKER

See subsection 4.3.1 of Ref. 141 for all information and references. See Appendix A of this report for Trade Parameters.

4.4 SIMS-B STAR TRACKER, RANDOM ACQUISITION FEASIBILITY

The following considerations show that it is possible to use the PPCS/PADS star tracker in a mode requiring no on-board star catalog. Unfortunately, this information became apparent too late in the program to be fully developed as the proper SIMS-B Star Tracker configuration in time for inclusion in this report. However, its promised merit for SIMS-B implementation should encourage further examination.

The mode of scanning that was defined for the SIMS-DB2 has been considered as a possibility by TRW (Ref. 161) with the following parameters:

PADS Eff. Aperture	= 42 cm ²
IFOV	= 170 ^{''}
Search FOV/cycle	= ±15°×0.5° (roll × pitch)
Gimbal Rate	= 7.2°/sec (roll)
Limiting Magnitude	= 3.5 ^M AO

To accomplish a complete scan cycle from +15° to -15° and return to +15° entails a total angular distance of 60° which is accomplished in a time

$$t_s = \frac{60^\circ}{7.2^\circ/\text{sec}} = 8.34 \text{ seconds}$$

~~The spacecraft pitch rate is the orbital rate of~~
0.206^{''}/millisecond. Thus, the field of view advances

$$0.206 \times t_s = 1.72 \times 10^3 \text{ } ^{\circ} \lesssim 0.5^\circ$$

and there will be no gaps within the ±15°×360° swath searched.

Next, we examine the dwell time for the IFOV. The number of dwell discrettes of $170''$ adjacent IFOVs that line up in the pitch direction to equal 0.5° is

$$N = \frac{(0.5^\circ)(3600''/\circ)}{170''} = 10.58$$

(We assume instant flyback after each pitch scan).

If the dwell time of each discrete IFOV is t_D , the total time consumed in moving the field-of-view 0.5° in the pitch direction relative to the space vehicle is

$$t_N = N t_D$$

But, in a time t_N the IFOV must move $170''$ at the rate $7.2^\circ/\text{sec}$, i.e.,

$$t_n = \frac{170''}{(7.2^\circ/\text{sec})(3600''/\circ)} = .00656 \text{ sec.}$$

Therefore,

$$t_D = \frac{t_N}{N} = .000614 = 614 \mu \text{ seconds.}$$

From LPL (Ref. 118) data (see Fig. 4-1, present report), the S-20 response to a 3.5^M AO star is 3.2×10^{-15} amps/effective aperture area of one cm^2 . Therefore

$$I_{3.5} = 1.34 \times 10^{-13} \text{ amps}$$

$$\frac{I_{3.5}}{e} = 0.835 \text{ photoelectrons}/\mu \text{ second}$$

$$t_D \frac{I_{3.5}}{e} = 512 \text{ photoelectrons per IFOV dwell}$$

$$B_s \approx \frac{1}{.000614} = 1630 \text{ Hz (signal bandwidth)}$$

The anode dark current for an F4004 (S-20) with approximately the same IEPD is .005 μ A with a tube gain of 2×10^6 . The equivalent cathode thermal photoemission rate is

$$\frac{I_D}{eG} = \frac{5 \times 10^{-9}}{(2 \times 10^6)(1.6 \times 10^{-19})} \approx .0156 \text{ photoelectrons}/\mu \text{ sec}$$

or, in one dwell time,

$$(614)(.0156) = 9.6 \text{ photoelectrons}$$

Thus, with a 1630 Hz bandwidth we should have a nominal

$$\frac{S}{N} = \frac{512}{9.6} = 53.4$$

However, let us assume a threshold for 95% probability of detection which implies we set the threshold detector at a value 1.64 σ below the average signal, i.e., $512 - 1.64 \sqrt{512} = 475$ and the effective S/N is

$$S/N = \frac{475}{9.6} = 49.5$$

so the false alarm rate should be negligible.

SECTION 5

ERROR STUDIES

5.1 INTRODUCTION

The objective of the present error studies was to determine the accuracy of attitude determination for three SIMS candidates which are fairly representative of today's technology and are briefly identified as follows:

<u>SIMS Candidate</u>	<u>Chief Characteristics</u>
A	Strapped-Down Gyros; Star Mapper
B	Strapped-Down Gyros; Gimbaled Star Tracker
D	Gyros Fully Gimbaled; Star Mapper

Each of the above candidates employs the gimbaled or strapped down set of gyros for continuous attitude information, and the star sensor to bound the errors.

Attitude determination in the present case implies determination, on the ground, of the inertial attitude of some spacecraft reference block at an arbitrary epoch using gyro and star measurement data received before and after that epoch. Since attitude determination is "after-the-fact", it involves the mathematical problem of smoothing.

The attitude determination accuracy desired by NASA is 0.001 deg (1σ) per axis. Determining the extent to which each of

the SIMS candidates meets this requirement was one of the primary objectives of this study. It is important to note that the extent to which a given candidate does so depends not only on the equipment on board the spacecraft but also on the ground technique used to process the data. There are a number of techniques for processing and smoothing data. Many of them, like the one used in this study, make use of a priori knowledge of the system errors and generate a solution in the least squares sense. The technique employed in the present effort was the Fraser two-filter smoother formulation which is described in Section 5.4 of Interim Technical Report No. 2¹⁴¹.

Since a number of different systems had to be analyzed in a relatively short time, certain simplifications were made in the error studies. One of these was to generate smoothed estimates of only the covariance matrix of the state (but not the state itself) since this gives a statistical indication of the accuracy for each SIMS candidate. In the present effort smoothed estimates were generated only for a nominal attitude history in a circular orbit in an inertially-fixed plane. It was felt that the results for this case would also be a pretty good indication of the performance when the attitude deviates from nominal by the small amount expected in this mission.

The statistics of all significant random-type error sources were modeled in the data smoothing technique since this was considered necessary. However, in the case of bias-type errors, only the bias drift of each gyro was modeled in the smoother formulation since this bias was considered to be by far the most important bias-type error in any of the candidates. To

account for a bias error in the smoother formulation requires that it be estimated along with spacecraft attitude. Since this results in a significant increase in computation, the number of biases handled in this manner was kept to a minimum. However, it should be noted that the inclusion of bias drift in the smoother estimation also accounts, in a round-about manner, for the other bias-type errors since most of them affect system performance in a similar manner. This is shown in Section 5.5 where rough estimates are made of the contributions made by some of these other bias-type error sources when they are not accounted for in the error analysis.

Early in the present effort it was decided that real star distributions should be used in analyzing each candidate. Steps were therefore taken to generate a large star catalog containing all stars down to at least the limiting detector magnitude of each detector of interest. Afterwards, star distribution plots were generated for each candidate star sensor showing those stars that would pass through the field-of-view of the star sensor for a specified orbit. The plots were generated for a 9 AM - 9 PM sun-synchronous orbit at various times in the year 1972. Although other sun-synchronous orbits are also being considered in the EOS mission, it was felt that the 9 AM - 9 PM orbit was sufficient for the purposes of this study. Most of the results of the star availability study were reported in Ref. 141. However, some later results are given in Section 5.2. In addition, those star distribution cases used in the error studies are identified in Section 5.2.5.

In Section 5.3 the state and measurement equations, previously given for SIMS-A and -B in Ref. 141 are repeated with additional details. This section also gives the state and measurement equations for SIMS-D which were not previously reported.

The performance results obtained with the smoother formulation for SIMS-A, -B, and -D are shown in Section 5.4. These results represent what the performance would be if the system had only the errors modeled in the smoother formulation. Any imperfect or incomplete modeling of the system errors in the smoother formulation would of course degrade the results. However, it is felt that the results give a fairly good indication of the accuracy attainable with each candidate. And, what is more important in terms of trade considerations, they give a very good indication of the relative performance of these systems except for certain error sources which were not included in the data processing. Examples of such error sources are gyro scale factor error and gyro input axis misalignment in SIMS-A and -B which are considered separately in Section 5.5.

In Section 5.4 it will be seen that under typical conditions the accuracy of attitude determination in SIMS-B and -D is well within the desired value of 0.001° (1σ) per axis after one orbit of data processing. For SIMS-A the performance results were generated for a star mapper using either a cadmium sulfide (CdS) or silicon (SIL) detector. With either the CdS or SIL star mapper the typical performance in pitch and roll was within the required accuracy after one orbit of data processing. However, the typical performance in yaw for the SIL star mapper

did not drop below 0.001° until after 4 orbits of data processing; while that for the CdS star mapper was still slightly above 0.001° after 16 orbits of data processing.

It should be noted that the nominal values of the error sources and some system parameters used to generate most of the performance results in Section 5.4 represented the best available estimates at the time they were used. In some cases, more recent values have become available and some are still subject to change. This has been found especially true with star mappers of which there are many different versions being considered by industry. In Section 5.4 the sensitivity of performance is given for most of the important error sources and parameters so that one can ascertain the performance for different values of these error sources and parameters.

Since the performance of SIMS-A is marginal in comparison with the EOS specification, a more detailed simulation of this candidate is now under way to establish the poorest accuracy achievable with this candidate. This will include certain error sources which are considered important by some individuals but were not present in the smoothing results of Section 5.4.

Examples of such error sources are gyro scale factor error and gyro input axis misalignment which were considered to some extent in Section 5.5. The detailed simulation will also include displacement and libration of the vehicle attitude from nominal by the prescribed amount. The smoother formulation will be modified so that it can generate a smoothed estimate of state which will still consist of the six parameters: pitch, roll, yaw, and the three gyro drift biases. Consideration is also being given to

changing some of the design parameters to reflect the latest thinking of companies such as Honeywell.

In the follow-on effort, consideration will also be given to using line-of-sight information provided by the payload sensor imagery to update the vehicle attitude. Continuous attitude information will be provided by the SIMS gyros.

5.2 STAR AVAILABILITY STUDIES

5.2.1 INTRODUCTION

The objective of the star availability studies is to acquire spatial distribution data on stars for each detector being considered in order to be able to select representative and worst-case distributions for use by the error analysis programs. These programs require as input a swath catalog containing all stars, down to a designated limiting detector magnitude and listed in order of acquisition, that fall within the field-of-view of the particular SIMS candidate's star mapper or tracker for the specified orbit.

The general approach to the solution of this problem has been to first obtain a general star catalog which contains a sufficient number of stars to include all stars down to the necessary limiting detector magnitude for any detector of interest. Then the detector magnitudes were calculated and the detector star catalogs generated for each detector being considered. Finally these detector catalogs were used in conjunction with the orbit specification and the characteristics of a particular SIMS candidate to generate statistical data and availability plots for visual inspection in order to make a selection of typical and worst cases for the error studies.

~~Most of the results for the star availability studies~~ were reported in Interim Technical Report No. 2 (Reference 141). In this report some recent work done in this area is reported. The general star catalog and the individual detector catalogs have been revised to incorporate recent stellar photometric data. New star mapper distribution plots for the CdS and Si detectors have been generated for different detector magnitude acceptance limits. New star distribution plots have also been

generated for the star tracker showing the stars that are picked by the star selection criterion when the maximum outer gimbal angle of the tracker is reduced to ± 30 and ± 15 degrees. Also, the star distribution cases used in the error studies for each SIMS candidate are identified in this report.

5.2.2 UPDATE OF GENERAL STAR CATALOG AND DETECTOR CATALOGS

Thirteen-color narrow-band photometry data for 364 southern stars was received from the University of Arizona in February 1972. This data, which includes the 139 southern stars for which we had preliminary data, has been incorporated in an updated general star catalog. This catalog now contains data for 9064 stars, of which 1213 have been taken from the 13-color photometry catalog, 170 from the UBVRIJKL photometry catalog, and 7681 from the Yale Bright Star Catalog.

The detector star catalogs have been regenerated from this new general catalog as before and a new composite listing of the 968 stars whose magnitude for any detector is 4.0 or brighter appears in Appendix B. Table 5-1 gives the statistical data on the number of stars that are brighter than a given detector magnitude for each detector. It can be seen by comparison to the previous table* that several of the updated stars have changed in detector magnitude, although not appreciably. These revised detector catalogs were used to generate the new star distribution results.

5.2.3 STAR MAPPER DISTRIBUTION PLOTS

Eight new star mapper distribution plots have been generated to illustrate the effect that the minimum usable detector magnitude has on the error analysis results. For cadmium sulfide the minimum usable magnitude was varied by ± 0.75 , and for the silicon detector by ± 0.40 . As before, the small

*Table 5-3, Reference 141.

Table 5-1

NUMBER OF STARS BRIGHTER THAN OR
EQUAL TO A GIVEN DETECTOR MAGNITUDE

<u>MAGNITUDE</u>	<u>STAR TRACKER DETECTOR</u>	<u>STAR MAPPER DETECTORS</u>		
	<u>S-20</u>	<u>S-20</u>	<u>CdS</u>	<u>Si</u>
0.0	4	4	3	9
1.0	14	14	13	24
2.0	50	50	48	85
3.0	132	132	127	296
4.0	362	364	354	930
5.0	1075	1088	1071	2532
6.0	3289	3325	3270	6561

Table 5-2

STELLAR MAGNITUDE RANGES
DENOTED BY VARIOUS SYMBOLS

<u>SYMBOL</u>	<u>MAGNITUDE RANGE</u>
*	$M \leq (MUM - 1.0)$
x	$(MUM - 1.0) < M \leq (MUM - 0.5)$
+	$(MUM - 0.5) < M \leq MUM$
.	$MUM < M \leq (MUM + 2.0)$

where MUM is the specified minimum usable magnitude.

dots represent stars that are up to two magnitudes below the limit and which might be a source of noise. The other figures are similarly scaled and summarized in table 5-2. The plots can be found in Appendix C.

5.2.4 STAR TRACKER DISTRIBUTION PLOTS

New star tracker distribution plots were generated showing the stars that were selected in the star selection criterion when the maximum allowable out-of-orbital plane angle (or star tracker outer gimbal angle) was reduced to ± 30 and ± 15 degrees. The plots (shown in Appendix C) were generated for the single date of July 1, 1972, with stars being selected every 8, 16, 20, or 40 degrees of orbital motion.

It should be noted that the star tracker distribution results previously given in Appendix C of Reference 141 are for the year 1972 and not for the year 1971.

5.2.5 STAR DISTRIBUTION CASES SELECTED FOR ERROR STUDIES

The star distribution cases used in the error studies were selected by visual inspection of the star distribution plots and consideration of the statistical data printed at the right margin of the plots.

The cases selected for the star mapper in SIMS-A and -D are shown in Table 5-3 where the right hand column indicates whether it was a worst, typical, or special distribution case. A worst case was considered to be one with the least number of usable stars per orbit. Preliminary error results for more than one worst case indicated that the number of stars was more important than the uniformity of separation between stars. A typical case was considered to be one with an average number

Table 5-3

STAR MAPPER DISTRIBUTIONS SELECTED
FOR ERROR STUDIES

Detector	Minimum Usable Magnitude	FOV (Deg)	Number Of Stars Per Orbit	Date In 1972	Distribution Case*
Cds ↓	4.00	4	5	11/10	W
	↓	4	11	10/21	T
	↓	6	18	↓	S
	↓	8	22	↓	↓
	↓	10	30	↓	T**
	3.25	4	5	11/14	T
	4.75	4	26	8/18	T
Si ↓	3.6	4	13	9/23	W
	↓	4	20	12/28	T
	↓	6	37	↓	S
	↓	8	42	↓	↓
	↓	10	55	↓	T
	3.2	4	12	11/26	T
	3.2	8	25	10/01	T
	4.0	4	31	7/01	T
	4.0	8	61	8/14	T

- * W = Worst case with least number of stars
 T = Typical case with average number of stars
 and most uniform distribution
 S = Special case where orbit for typical at
 4° FOV was used for larger FOV's.

** For a 4° FOV and a minimum usable magnitude of 3.25 there are very few stars available in many orbits. Although the typical number of stars was 5, there were cases with only 2 stars per orbit. Based on the results of the error studies, even 5 stars per orbit would not be sufficient for SIMS-A.

of usable stars per orbit and a uniform star separation. The special cases are those where a larger star mapper FOV (6, 8, and 10 degrees) was used for the same orbit associated with the typical case selected for the 4 degree FOV. The star distribution cases for the silicon detector were used in SIMS-A and -D since both used the same star mapper.

No effort was made to select a worst star distribution case for SIMS-B since there was always a large number of usable stars within the angular range of the star tracker per orbit. In fact, a star selection technique was used to reduce the number of stars to a reasonable value and to establish some regularity in star measurement times. The orbit selected for all of the error studies was that associated with the star distribution plot for July 1, 1972 shown on page C-15 of Reference 141. The maximum star count for this plot (126 stars) was nearest the average for the six plots of this type. The star distribution cases used in the error analysis were generated by selecting stars at uniformly distributed points of spacecraft position (or true anomaly) in accordance with the criterion explained in Section 5.3.5.2 of Reference 141. Use was made of step sizes in true anomaly of 8, 16, 20, and 40 degrees, which correspond to 2.3, 4.7, 5.8 and 11.5 minute time intervals between successive star updates in a 105 minute orbit.

5.3 SYSTEM EQUATIONS

5.3.1 INTRODUCTION

In the following sub-sections the state and measurement equations are presented separately for each of the three SIMS candidates. Although some of the equations for SIMS-A and -B were previously given in Reference 141, it was felt that they should be repeated for completeness.

These equations employ various coordinate systems which were previously identified in ref. 141 as follows:

- Basic Inertial (I-frame)
- Orbit-Oriented Inertial (O-frame)
- Body-Fixed (B-frame)
- Star Tracker (for SIMS-B)
- Platform (for SIMS-D)

The matrix transformations between the above coordinate systems are also given in ref. 141.

In the present study use is made of the Fraser two-filter smoother formulation (See Section 5.4 of ref. 141) to evaluate the performance of each SIMS candidate. This formulation uses two "Kalman" filters, one to process the data forward from the beginning of the data interval to a point of interest, and the other to process the data backwards from the end of the data interval to the same point of interest. The resulting estimates of the two filters at the point of interest are then combined in an optimal manner to obtain a smoothed estimate. In the present effort smoothed estimates are made of only the covariance matrix of the state (but not the state itself) since this gives a statistical measure of the obtainable accuracy for each SIMS candidate.

~~-----~~The smoother formulation requires the state and measurement equations to be linear. In deriving these equations certain assumptions were made to reduce the computational load. One of the most important of these was the decision to use the smoother formulation to analyze the performance of each candidate for only a nominal attitude history. Although the actual vehicle attitude in an EOS mission may deviate (or librate) from nominal as much as 1.1 degrees about each axis, it is felt that the

nominal results will be a very good indication of the performance for these cases since the deviations are small. This is especially true if certain errors such as mounting and gyro scale factor errors are not present. The type of errors being referred to here are those that make their presence known only when the attitude deviates from nominal. Since these types of errors are not being accounted for in the present state and measurement equations, and only the covariance matrix of the state is being estimated in the smoother formulation, it is felt that the inclusion of attitude librations in the state equations is an unnecessary complication. However, it should not be inferred that these type of errors are being entirely neglected in the present effort since Section 5.5 gives some indication of the effect of these errors.

5.3.2 SYSTEM EQUATIONS FOR SIMS-A

5.3.2.1 State Equation for SIMS-A

For SIMS-A, expressing the state (or vehicle attitude) in terms of the inertial attitude angles θ , ϕ , and ψ results in a non-linear state equation. However, a linear state equation can be derived by using state vector elements that are perturbations of the three attitude angles. Perturbations in gyro bias drift have also been included in the state vector. The resulting linearized state vector is expressed as:

$$\underline{x} = \begin{bmatrix} \delta\theta \\ \delta\phi \\ \delta\psi \\ \delta B_x \\ \delta B_y \\ \delta B_z \end{bmatrix} \quad (5-1)$$

With the assumption of a circular orbit and a nominal attitude history, the state equation is:

$$\dot{\underline{x}} = \begin{bmatrix} 0 & 0 & 0 & | & 0 & -1 & 0 \\ 0 & 0 & -\omega_0 & | & 1 & 0 & 0 \\ 0 & \omega_0 & 0 & | & 0 & 0 & -1 \\ \hline & & & & 0 & & 0 \end{bmatrix} \underline{x} + \begin{bmatrix} 0 & -1 & 0 \\ 1 & 0 & 0 \\ 0 & 0 & -1 \\ \hline & & & 0 \end{bmatrix} \underline{u} \quad (5-2)$$

where ω_0 is the constant orbital rate, and \underline{u} is the noise introduced by gyro random drift and quantization effects. The matrix associated with \underline{u} is the matrix $G(t)$ required in the smoother formulation.

The transition matrix for this case is:

$$\Phi_{k,k-1} = \begin{bmatrix} 1 & 0 & 0 & | & 0 & -\Delta t_k & 0 \\ 0 & c\xi & -s\xi & | & s\xi/\omega_0 & 0 & (1-c\xi)/\omega_0 \\ 0 & s\xi & c\xi & | & (1-c\xi)/\omega_0 & 0 & -s\xi/\omega_0 \\ \hline & 0 & & & & I & \end{bmatrix} \quad (5-3)$$

where the subscripts k and $k-1$ correspond to the times t_k and t_{k-1} , at which updates are made with star mapper measurements; $\Delta t_k = t_k - t_{k-1}$; $\xi = \omega_0 \Delta t_k$; I is the identity matrix; and s and c are used to denote sine and cosine.

The gyro noise matrix V_k required in the smoother formulation is:

$$V_k = G_k Q_k G_k^T \quad (5-4)$$

where

$$G_k = (6 \times 3) \text{matrix} = \begin{bmatrix} 0 & -1 & 0 \\ 1 & 0 & 0 \\ 0 & 0 & -1 \\ \hline & 0 & \end{bmatrix} \quad (5-5)$$

and

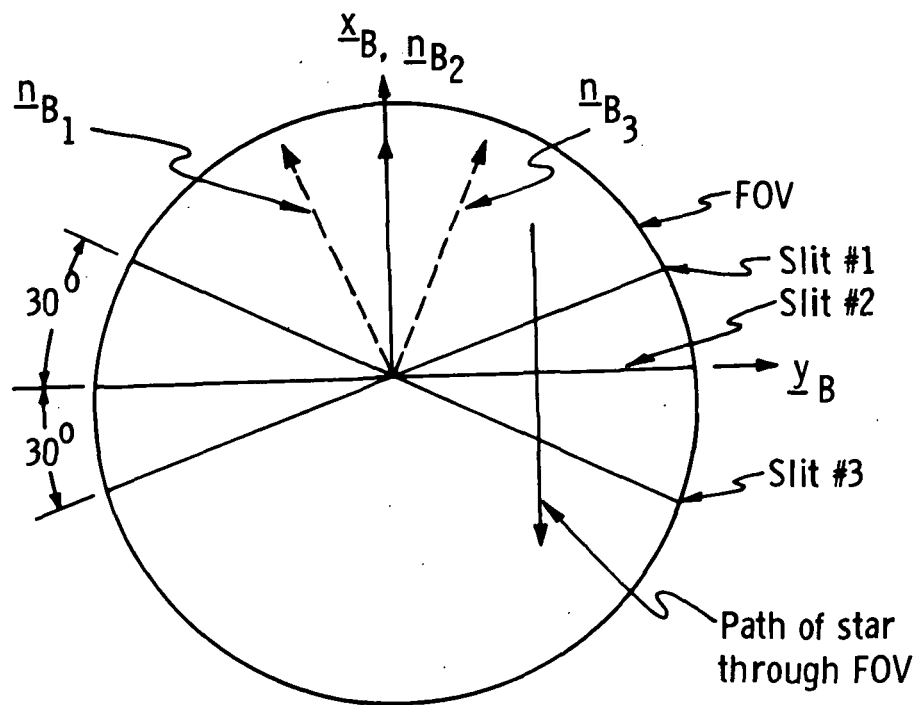
$$Q_k = q^2 \Delta t_k I \quad (5-6)$$

where q^2 represents the low frequency gyro drift power spectral density for each gyro. For SIMS-A (and SIMS-B) the gyro random drift rate has nominally been assumed to be a white noise process, although some error results were generated for SIMS-A using a random walk model.

5.3.2.2 Measurement Equations For SIMS-A

The star mapper is a fixed instrument using relatively small-FOV concentric optics (4 deg. FOV) to focus the star field onto the detector surface. The detector consists of several photo-sensitive elements called slits. As the vehicle rotates in inertial space the stars transit the slits as shown in Figure 5-1. Each slit and the optical axis of the mapper defines a fixed plane in body-fixed coordinates. When a star image crosses one of the slits the direction of the star is known to be in the plane of the associated slit. In the present studies it is assumed that the mapper has three slits and its optical axis is nominally pointing towards zenith, although some performance results have been obtained for the mapper pointing 30 degrees ahead of zenith in the orbital plane.

Two different techniques (with their associated measurement equations) have been used in the present effort to process



Note: Optical axis is normal to figure at center of FOV and directed outwards

Figure 5-1 Slit Pattern of Star Mapper

the star transits for SIMS-A. One essentially represents the technique in SPARS where the attitude is updated for each star transit of a slit. This technique is the original technique (denoted as such) used to generate most of the results in the present effort. The second technique (denoted as the alternate technique) does the same thing as the original technique for Slit #2, but combines the star transits of the other two slits to obtain the line-of-sight to a star.

5.3.2.2.1 Original Technique of Measurement

At the time of star transit, a measure of the attitude error is obtained by the following dot product:

$$\text{DOT} = \underline{n}_{B_j} \cdot \left[T_{BO} T_{OI} \underline{s}_I \right] \quad (5-7)$$

where \underline{n}_{B_j} is the unit normal vector of the j^{th} slit plane in body-fixed coordinates and \underline{s}_I is the unit vector of the cataloged star in basic inertial coordinates, which is transformed to body-fixed coordinates using T_{BO} and T_{OI} , where T_{BO} has been computed for the time of transit and T_{OI} is assumed to be fixed and known. Ideally DOT would be zero if there were no errors in the star mapper measurement and the vehicle attitude as expressed by T_{BO} . Since DOT is a small quantity for the level of errors expected in this type of mission, it can be interpreted (except for mapper error) as being the attitude error in radians about an axis normal to \underline{n}_{B_j} and the estimated star direction. However, note that DOT is only a one-dimensional measure of the attitude error and does not indicate how much error exists about each of the three body axes. If a slit is parallel to one of the vehicle axes (as is the case for Slit #2 and the pitch axis \underline{y}_B in Figure 5-1) DOT will be a good indication of the error about that axis. However, for Slits #1 or #3 in Figure 5-1 the same value of DOT can be obtained for different combinations of

pitch, roll, and yaw error. In the present technique (i.e., original technique) a given value of DOT for Slit #1 or #3 is used to update pitch, roll, and yaw by using weighting factors in accordance with the trigonometric resolution of DOT into pitch, roll, and yaw components. Obviously, this can lead to errors in updating pitch, roll, and yaw for a given star transit and this particular aspect has bothered some individuals and is the reason for implementation of the alternate technique. Other techniques are also being considered for this purpose. It should be noted, however, that incorrect updates for one slit will be essentially cancelled by incorrect updates for another slit because of symmetry of the slit pattern. Also, it is presently felt that such errors in update are gradually washed out when processing a reasonable amount of data.

The measurement equation for this technique is

$$z_k = H_k x_k + v_k \quad (5-8)$$

where z_k denotes the star measurement (DOT) at t_k , H_k is the geometry matrix relating perturbations in state to perturbations in measurement, and v_k is the noise in the measurement. In the present case, z_k is a scalar and the elements of H_k are

$$H_x = \frac{\partial}{\partial x} (\text{DOT}) \quad (x=\theta, \phi, \psi, \dots) \quad (5-9)$$

$$H_x = n_{B_j} \cdot \left\{ \frac{\partial}{\partial x} \left[T_{BO} \right] T_{OI} s_I \right\} \quad (5-10)$$

Using the expression for T_{BO} in Equation 5-3 of ref. 141 we have

$$H_{\theta} = \underline{n}_{B_j} \cdot \begin{bmatrix} -c\psi c\theta & -c\psi s\theta & 0 \\ -s\psi s\phi s\theta & +s\psi c\theta s\phi & 0 \\ -s\psi c\theta & -s\psi s\theta & 0 \\ +c\psi s\phi s\theta & -c\psi c\theta s\phi & 0 \\ c\phi s\theta & -c\phi c\theta & 0 \end{bmatrix} T_{OI} \underline{s}_I \quad (5-11)$$

$$H_{\phi} = \underline{n}_{B_j} \cdot \begin{bmatrix} s\psi c\phi c\theta & s\psi s\theta c\phi & -s\psi s\phi \\ -c\psi c\phi c\theta & -c\psi s\theta c\phi & c\psi s\phi \\ s\phi c\theta & s\phi s\theta & c\phi \end{bmatrix} T_{OI} \underline{s}_I \quad (5-12)$$

$$H_{\psi} = \underline{n}_{B_j} \cdot \begin{bmatrix} s\psi s\theta & -s\psi c\theta & c\psi c\phi \\ +c\psi s\phi c\theta & +c\psi s\theta s\phi & 0 \\ -c\psi s\theta & c\psi c\theta & s\psi c\phi \\ +s\psi s\phi c\theta & +s\psi s\theta s\phi & 0 \\ 0 & 0 & 0 \end{bmatrix} T_{OI} \underline{s}_I \quad (5-13)$$

$$H_{B_x} = H_{B_y} = H_{B_z} = 0 \quad (5-14)$$

Note that the above expressions for H_x are correct for all values of θ , ϕ , and ψ . Since we are only analyzing the performance for a nominal attitude history (i.e., $\phi = \psi = 0$) the above expressions can be simplified as follows:

$$H_{\theta} = \underline{n}_{B_j} \cdot \begin{bmatrix} -c\theta & -s\theta & 0 \\ 0 & 0 & 0 \\ s\theta & -c\theta & 0 \end{bmatrix} \underline{s}_O \quad (5-15)$$

$$H_{\phi} = \underline{n}_{B_j} \cdot \begin{bmatrix} 0 & 0 & 0 \\ -c\theta & -s\theta & 0 \\ 0 & 0 & 1 \end{bmatrix} \underline{s}_O \quad (5-16)$$

$$H_{\psi} = \underline{n}_{B_j} \cdot \begin{bmatrix} 0 & 0 & 1 \\ -s\theta & c\theta & 0 \\ 0 & 0 & 0 \end{bmatrix} \underline{s}_O \quad (5-17)$$

where $\underline{s}_O = T_{OI} \underline{s}_I$. Except for a change in notation, it is seen that H_{θ} , H_{ϕ} , and H_{ψ} are same as reported in Section 5.4.3.2 of ref. 141.

Since the star mapper measurement z_k in Equation 5-8 is a scalar, the matrix H_k will be a 1×6 matrix as follows:

$$H_k = [H_{\theta}, H_{\phi}, H_{\psi}, 0, 0, 0] \quad (5-18)$$

The covariance matrix of the measurement noise v_k is R_k which is given as a scalar quantity.

As previously indicated, this technique is essentially the same as that used in SPARS. The differences between the two approaches are discussed in detail in Appendix D. These differences are in the definitions of the orbit-oriented inertial coordinate system and the attitude angles. In addition, the expressions for H_{θ} , H_{ϕ} , and H_{ψ} have been simplified in the present effort by setting $\phi = \psi = 0$ since most of the studies are for a nominal attitude history. This same simplification could have been made in the SPARS equations for a nominal attitude history.

5.3.2.2.2 Alternate Technique of Measurement

The alternate technique of measurement with the star mapper is the same as the original technique in the case of star transits of Slit #2 since this slit is presently assumed to be parallel to the pitch axis. However, for Slits #1 and #3 of Figure 5-1, the transit data is used in such a way as to determine a complete line-of-sight to a star. It is assumed that only stars which transit both of these slits would be used in this method.

The manner in which the line-of-sight to a star is determined is as follows: Let us assume that a star transits Slits #1 and #3 at times t_1 and t_3 , respectively. Each slit defines a fixed plane in body coordinates. For Slits #1 and #3 the corresponding planes are mathematically represented in body coordinates by the unit normal vectors \underline{n}_{B_1} and \underline{n}_{B_3} . Although these planes are fixed in body coordinates, their orientations with respect to inertial space are continuously changing because of vehicle attitude motion. At time t_1 the star is in the body fixed plane defined by \underline{n}_{B_1} . At time t_3 the star is in the body-fixed plane defined by \underline{n}_{B_3} . Each of these planes at their associated time of transit defines a plane in inertial space containing the star. To obtain in body coordinates at time t_3 the orientation of the plane defined by \underline{n}_{B_1} at t_1 the following transformation is performed:

$$\underline{n}_{B_1}(t_3) = T_{BO}(t_3) T_{OB}(t_1) \underline{n}_{B_1} \quad (5-19)$$

where $T_{BO}(t_3)$ and $T_{OB}(t_1)$ represent transformations between the body and orbit-oriented coordinate systems.

At time t_3 we therefore have two different planes (represented by \underline{n}_{B_3} and $\underline{n}_{B_1}(t_3)$) which contain the star.

Consequently, the direction of the star must be along the line of intersection of the two planes. This direction is defined by the unit vector \underline{s}_B where:

$$\underline{s}_B = \text{UNIT} [\underline{n}_{B_3} \times \underline{n}_{B_1}(t_3)] \quad (5-20)$$

In the present case, \underline{s}_B represents the measured direction of the star in body coordinates. The estimated direction \underline{s}'_B of the star in body coordinates is:

$$\underline{s}'_B = T_{B_0}(t_3) \underline{s}_0 \quad (5-21)$$

where \underline{s}_0 is the unit vector of the cataloged direction of the star in orbit-oriented coordinates.

In the present application it can be shown¹⁵⁰ that the measured star direction \underline{s}_B is essentially independent of the state elements $\delta\theta$, $\delta\phi$, and $\delta\psi$. However, it is dependent upon the state elements δB_x , δB_y , and δB_z as shown by the following approximate expression for \underline{s}_B taken from Reference 150:

$$\underline{s}_B \approx \frac{1}{2} \left\{ \begin{bmatrix} -s\Delta\theta \\ \sqrt{3} s\Delta\theta \\ -2 \end{bmatrix} + \begin{bmatrix} -1 \\ \sqrt{3} \\ s\Delta\theta \end{bmatrix} \Delta t \delta B_y + \begin{bmatrix} \frac{1}{\sqrt{3}} \\ -1 \\ -\sqrt{3} s\Delta\theta \end{bmatrix} \Delta t \delta B_x + \begin{bmatrix} 0 \\ 0 \\ \sqrt{3} - \frac{1}{\sqrt{3}} \end{bmatrix} \Delta t \delta B_z \right\} \quad (5-22)$$

where $\Delta\theta = \theta(t_3) - \theta(t_1)$ and $\Delta t = t_3 - t_1$.

To determine the H matrix for this technique it would seem that the approach would be different from that used for the star tracker in SIMS-B due to the following reason: Although \underline{s}_B' , in both cases, has the same dependence on $\delta\theta$, $\delta\phi$, and $\delta\psi$, the new technique also has the additional dependence of \underline{s}_B on δB_x , δB_y , and δB_z . In the approach taken until now, the dependence of \underline{s}_B on δB_x , δB_y , and δB_z has been neglected since preliminary calculations indicate that the errors introduced by the initial values used for δB_x , δB_y , and δB_z are not large enough to prevent rapid reduction in the magnitudes of δB_x , δB_y , and δB_z to values which have negligible effect on \underline{s}_B during normal data processing. Consequently, the same measurement equation (and H matrix), given for SIMS-B in Section 5.4.3.3 of ref. 141 and in Section 5.3.3.2 of this report, has been used in this technique, except for the difference in error sources. This measurement equation is as follows:

$$\underline{z}_k = \begin{bmatrix} \underline{H}_\theta & \underline{H}_\phi & \underline{H}_\psi & 0 & 0 & 0 \\ 0 & 0 & 0 & 0 & 0 & 0 \end{bmatrix} \underline{x}_k + A_k \begin{bmatrix} v_1 \\ v_3 \end{bmatrix} \quad (5-23)$$

where v_1 and v_3 are the measurement noises of Slits #1 and #3, respectively. The elements of the matrix H_k are two dimensional vectors as follows:

$$\underline{H}_\theta = \begin{bmatrix} -c\theta & -s\theta & 0 \\ 0 & 0 & 0 \end{bmatrix} \underline{s}_0 \quad (5-24)$$

$$\underline{H}_\phi = \begin{bmatrix} 0 & 0 & 0 \\ -c\theta & -s\theta & 0 \end{bmatrix} \underline{s}_0 \quad (5-25)$$

$$\underline{H}_\psi = \begin{bmatrix} 0 & 0 & 1 \\ -s\theta & c\theta & 0 \end{bmatrix} \underline{s}_0 \quad (5-26)$$

The matrix A_k can be shown (Reference 150) to be approximately:

$$A_k = \begin{bmatrix} \frac{1}{\sqrt{3}} & \frac{1}{\sqrt{3}} \\ -1 & 1 \end{bmatrix} \quad (5-27)$$

and the covariance matrix R_k used in the smoother formulation is:

$$R_k = A_k \begin{bmatrix} \sigma_{v_1}^2 & 0 \\ 0 & \sigma_{v_3}^2 \end{bmatrix} A_k^T \quad (5-28)$$

5.3.3 SYSTEM EQUATIONS FOR SIMS-B

5.3.3.1 State Equation for SIMS-B

Since SIMS-B has strapped-down gyros like SIMS-A, the attitude and gyro bias drift estimation problem is the same. For this reason, the linearized state equations, the transition matrix, and the gyro-noise matrix are the same as for SIMS-A.

5.3.3.2 Measurement Equation for SIMS-B

SIMS-B has a two-gimbal star tracker with the gimbal angles defined as shown in Figure 5-3 of ref. 141. This figure shows the outer gimbal angle ϕ , about the body roll axis x_B , and the inner gimbal angle, θ_T , about an axis displaced from the body pitch axis y_B by the angle ϕ . In the error studies

the star tracker is pointing towards zenith when the gimbal angles are zero. The outer gimbal can rotate through ± 45 degrees and the inner gimbal through ± 15 degrees. It is not required that a star be exactly at the center of the FOV since the displacement of the star in the FOV is indicated by two small angles, α_T and β_T , as shown in Figure 5-4 of ref. 141.

The measured direction of a star in body-fixed coordinates is given by the following unit vector:

$$\underline{s}_B = \begin{bmatrix} \beta_T c\theta_T - s\theta_T \\ -\alpha_T c\phi + \beta_T s\theta_T s\phi + c\theta_T s\phi \\ -\alpha_T s\phi - \beta_T s\theta_T c\phi - c\theta_T c\phi \end{bmatrix} \quad (5-29)$$

The estimated direction of a star in body-fixed coordinates is given by the following unit vector:

$$\underline{s}'_B = T_{BO} \underline{s}_O \quad (5-30)$$

where \underline{s}_O is the cataloged star direction in orbit-oriented coordinates.

As before, the measurement equation is

$$\underline{z}_k = H_k \underline{x}_k + \underline{v}_k \quad (5-31)$$

where the components of H_k are

$$\underline{H}_x = \frac{\partial}{\partial \underline{x}} \left[T_{BO} \right] \underline{s}_O \quad (\underline{x} = \theta, \phi, \psi, \dots) \quad (5-32)$$

Since \underline{s}_B and \underline{s}'_B are unit vectors the measurement equation requires only two components of each vector. The measurement equation in this case is:

$$\underline{z}_k = \begin{bmatrix} \underline{H}_\theta & \underline{H}_\phi & \underline{H}_\psi & 0 & 0 & 0 \\ 0 & 0 & 0 & 0 & 0 & 0 \end{bmatrix} \underline{x}_k + A_k \begin{bmatrix} v_{\theta_T} \\ v_{\phi} \\ v_{\alpha_T} \\ v_{\beta_T} \end{bmatrix} \quad (5-33)$$

where the v 's are the noises associated with the star tracker measurement angles, and the elements of the matrix H_k are two-dimensional vectors as follows:

$$\underline{H}_\theta = \begin{bmatrix} -c\theta & -s\theta & 0 \\ 0 & 0 & 0 \end{bmatrix} \underline{s}_0 \quad (5-34)$$

$$\underline{H}_\phi = \begin{bmatrix} 0 & 0 & 0 \\ -c\theta & -s\theta & 0 \end{bmatrix} \underline{s}_0 \quad (5-35)$$

$$\underline{H}_\psi = \begin{bmatrix} 0 & 0 & 1 \\ -s\theta & c\theta & 0 \end{bmatrix} \underline{s}_0 \quad (5-36)$$

Note that the above expressions for \underline{H}_x are simple since we are considering the performance of the smoother formulation for only a nominal attitude history.

The components of the noise transformation matrix A_k can be obtained by appropriate differentiation of the expression for \underline{s}_B in Equation 5-29 with respect to each measurement angle. The matrix in this case is:

$$A_k = \begin{bmatrix} -\beta_T s\theta_T - c\theta_T & 0 & 0 & c\theta_T \\ -s\phi(s\theta_T - \beta_T c\theta_T) & c\phi(c\theta_T + \beta_T s\theta_T) + \alpha_T s\phi & -c\phi & s\phi s\theta_T \end{bmatrix} \quad (5-37)$$

where θ_T , ϕ , α_T , and β_T are the star tracker measurements at time t_k .

The covariance matrix R_k required in the smoother formulation is:

$$R_k = A_k \begin{bmatrix} \sigma_{\theta_T}^2 & 0 & 0 & 0 \\ 0 & \sigma_{\phi}^2 & 0 & 0 \\ 0 & 0 & \sigma_{\alpha_T}^2 & 0 \\ 0 & 0 & 0 & \sigma_{\beta_T}^2 \end{bmatrix} A_k^T \quad (5-38)$$

5.3.4 SYSTEM EQUATIONS FOR SIMS-D

SIMS-D utilizes a 3-gimbaled gyro system, and the gyro platform is fully stabilized with respect to inertial space. Due to the existence of a stabilized gyro platform, one can now define the attitude that is to be estimated to be that of the gyro platform instead of the vehicle. The advantage of this is that the attitude of the platform can be immediately expressed in a linear state equation while that for the vehicle requires linearization. Once the attitude of the platform has been determined with respect to the orbit-oriented coordinate system, the attitude of the vehicle with respect to this coordinate system can be obtained by merely using the gimbal angles at the time of interest. If the axes of the gyro platform are coincident with those of the orbit-

oriented coordinate system, and the proper gimbal angle sequence is chosen, the gimbal angles will be a direct indication of the angles θ , ϕ , and ψ used in SIMS-A and -B.

For SIMS-D the smoother formulation was only used to obtain the accuracy of attitude determination for the platform. The results were then transformed to body-fixed coordinates to show the equivalent accuracy of attitude determination for the vehicle. In doing this, no allowance was made in the computer results for the additional errors associated with the reading of the gimbal angles. However, it should be noted that the effect of these additional error sources can be reduced by using a second smoother to process multiple sets of gimbal angle readings. Such a smoother was not considered in the present effort, but one can make reasonably good estimates of what the results would be for a few sets of gimbal angle readings. Examples of this are given later with the results.

For SIMS-D it is assumed that the platform coordinate system coincides with the orbit-oriented coordinate system except for small misalignment angles α , β , and γ which are used in an Euler sequence as shown in Figure 5-2. The transformation from orbital to platform coordinates is given approximately by:

$$T_{PO} \approx \begin{bmatrix} 1 & 0 & 0 \\ 0 & 1 & -\gamma \\ 0 & -\gamma & 1 \end{bmatrix} \begin{bmatrix} 1 & 0 & -\beta \\ 0 & 1 & 0 \\ \beta & 0 & 1 \end{bmatrix} \begin{bmatrix} 1 & \alpha & 0 \\ -\alpha & 1 & 0 \\ 0 & 0 & 1 \end{bmatrix}$$

$$T_{PO} \approx \begin{bmatrix} 1 & \alpha & -\beta \\ -\alpha & 1 & \gamma \\ \beta & -\gamma & 1 \end{bmatrix} \quad (5-39)$$

The orientation of the body-fixed coordinate system with respect to the platform axes is given by three gimbal

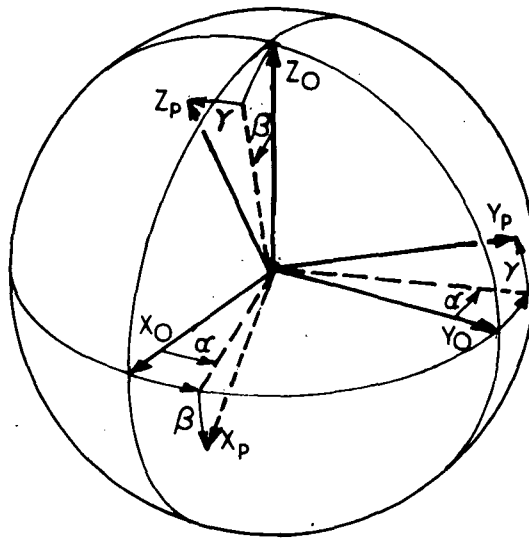


Figure 5-2 Platform and Orbital-Inertial Coordinate Systems

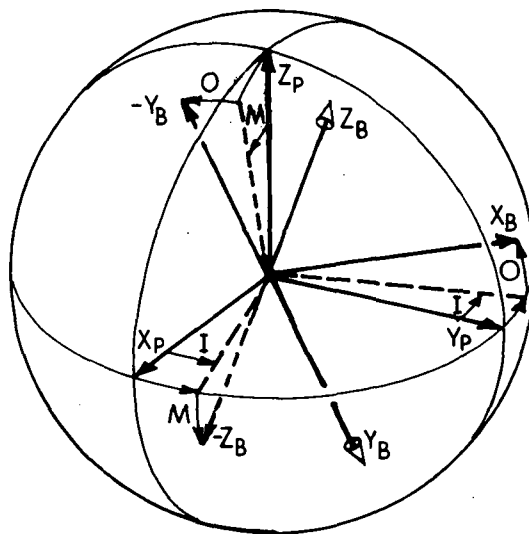


Figure 5-3 Body-Fixed and Platform Coordinate Systems

angles I, M, and O, which are respectively the inner, middle, and outer gimbal angles. The sequence of gimbal angle transformations shown in Figure 5-3 was chosen so that I, M, and O would correspond to the Euler angles θ , ϕ , and ψ used in SIMS-A and -B. If there were no misalignment between the platform and orbit-oriented coordinate systems, the angles I, M, and O would equal θ , ϕ , and ψ , respectively. The transformation from platform to body-fixed coordinates is given by:

$$T_{BP} = \begin{bmatrix} 0 & 1 & 0 \\ 0 & 0 & -1 \\ -1 & 0 & 0 \end{bmatrix} \begin{bmatrix} 1 & 0 & 0 \\ 0 & cO & sO \\ 0 & -sO & cO \end{bmatrix} \begin{bmatrix} cM & 0 & -sM \\ 0 & 1 & 0 \\ sM & 0 & cM \end{bmatrix} \begin{bmatrix} cI & sI & 0 \\ -sI & cI & 0 \\ 0 & 0 & 1 \end{bmatrix} \quad (5-40)$$

5.3.4.1 State Equation for SIMS-D

In SIMS-D the relationship between the Euler angle rates $\dot{\alpha}$, $\dot{\beta}$, and $\dot{\gamma}$ and the platform rates ω_x , ω_y , and ω_z can be expressed as follows:

$$\begin{bmatrix} \dot{\alpha} \\ \dot{\beta} \\ \dot{\gamma} \end{bmatrix} = \begin{bmatrix} 1 & s\beta \, s\gamma/c\beta & s\beta \, c\gamma/c\beta \\ 0 & c\gamma & -s\gamma \\ 0 & s\gamma/c\beta & c\gamma/c\beta \end{bmatrix} \begin{bmatrix} \omega_z \\ \omega_y \\ \omega_x \end{bmatrix} \quad (5-41)$$

Since the platform is stabilized, the rates ω_z , ω_y , and ω_x will be simply the gyro bias drift rates B_z , B_y , and B_x , respectively, where gyro random drift rates have been neglected.

If we assume that α , β , and γ are very small, Equation 5-41 can be expressed as follows:

$$\begin{bmatrix} \dot{\alpha} \\ \dot{\beta} \\ \dot{\gamma} \end{bmatrix} = \begin{bmatrix} 1 & 0 & 0 \\ 0 & 1 & 0 \\ 0 & 0 & 1 \end{bmatrix} \begin{bmatrix} B_z \\ B_y \\ B_x \end{bmatrix} \quad (5-42)$$

Using the above relationship, we can now give a state equation for the state parameters α , β , γ , B_z , B_y , and B_x as follows:

$$\dot{\underline{x}} = \begin{bmatrix} & & & 1 & 0 & 0 \\ & 0 & & 0 & 1 & 0 \\ - & - & - & 0 & 0 & 1 \\ & 0 & & & 0 & \end{bmatrix} \underline{x} + \begin{bmatrix} 1 & 0 & 0 \\ 0 & 1 & 0 \\ 0 & 0 & 1 \\ 0 & & \end{bmatrix} \underline{v} \quad (5-43)$$

where \underline{v} is the noise introduced by gyro random drift and \underline{x} is the following state vector

$$\underline{x} = \begin{bmatrix} \alpha \\ \beta \\ \gamma \\ B_z \\ B_y \\ B_x \end{bmatrix} \quad (5-44)$$

The transition matrix for this case is

$$\Phi_{k,k-1} = \begin{bmatrix} & & & \Delta t_k & 0 & 0 \\ & I & & 0 & \Delta t_k & 0 \\ - & - & - & 0 & 0 & \Delta t_k \\ & 0 & & & I & \end{bmatrix} \quad (5-45)$$

where Δt_k is the time between successive star measurements at times t_k and t_{k-1} , and O and I are 3×3 null and identity matrices, respectively.

The gyro noise matrix V_k required in the smoother formulation is:

$$V_k = G_k Q_k G_k^T \quad (5-46)$$

where

$$G_k = 6 \times 3 \text{ matrix} = \begin{bmatrix} I \\ - \\ 0 \end{bmatrix} \quad (5-47)$$

and

$$Q_k = q^2 \Delta t_k^2 I \quad (5-48)$$

where the gyro random drift error is now based on the TGG noise model of subsection 5.5 of ref. 141, although some results were obtained for a white noise as given by the expression for Q_k in Equation 5-6.

5.3.4.2 Measurement Equations for SIMS-D

Two different techniques (analogous to those employed in SIMS-A) were used to process the star transits of the mapper. These techniques are also denoted as the "original" and "alternate" techniques of measurement, and separate equations are given for each. Most of the error results generated in the present effort for SIMS-D used the original technique which is treated as nominal. However, some results were generated with the alternate technique for purposes of comparison.

5.3.4.2.1 Original Technique of Measurement

This technique is similar to the original technique described for SIMS-A in Section 5.3.2.2.1 except that the dot

product is computed for two vectors in platform coordinates instead of body-fixed coordinates:

$$\text{DOT} = \underline{n}_{P_j} \cdot \begin{bmatrix} T_{PO} & T_{OI} & \underline{s}_I \end{bmatrix} \quad (5-49)$$

where \underline{s}_I is the unit vector of the cataloged star in basic inertial coordinates, which is transformed to platform coordinates using T_{PO} and T_{OI} , where T_{PO} is given in Equation 5-39 and T_{OI} is assumed to be fixed and known. The vector \underline{n}_{P_j} is the unit normal vector of the j^{th} slit plane in platform coordinates obtained as follows:

$$\underline{n}_{P_j} = T_{BP}^{-1} \underline{n}_{B_j} \quad (5-50)$$

where \underline{n}_{B_j} is the unit normal vector of the j^{th} slit plane in body-fixed coordinates and T_{BP} is given in Equation 5-40.

The measurement equation for this technique is:

$$z_k = \begin{bmatrix} H_\alpha & H_\beta & H_\gamma & 0 & 0 & 0 \end{bmatrix} \underline{x}_k + A_k \begin{bmatrix} v_I \\ v_M \\ v_O \\ v_S \end{bmatrix} \quad (5-51)$$

where v_I , v_M , v_O , and v_S are the errors in the measurement of the inner, middle, and outer gimbal angles and the star mapper. The elements of the matrix H_k are:

$$H_x = \frac{\partial}{\partial x} (\text{DOT}) \quad (x=\alpha, \beta, \gamma) \quad (5-52)$$

$$H_x = \underline{n}_{P_j} \cdot \left\{ \frac{\partial}{\partial x} \begin{bmatrix} T_{PO} \end{bmatrix} T_{OI} \underline{s}_I \right\} \quad (5-53)$$

$$H_{\alpha} = \underline{n}_{P_j} \cdot \begin{bmatrix} 0 & 1 & 0 \\ -1 & 0 & 0 \\ 0 & 0 & 0 \end{bmatrix} \underline{s}_O \quad (5-54)$$

$$H_{\beta} = \underline{n}_{P_j} \cdot \begin{bmatrix} 0 & 0 & -1 \\ 0 & 0 & 0 \\ 1 & 0 & 0 \end{bmatrix} \underline{s}_O \quad (5-55)$$

$$H_{\gamma} = \underline{n}_{P_j} \cdot \begin{bmatrix} 0 & 0 & 0 \\ 0 & 0 & 1 \\ 0 & -1 & 0 \end{bmatrix} \underline{s}_O \quad (5-56)$$

where $\underline{s}_O = T_{OI} \underline{s}_I$.

The noise transformation matrix A_k is the following 1×4 matrix:

$$A_k = [A_I, A_M, A_O, A_S] \quad (5-57)$$

where

$$A_S = 1$$

$$A_x = \frac{\partial}{\partial x} \text{ (DOT)} \quad (x=I, M, O) \quad (5-58)$$

$$A_x = \left\{ \frac{\partial}{\partial x} \left[T_{BP}^{-1} \right] \underline{n}_{B_j} \right\} \cdot \left\{ T_{PO} T_{OI} \underline{s}_I \right\} \quad (5-59)$$

$$A_I = \begin{bmatrix} -s_O s_M s_I & c_O s_M s_I & c_M s_I \\ -c_O c_I & -s_O c_I & \\ s_O s_M c_I & -c_O s_M c_I & -c_M c_I \\ -c_O s_I & -s_O s_I & \\ 0 & 0 & 0 \end{bmatrix} \underline{n}_{B_j} \cdot \underline{s}_P \quad (5-60)$$

$$A_M = \begin{bmatrix} sOcMcI & -cOcMcI & sMcI \\ sOcMsI & -cOcMsI & sMsI \\ -sOsM & cOsM & cM \end{bmatrix} \underline{n}_{B_j} \cdot \underline{s}_p \quad (5-61)$$

$$A_O = \begin{bmatrix} cOsMcI & sOsMcI & 0 \\ +sOsI & -cOsI & 0 \\ cOsMsI & sOsMsI & 0 \\ -sOcI & +cOcI & 0 \\ cOcM & sOcM & 0 \end{bmatrix} \underline{n}_{B_j} \cdot \underline{s}_p \quad (5-62)$$

where $\underline{s}_p = T_{PO} T_{OI} \underline{s}_I$.

Since the smoothing formulation is being used to analyze only the nominal gimbal angle situation (i.e., $M=0=0$), the following simplification can be made:

$$A_I = \begin{bmatrix} -cI & 0 & sI \\ -sI & 0 & -cI \\ 0 & 0 & 0 \end{bmatrix} \underline{n}_{B_j} \cdot \underline{s}_p \quad (5-63)$$

$$A_M = \begin{bmatrix} 0 & -cI & 0 \\ 0 & -sI & 0 \\ 0 & 0 & 1 \end{bmatrix} \underline{n}_{B_j} \cdot \underline{s}_p \quad (5-64)$$

$$A_O = \begin{bmatrix} 0 & -sI & 0 \\ 0 & cI & 0 \\ 1 & 0 & 0 \end{bmatrix} \underline{n}_{B_j} \cdot \underline{s}_p \quad (5-65)$$

The covariance matrix R_k required in the smoother formulation is the following scalar:

If the effects of gyro bias drift on the measurement are neglected, the measurement equation can be expressed as follows:

$$\underline{z}_k = \begin{bmatrix} \underline{H}_\alpha & \underline{H}_\beta & \underline{H}_\gamma & 0 & 0 & 0 \\ 0 & 0 & 0 & 0 & 0 & 0 \end{bmatrix} \underline{x}_k + A_k \underline{v}_k \quad (5-71)$$

where \underline{H}_α , \underline{H}_β , and \underline{H}_γ are two-dimensional vectors constructed with the first two components of the following vectors:

$$\underline{H}_x = \frac{\partial}{\partial x} \begin{bmatrix} T_{PO} \end{bmatrix} \underline{s}_0 \quad (x=\alpha, \beta, \gamma) \quad (5-72)$$

$$\underline{H}_\alpha = \begin{bmatrix} 0 & 1 & 0 \\ -1 & 0 & 0 \\ 0 & 0 & 0 \end{bmatrix} \underline{s}_0 \quad (5-73)$$

$$\underline{H}_\beta = \begin{bmatrix} 0 & 0 & -1 \\ 0 & 0 & 0 \\ 1 & 0 & 0 \end{bmatrix} \underline{s}_0 \quad (5-74)$$

$$\underline{H}_\gamma = \begin{bmatrix} 0 & 0 & 0 \\ 0 & 0 & 1 \\ 0 & -1 & 0 \end{bmatrix} \underline{s}_0 \quad (5-75)$$

In the present technique there are eight random errors associated with the measurement. In addition to the errors v_1 and v_3 for Slits #1 and #3, there are the errors associated with the reading of the gimbal angles I, M, and O at times t_1 and t_3 . It is assumed that the gimbal angle errors at t_1 are independent of those at t_3 . The error vector \underline{v}_k in Equation 5-71 can therefore be expressed as follows:

$$\underline{v}_k^T = \left[v_{I_1}, v_{M_1}, v_{O_1}, v_{I_3}, v_{M_3}, v_{O_3}, v_1, v_3 \right] \quad (5-76)$$

where the subscripts 1 and 3 for the gimbal angle errors correspond to times t_1 and t_3 .

The noise transformation matrix A_k is the following 2×8 matrix:

$$A_k = \left[\underline{A}_{I_1} \mid \underline{A}_{M_1} \mid \underline{A}_{O_1} \mid \underline{A}_{I_3} \mid \underline{A}_{M_3} \mid \underline{A}_{O_3} \mid \underline{A}_{v_1} \mid \underline{A}_{v_3} \right] \quad (5-77)$$

where the first six elements are two dimensional vectors constructed with the first two components of the following vectors:

$$\underline{A}_{w_j} = \frac{\partial}{\partial w_j} (\underline{s}_p) \quad \begin{cases} w = (I, M, O) \\ j = (1, 3) \end{cases} \quad (5-78)$$

$$\underline{A}_{w_1} = \text{UNIT} \left\{ \left[T_{PB}(t_3) \underline{n}_{B_3} \right] \times \left[\frac{\partial T_{PB}(t_1)}{\partial w_1} \underline{n}_{B_1} \right] \right\} \quad (5-79)$$

$$\underline{A}_{w_3} = \text{UNIT} \left\{ \left[\frac{\partial T_{PB}(t_3)}{\partial w_3} \underline{n}_{B_3} \right] \times \left[T_{PB}(t_1) \underline{n}_{B_1} \right] \right\} \quad (5-80)$$

It should be noted that the angles M and O were set to zero after derivation of each of the above vectors since the smoother formulation was only used to generate results for the nominal case.

The remaining two elements of the matrix A_k are:

$$\underline{A}_{v_1} = \begin{bmatrix} \frac{1}{\sqrt{3}} \\ -1 \end{bmatrix} \quad \text{and} \quad \underline{A}_{v_3} = \begin{bmatrix} \frac{1}{\sqrt{3}} \\ 1 \end{bmatrix} \quad (5-81)$$

If the effects of gyro bias drift on the measurement are neglected, the measurement equation can be expressed as follows:

$$\underline{z}_k = \begin{bmatrix} \underline{H}_\alpha & \underline{H}_\beta & \underline{H}_\gamma & 0 & 0 & 0 \\ 0 & 0 & 0 & 0 & 0 & 0 \end{bmatrix} \underline{x}_k + A_k \underline{v}_k \quad (5-71)$$

where \underline{H}_α , \underline{H}_β , and \underline{H}_γ are two-dimensional vectors constructed with the first two components of the following vectors:

$$\underline{H}_x = \frac{\partial}{\partial x} \begin{bmatrix} T_{PO} \end{bmatrix} \underline{s}_0 \quad (x=\alpha, \beta, \gamma) \quad (5-72)$$

$$\underline{H}_\alpha = \begin{bmatrix} 0 & 1 & 0 \\ -1 & 0 & 0 \\ 0 & 0 & 0 \end{bmatrix} \underline{s}_0 \quad (5-73)$$

$$\underline{H}_\beta = \begin{bmatrix} 0 & 0 & -1 \\ 0 & 0 & 0 \\ 1 & 0 & 0 \end{bmatrix} \underline{s}_0 \quad (5-74)$$

$$\underline{H}_\gamma = \begin{bmatrix} 0 & 0 & 0 \\ 0 & 0 & 1 \\ 0 & -1 & 0 \end{bmatrix} \underline{s}_0 \quad (5-75)$$

In the present technique there are eight random errors associated with the measurement. In addition to the errors v_1 and v_3 for Slits #1 and #3, there are the errors associated with the reading of the gimbal angles I, M, and O at times t_1 and t_3 . It is assumed that the gimbal angle errors at t_1 are independent of those at t_3 . The error vector \underline{v}_k in Equation 5-71 can therefore be expressed as follows:

$$\underline{v}_k^T = \left[v_{I_1}, v_{M_1}, v_{O_1}, v_{I_3}, v_{M_3}, v_{O_3}, v_1, v_3 \right] \quad (5-76)$$

where the subscripts 1 and 3 for the gimbal angle errors correspond to times t_1 and t_3 .

The noise transformation matrix A_k is the following 2×8 matrix:

$$A_k = \left[\underline{A}_{I_1} \mid \underline{A}_{M_1} \mid \underline{A}_{O_1} \mid \underline{A}_{I_3} \mid \underline{A}_{M_3} \mid \underline{A}_{O_3} \mid \underline{A}_{v_1} \mid \underline{A}_{v_3} \right] \quad (5-77)$$

where the first six elements are two dimensional vectors constructed with the first two components of the following vectors:

$$\underline{A}_{w_j} = \frac{\partial}{\partial w_j} (\underline{s}_p) \quad \begin{cases} w = (I, M, O) \\ j = (1, 3) \end{cases} \quad (5-78)$$

$$\underline{A}_{w_1} = \text{UNIT} \left\{ \left[T_{PB}(t_3) \mid \underline{n}_{B_3} \right] \times \left[\frac{\partial T_{PB}(t_1)}{\partial w_1} \mid \underline{n}_{B_1} \right] \right\} \quad (5-79)$$

$$\underline{A}_{w_3} = \text{UNIT} \left\{ \left[\frac{\partial T_{PB}(t_3)}{\partial w_3} \mid \underline{n}_{B_3} \right] \times \left[T_{PB}(t_1) \mid \underline{n}_{B_1} \right] \right\} \quad (5-80)$$

It should be noted that the angles M and O were set to zero after derivation of each of the above vectors since the smoother formulation was only used to generate results for the nominal case.

The remaining two elements of the matrix A_k are:

$$\underline{A}_{v_1} = \begin{bmatrix} \frac{1}{\sqrt{3}} \\ -1 \end{bmatrix} \quad \text{and} \quad \underline{A}_{v_3} = \begin{bmatrix} \frac{1}{\sqrt{3}} \\ 1 \end{bmatrix} \quad (5-81)$$

As a matter of interest, error results were also generated using a measurement equation where all three components of the vectors \underline{H}_x and \underline{A}_{wj} were used. The results were essentially the same as for Equation 5-71.

5.4 ERROR STUDY RESULTS

5.4.1 INTRODUCTION

The results presented in this section represent the performance obtained for each SIMS candidate using real star distributions and the Fraser two filter smoother formulation described in Section 5.4 of ref. 141. The performance is indicated by the uncertainties in the smoothed estimates of the state parameters (pitch, roll, yaw, etc) after processing star measurements over one or more orbits with the smoother formulation. This formulation uses two "Kalman" filters, one of which processes the data forward from the beginning of the data interval to the point of interest, while the other works backward to this point from the end of the data interval. The results at the point of interest are then combined in an optimal manner to obtain the smoothed results. This point of interest was usually chosen at the middle of the data interval although some results were generated for other points uniformly distributed throughout the interval.

Due to the limited scope of the present effort and the relatively short time remaining to complete the study, the following steps were taken in the use of the smoother formulation:

- 1) Only the covariance matrix of the state (but not the state itself) was processed in the smoother formulation since this is more indicative of the statistical accuracy of each SIMS candidate.

- 2) Only a nominal attitude history was used with each SIMS candidate since the performance for this case is considered to be a very good indication of what the performance will be for an actual EOS mission, where the deviations in attitude and attitude rate from nominal are within $0.5^{\circ} + 0.2^{\circ}(1\sigma)$ and 0.005 degrees per second (3σ), respectively. Using a nominal attitude history also permitted certain simplifications to be made in the smoother formulation and its associated equations. It should also be noted that a circular orbit was assumed for this study.
- 3) In the state and measurement equations, the state to be estimated was restricted to six elements which represented the three attitude angles (pitch, roll, yaw) and the bias drift of each gyro. In SIMS-D the attitude angles were those of the gyro platform instead of the spacecraft since this resulted in simpler equations. The other bias type errors, such as those associated with gyro scale factor and gyro input axis alignment, were not included in the estimated state for the following reasons: These bias-type errors are usually not as important as gyro bias drift; the addition of these errors to the estimated state would have caused a significant increase in the complexity of the equations; and by including gyro bias drift in the estimated state this accounts to a great extent for the other gyro bias errors since their effects are somewhat similar and, in fact, are indistinguishable when there is no deviation from the nominal attitude history. In Section 5.5 rough estimates are made of the contributions made by these error sources when they are not accounted for in the smoother formulation.

The performance results using the Fraser two-filter smoother formulation are given separately for each SIMS candidate in the following sub-sections. The nominal values of the error sources and parameters used in the generation of the results are also presented at the beginning of each sub-section. In some cases the nominal value used for an error source or parameter does not represent the latest estimate for that source or parameter due to the delay in getting that information. However, sensitivity results are given for the most important error sources and parameters so that one can extrapolate the results. The star distribution cases used to generate the results in the following subsections are identified in Section 5.2.5.

5.4.2 ERROR STUDY RESULTS FOR SIMS-A

Unless otherwise noted, the nominal values of the error sources and parameters used to generate most of the results in this subsection are the following:

Initial State Uncertainties (1σ)

Pitch, Roll, Yaw	-	60 arcsec (each)
Gyro Bias Drift	-	0.15 deg/hr (each)

Star Mapper

Field-of-View	=	4 degrees
Pointing Direction	-	towards zenith
Measurement Error (1σ):		
CDS Mapper	=	1.6 arcsec
SIL Mapper	=	1.1 arcsec
Star Distribution	-	typical for CDS and SIL
Detector Magnitude Threshold:		
CDS Mapper	=	4
SIL Mapper	=	3.6
Measurement Technique	-	original

Gyro (GG334A)

Random Drift Rate (1σ) = 0.01 deg/hr (white noise)
Constant Angle Noise (quantization, etc.) (1σ) =
0.1 arcsec

Performance results have been generated for SIMS-A with a star mapper using either a cadmium sulfide (CDS) detector or a silicon (SIL) detector. This was done to show the relative merits of each detector since both are under serious consideration by industry for this application. One of the advantages of SIL over CDS is its greater sensitivity to stellar radiation in the red and infra-red portions of the spectrum, which enables SIL to see more stars than CDS for the same detector magnitude threshold. For example, in the typical star distribution cases used in this study (see Section 5.2.5), the SIL detector could see 20 stars brighter than the detector magnitude threshold of 3.6, while the CDS detector could only see 11 stars brighter than the detector magnitude threshold of 4.0. However, as previously noted, the nominal values used for the detector magnitude threshold and sensor measurement accuracy do not necessarily represent the latest estimates. Consequently, sensitivity results were generated to show the effects of variation in the detector magnitude threshold, the measurement error, and the field-of-view.

SIMS-A Performance Versus Data Interval Size

In Figures 5-4 and 5-5 the effect of variation in data processing interval size is shown for a nominal SIMS-A system using the SIL and CDS mappers. Note that for a typical star field (or star distribution case) the uncertainties in the smoothed estimates of pitch and roll are below the required level of 0.001 degrees (or 3.6 arcsecs) after 1 orbit of data

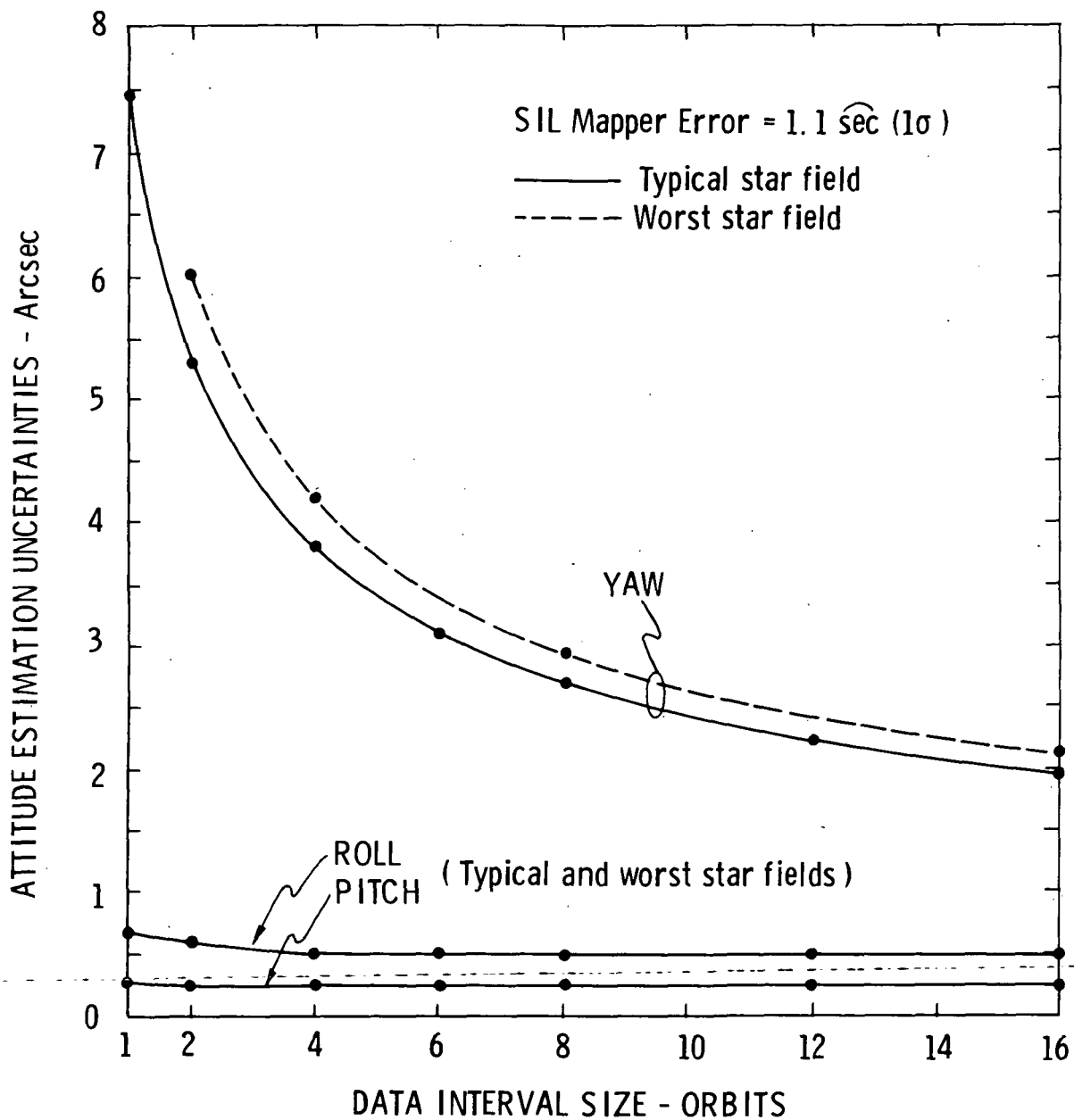


Figure 5-4 SIMS-A Performance Versus Data Processing Interval Size Using SIL Mapper

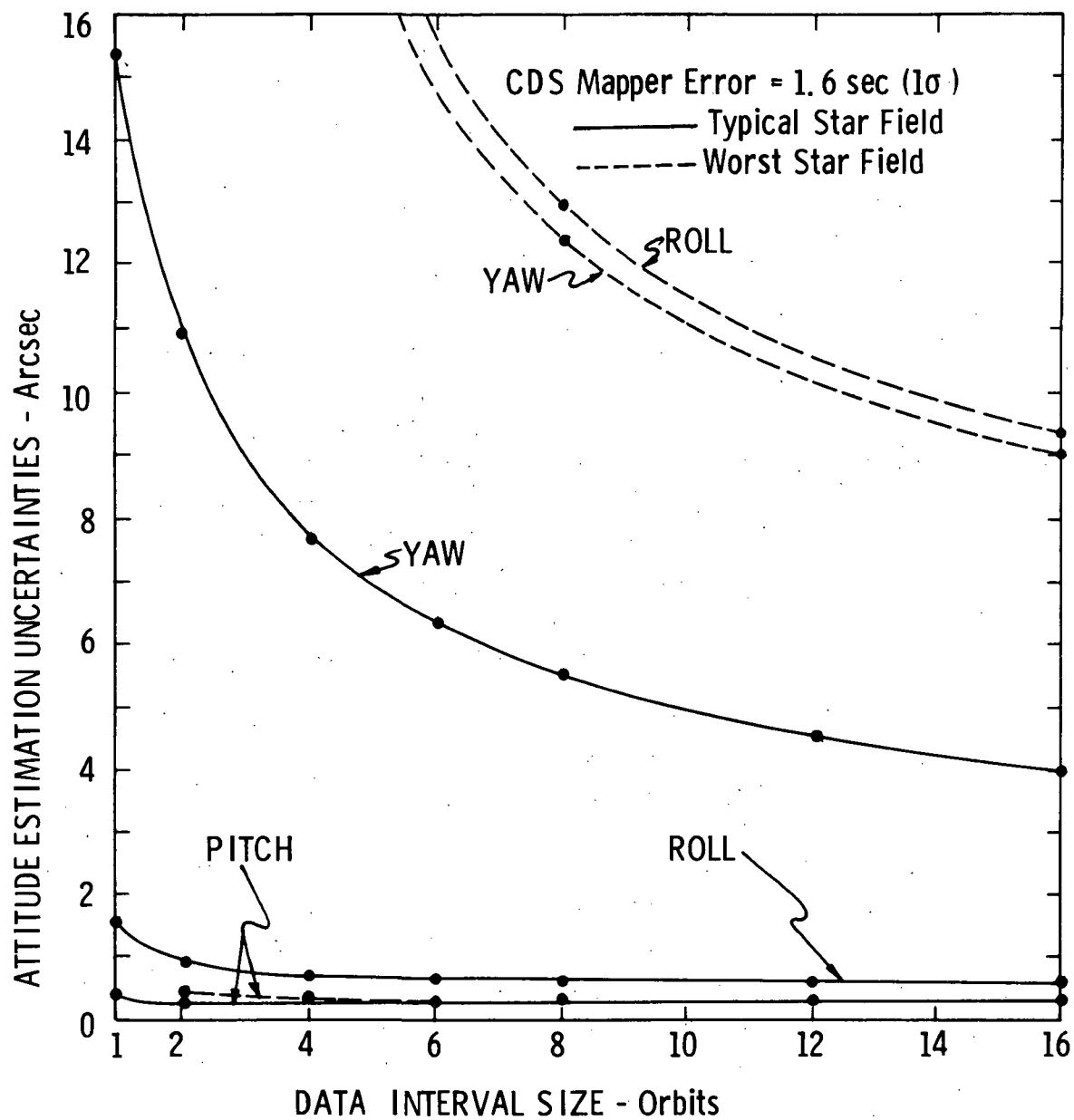


Figure 5-5 SIMS-A Performance Versus Data Processing Interval Size Using CDS Mapper

processing, and that they reach steady state values of less than 1 arcsec after a few orbits of data processing. However, the uncertainties in the smoothed estimates of yaw are much higher and continue to drop after 16 orbits of data processing. For the SIL mapper the yaw uncertainty drops below 3.6 arcsecs after 5 orbits, while that for the CDS mapper is still about 4 arcsecs after 16 orbits.

In Figures 5-4 and 5-5 the results are also shown for the worst star fields (identified in Section 5.2.5). Note there is very little difference between the results for the worst and typical star fields of the SIL mapper, even though the worst star field has only 12 usable stars per orbit as compared to 20 for the typical star field. However, the difference between the results for the worst and typical star fields of the CDS mapper is much larger due to the very small number of stars (5) available per orbit for the worst star field.

SIMS-A Sensitivity To Star Mapper Pointing Direction

In Tables 5-4 and 5-5 performance results are given for two different pointing directions of the SIL and CDS mappers. These directions are denoted by the angle β where $\beta=0^\circ$ for the nominal case of pointing towards zenith, and $\beta=-30^\circ$ for the mapper pointing 30° ahead of zenith in the orbital plane. For $\beta=0^\circ$ the results are the same as given previously in Figures 5-4 and 5-5. Note that the tables also include the uncertainties in the smoothed estimates of gyro bias drift. The primary reason for generating results with $\beta=-30^\circ$ was to determine how much improvement would occur in yaw. It is seen that yaw improves a little but at a significant expense to roll.

SIMS-A Sensitivity to Initial State Uncertainties

In Table 5-6 the sensitivity of performance to initial uncertainties in attitude and gyro bias drift is given for

Table 5-4

SIMS-A SENSITIVITY TO SIL MAPPER
POINTING DIRECTION

β (deg)	Interval Size (Orbits)	Uncertainty (1σ) At Middle of Interval					
		Attitude (arcsec)			Gyro Bias Drift (10^{-3} deg/hr)		
		Pitch	Roll	Yaw	Y	X	Z
0 ↓	1	0.3	0.7	7.5	0.17	7.5	0.5
	2		0.6	5.3	0.09	5.3	0.3
	4		0.5	3.8	0.06	3.8	0.2
	6		0.5	3.1	0.05	3.0	0.2
	8		0.5	2.7	0.04	2.6	0.2
	12			2.2	0.03	2.2	0.1
	16	↓	↓	1.9	0.03	1.9	0.1
-30 ↓	2	0.3	2.7	4.6	0.09	4.6	2.7
	4		1.9	3.3	0.06	3.2	1.9
	8		1.4	2.3	0.05	2.3	1.3
	16	↓	1.1	1.7	0.03	1.7	1.0

NOTES: SIL Mapper Error (1σ) = 1.1 arcsec

$\beta = 0^\circ$ for Mapper Pointing Towards Zenith (nominal case)

$\beta = -30^\circ$ for Mapper Pointing 30° Ahead of Zenith in
Orbit Plane

Table 5-5

SIMS-A SENSITIVITY TO CDS MAPPER
POINTING DIRECTION

β (deg)	Interval Size (Orbits)	Uncertainty (1σ) At Middle of Interval					
		Attitude (arcsec)			Gyro Bias Drift (10^{-3} deg/hr)		
		Pitch	Roll	Yaw	Y	X	Z
0 ↓	1	0.4	1.6	15.5	0.21	15.5	0.8
	2	0.3	0.9	10.9	0.09	11.0	0.6
	4	↓	0.7	7.8	0.06	7.3	0.5
	6	↓	0.6	6.4	0.05	6.3	0.3
	8	↓	↓	5.5	0.03	5.6	0.3
	12	↓	↓	4.5	↓	4.5	0.2
	16	↓	↓	3.9	↓	3.9	0.2
-30 ↓	2	0.3	5.5	9.5	0.09	9.5	0.5
	4	↓	3.9	6.7	0.06	6.8	0.4
	8	↓	2.8	4.8	0.03	4.8	0.3
	16	↓	2.0	3.4	↓	3.3	0.2

NOTES: CDS Mapper Error (1σ) = 1.6 arcsec

$\beta = 0^\circ$ for Mapper Pointing Towards Zenith (nominal case)

$\beta = -30^\circ$ for Mapper Pointing 30° Ahead of Zenith
in Orbit Plane

Table 5-6

SIMS-A SENSITIVITY TO INITIAL STATE UNCERTAINTIES

Initial Uncertainty (per axis)		Uncertainty (1σ) at Middle of Interval					
Attitude (arcsec)	Gyro Bias Drift (deg/hr)	Attitude (arcsec)			Gyro Bias Drift (10 ⁻³ deg/hr)		
		Pitch	Roll	Yaw	Y	X	Z
0.5	0.15	0.3	0.50	0.9	0.05	0.8	0.2
1	(Nominal)			1.2		1.1	
2				1.7		1.7	
10				2.6		2.5	
30				2.7		2.6	
60							
240							
600							
60	0.0015			1.4		1.3	
(Nominal)	0.0030			2.0		2.0	
	0.0075			2.5		2.5	
	0.015			2.7		2.6	
	0.030						
	0.075						
	0.15						
	0.60						

NOTES: Data Interval = 8 Orbits

SIL Mapper Error (1σ) = 1.1 arcsec

SIMS-A using the SIL mapper. The results are for 8 orbits of data processing. It is seen that the results are somewhat independent of the initial state (i.e., attitude and gyro bias drift) uncertainties. There is some improvement in performance for very small initial state uncertainties; however, it is felt that this improvement would be less if the data interval was greater than 8 orbits. This is based upon the assumption that, given a large enough data processing interval, the limiting performance will be dictated by the errors in the system and not by the initial uncertainties used in the data processing. It should be noted that the nominal values of the initial attitude and gyro bias drift uncertainties used to generate most of the results for SIMS-A and -B are 60 arcsecs and 0.15 degrees per hour, respectively. These values are what might be expected immediately following launch or after the system has been inactive. After processing data for so many orbits, the state uncertainties will be much smaller than those previously mentioned and one would think the new values should be used as the uncertainties for processing data in later orbits in order to gain the slight improvement in performance indicated in Table 5-6. However, note in Table 5-6 that these new initial uncertainties would have to be very small and there is no guarantee that the errors will remain that small many orbits later because of the presence of error sources which are not being fully accounted for in the smoothing process.

SIMS-A Performance at Various Points in Data Interval

In Table 5-7 the uncertainties in the smoothed estimates of state are shown for various points uniformly distributed throughout an 8 orbit data processing interval. The results are for a nominal SIMS-A using the CDS mapper. It is seen that there is essentially no difference in performance throughout the interval, and this is what one would expect in

Table 5-7

SIMS-A PERFORMANCE AT VARIOUS POINTS IN 8 ORBIT DATA
PROCESSING INTERVAL USING CDS MAPPER

Time Since Start of Interval (secs)	Uncertainty (1σ) at Indicated Times					
	Attitude (arcsec)			Gyro Bias Drift (10^{-3} deg/hr)		
	Pitch	Roll	Yaw	Y	X	Z
4200	0.3	0.6	5.5	0.03	5.5	0.3
8400	↓	0.8	↓	↓	↓	↓
16800	↓	0.5	↓	↓	↓	↓
25200	↓	0.6	↓	↓	↓	↓
33600	↓	0.8	↓	↓	↓	↓
42000	↓	0.6	↓	↓	↓	↓
46200	↓	0.9	↓	↓	↓	↓

NOTES: CDS Mapper Error (1σ) = 1.6 arcsec
8 Orbits = 50400 seconds

the smoothing process. One may therefore conclude that the uncertainties in the smoothed estimates of state at a particular point, such as at the middle of the data interval, are indicative of the performance throughout the interval.

SIMS-A Sensitivity to Mapper Measurement Error

In Figures 5-6 and 5-7 the sensitivity of performance to SIL and CDS mapper measurement errors are shown for 2, 8, and 16 orbits of data processing. It is seen that the performance is a linear function of mapper measurement error; and the yaw component is considerably more sensitive than pitch and roll. In Figures 5-6 and 5-7 it is seen that, for the same measurement error, the performance is better for the SIL mapper. This is due to the fact that the typical star distribution case for the SIL mapper contains 20 usable stars per orbit, while that for the CDS mapper contains only 11 usable stars per orbit, even though CDS has a more favorable detector magnitude threshold.

SIMS-A Sensitivity to Mapper FOV

In Figures 5-8 and 5-9 the sensitivity of performance to the size of field-of-view (FOV) of the SIL and CDS mappers is shown for 8 orbits of data processing. This data is also shown with some other results in Table 5-8. It is seen that the performance in pitch and roll is essentially independent of FOV size. However, a significant improvement can be obtained in yaw by increasing the FOV above the nominal value of 4 degrees. Note that the yaw performance increases by at least a factor of two when the FOV is increased from 4 to 6 degrees. This improvement is due not only to the greater number of stars which can be seen per orbit but also to the improvement in geometry of the measurement. In other words, measurements on stars further away from zenith give more

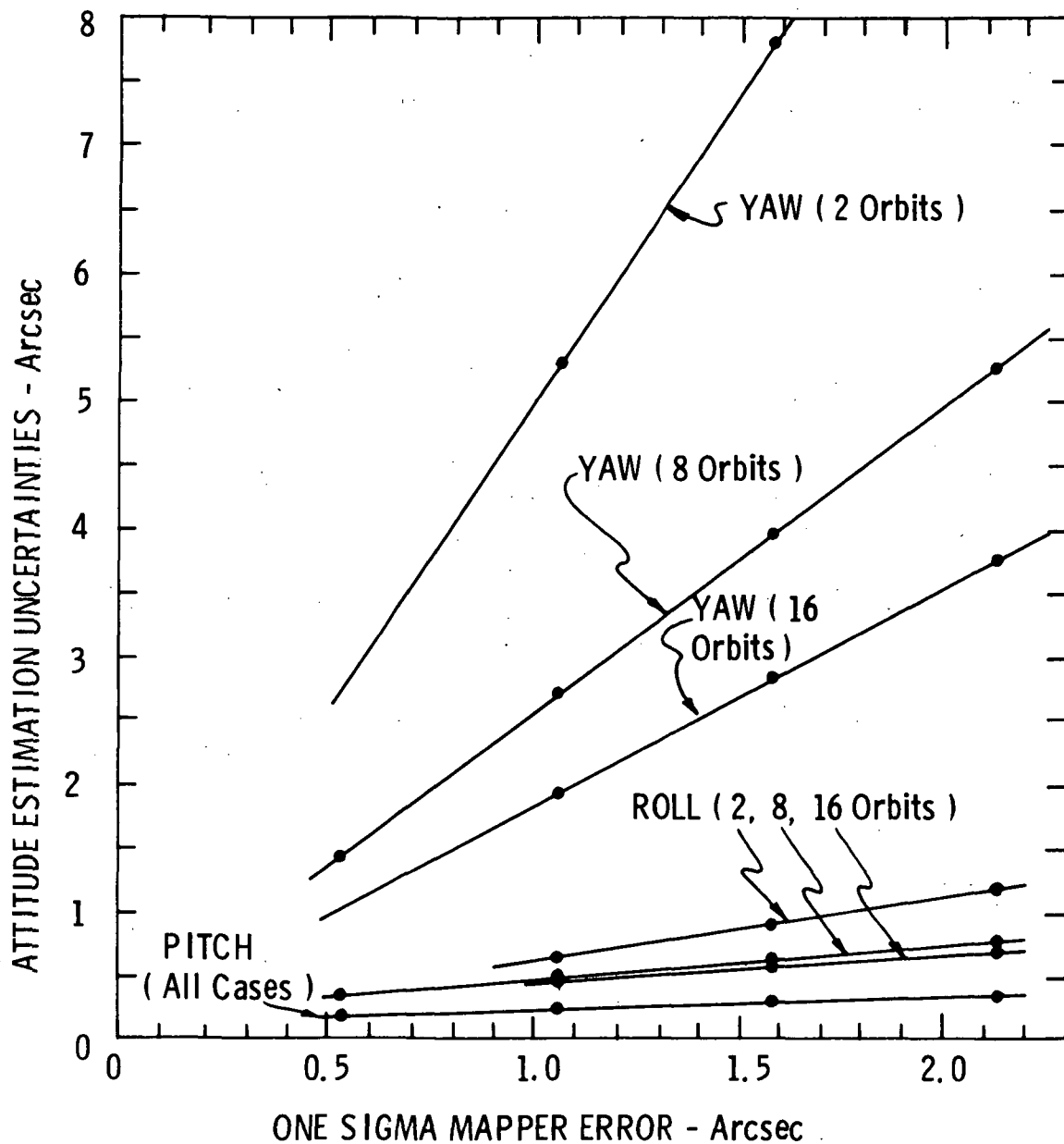


Figure 5-6 SIMS-A Sensitivity to SIL Mapper Measurement Error

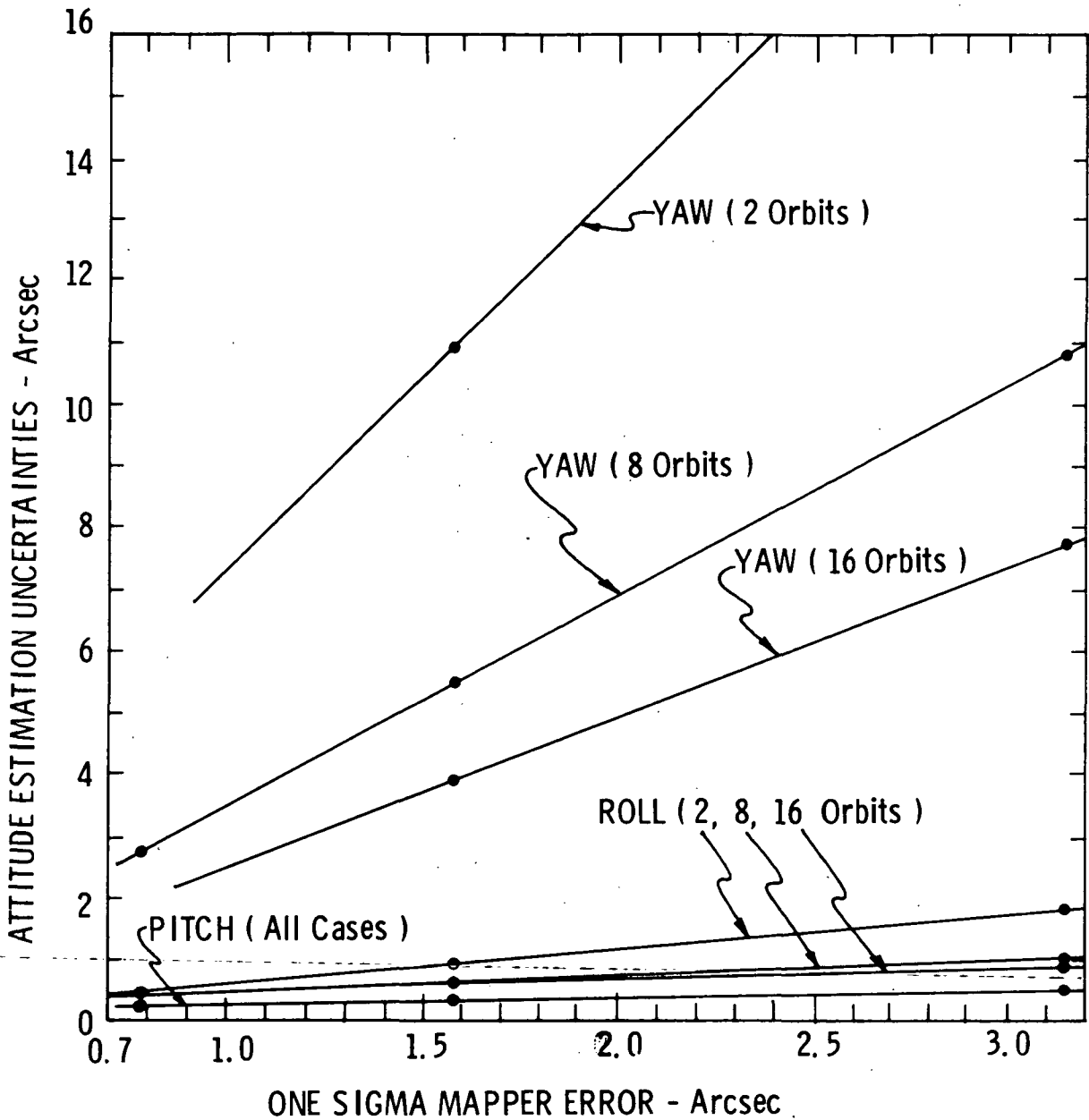


Figure 5-7 SIMS-A Sensitivity to CDS Mapper Measurement Error

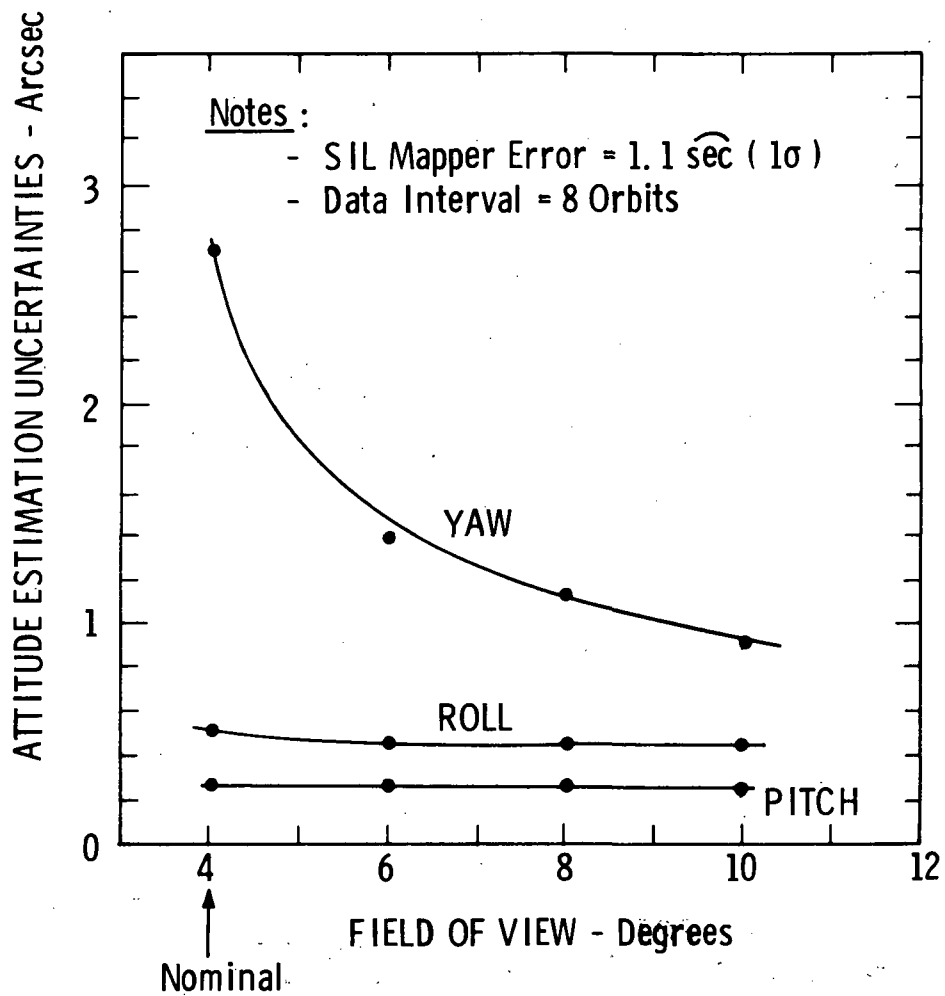


Figure 5-8 SIMS-A Sensitivity to FOV of SIL Mapper

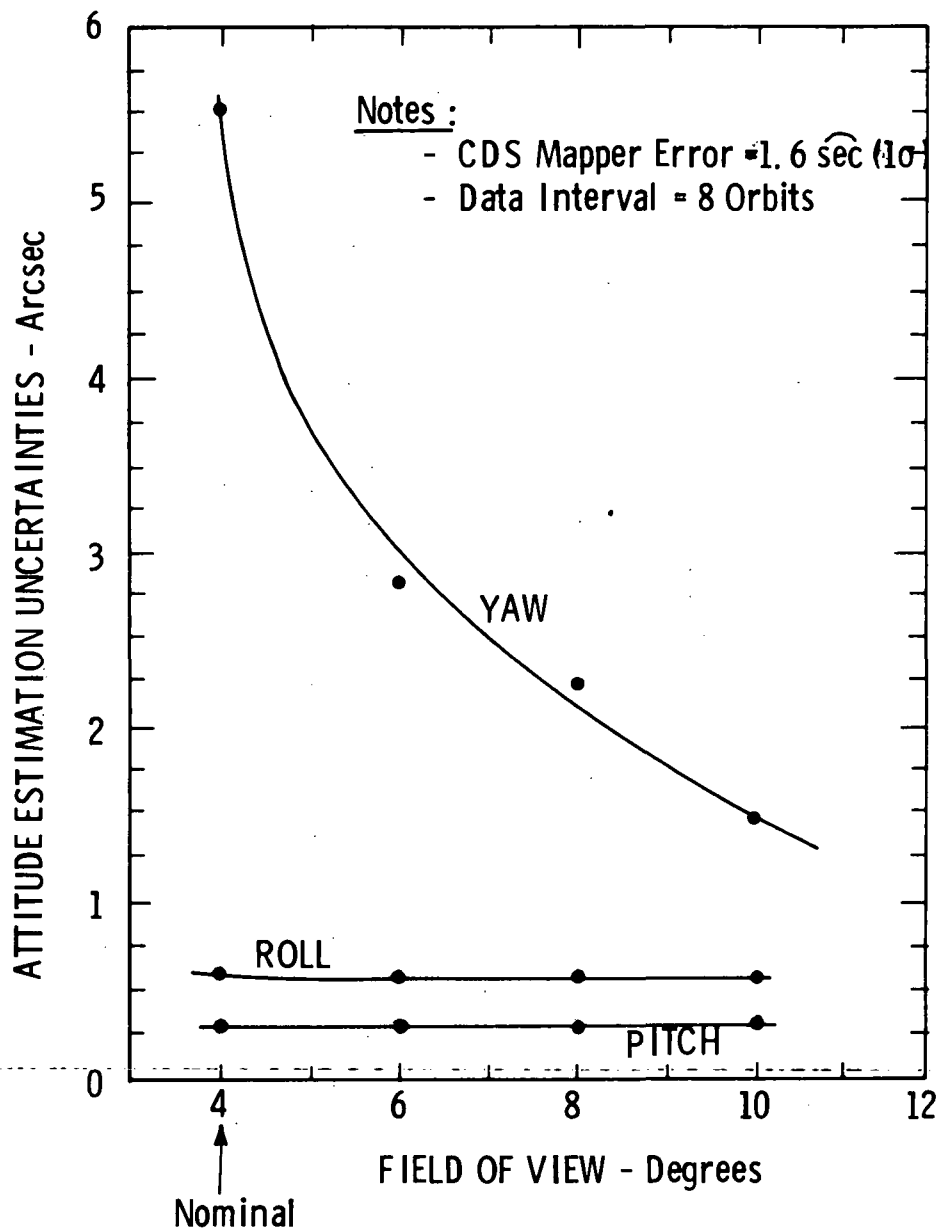


Figure 5-9 SIMS-A Sensitivity to FOV of CDS Mapper

SIMS-A SENSITIVITY TO STAR MAPPER FOV

NOTE: SIL Mapper Error (1σ) = 1.1 arcsec
CDS Mapper Error (1σ) = 1.6 arcsec

information about the yaw component of attitude error. More will be said about the influence of these two factors in the following discussion of sensitivity to detector magnitude threshold. Although these results were generated independent of any studies in process at Honeywell, it is interesting to note that Honeywell is now seriously considering CDS and SIL mappers with a FOV of 10 degrees.

SIMS-A Sensitivity to Detector Magnitude Threshold

In Figures 5-10 and 5-11 the sensitivity of performance to detector magnitude threshold of the SIL and CDS mappers is shown for 8 orbits of data processing. The numbers next to the data points for the yaw curves indicate the number of stars brighter than the indicated detector magnitude threshold for the star distribution cases used to generate the results. In Figure 5-10 the sensitivity to detector magnitude threshold is also shown for a SIL mapper with a FOV of 8 degrees. For both the SIL and CDS mapper it is seen that the performance in pitch and roll is essentially at a steady state level and is somewhat independent of detector magnitude threshold. However, some improvement can be made in yaw performance by increasing the detector magnitude threshold so that additional (but less bright) stars can be used. It should be noted that the yaw curve for CDS appears much steeper than the corresponding one for SIL partly because of the difference in scaling of the abscissa.* In Figure 5-10 one can clearly see the improvement in yaw performance due only to the increase in geometry when the FOV is increased from 4 to 8 degrees. Note that the yaw performance for an 8 degree FOV at a magnitude threshold of 3.2 is better than that of a 4 degree FOV at a magnitude threshold of 4.0, even though there are more stars in the latter.

* Recent test results verify (as was previously suspected) that the yaw uncertainty at the magnitude threshold of 3.25 should be larger than as shown in Figure 5-11. At this threshold only five stars were available per orbit; this makes the performance somewhat sensitive to individual star locations. When there are ten

(Footnote continued - page 5-62)

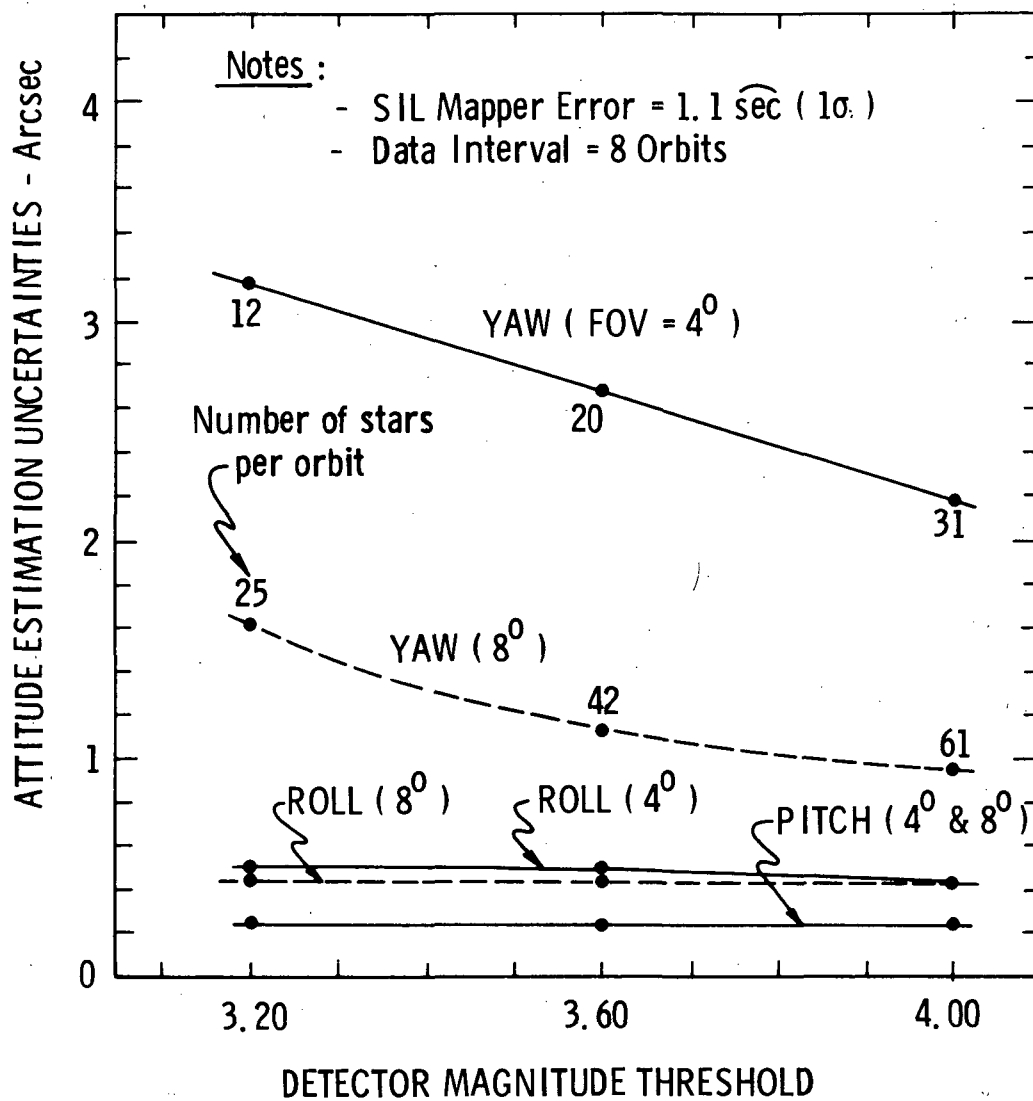


Figure 5-10 SIMS-A Sensitivity to Detector
Magnitude Threshold of SIL Mapper

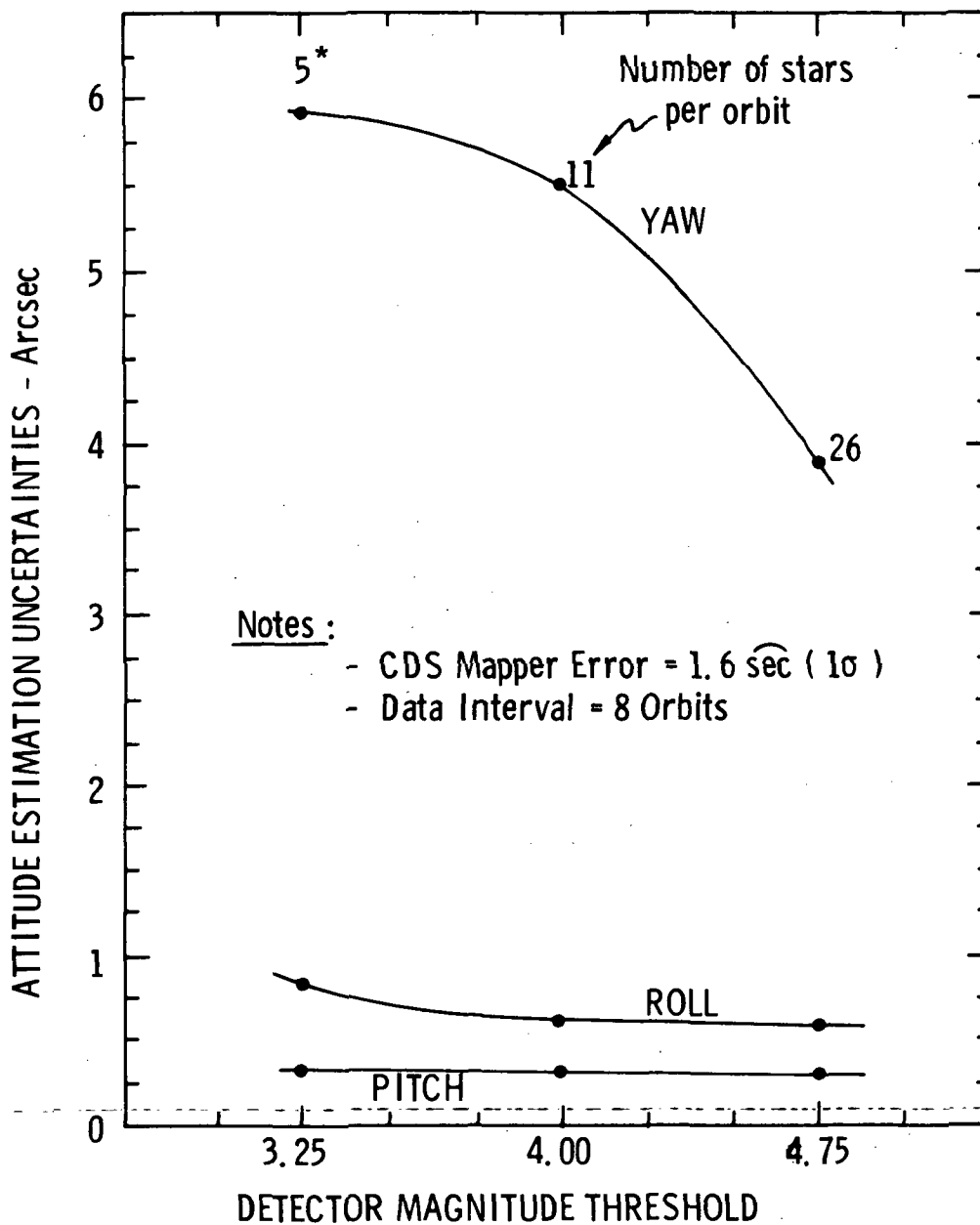


Figure 5-11 SIMS-A Sensitivity to Detector
Magnitude Threshold of CDS Mapper

* Refer to footnotes on pages 5-11 and 5-59.

SIMS-A Sensitivity to Gyro Noise

In Figures 5-12 and 5-13 the sensitivity of performance to gyro random drift and constant angle noise (quantization, etc) is shown for 8 orbits of data processing. This data was generated for SIMS-A using the SIL mapper. The gyro random drift rate was modeled as a white noise extending from 0 to 0.5 hertz, as indicated by Honeywell for the GG334 gyro. It is seen that the sensitivity to gyro random drift and constant angle noise is not very large. For example, one could get about the same performance as nominal if the one sigma gyro random drift rate was ten times nominal. This result seems to indicate that gyros with less strict requirements could be used in SIMS-A.

SIMS-A Performance for Two Techniques of Star Measurement

In Table 5-9 the performance is shown for the two different techniques of star mapper measurement described in Section 5.3.2.2. These are identified as the 'original' and 'alternate' techniques of measurement, where the former has been used as the nominal technique. The results were generated using the SIL mapper. It is seen that there is very little difference in the results for the two techniques.

5.4.3 ERROR STUDY RESULTS FOR SIMS-B

Unless otherwise noted, the nominal values of the error sources and parameters used to generate most of the results in this subsection are the following:

Initial State Uncertainties (1σ)

Pitch, Roll, Yaw	- 60 arcsec (each)
Gyro Bias Drift	- 0.15 deg/hr (each)

(Footnote continued from page 5-59) or more stars per orbit, it has been found that there is very little variation in performance for different star distributions having the same number of stars. Consequently, it is felt that this data point should be higher so that the shape of the yaw curve would then be more like the ones shown for the SIL mapper in Figure 5-10.

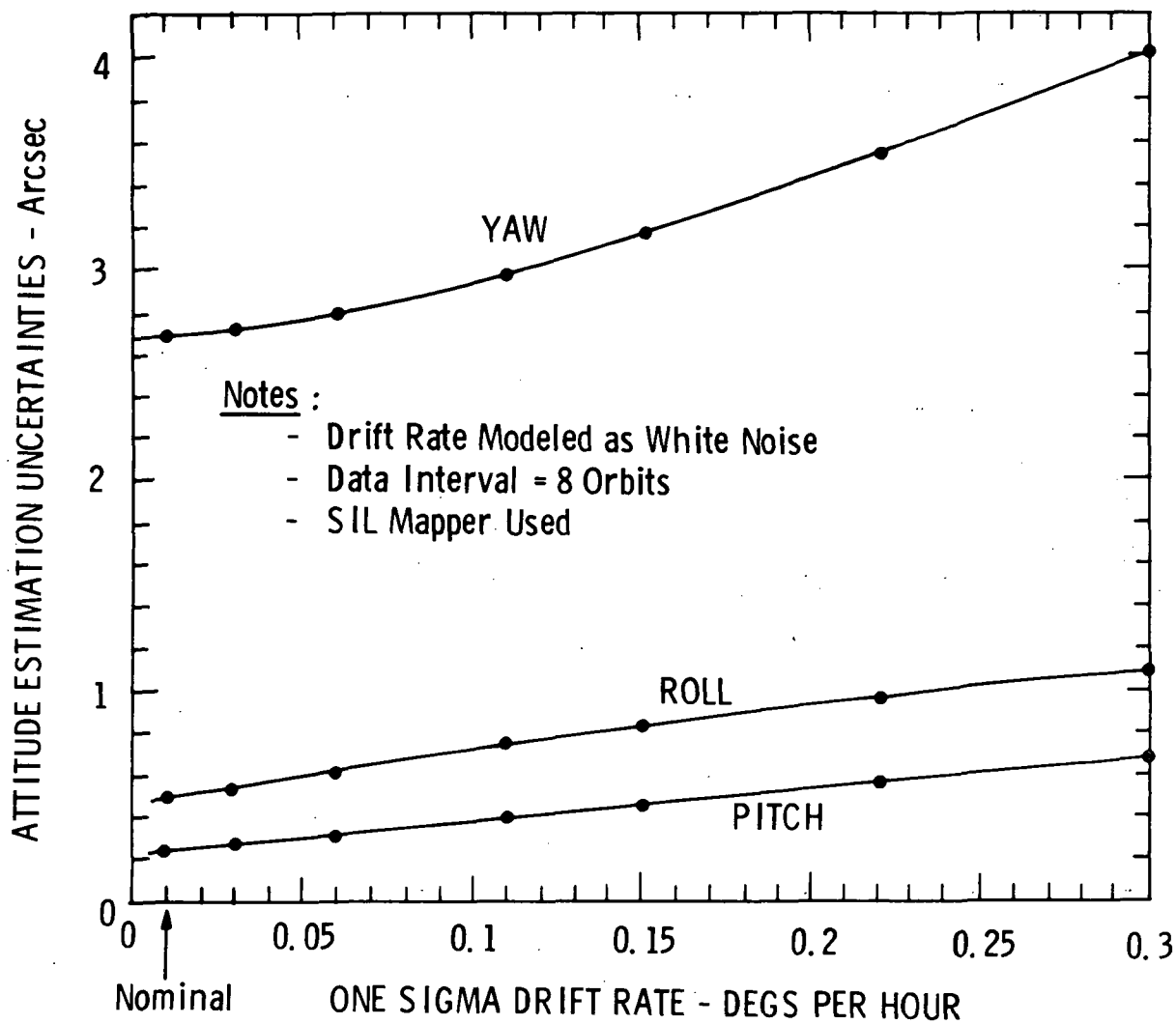


Figure 5-12 SIMS-A Sensitivity to Gyro Random Drift

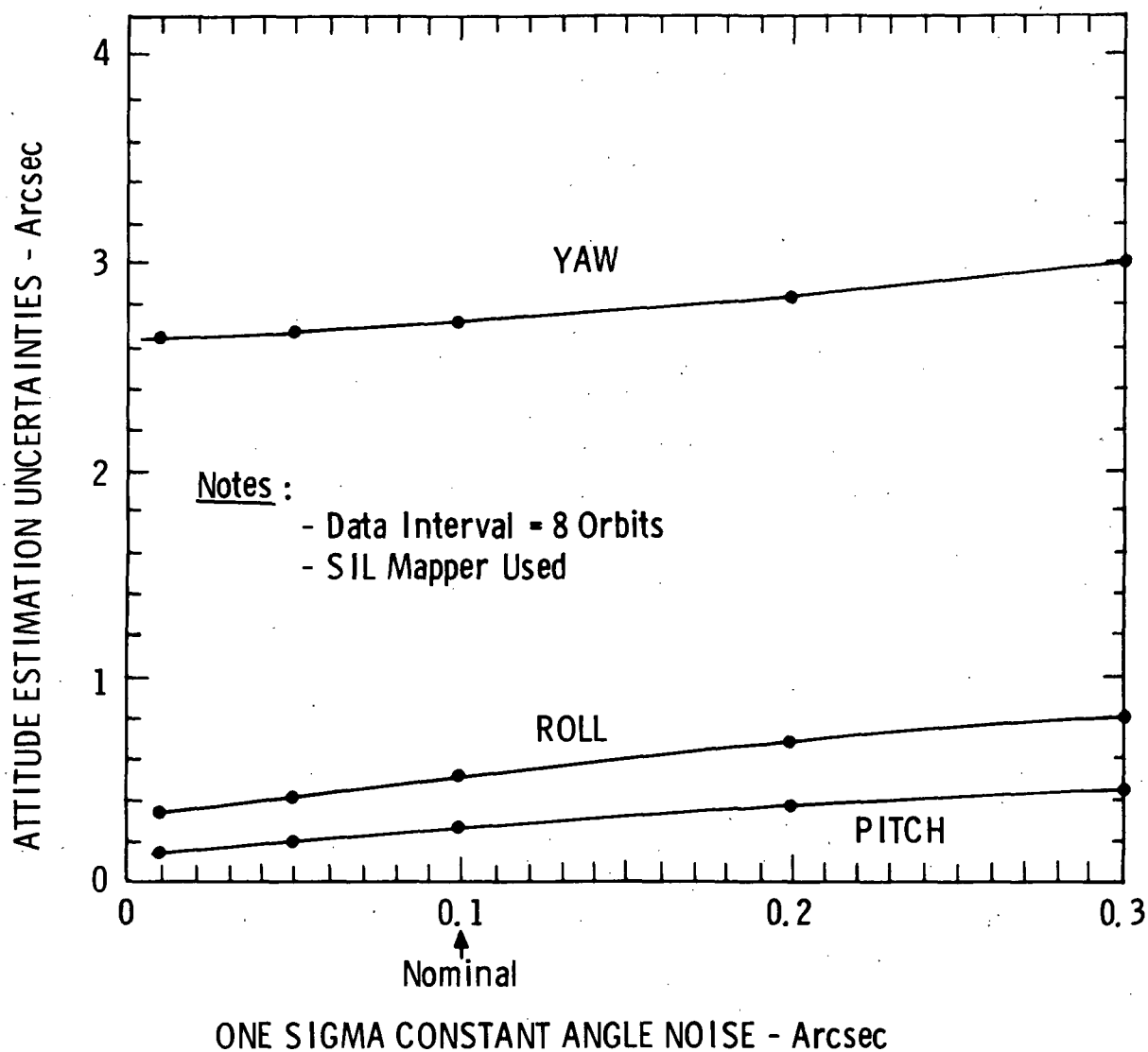


Figure 5-13 SIMS-A Sensitivity to Gyro
Constant Angle Noise

Table 5-9

SIMS-A PERFORMANCE FOR TWO TECHNIQUES
OF STAR MEASUREMENT

Measure- ment Technique	Interval Size (Orbits)	Uncertainty (1σ) at Middle of Interval					
		Attitude (arcsec)			Gyro Bias Drift (10^{-3} deg/hr)		
		Pitch	Roll	Yaw	Y	X	Z
Original (Nominal) ↓	1	0.3	0.7	7.5	0.17	7.5	0.5
	2	↓	0.6	5.3	0.09	5.3	0.3
	4	↓	0.5	3.8	0.06	3.8	0.2
	8	↓	↓	2.7	0.05	2.6	0.2
	12	↓	↓	2.2	0.03	2.2	0.1
Alternate ↓	1	0.3	0.7	8.3	0.15	8.3	0.5
	2	0.2	0.6	5.8	0.08	5.8	0.3
	4	↓	0.5	4.2	0.05	4.1	0.2
	8	↓	↓	3.0	0.03	2.9	0.2
	12	↓	↓	2.4	0.03	2.4	0.1

NOTES: SIL Mapper Error (1σ) = 1.1 arcsec

Star Tracker

Gimbal Angle Limits:

Outer (Roll) - ± 45 degrees

Inner (Pitch) - ± 15 degrees

Zero Gimbal Pointing Direction - towards zenith

Measurement Errors (1σ):

Outer Gimbal (ϕ) = 1.2 arcsec

Inner Gimbal (θ_T) = 1.2 arcsec

Alpha (α_T) = 1.5 arcsec

Beta (β_T) = 1.5 arcsec

Detector Magnitude Threshold (S-20) = 3.5

Star Distribution - star selected every 20 degrees
of orbital motion for orbit of
7/1/72

Gyro (GI-K7G)

Random Drift Rate (1σ) = 0.002 deg/hr (white noise)

Constant Angle Noise (quantization, etc) (1σ) = 0.1 arcsec

SIMS-B Performance Versus Data Interval Size

In Figure 5-14 the effect of variation in data processing interval size is shown for a nominal SIMS-B using a star update every 20 degrees of orbital motion. This star update interval corresponds to about 5.8 minutes between updates and permits about 18 star updates per orbit. It is seen in Figure 5-14 that the uncertainties in the smoothed estimates of pitch, roll, and yaw are less than about 1 arcsec after one orbit of data processing, and, after a few orbits of data processing, settle out around 0.4 arcsecs. It is apparent that this candidate more than meets the required accuracy of 3.6 arcsecs and this will be found to be the case throughout the results of this subsection. One of the most significant differences between the performance of SIMS-A and -B is the large improvement in yaw for

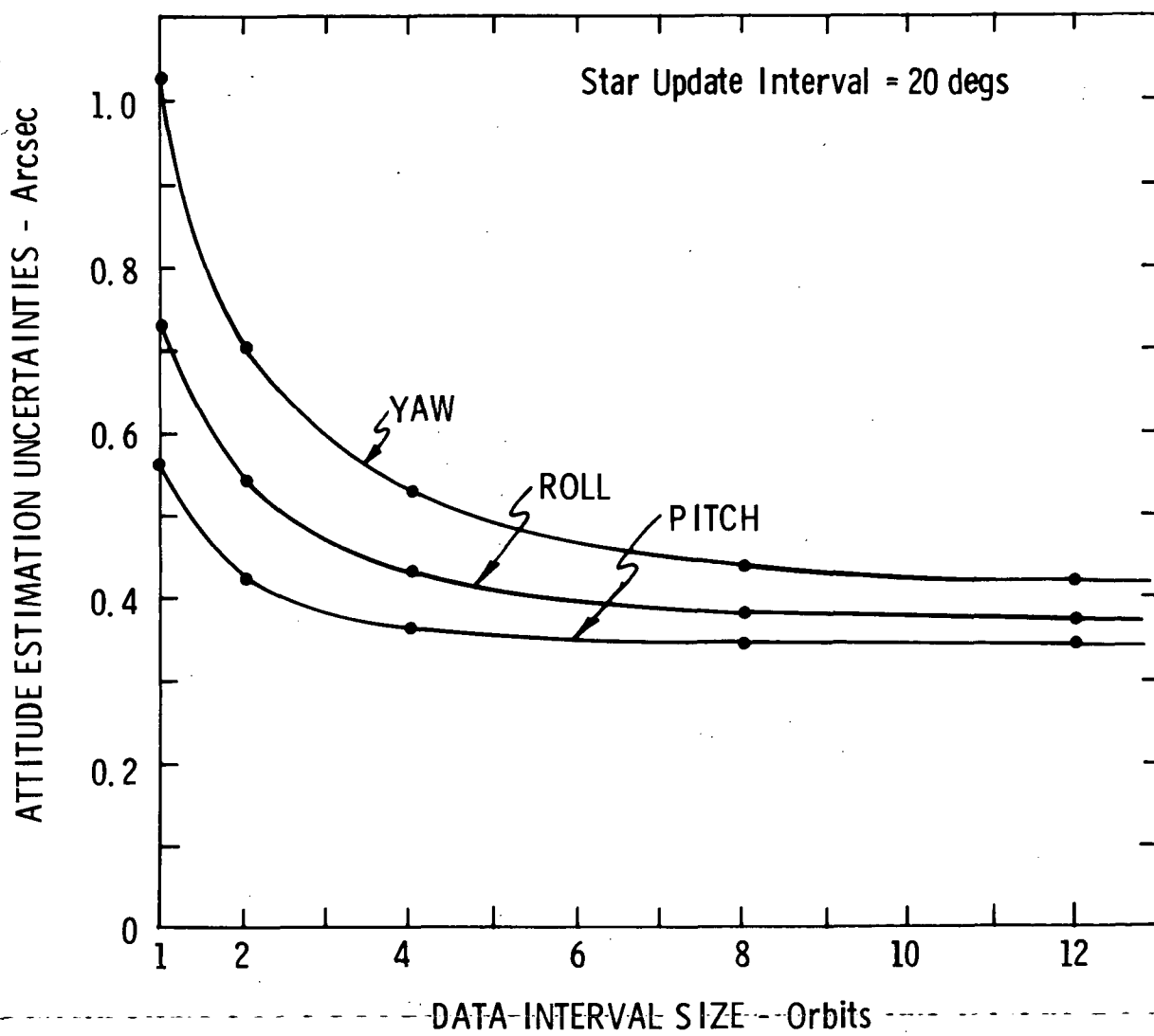


Figure 5-14 SIMS-B Performance Versus Data Processing Interval Size

SIMS-B. This is due to the fact that measurements are now being made on stars further away from zenith. It was noted in the results for SIMS-A that similar improvement in yaw could be obtained by increasing the FOV.

SIMS-B Performance Versus Star Update Interval Size

In Table 5-10 the performance is shown for star update intervals of 8, 16, 20, and 40 degrees. The table also shows the performance for various data processing interval sizes. Here it is seen that even with a star update interval of 40 degrees, which corresponds to about 9 star updates per orbit, the performance is about the same as for the other cases.

SIMS-B Sensitivity to Initial State Uncertainties

In Table 5-11 the sensitivity of performance to initial uncertainties in attitude and gyro bias drift is shown for 4 orbits of data processing. It is seen that the results are independent of the initial state uncertainties and supports the comment made on this subject in Section 5.4.2 for SIMS-A.

SIMS-B Sensitivity to Star Tracker Measurement Errors

In Figure 5-15 and Table 5-12 the sensitivity of performance to star tracker measurement errors is shown for 8 orbits of data processing. Figure 5-15 shows the effect of simultaneous variation of the one sigma values of the errors in Φ , θ_T , α_T , and β_T . The one sigma values are expressed relative to their nominal values. It is seen that the uncertainties in the smoothed estimates of pitch, roll, and yaw are still less than one arcsec even when the one sigma values are twice nominal. Table 5-12 shows the effect of variation in the one sigma value of each error source when the remaining three are nominal. Note that there is very little difference in the performance for the cases analyzed.

Table 5-10

SIMS-B PERFORMANCE VERSUS STAR UPDATE INTERVAL SIZE

Star Update Interval (Deg)	Interval Size (Orbits)	Uncertainty (1σ) at Middle of Interval					
		Attitude(arcsec)			Gyro Bias Drift(10^{-3} deg/hr)		
		Pitch	Roll	Yaw	Y	X	Z
8	1	0.4	0.5	0.7	0.30	0.6	0.3
	2	0.4	0.4	0.5	0.11	0.4	0.2
	4	0.3	↓	0.4	0.06	0.3	0.2
	8	↓	↓	↓	0.05	0.2	0.1
	12	↓	↓	↓	0.03	0.2	0.1
16	1	0.5	0.7	1.0	0.27	0.8	0.4
	2	0.4	0.5	0.6	0.11	0.5	0.3
	4	0.4	0.4	0.5	0.06	0.4	0.2
	8	0.3	↓	0.4	0.03	0.3	0.2
	12	0.3	↓	0.4	0.03	0.2	0.1
20	1	0.6	0.7	1.0	0.32	0.8	0.5
	2	0.4	0.5	0.7	0.12	0.6	0.3
	4	0.4	0.4	0.5	0.06	0.4	0.2
	8	0.3	↓	0.4	0.03	0.3	0.2
	12	0.3	↓	0.4	0.02	0.2	0.1
40	1	0.8	1.0	1.3	0.47	1.1	0.6
	2	0.6	0.7	1.0	0.17	0.8	0.5
	4	0.4	0.5	0.7	0.06	0.5	0.3
	8	↓	0.4	0.5	0.03	0.4	0.2
	12	↓	0.4	0.5	0.02	0.3	0.2

Table 5-11

SIMS-B SENSITIVITY TO INITIAL STATE UNCERTAINTIES

Initial Uncertainty (per axis)		Uncertainty (1σ) at Middle of Interval					
Attitude (arcsec)	Gyro Bias Drift (deg/hr)	Attitude (arcsec)			Gyro Bias Drift (10^{-3} deg/hr)		
		Pitch	Roll	Yaw	Y	X	Z
0.5	0.15	0.4	0.4	0.5	0.05	0.4	0.2
1	(Nominal)	↓	↓	↓	↓	↓	↓
2							
10							
30							
60							
240							
600							
60	0.0015	↓	↓	↓	↓	↓	↓
(Nominal)	0.0030						
	0.0075						
	0.015						
	0.030						
	0.075						
	0.15						
	0.6						

NOTES: Data Interval = 4 Orbits
 Star Update Interval = 20 degrees

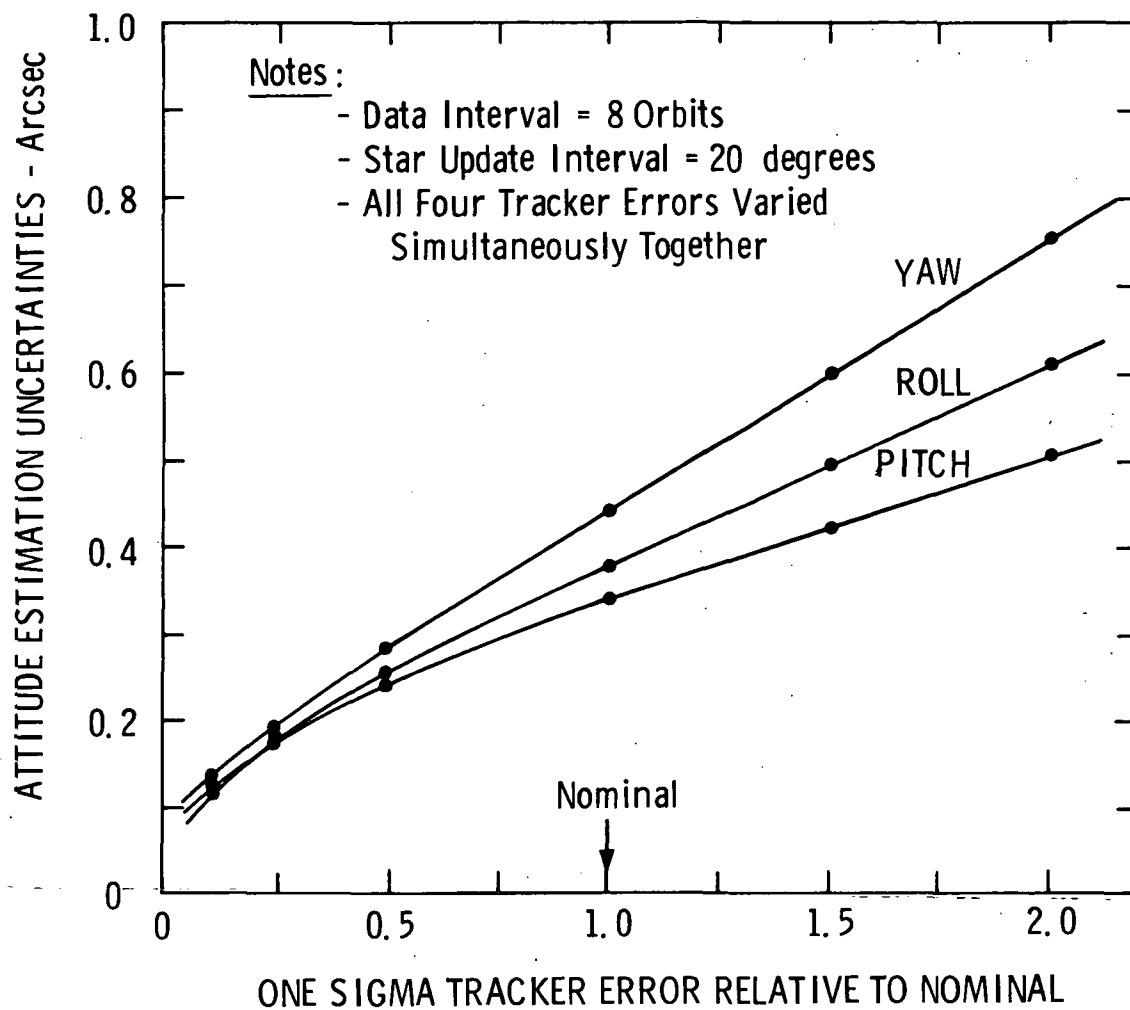


Figure 5-15 SIMS-B Sensitivity to Star Tracker Measurement Error

Table 5-12

SIMS-B SENSITIVITY TO STAR TRACKER MEASUREMENT ERRORS

Error Source Being Changed	One Sigma Relative To Nominal	Uncertainty (1σ) at Middle of Interval					
		Attitude(arcsec)			Gyro Bias Drift(10^{-3} deg/hr)		
		Pitch	Roll	Yaw	Y	X	Z
All 4	0.25	0.2	0.2	0.2	0.03	0.1	0.1
	0.5	0.2	0.3	0.3		0.2	0.1
	1.0	0.3	0.4	0.4		0.3	0.2
	1.5	0.4	0.5	0.6		0.4	0.2
	2.0	0.5	0.6	0.8		0.6	0.3
Inner Gimbal (θ_T)	0.25	0.3	0.4	0.4		0.2	0.2
	0.5	0.3	↓	↓		0.2	↓
	1.0	0.3	↓	↓		0.3	↓
	1.5	0.4	↓	0.5		0.3	↓
	2.0	0.4	↓	0.5		0.4	↓
Outer Gimbal (ϕ)	0.25	0.3	0.3	0.4		0.3	0.1
	0.5	↓	0.4	↓		↓	0.1
	1.0	↓	↓	↓		↓	0.2
	1.5	↓	↓	0.5		↓	↓
	2.0	↓	0.5	0.5		↓	↓
α_T	0.25	0.3	0.3	0.4			0.1
	0.5	↓	0.3	↓			0.1
	1.0	↓	0.4	↓			0.2
	1.5	↓	0.4	0.5			0.2
	2.0	↓	0.5	0.5		↓	0.3
β_T	0.25	0.3	0.4	0.4		0.2	0.2
	0.5	↓	↓	↓		0.2	↓
	1.0	↓	↓	↓		0.3	↓
	1.5	0.4	↓	0.5		0.4	↓
	2.0	0.5	↓	0.6		0.5	↓

NOTES: Data Interval = 8 Orbits

Star Update Interval = 20 degrees

SIMS-B Sensitivity to Star Tracker Outer Gimbal Limit

In Figure 5-16 and Table 5-13 the sensitivity of performance to star tracker outer gimbal limit is shown for 8 orbits of data processing and a star update interval of 20 degrees. Table 5-13 also shows the results for star update intervals of 8, 16, and 40 degrees. The outer gimbal limit, in this case, represents the maximum angle that the optical axis of the tracker can be directed to either side of the orbital plane. Only stars within these angular limits were used for updates. It should be noted that the data for the outer gimbal limit of ± 2 degrees was generated using the typical star distribution case of the SIL mapper and the nominal error values for the SIMS-A gyro. In other words, the star tracker was forced to use the stars of that distribution. However, it is felt that the results are indicative of SIMS-B performance at ± 2 degrees since the difference between the two gyros is not important and the typical star distribution case for silicon has about the same number of stars as that for a star update interval of 20 degrees.

For a given star update interval there was also some reduction in the number of stars that could be used per orbit when the outer gimbal limit was reduced from ± 45 to ± 30 and ± 15 degrees. However, this reduction was not large enough to have any significant effect on the results in Figure 5-16 and Table 5-13.

It is interesting to note that SIMS-B could probably meet the performance requirement of 3.6 arcsecs for outer gimbal limits on the order of ± 10 degrees or less.

SIMS-B Sensitivity to Gyro Noise

In Figures 5-17 and 5-18 the sensitivity of performance to gyro random drift and constant angle noise (quantization,

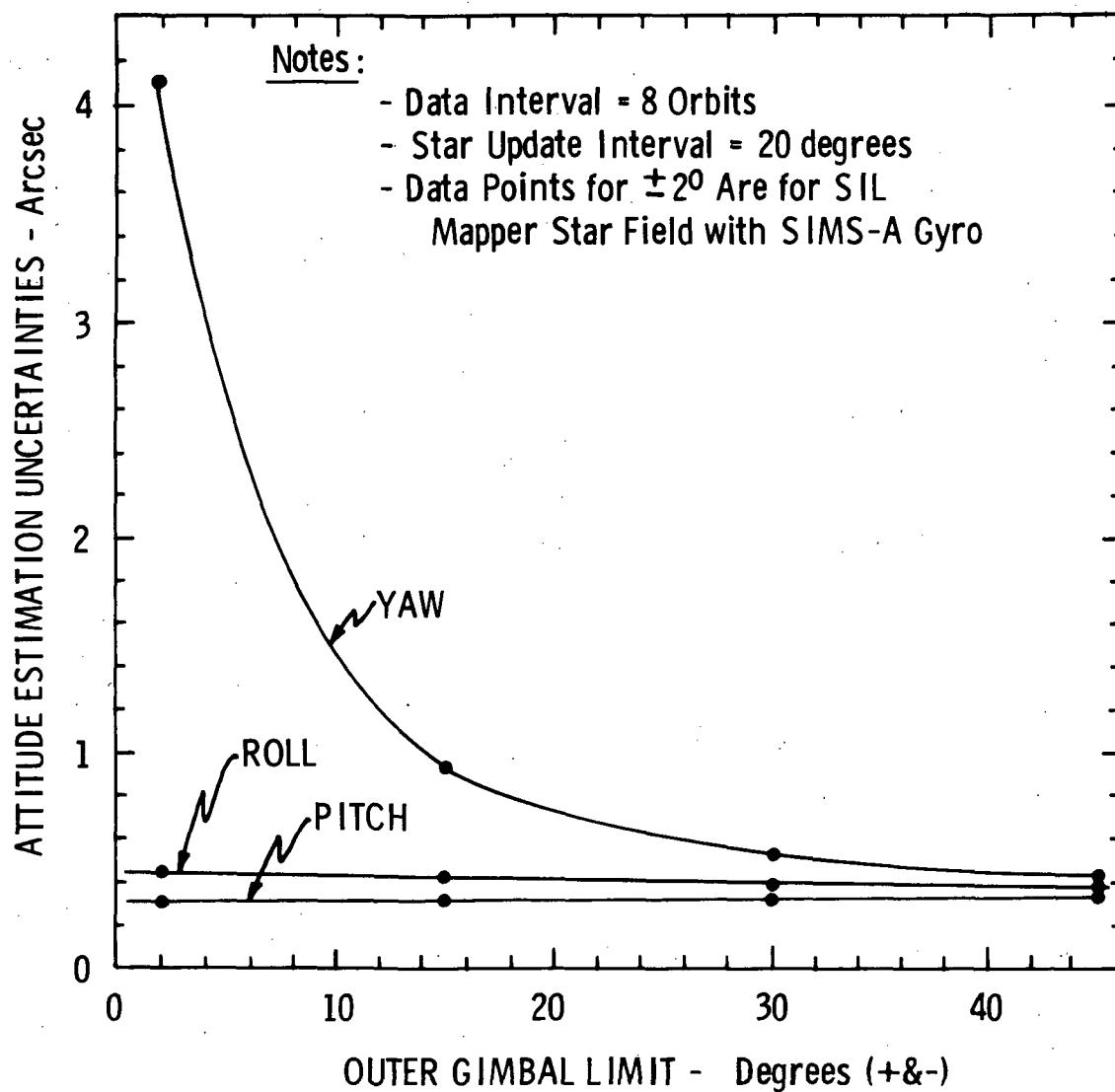


Figure 5-16 SIMS-B Sensitivity to Star Tracker Outer Gimbal Limit

Table 5-13

SIMS-B SENSITIVITY TO STAR TRACKER OUTER GIMBAL LIMIT

Outer (Roll) Gimbal Limit (deg)	Star Update Interval (deg)	Uncertainty (1σ) at Middle of Interval					
		Attitude (arcsec)			Gyro Bias Drift (10^{-3} deg/hr)		
		Pitch	Roll	Yaw	Y	X	Z
±45	8	0.3	0.4	0.4	0.03	0.2	0.1
	16	↓	↓	↓	↓	0.3	0.2
	20	↓	↓	↓	↓	0.3	0.2
	40	0.4	↓	0.5	↓	0.4	0.2
±30	8	0.3	↓	0.4	↓	0.3	0.1
	16	↓	↓	0.5	↓	0.4	0.2
	20	↓	↓	0.5	↓	0.4	0.2
	40	↓	↓	0.7	↓	0.5	0.2
±15	8	↓	↓	0.6	↓	0.5	0.1
	16	↓	↓	0.9	↓	0.8	0.2
	20	↓	↓	0.9	↓	0.9	0.2
	40	↓	0.5	1.6	↓	1.5	0.3
±2 (See Note)		↓	0.4	4.1	0.05	4.1	0.1

NOTES: Data Interval = 8 Orbits

±2 Degree Case is for Star Tracker using

Typical Star Field of SIL Mapper and

SIMS-A Gyro

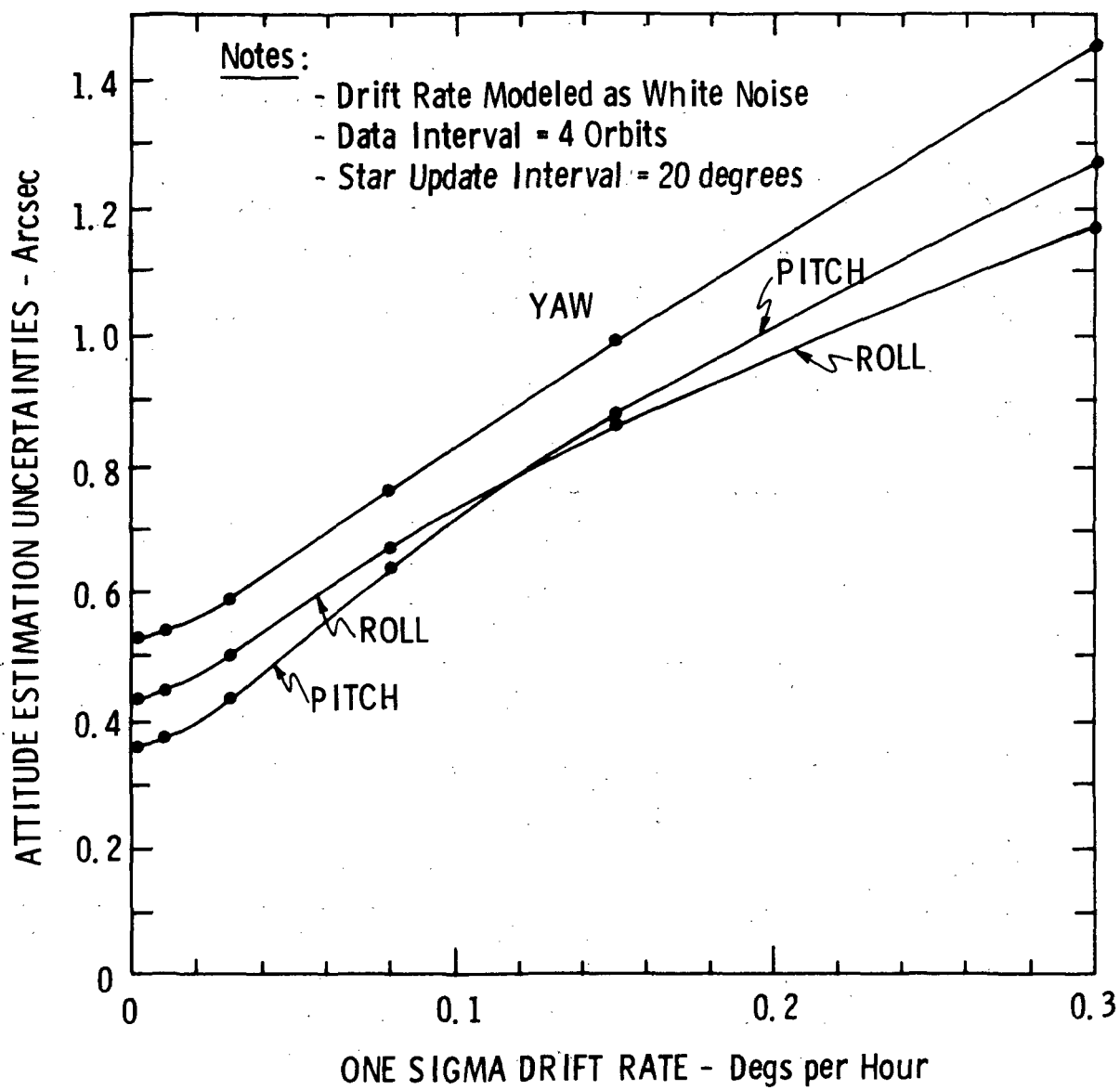


Figure 5-17 SIMS-B Sensitivity to Gyro Random Drift

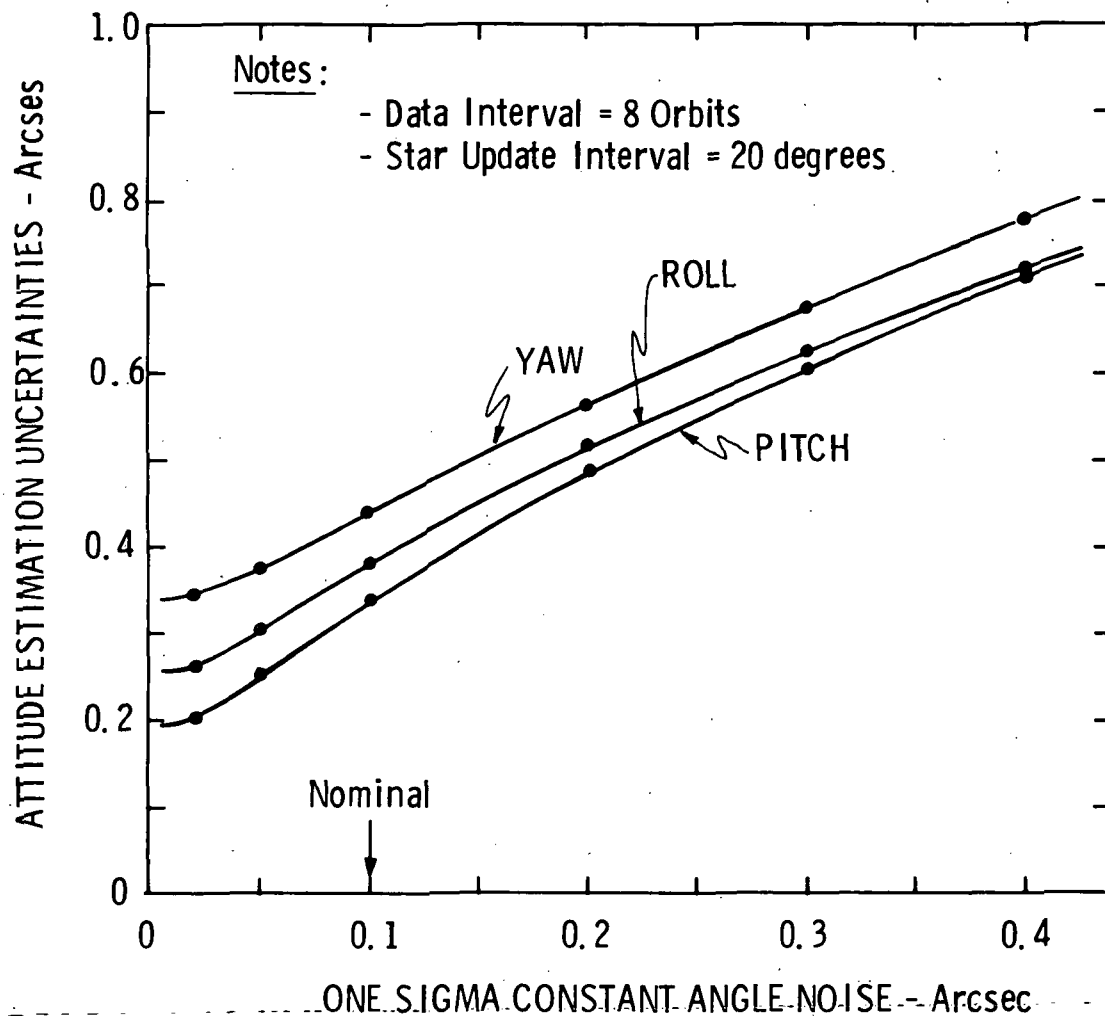


Figure 5-18 SIMS-B Sensitivity to Gyro
Constant Angle Noise

etc) is shown for 4 orbits of data processing. The gyro random drift rate was modeled as a white noise from 0 to 0.5 hertz. It is seen that the gyro noise would not have a serious effect on performance if it were a few times larger than nominal.

SIMS-B Performance Using Star Field of SIL Mapper and
SIMS-A Gyro

In Table 5-14 the performance of SIMS-B is shown for the case where the gyro is that of SIMS-A and the star tracker is forced to use the stars of the typical star distribution of the SIL mapper with a 4° FOV. These results were generated as a rough check of the performance obtained in SIMS-A. It is seen that the results are in reasonable agreement with those of SIMS-A in Figure 5-4. The small difference between the two is primarily due to the larger measurement error of the tracker as compared with the SIL mapper. These results tend to indicate that the original technique of measurement in SIMS-A is satisfactory.

5.4.4 ERROR STUDY RESULTS FOR SIMS-D

Unless otherwise noted, the nominal values of the error sources and parameters used to generate the results in this subsection are the following:

Initial State Uncertainties (1σ)

Pitch, Roll, Yaw - 60 arcsec (each)
Gyro Bias Drift - 0.03 deg/hr (each)

Star Mapper (SIL)

Field-of-View = 4 degrees
Pointing Direction - towards zenith
Measurement Error (1σ) = 1.1 arcsec
Detector Magnitude Threshold = 3.6
Star Distribution - typical for SIL mapper
Measurement Technique - original

Table 5-14

SIMS-B PERFORMANCE USING STAR FIELD OF SIL MAPPER
AND SIMS-A GYRO

Interval Size (Orbits)	Uncertainty (1σ) at Middle of Interval					
	Attitude(arcsec)			Gyro Bias Drift (10^{-3} deg/hr)		
	Pitch	Roll	Yaw	Y	X	Z
2	0.3	0.4	8.1	0.11	8.0	0.21
4	↓	↓	5.8	0.05	5.8	0.15
8	↓	↓	4.1	0.04	4.1	0.11
12	↓	↓	3.4	0.03	3.3	0.09

Gyro (TGG)

Random Drift - modeled so that the resulting
variance in angle is $10^{-10} t^2$ arcsec²
Constant Angle Noise (1σ) = 0.01 arcsec

IARU Gimbal Angle Error (1σ)

Middle, Outer - 1.3 arcsec (each)
Inner - 2.2 arcsec

In SIMS-D only the SIL mapper of SIMS-A was used for star measurements. As previously noted, the nominal characteristics of the SIL mapper used in this study do not represent the latest thinking on this sensor. However, it is felt that the sensitivity results for certain error sources and parameters of the mapper will enable one to predict fairly well what the performance would be for different values of these error sources and parameters.

As previously indicated in Section 5.3.4, the smoother formulation for SIMS-D is used to generate smoothed estimates of the uncertainties in the orientation of the gyro platform. This data is then converted to the equivalent uncertainties in vehicle pitch, roll, and yaw. In doing this, no allowance was made for the additional error associated with reading the IARU gimbal angles. It was indicated in Section 5.3.4 that one could reduce the effects of this additional error source by using a second smoother formulation to smooth more than one set of gimbal angle readings. A rough estimate of what the overall performance would be after smoothing a few closely-spaced sets of gimbal angle readings is as follows: In SIMS-D the gimbal angle sequence was chosen so that the inner, middle, and outer gimbal axes correspond to the vehicle pitch, roll, and yaw axes, respectively. Consequently, errors in the inner, middle, and outer gimbal angles correspond to errors in pitch, roll, and

yaw, respectively. The nominal one sigma values of the errors in the inner, middle, and outer gimbal angles are 2.2, 1.3, and 1.3 arcsecs, respectively. As will be seen later in Figure 5-19, the uncertainties in pitch, roll, and yaw estimated by the Fraser two-filter smoother formulation are about 0.2, 0.5, and 0.5 arcsecs, respectively, for 8 orbits of data processing. For a single set of gimbal angles, the overall performance will be the RSS of these values which are 2.2, 1.4, and 1.4 arcsecs, respectively. If 4 sets of closely-spaced but independent gimbal angle readings are taken and smoothed, the gimbal errors will be reduced by a factor of two (i.e., the square root of the number of sets). The overall performance in pitch, roll, and yaw for the latter case would now be 1.1, 0.8, and 0.8 arcsecs, respectively.

SIMS-D Performance Versus Data Interval Size

In Figure 5-19 the effect of variation in data processing interval size is shown for a nominal SIMS-D using the SIL mapper. Note that the performance is similar to that of SIMS-B in Figure 5-14. In comparison with SIMS-A a significant improvement has been made in yaw performance. This is due to the continuous change in geometry between the star mapper and the gyro package of SIMS-D. In SIMS-A the star mapper and gyros are fixed to the vehicle and the star mapper provides attitude information mostly in pitch and roll when pointing towards zenith. In SIMS-D the star mapper rotates with respect to the gyro platform and provides good attitude information about all axes of the gyro platform.

SIMS-D Sensitivity to Initial State Uncertainties

In Table 5-15 the sensitivity of performance to initial uncertainties in attitude and gyro bias drift is given for 4 orbits of data processing. It is seen that the results are essentially independent of initial state uncertainties, and supports the comments made on this subject in Section 5.4.2 for SIMS-A.

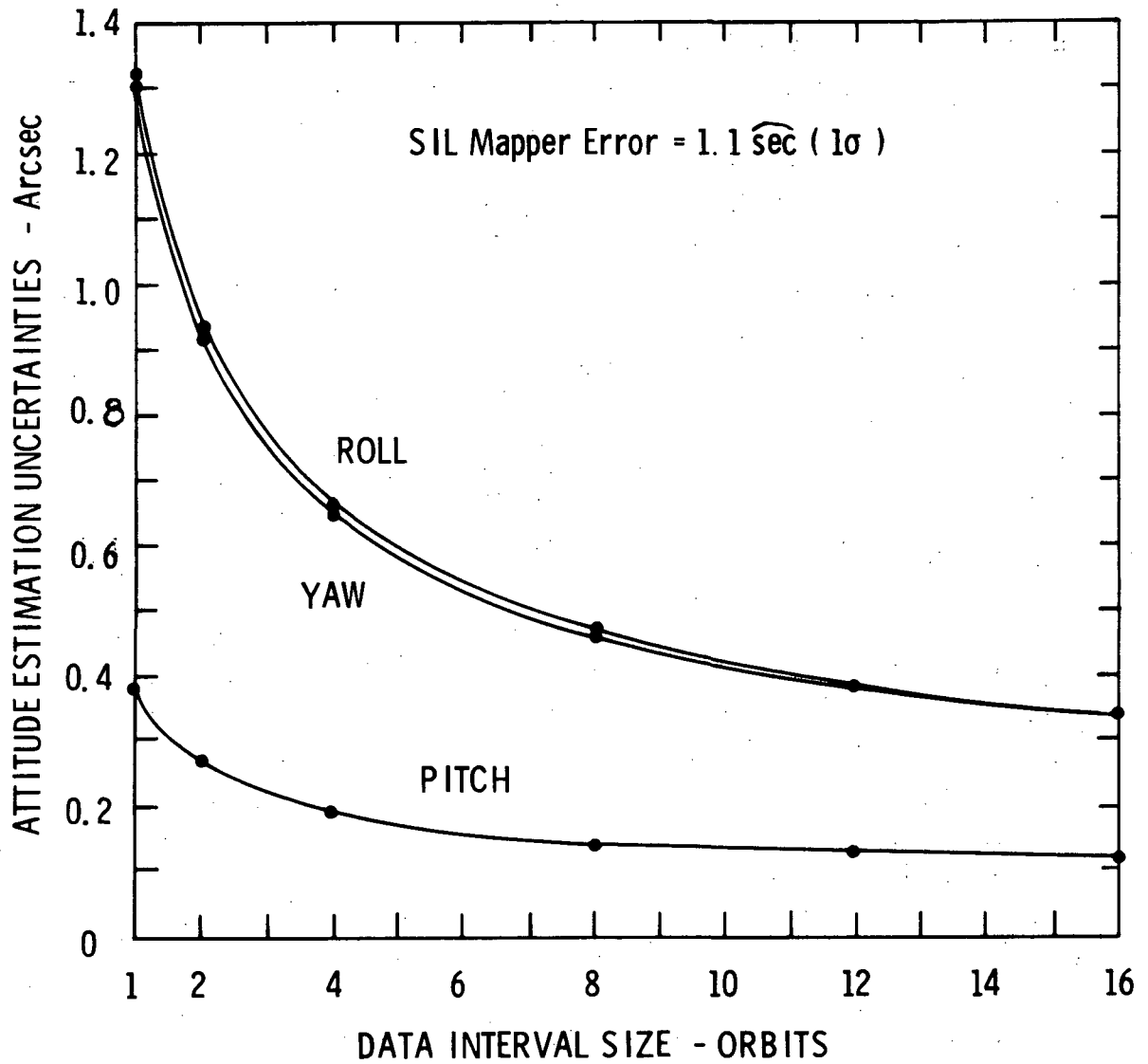


Figure 5-19 SIMS-D Performance Versus Data Processing Interval Size

Table 5-15

SIMS-D SENSITIVITY TO INITIAL STATE UNCERTAINTIES

Initial Uncertainty (per axis)		Uncertainty (1σ) at Middle of Interval					
Attitude (arcsec)	Gyro Bias Drift (deg/hr)	Attitude (arcsec)			Gyro Bias Drift (10^{-3} deg/hr)		
		Pitch	Roll	Yaw	Z	Y	X
0.5	0.03	0.2	0.6	0.6	0.03	0.1	0.06
1	(Nominal)		0.7	0.7			0.07
2							0.09
5							0.10
10							
30							
60							
120							
240							
60	0.0015						
(Nominal)	0.0030						
	0.0075						
	0.015						
	0.030						
	0.075						
	0.15						
	0.30						
	0.60						

NOTES: Data Interval = 4 Orbits

SIL Mapper Error (1σ) = 1.1 arcsec

SIMS-D Performance at Various Points in Data Interval

In Table 5-16 the uncertainties in the smoothed estimates of state are shown for various points uniformly distributed throughout an 8 orbit data processing interval. It is seen that the performance is somewhat the same throughout the interval.

SIMS-D Sensitivity to Mapper Measurement Error

Figure 5-20 shows the sensitivity of performance to SIL mapper measurement error for 4 orbits of data processing. It is seen that there is very little degradation in performance when the measurement error is twice nominal (which is 1.1 arcsec).

SIMS-D Sensitivity to Mapper FOV

In Figure 5-21 the sensitivity of performance to the size of the field-of-view (FOV) of the SIL mapper is shown for 4 orbits of data processing. Note there is some improvement when the FOV is increased from 4 to 6 degrees, but this improvement is not considered necessary in SIMS-D since the performance is well within the required accuracy of 3.6 arcsecs.

SIMS-D Sensitivity to Detector Magnitude Threshold

Figure 5-22 shows the sensitivity of performance to detector magnitude threshold of the SIL mapper for 4 orbits of data processing. The results are given for an FOV of 4 and 8 degrees. The numbers next to the data points for the yaw curves indicate the number of stars brighter than the indicated detector magnitude threshold for the star distribution cases used to generate the results. It is seen that the roll and yaw performance for an 8° FOV at a magnitude threshold of 3.2 is the same as that for a 4° FOV at a magnitude threshold of 4.0. However, the overall performance would be considered acceptable even if a magnitude threshold of 3.2 were used with a 4° FOV.

Table 5-16

SIMS-D PERFORMANCE AT VARIOUS POINTS IN
8 ORBIT DATA PROCESSING INTERVAL

Time Since Start of Interval (secs)	Uncertainty (1σ) at Indicated Times					
	Attitude (arcsec)			Gyro Bias Drift (10^{-3} deg/hr)		
	Pitch	Roll	Yaw	Z	Y	X
6300	0.2	0.8	0.8	0.01	0.03	0.03
12600	↓	0.6	0.6	↓	↓	↓
18900	↓	0.5	0.5	↓	↓	↓
25200	0.1	↓	↓	↓	↓	↓
31500	0.2	↓	↓	↓	↓	↓
37800	↓	0.6	0.6	↓	↓	↓
44100	↓	0.8	0.8	↓	↓	↓

NOTES: SIL Mapper Error (1σ) = 1.1 arcsec
8 Orbits = 50400 seconds

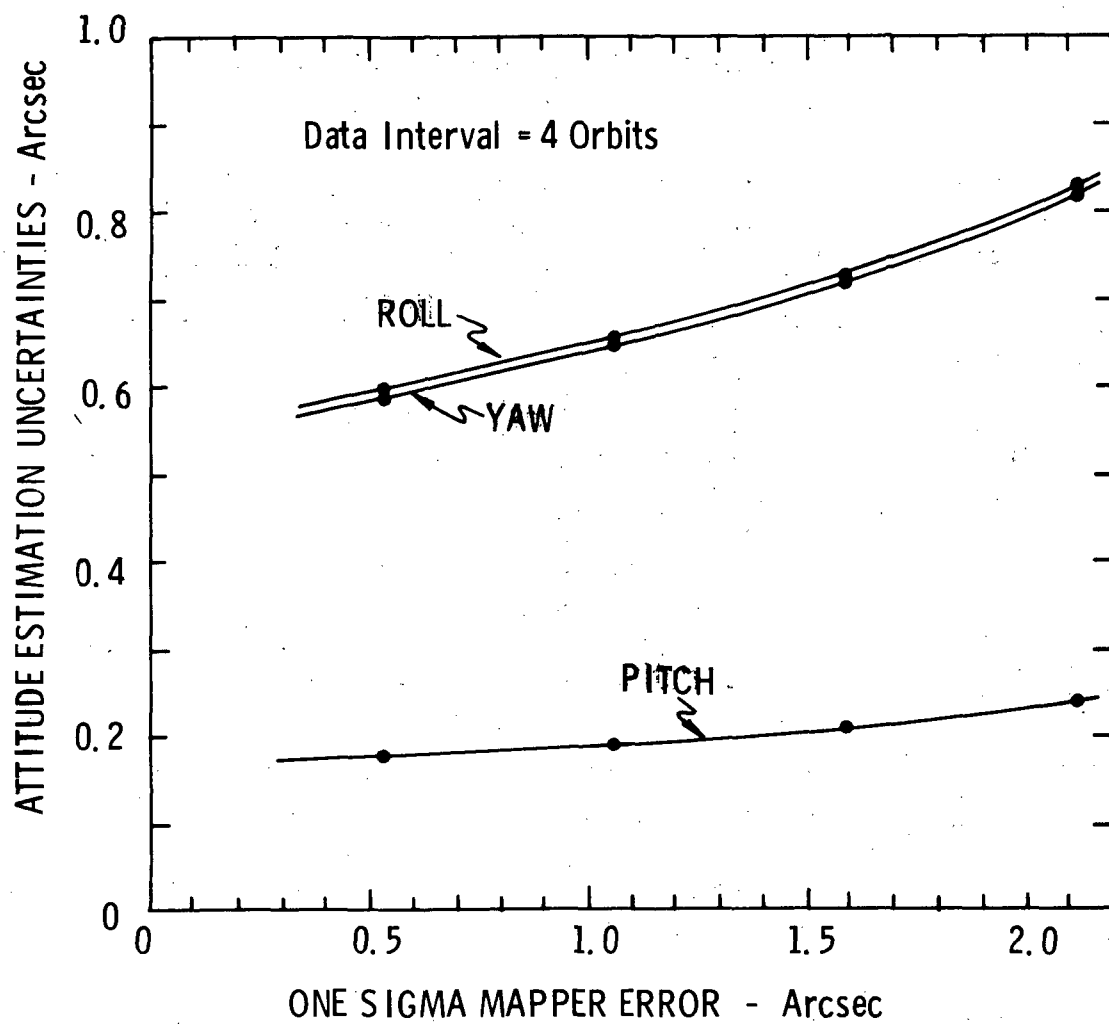


Figure 5-20 SIMS-D Sensitivity to SIL Mapper Measurement Error

Notes SIL Mapper Error (1σ) = 1.1 sec
Data Interval = 4 Orbits

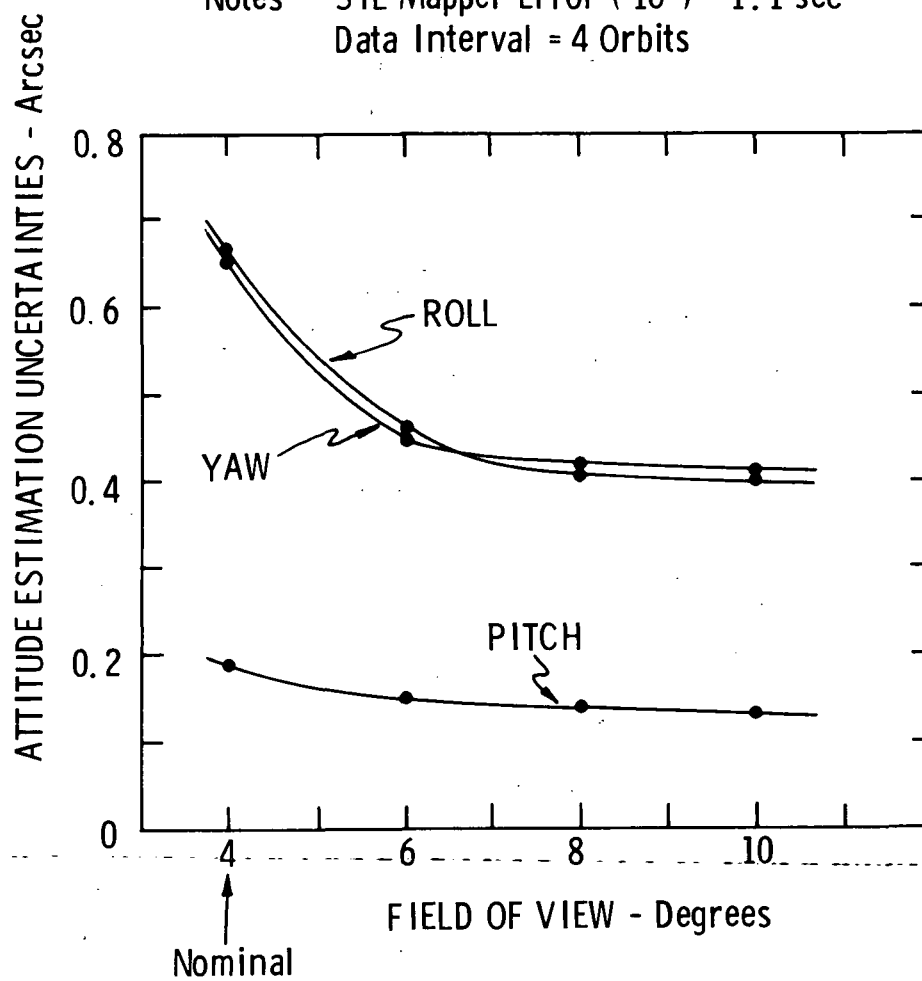


Figure 5-21 SIMS-D Sensitivity to FOV of SIL Mapper

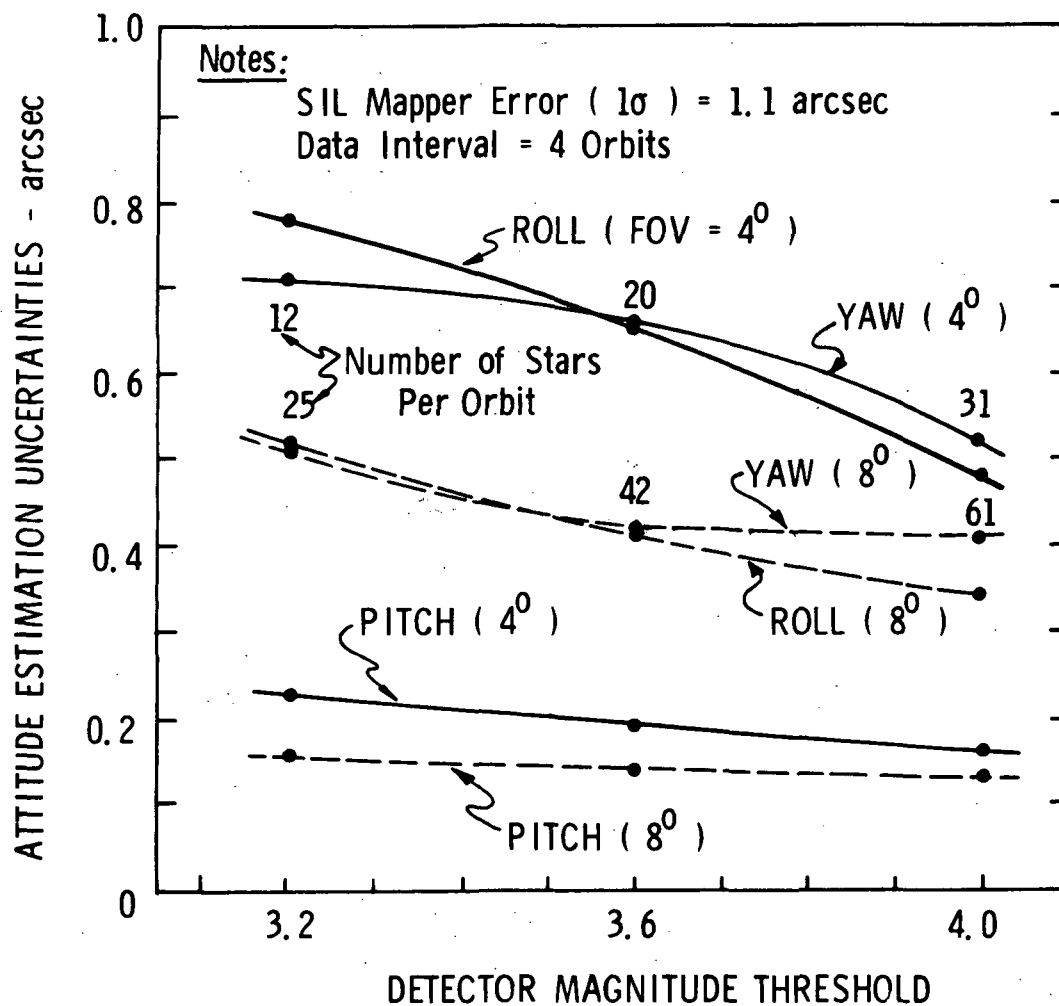


Figure 5-22 SIMS-D Sensitivity to Detector Magnitude Threshold of SIL Mapper

SIMS-D Sensitivity to IARU Gimbal Errors

In Figure 5-23 and Table 5-17 the sensitivity of performance to IARU gimbal errors is shown for 4 orbits of data processing. Figure 5-23 shows the effect of simultaneous variation of the one sigma values of the inner, middle, and outer gimbal angle errors. The one sigma values are expressed relative to their nominal values. It is seen that the uncertainties are still no more than about 1.2 arcsecs when the one sigma values are twice nominal. Table 5-17 shows the effect of variation in the one sigma value of each gimbal angle error when the remaining two are nominal.

SIMS-D Sensitivity to Gyro Random Drift

In Figures 5-24 and 5-25 the sensitivity of performance to gyro random drift is shown for two different models of random drift rate. Figure 5-24 shows the results when the noise model adopted as nominal for the TGG gyro is used (see subsection 5.5 of ref. 141). This noise model causes an angular error whose variance is a function of t^2 . Figure 5-25 shows the results when a white noise model is used, such as was the case for SIMS-A and -B. For either model it is seen that a stringent requirement is not required on gyro random drift.

SIMS-D Sensitivity to Gyro Constant Angle Noise

In Figure 5-26 the sensitivity of performance to gyro constant angle noise is shown for 4 orbits of data processing. It is seen that this noise could be many times larger than the nominal value without seriously affecting the performance.

SIMS-D Performance for Two Techniques of Star Measurement

In Table 5-18 the performance is shown for the two different techniques of star mapper measurement described in

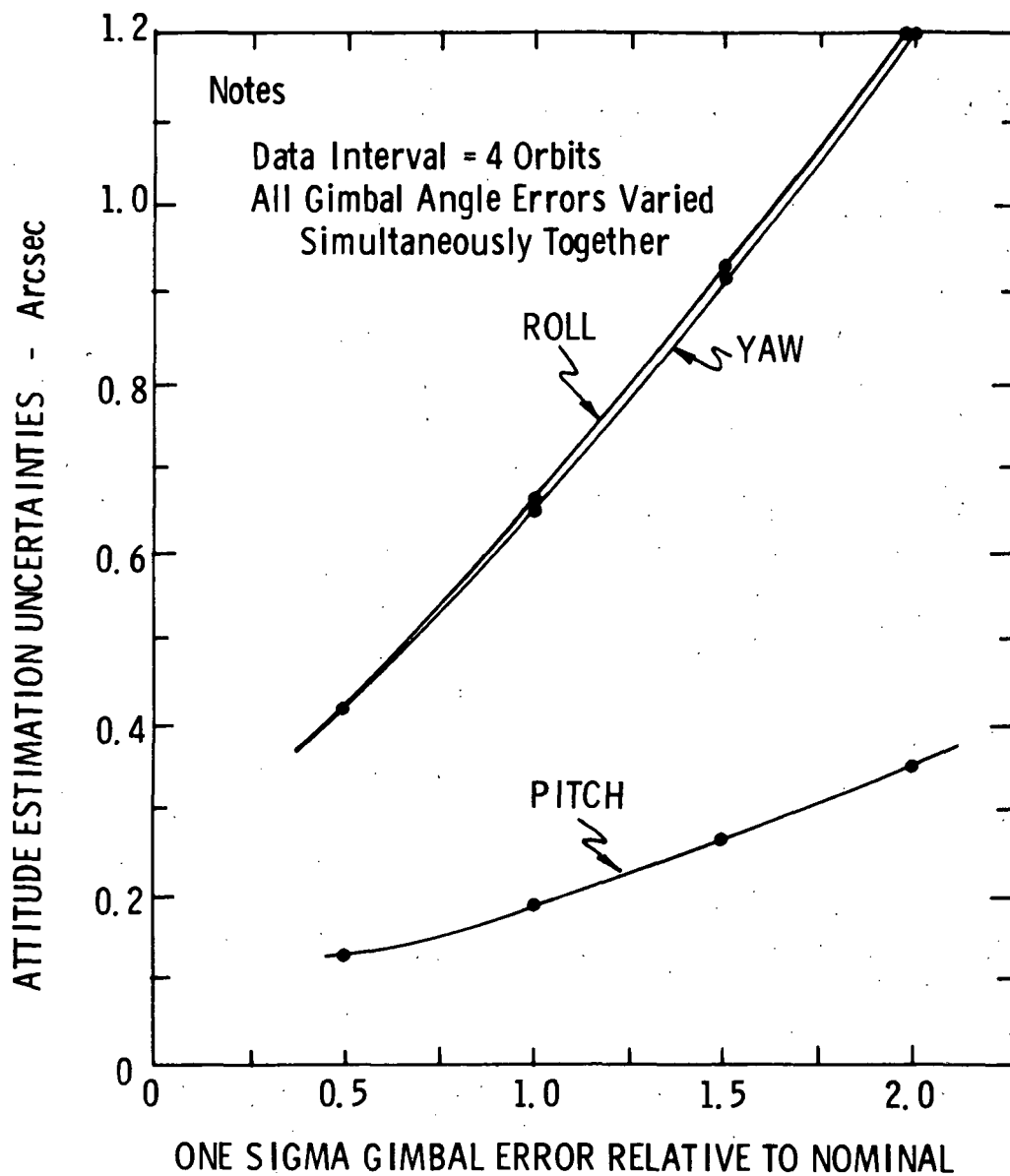


Figure 5-23 SIMS-D Sensitivity to IARU Gimbal Errors

Table 5-17

SIMS-D SENSITIVITY TO IARU GIMBAL ERRORS

Gimbal Error Being Changed	One Sigma Relative To Nominal	Uncertainty (1σ) at Middle of Interval					
		Attitude(arcsec)			Gyro Bias Drift(10 ⁻³ deg/hr)		
		Pitch	Roll	Yaw	Z	Y	X
All 3	0.5	0.1	0.4	0.4	0.02	0.06	0.06
	1.0	0.2	0.7	0.7	0.03	0.09	0.09
	1.5	0.3	0.9	0.9	0.03	0.12	0.12
	2.0	0.4	1.2	1.2	0.05	0.17	0.17
Inner	0.5	0.1	0.5	0.5	0.02	0.06	0.06
	1.0	0.2	0.7	0.7	0.03	0.09	0.09
	1.5	0.3	0.9	0.9	0.03	0.12	0.12
	2.0	0.3	1.1	1.1	0.05	0.15	0.15
Middle	0.5	0.2	0.6	0.6	0.09	0.09	0.03
	1.0	↓	0.7	0.7	0.03	↓	0.09
	1.5	↓	0.7	0.7	↓	↓	0.09
	2.0	↓	0.8	0.8	↓	0.10	0.10
Outer	0.5	0.2	0.7	0.7	0.03	0.09	0.09
	1.0	↓	↓	↓	↓	↓	↓
	1.5	↓	↓	↓	↓	↓	↓
	2.0	↓	↓	↓	↓	↓	↓

NOTES: Data Interval = 4 Orbits

$$\text{Nominal Gimbal Errors (1}\sigma\text{)} = \begin{cases} \text{Inner} = 2.2 \text{ } \overline{\text{sec}} \\ \text{Middle} = 1.3 \text{ } \overline{\text{sec}} \\ \text{Outer} = 1.3 \text{ } \overline{\text{sec}} \end{cases}$$

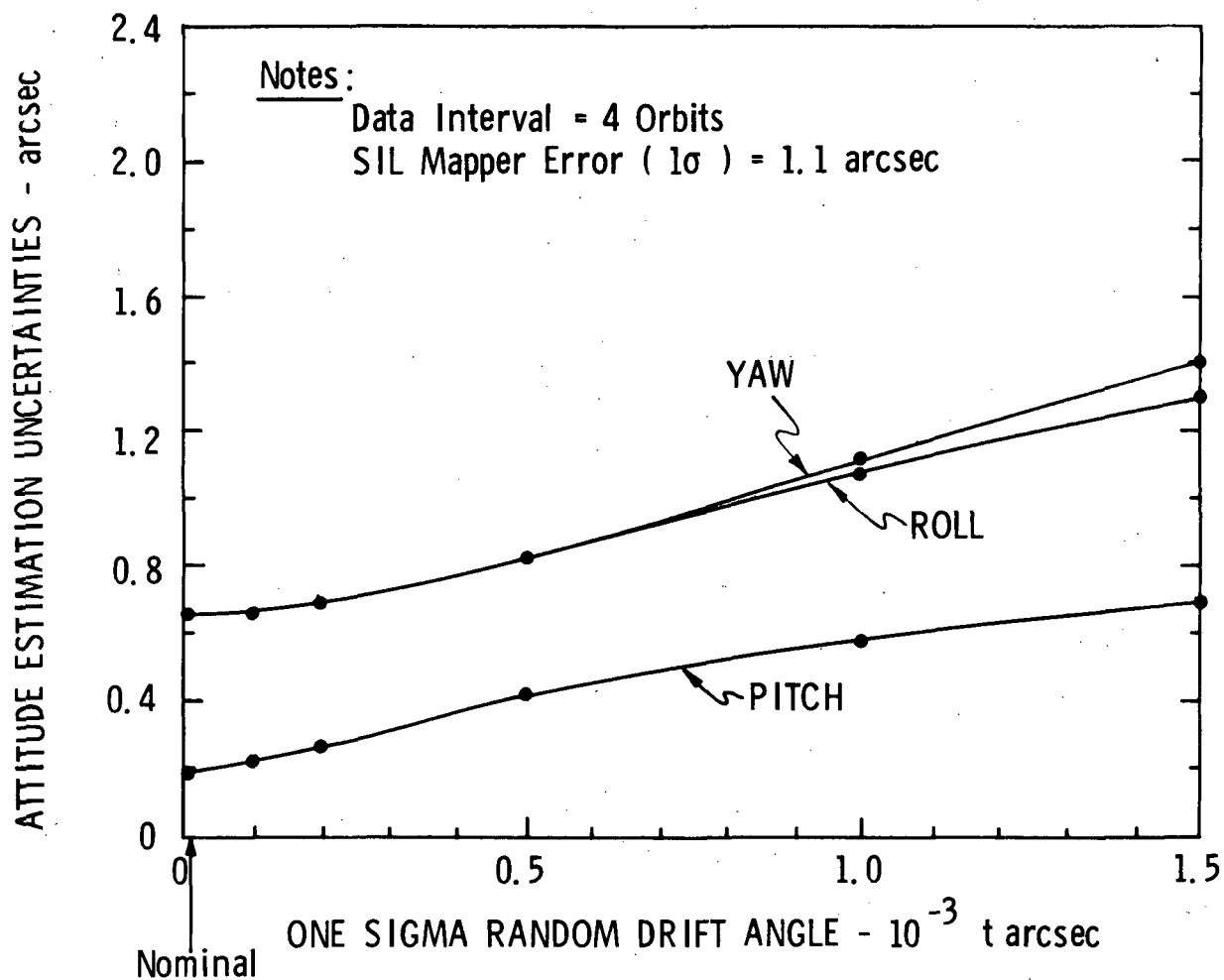


Figure 5-24 SIMS-D Sensitivity to Gyro Random Drift as Modeled for TGG gyro

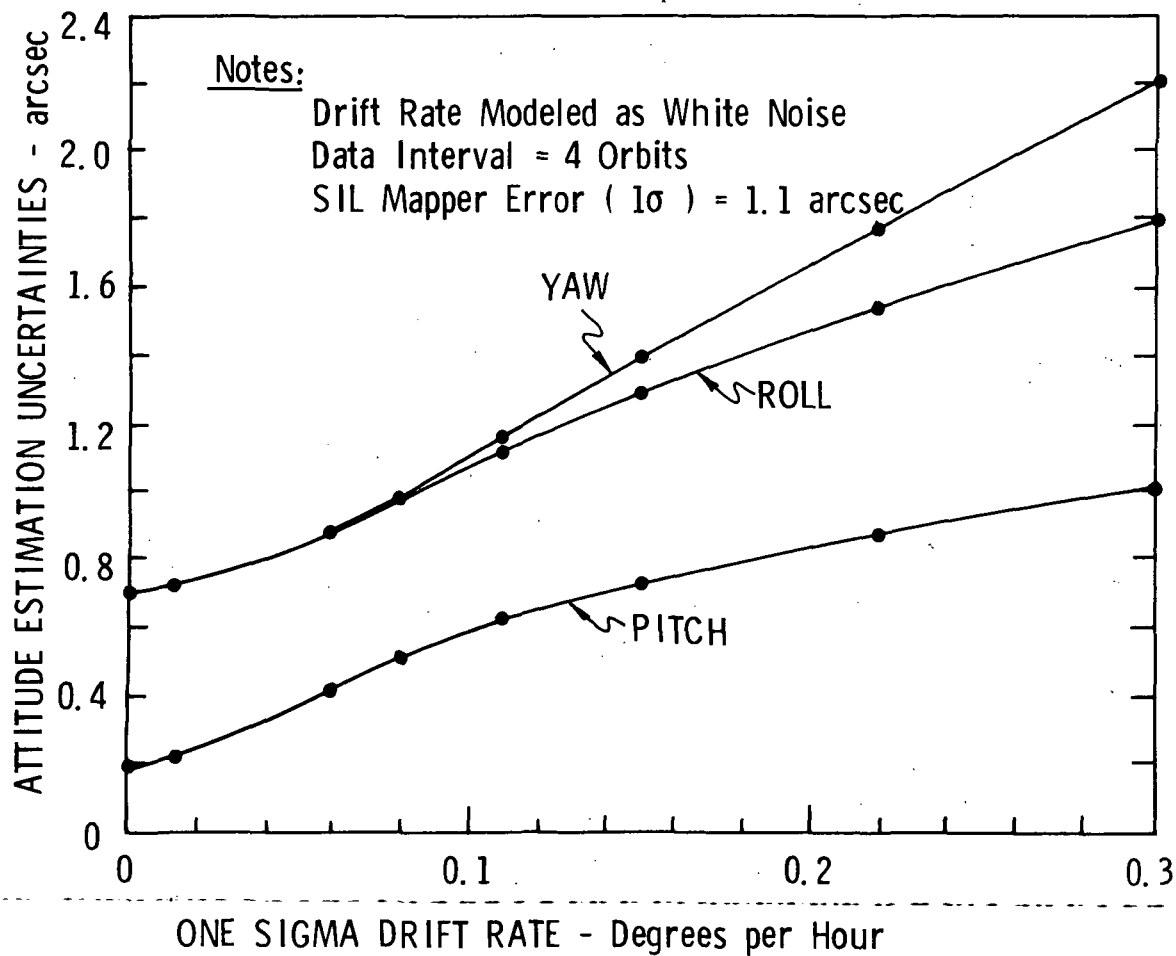


Figure 5-25 SIMS-D Sensitivity to Gyro Random
Drift Rate Modeled as White Noise

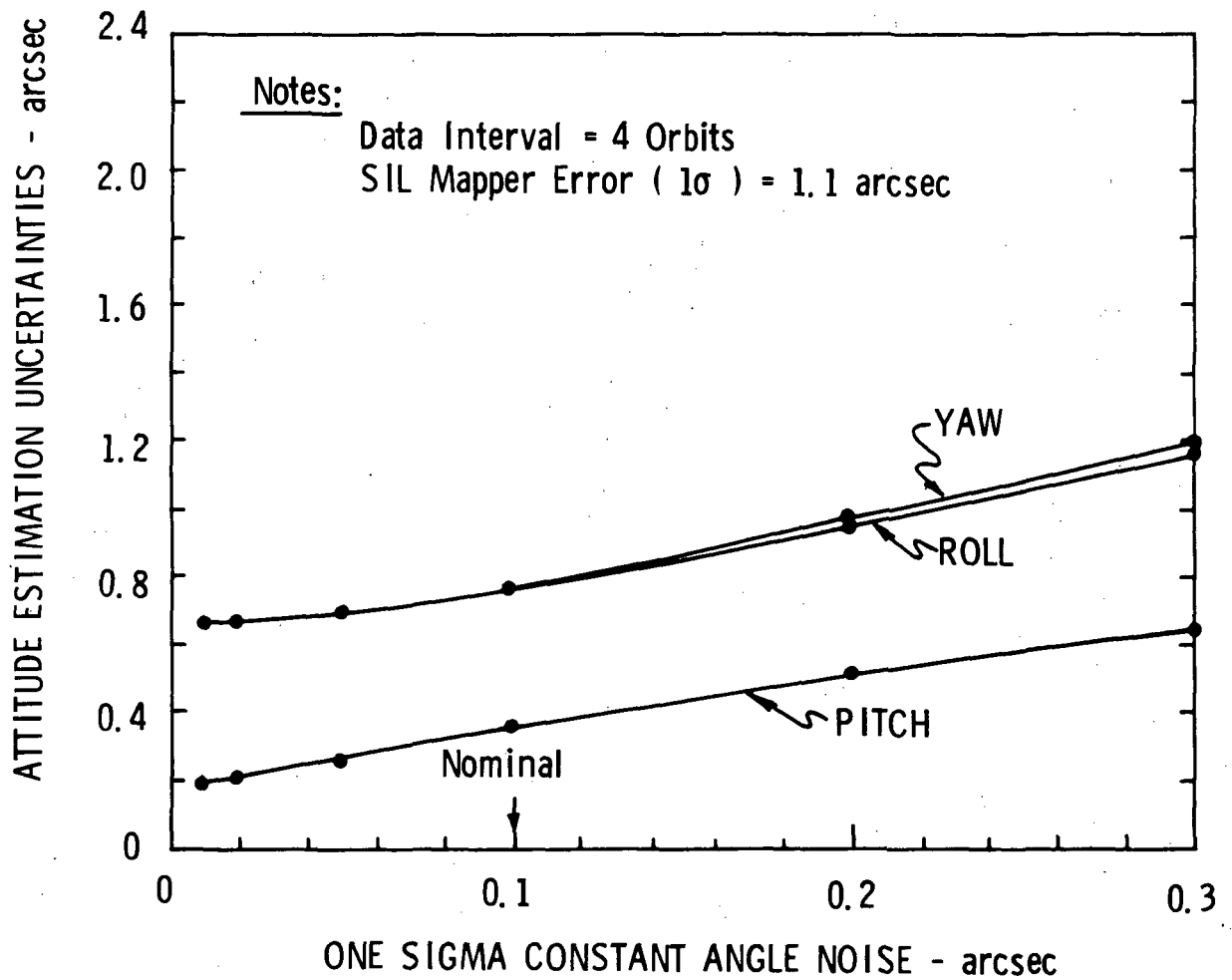


Figure 5-26 SIMS-D Sensitivity to Gyro Constant Angle Noise

Table 5-18

SIMS-D PERFORMANCE FOR TWO TECHNIQUES
OF STAR MEASUREMENT

Star Measurement Technique	Interval Size (Orbits)	Uncertainty (1σ) at Middle of Interval					
		Attitude(arcsec)			Gyro Bias Drift(10^{-3} deg/hr)		
		Pitch	Roll	Yaw	Z	Y	X
Original (Nominal) ↓	1	0.4	1.3	1.3	0.22	0.68	0.93
	2	0.3	0.9	0.9	0.25	0.08	0.27
	4	0.2	0.7	0.7	0.03	0.09	0.09
	8	0.1	0.5	0.5	0.01	0.03	0.03
	12	↓	0.4	0.4	↓	0.03	0.03
	16	↓	0.3	0.3	↓	0.01	0.01
Alternate ↓	1	0.4	1.5	1.4	0.22	0.74	1.02
	2	0.3	1.0	1.0	0.08	0.27	0.29
	4	0.2	0.7	0.7	0.03	0.11	0.11
	8	0.2	0.5	0.5	0.01	0.03	0.03
	12	0.1	0.4	0.4	↓	0.02	0.02
	16	0.1	0.4	0.4	↓	0.01	0.01

NOTES: SIL Mapper Error (1σ) = 1.1 arcsec

subsec. 5.3.4.2. These are identified as the 'original' and 'alternate' techniques of measurement, where the former has been used as the nominal technique. It is seen that there is very little difference in the results for the two techniques.

5.5 CONSIDERATION OF ADDITIONAL ERROR SOURCES

5.5.1 INTRODUCTION

The primary purpose of this section is to consider to some extent those error sources which were not accounted for in the performance results of subsec. 5.4. In doing this, various simplifying assumptions were made in order to obtain rough estimates of the contributions made by some of these sources. Although these rough estimates are obviously not as good as those which could be obtained through computer simulation, it is felt that they at least give some indication of the magnitude and nature of the contributions made by these sources. In some cases only brief comments are made about an error source since its effect on system performance is sometimes complex and really requires computer simulation. It should be noted that the effect of some of these error sources on the performance of SIMS-A will be analyzed in greater detail in the follow-on effort.

Most of the error sources in this category are bias-type error sources. With the exception of gyro bias drift, the other bias-type error sources were not modeled in the smoother formulation for the following reasons:

- 1) Gyro bias drift is considered to be the most significant bias-type error in any of the candidates.
- 2) To account for a bias-type error in the smoothing formulation, one must usually include it as an additional parameter to be estimated along with the

spacecraft attitude. Since this results in a significant increase in computation, the number of biases handled in this manner were kept to a minimum.

- 3) By including gyro bias drift in the smoothing estimates, one has also accounted, to some extent, for gyro scale factor bias error and gyro misalignment bias which have somewhat the same effect as bias drift when the deviations in attitude rates are small as expected in this type of mission. In fact, the bias drift estimates will include the contributions made by these two other sources except for those components associated with the changes in attitude rate. If the changes in attitude rate are known, one can sometimes roughly estimate what these additional errors will be.
 - 4) In the present study effort, the smoother formulation was only used to study the candidates for a nominal attitude history and a circular orbit. Under these circumstances, there was no change in the attitude rates. Consequently, there was nothing to be gained by estimating gyro scale factor bias error and gyro misalignment bias in the smoother formulation.
-

In addition to bias-type errors, there are also some random-type errors which were not specifically accounted for in the smoother formulation. Examples of these are the random components of gyro scale factor error and gyro misalignment. Although these were found to be insignificant, they were also considered in this section.

In the following sub-sections, separate consideration is given to gyro scale factor error and gyro misalignment since these are considered to be the next most important gyro errors after bias drift in SIMS-A and -B. This is primarily due to the fact that these two error sources, like bias drift, produce an unbounded error which grows with time. It should be noted that we are concerned with only the unknown component of a gyro bias error in this section since one can compensate for the known component. Consequently, the bias errors in the following discussion should be looked upon as being the unknown components.

5.5.2 GYRO SCALE FACTOR ERROR

The angular rate measured by a gyro can be expressed as:

$$\omega_m = (1 + b_{SF} + n_{SF})\omega_T + b_D + n_D \quad (5-82)$$

where

ω_T = true angular rate sensed by the gyro

b_{SF} = scale factor bias error

n_{SF} = scale factor noise error

b_D = drift rate bias (usually referred to as bias drift)

n_D = drift rate noise (usually referred to as random drift)

Note that Equation 5-82 can be re-arranged as follows:

$$\omega_m = \omega_T + b_{SF}\omega_T + b_D + n_{SF}\omega_T + n_D \quad (5-83)$$

where the first term on the right represents the rate that we wish to measure about the gyro input axis and the remaining terms are the quantities which prevent the gyro from correctly measuring this rate.

To estimate the effects of gyro scale factor error, two cases will be considered: In one, there are no changes in the attitude rates; in the other, there are attitude rate changes of the magnitude anticipated in the EOS mission.

Case of No Attitude Rate Change

If there are no changes in the attitude rates, the true angular rate ω_T about the gyro input axis will remain fixed. Consequently, $b_{SF}\omega_T$ will be indistinguishable from the bias drift b_D and will be included in the estimation of b_D by the smoother formulation. This would be the case for a nominal attitude history in a circular orbit in an inertially-fixed plane. It is also the case for a vehicle attitude displaced from nominal by a fixed amount.

For a nominal attitude history the roll (X) and yaw (Z) gyros are in the orbital plane, and the pitch (Y) gyro is perpendicular to this plane. For this case the roll and yaw gyros do not sense any angular rate ω_T and that sensed by the Y gyro is equal to the constant orbital rate ω_0 .

In the EOS mission it is understood that the attitude control system will maintain all axes to within 0.2° (1σ) of an attitude which is within $\pm 0.5^\circ$ of nominal. In addition, the attitude control rates will be within 0.005 degrees per second (3σ) of nominal.

If the vehicle attitude is displaced from nominal by a fixed amount of 0.5 degrees about the roll and yaw axes, the rates sensed by the roll and yaw gyros will each be about $\omega_0 \sin(0.5^\circ) = 1.8$ degrees per hour, where ω_0 is assumed to be 206.5 degrees per hour for an EOS mission. In this case the pitch gyro for all practical purposes will continue to sense the full value of ω_0 . If the nominal value of 10 parts per million (PPM) is assumed for b_{SF} in SIMS-A and -B, the following values will exist for the term $b_{SF}\omega_T$:

$$\begin{aligned} \text{Y Gyro} & - (10^{-5})(206.5) \cong 2 \times 10^{-3} \text{ deg/hr} \\ \text{X Gyro} & - (10^{-5})(1.8) \cong 2 \times 10^{-5} \text{ deg/hr} \\ \text{Z Gyro} & - (10^{-5})(1.8) \cong 2 \times 10^{-5} \text{ deg/hr} \end{aligned} \quad (5-84)$$

Here it is seen that the above values are insignificant in comparison to what is expected for b_D even though both will be included in the estimation of b_D by the smoother formulation. For this case it would seem that one could permit even larger values for b_{SF} such as 50 PPM.

In Equation 5-83 it is seen that $n_{SF}\omega_T$ and n_D would also be indistinguishable if both had the same noise characteristics. In the performance results of Section 5.4, n_D was assumed to be a white noise with one sigma values of 0.01 and 0.002 degrees per hour for SIMS-A and -B, respectively. Little is known about the noise characteristics of n_{SF} ; however, if n_{SF} were assumed to be a white noise with a one sigma value of 5 PPM, then the term $n_{SF}\omega_T$ would be indistinguishable from n_D and the following values would exist for $n_{SF}\omega_T$ when the attitude is displaced from nominal

by 0.5 degrees about the roll and yaw axes:

$$\begin{aligned} \text{Y Gyro} &- (5 \times 10^{-6})(206.5) \cong 10^{-3} \text{ deg/hr} \\ \text{X Gyro} &- (5 \times 10^{-6})(1.8) \cong 10^{-5} \text{ deg/hr} \\ \text{Z Gyro} &- (5 \times 10^{-6})(1.8) \cong 10^{-5} \text{ deg/hr} \end{aligned} \quad (5-85)$$

Here it is seen that the above values for the X and Z gyros are insignificant, and that for the Y gyro is half as large as the nominal value of n_D for SIMS-B. It should be noted, however, that the sensitivity results in Section 5.4 indicate that even the nominal values used for n_D do not have any significant effect on system performance.

Case of Attitude Rate Change

If there are changes in the attitude rates, the true angular rate ω_T sensed by each gyro will also change. In this case there are two sources of change in ω_T . One is the additional rate (besides nominal) introduced by the attitude control system. In this report this rate is referred to as the libration rate ω_L . The other source of change in ω_T is due to the change in orientation of the vehicle which causes the gyros to sense a different component of the orbital rate.

First, let us consider the libration rate which is understood to be periodic in nature and is no larger than 0.005 degrees per second (3σ) about each axis. If it is assumed for the worst case that the attitude control system is limit cycling between ± 0.6 degrees (3σ) with a rate of 0.005 degrees per second, it

would take 120 seconds to go from 0 to 0.6 degrees. During this excursion the angular error introduced by b_{SF} for libration rate alone will build up to:

$$(10^{-5})(0.005)(120) = 6 \times 10^{-6} \text{ degrees.} \quad (5-86)$$

Afterwards, the libration rate will reverse polarity and the error will build up in the opposite direction by the same amount.

Next, let us consider the change in the component of orbital rate sensed by a gyro when the attitude deviates from a fixed orientation relative to nominal because of libration. To simplify matters let us assume that the attitude is nominal except for the libration which causes the attitude to deviate from nominal by ± 0.6 degrees about each axis. In this particular case the error due to the b_{SF} of the Y gyro will remain essentially fixed at the value previously given (i.e., 10^{-3} deg/hr) and will be included in the estimate of bias drift by the smoother formulation. However, the error due to the b_{SF} of the X and Z gyros will appear to be a bias drift which periodically varies with time in accordance with Figure 5-27. Note that we are only considering that portion of the b_{SF} error which is due to the departure of attitude from nominal because of libration. For example, when the X gyro is in the orbital plane, it does not sense the orbital rate ω_0 . However, when the X gyro deviates by a small angle δ out of the orbital plane, it will sense a rate equal to $\omega_0 \sin \delta$ which is ≈ 2.2 degrees per hour for $\delta = 0.6$ degrees. For a b_{SF} of 10 PPM the peak error in rate is $(10^{-5})(2.2) = 2.2 \times 10^{-5}$ degrees per hour (or 2.2×10^{-5} arcsecs per second) as shown in Figure 5-27. For the libration frequency shown in Figure 5-27 the

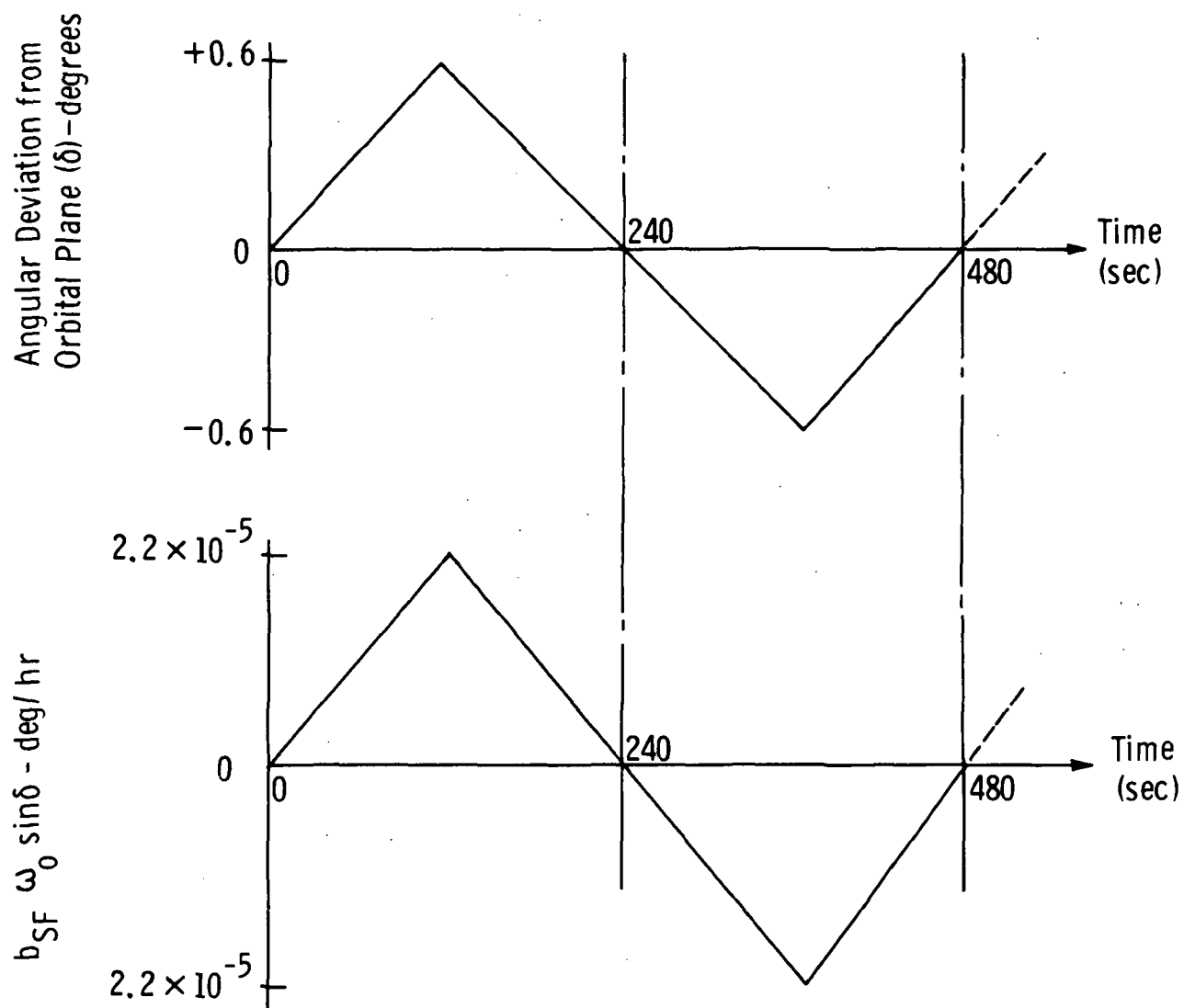


Figure 5-27 Rate Error Introduced by
Scale Factor Bias Error
When the Vehicle Attitude
Departs from Nominal

peak angle error due to the rate error will be $(120)(1.1 \times 10^{-5}) \approx 1.3 \times 10^{-3}$ arcsec. Even if the libration was such that it took 7 hours (i.e., 4 orbits) to go from zero to 0.6 degrees and back (highly unlikely), the peak angle error would be about 0.14 arcsec. It should be noted that on the average this error will be zero.

From the results generated in this section it would seem that gyro scale factor error does not have much effect on system performance if the nominal values assumed for this error are used. In fact, one could possibly relax the requirements on this error and still meet the desired system performance without having to estimate scale factor bias error in the smoother formulation.

5.5.3 GYRO INPUT AXIS MISALIGNMENT

Gyro input axis misalignment refers to incorrect alignment of the input axes of the gyros relative to each other. Ideally, the input axes of the three gyros should be orthogonal so that their integrated outputs may be interpreted by means of an orthogonal coordinate transformation. Incorrect knowledge of the directions of the gyro input axes causes the rates to be integrated about the wrong axes.

The input axis of a gyro can have two components of misalignment. For a given gyro these components are normally specified as small angles of rotation about the input axes of the other two gyros. In the present discussion the misalignment components of the roll (X) or the yaw (Z) gyro will normally be referred to as the in-plane and out-of-plane components. In general, it is the out-of-plane component of the X and Z gyros that is important. For the pitch (Y) gyro, both components are important because of the symmetry of this gyro with respect to orbital rate.

In SIMS-A and -B the nominal one sigma uncertainties assumed for the bias and random components of input axis misalignment are 10 and 5 arcsecs, respectively. It should be noted that only the uncertainty in the bias (i.e., the unknown value) will be considered in the present analysis since the known component can be compensated for.

In considering gyro input-axis misalignment frequent use will be made of the following truncated trigonometric series:

$$\sin(\delta + \epsilon) \cong \sin \delta + \epsilon \cos \delta \quad (5-87)$$

$$\cos(\delta + \epsilon) \cong \cos \delta - \epsilon \sin \delta - \epsilon^2 \cos \delta / 2 \quad (5-88)$$

where δ is the vehicle displacement from nominal about some vehicle axis and ϵ is the misalignment of the input axis of a gyro about the same vehicle axis.

The effects of input axis misalignment shall be considered for two different attitude situations just as was done for scale factor error in subsection 5.5.2. In one of these situations there are no changes in the attitude rates; in the other there are changes in the attitude rates of the amplitudes anticipated in the EOS mission.

Case of No Attitude Rate Change

If there is no change in the attitude rates, the gyro outputs will remain constant and that component of each output due to input axis misalignment will appear to be an equivalent bias drift and will be estimated along with bias drift by the smoother formulation. Typical values of the equivalent bias drift caused by the expected values of input-axis misalignment are as follows:

For a nominal attitude history in a circular orbit in an inertially-fixed plane, only the Y gyro should be sensing the orbital rate. If the input axis of the Y gyro happens to be misaligned by 10 arcsecs, the resulting error in the rate sensed by this gyro will be the following where use is made of only the last term on the right of Equation (5-88).

$$\begin{aligned}\omega_0 \left[-\epsilon^2/2 \right] &= -(206.5)(4.848 \times 10^{-5})^2/2 \\ &= 2.4 \times 10^{-7} \text{ degrees per hour} \quad . \quad (5-89)\end{aligned}$$

If either the X or Z gyro has an out-of-plane component of misalignment of 10 arcsecs, the resulting error in the rate sensed by the gyro will be the following where use is made of only the last term on the right of Equation 5-87;

$$\begin{aligned}\omega_0 \epsilon &= (206.5)(4.848137 \times 10^{-5}) \\ &= 0.0100114 \text{ degrees per hour} \quad . \quad (5-90)\end{aligned}$$

If the vehicle attitude is always displaced from nominal by a fixed amount of 0.6 degrees about either the X or Z axis, a 10 arcsec misalignment of the Y gyro will cause the following rate error:

$$\begin{aligned}\omega_0 \left[-\epsilon \sin \delta - \epsilon^2 \cos \delta/2 \right] &\approx \omega_0 \left[-\epsilon \sin \delta \right] \\ &\approx - (206.5)(4.848 \times 10^{-5})(\sin 0.6^\circ) \\ &\approx - 10^{-4} \text{ degrees per hour} \quad (5-91)\end{aligned}$$

If this vehicle displacement happens to be about the Z axis, a 10 arcsec out-of-plane misalignment of the X gyro will cause the following rate error:

$$\begin{aligned}\omega_0 \epsilon \cos \delta &= (206.5) (4.848137 \times 10^{-5}) (\cos 0.6^\circ) \\ &= 0.0100110 \text{ degrees per hour} \quad (5-92)\end{aligned}$$

which is essentially the same as that given in Equation (5-90). It is apparent that the same result will be obtained for the Z gyro if the displacement is about the X axis.

From the results generated above for the bias components of input-axis misalignment it is apparent that the contributions made by the random components will be even smaller. For the Y gyro a random component of input-axis misalignment of 5 arcsecs will have essentially no effect on system performance. For the X and Z gyros a random component of 5 arcsecs will introduce an equivalent random drift of about 0.005 degrees per hour which according to the results of subsection 5.4 will also have little effect on system performance.

Case of Attitude Rate Change

For the case of attitude rate change, we will again consider separately the libration rate and the change in the component of orbital rate sensed by a gyro when the attitude deviates from nominal.

First, let us consider the libration rate, which shall be assumed to be periodic and is no larger than 0.005 degrees per second (3σ) about a given axis. If it is assumed for a worst case that the attitude control system is limit cycling between ± 0.6 degrees (3σ) with a rate of 0.005 degrees per second about a given axis, it will take 240 seconds to go from one limit to the other. If this libration is about the Y axis, a 10 arcsec out-of-plane misalignment of the X or Z gyro will introduce an error in the libration rate sensed by that gyro of:

$$(0.005)\sin \epsilon = 2.4 \times 10^{-7} \text{ degrees per second}$$

$$= 8.6 \times 10^{-4} \text{ arcsecs per second} \quad (5-93)$$

Since the polarity of the libration rate is periodically reversing, the average value of the rate error over a complete limit cycle is zero. However, this error rate will cause a periodic angle error with a peak value of:

$$\begin{aligned} \left(\frac{\text{Limit Cycle Period}}{4} \right) \times \text{Rate Error} &= (120) (8.6 \times 10^{-4}) \\ &= 0.1 \text{ arcsec} \end{aligned} \quad (5-94)$$

which is not significant in the present system requirements.

Next, let us consider the change in the component of orbital rate sensed by a gyro when the attitude deviates from nominal by ± 0.6 degrees about a particular axis. It is recalled that values were previously given for the rate error caused by input axis misalignment when the vehicle attitude was nominal or displaced by 0.6 degrees from nominal. These are the values which would be treated as equivalent bias drifts by the smoother formulation if the vehicle attitude remained fixed. If the attitude is changing with respect to nominal, some of these error rates will change and these changes, which are not accounted for in the smoother formulation, will cause error in attitude estimation.

For the Y gyro it was previously shown in Equations (5-89) and (5-91) that a 10 arcsec misalignment would cause error rates of 2.4×10^{-7} and 10^{-4} degrees per hour at the nominal attitude and 0.6 degrees from nominal about either the X or z axis, respectively. Consequently, if the vehicle attitude is librating by ± 0.6 degrees about the X or Z axis, the error rate will vary

between $\pm 10^{-4}$ degrees per second. For the libration case shown previously in Figure 5-27, this rate error will look like the rate error for scale factor in Figure 5-27 except that the peak value will be $\pm 10^{-4}$ degrees per second (i.e., about 5 times larger than that for a scale factor error of 10 PPM). For the libration frequency used in that case the rate error will cause a periodic angle error with an amplitude of about:

$$\left(\frac{\text{Limit Cycle Period}}{4} \right) \left(\frac{\text{Peak Error Rate}}{2} \right) \\ = (120)(10^{-4}/2) = 0.006 \text{ arcsec} \quad (5-95)$$

If the libration period was larger, the peak angle error would of course be larger. However, even if the period was the unlikely value of 14 hours (i.e., 8 orbits) the peak angle error would be no more than about $(12,600)(10^{-4}/2) \approx 0.6 \text{ arcsec}$.

For the X or Z gyro it was previously shown in Equation (5-90) and (5-92) that a 10 arcsec out-of-plane misalignment causes about the same rate error when the attitude is nominal or 0.6 degrees from nominal. Consequently, this component of the error rate is fully accounted for when estimating bias drift with the smoother formulation.

The results generated in this section seem to indicate that gyro input axis misalignment does not have much effect on system performance if the nominal values assumed for this error are used. However, further studies will be made in the follow-on effort for SIMS-A to determine whether or not this is true.

5.5.4 OTHER ERROR SOURCES

Other sources of error which have not been considered in the performance results of Section 5.4 are such sources as gyro package misalignment with respect to the star sensor in

SIMS-A and -B, misalignment of the IARU mounting base with respect to the star mapper in SIMS-D, bias and systematic type errors in the gimbal angle indicators, non-orthogonality of the gimbals, and certain error sources in the star sensors which are usually minor but are not always firmly established for a particular star sensor.

Most of these sources are bias type error sources which introduce an error in attitude determination only when there are certain changes in the physical geometry of the system during its operation. For example, a small misalignment in pitch for the gyro package in SIMS-A and -B or the IARU mounting base in SIMS-D would have no effect on system performance during a nominal attitude history. Only when there is a change in roll or yaw would this error make its presence known and this would only be to a small extent since the expected changes in roll and yaw are small. In general, the contributions made by most of these bias type error sources are smaller than the magnitudes of these sources. One possible exception may be gyro package misalignment in SIMS-A and -B which seems to be somewhat analogous to gyro input axis misalignment.

None of the above error sources were analyzed in the manner given for gyro scale factor error and input axis misalignment; there was insufficient time to perform a thorough analysis and the results would have been expected to be of trivial importance.

SECTION 6

CONFIGURATION TRADES

6.1 HIGHLIGHTS OF THE SIMS TRADE STUDY

Implementation of Simulation Capability —

The most outstanding achievement in the SIMS Trade Study was the creation of a simulation capability at the CSDL in which SIMS and SIMS-like concepts can be tested for a variety of configurations and sensor types, and with real star distributions. The need for simulations became obvious when, shortly after the CSDL made its commitment to perform the SIMS Study, Tasks 4 and 5 of the Statement of Work (see Appendix A of the First Interim Report⁸⁵), which pertain to error analysis and error sensitivity, were reviewed by the SIMS Study group. Some of the major IARU error sources give rise to uncertainty in attitude rate, and consequently to uncertainty in attitude that increases with time. The latter can be bounded in SIMS only through the use of stellar data. The SIMS Study group concluded that, to establish quantitatively how well stellar data bounds the attitude uncertainty, dynamic error simulations are essential. Therefore, each of the SIMS candidates was simulated in the specified EOS orbits using current IARU and star sensor error models and performance figures, and with typical and worst-case signal-star distributions derived from a star availability study. This work is covered under "Error Studies" — Section 5 of this and the Second Interim Technical Report¹⁴¹.

Although the error studies have produced a good deal of useful data, to keep within the available resources a number of approximations and simplifying assumptions were made in the simulations. An expanded simulation capability that removes the more significant of those defects, and continued efforts to refine the error models for the IARUs and star sensors, is needed for high assurance of reliable results. (See recommendation 1 of subsection 6.3).

SIMS-D Configuration Proposed —

The SIMS Statement of Work* requires that "MIT/CSDL shall propose one or two versions of Configuration D." Actually, six versions were identified in the First Interim Technical Report⁸⁵. By the time of the Second Interim Technical Report¹⁴¹ all but one, SIMS-D1-A (now called SIMS-D), were eliminated. Its two key subsystems are a gyro-stabilized platform gimbaled in 3 axes, and a silicon-detector starmapper. Except in relation to system availability and non-recurring costs it shows up well in the configuration trades.

Two of the configurations eliminated, designated SIMS-D1-B1 and -B2, also characterized by fully gimbaled gyros, but employing a gimbaled star tracker rather than a starmapper, possess greater capability than can be justified in relation to SIMS requirements. They are mentioned in subsection 6.2.8 in connection with growth potential.

Preliminary Design of SIMS-D IARU —

Preliminary designs were executed for two IARUs, one

* See Appendix A of Ref. 85.

based on TGGs¹⁴¹, and the other on 13-IRIGs* (see subsection 3.3.3). The chief virtue of the former is that its drift rate uncertainty is so low that it can operate over very long periods without stellar data. An overall error of less than $2.5''$ was established as the target for both IARUs. This error was initially budgeted equally (on an RSS basis) to the four major contributors: gyro drift; gimbal-servos; gimbal angle indicators; gimbal geometry. The specialists in the appertaining technology who performed the various design tasks indicated confidence that their respective accuracy goals are attainable.

Star Sensors Evaluated —

Four star sensors — three starmappers and a gimbale star tracker — were studied in depth. The starmappers all employ solid-state detectors, the photomultiplier tube having been rejected on technical grounds. (These grounds are challenged in subsection 6.2.8, and a recommendation for development of a starmapper prototype with a photomultiplier detector appears in subsection 6.3.) For reasons given in Section 4, the starmapper chosen for SIMS-A

* The Statement of Work states: "Available state-of-the-art candidate sensors should be listed which can meet these (performance) specifications, and also a three to five years design life requirement. Trade study of the candidate sensors need not be done." Since the gyros chosen for all of the SIMS configurations were designed and developed at the CSDL, and the starmapper chosen for SIMS-A and -D was developed under the direction of a former head of the CSDL Division that conducted the SIMS Study, it is reasonable to suspect that the choices were based on biased judgements. Nonetheless, the point emphasized here is that CSDL was under no obligation to conduct a formal trade study of candidate sensors. Indeed, such studies are recommended in subsection 6.3.

and -D is a silicon-detector unit by Honeywell Radiation Center*. Since the CSDL does not have direct experience with this kind of sensor it was necessary to rely on paper analyses and data provided by the manufacturer. Questions remain about the performance of the optics, the signal-to-noise ratio achievable with the detector and preamplifier for the weakest signal-star, and the effects of channel dynamics. However, a fairly high confidence was developed in the ability of the sensor to provide stellar data with the accuracy required for SIMS.

The star tracker for SIMS-B is an improved version of the prototype that TRW developed for its Precision Attitude Determination System^{33,34,35}. Besides evaluating this sensor for SIMS, the CSDL identified a number of attractive design and moding options it offers: the avoidance of computer-directed star acquisition by employing a random acquisition scheme; reduction of the noise-equivalent angle by sampling the tracker and IARU gimbal angles a number of times for each star⁸⁵; elimination or simplification of one gimbal; mounting arrangements that allow for strong backup in the event of IARU failure. (See also subsection 6.2.8.)

Configuration Trades Completed —

When the SIMS Trade Study was accepted there was some doubt at the CSDL concerning the possibility of getting all of the information and executing all of the tasks necessary for defining and evaluating every candidate. The next subsection shows that most of the objectives — reasonably defined — have been met. Table 6-1 represents an attempt to grade the three candidate configurations relative to the various trade criteria.

* See previous footnote.

Table 6-1

COMPARISON OF SIMS CANDIDATES

The grade scales are +1 to +5 and -1 to -5. + signifies that quality increases with increasing magnitude; - signifies that quality decreases with increasing magnitude. That is, highest quality corresponds to a grade of +5 or -1. 0 signifies no discernible differences.

CRITERION	SIMS-A ¹	SIMS-B ¹	SIMS-D
1. COST	-3.5	----	-4.2 ² , -5.0 ³
2. ACCURACY	-5	-2	-2
3. WEIGHT	-1.8	-4.1 ⁴ , -5.0 ⁵	-1.8 ² , -2.6 ³
4. POWER	-3.1	-5.0	-3.2 ² , -4.4 ³
5. TELEMETRY REQUIREMENT	-5.0	-5.0	-1.3
6. TOTAL UNOBSTRUCTED FIELD OF VIEW REQUIRED	-1	-5	-1
7. SIMPLICITY OF DESIGN AND RELIABILITY	0	0	0
8. MODULARITY OF DESIGN AND GROWTH POTENTIAL ⁶	+1	+1	+5
9. COST OF GROUND SUPPORT EQUIPMENT	0	0	0
10. COMPLEXITY OF GROUND/ CONTROL/COMMAND/DATA PROCESSING OPERATIONS	0	0	0
11. SYSTEM AVAILABILITY	-1	-2	-5

- NOTES**
1. IARU attitude algorithm computation done on the ground.
 2. The IARU employs 13-IRIGs.
 3. The IARU employs TGGs.
 4. Beryllium gimbal structure
 5. Aluminum gimbal structure
 6. All candidates are equally modular; the grade refers to growth potential.

6.2 TRADES

6.2.1 CRITERION 1 -- COST

A method of arriving at total costs in a way that makes the various major items visible was formulated by the SIMS Study group and transmitted to the appropriate manufacturers.

Items to be costed:

1. Engineering prototype
2. Qualification test model
3. Flight model
4. Spare
5. Cost per unit in excess of 1-4 above
6. Dedicated laboratory facility for item 1
7. Laboratory test facility for item 2
8. Production facility for items 2, 3, and 4
9. GSE for items 3 and 4
10. Analytical support
11. Documentation

As a possible guide in filling out the list, the various development stages and typical outputs were summarized as follows:

Design

Electrical

Mechanical

Thermal

Optical

Analysis

Fabrication

Procurement

Subcontracts

Special equipment

Special parts

Assembly

Debug

Test (at acceptance and qualification levels)

Performance (system and subsystem peculiar)

Environmental

Temperature

Shock and vibration

Vacuum

Lifetime

Calibration

Documentation

Electrical schematics

Mechanical drawings

Wiring diagrams

Packaging layouts and potting information

Parts lists

Operating manuals

Alignment and calibration procedures

Test reports

Progress reports

Mission support

Pre-launch check-out

Flight progress monitoring

Data reduction and evaluation

The response¹⁶⁵ from Honeywell Aerospace, the manufacturer of the SIMS-A candidate, accords closely with that requested except in regard to GSE costs, and is otherwise fully satisfactory. The response from TRW, the manufacturer of the SIMS-B candidate, did not contain costs. Since NASA is

the sponsor for that candidate the missing cost figures are assumed to be accessible to the NASA monitor of the SIMS Study. For SIMS-D it was not practical, without an advanced system design as a basis, to carry out the effort necessary to evaluate every cost item. The approach taken was to adopt the SIMS-A cost breakdown with IARU cost estimates replaced by those for the SIMS-D IARU. For all of the SIMS candidates those itemized costs that were obtained are presented in Appendix A, and gross costs are summarized below.

SIMS-A

Qualified Prototype	540K
Three Flight Systems	942K
Other Non-Recurring Costs	<u>2815K</u>
Total	4297K
Per-Unit Cost Thereafter	247K

SIMS-B

TRW declined to provide costs to avoid compromising competitive advantage, primarily for subcontractors.

SIMS-D (13-IRIG Version)

Qualified Prototype	626K
Three Flight Systems	1060K
Other Non-Recurring Costs	<u>3487K</u>
Total	5173K
Per-Unit Cost Thereafter	371K

SIMS-D (TGG Version)

Qualified Prototype	956K
Three Flight Systems	1705K
Other non-Recurring Costs	<u>3487K</u>
Total	6148K
Per-Unit Cost Thereafter	441K

(Cont.)

CONDENSED SUMMARY (z)

<u>Candidate</u>	<u>Initial Cost</u>	<u>Subsequent Per-Unit Cost</u>
SIMS-A	4.3M	250K
13-IRIG SIMS-D	5.2M	270K
TGG SIMS-D	6.2M	440K

The foregoing estimates do not include the cost of the instrument mounting structure, the temperature regulator, the programmer (or computer for SIMS-B), or interface electronics. The details of mission planning were deemed inadequate for the pertinent design exercises.

The estimate for SIMS-A is based on the assumption that no on-board IARU attitude algorithm computer is required. A space-qualified Control Data computer (Model 469) that will do the job costs 50 - 100K.

6.2.2 CRITERION 2 - ACCURACY

This criterion is the subject of Section 5 of this and the Second Interim Report¹⁴¹, and aspects of it are covered in most of the other sections. Therefore, only a few comments are made here.

Perhaps the two most important statements that can be made about accuracy are: the error studies show that the three candidates meet, with varying degrees of success, the 0.001° (1σ) required for a SIMS; the results of the error studies are probably optimistic - as the studies become more comprehensive the errors will probably get worse. The bases for these two statements are reviewed briefly below.

Performance* -

Three prominent characteristics of SIMS-A performance are: the settling time is long, typically eight or more orbital periods; it depends on a stellar data rate that is just about all current starmappers are capable of; the settled error in spacecraft orientation about the starmapper optical axis is high.

SIMS-B settles in about two orbital periods to estimation uncertainties well below the SIMS specification. Moreover, even without a complicated smoothing computation it probably will provide attitude at or below the SIMS specification in a few minutes.

SIMS-D settles in four orbital periods to about the same estimation uncertainties as does SIMS-B. Although the roll and yaw uncertainties are about three times larger than in pitch,

* All of the generalizations made here are derived from subsection 5.4.

the absolute values are very small compared to the SIMS specification. SIMS-D can probably tolerate a gross reduction in the number of available stars without significant performance degradation.

Sources of Error Underestimated -

Although the error studies have progressed much further than was expected at the time when the SIMS Study began, they are by no means complete (see subsections 5.5 and 6.3). Among the tasks remaining are:

- a) Incorporate the most comprehensive and up-to-date error models and design parameters.
- b) Simulate the rotational environment to the fullest extent practicable.
- c) Simulate the attitude algorithm computation for SIMS-A and -B.
- d) Investigate digital filtering as a way of smoothing SIMS-D IARU gimbal angle data, and the corresponding data derived by the attitude algorithm operating on SIMS-A or -B angle increments.
- e) Evaluate the effects of noise stars on SIMS-A and -D starmapper data.

A detailed discussion of every item in the list is omitted here. However, just one aspect of item a) is taken up in the hope that the illustration it provides will emphasize the point made by the list - that further studies are indeed in order.

The design goals for the starmapper errors in the Air Force system under development¹⁵³ are $8''$ (1σ) noise, and $4''$ (1σ) bias. The combined error is almost an order of magnitude larger

than used in the SIMS error studies ($1.1''$, 1σ , for the silicon starmapper). Although Honeywell's goals for the SIMS version are $2''$ (1σ) noise, and $2''$ (1σ) bias, verification of their achievability should be the object of a critical design review. The bias, which is an alignment shift expected to occur during launch, is particularly troublesome. Techniques for estimation using only SIMS data would not detect it. The corresponding error for the SIMS-B tracker is not known at the CSDL, but the complexity of the tracker compared to the mapper suggests that the error is greater for the tracker.

6.2.3 CRITERION 3 - WEIGHT

The sources for weight estimates* are: Reference 153 for SIMS-A; Reference 35 for the SIMS-B star tracker; CSDL experience for the SIMS-D IARUs; one employing TGGs and the other 13-IRIGs. The SIMS-B IARU is assumed to be the same as for SIMS-A. Honeywell Radiation Center's silicon-detector star mapper is assumed for SIMS-A and SIMS-D. The estimates do not include the instrument mounting structure, programmer (computer for SIMS-B), temperature regulator, or interface electronics.

SIMS-A	Weight (lbs)
IARU (13-IRIG)	16
Star sensor and electronics	5
Sun shield	1
Total	22

SIMS-B	Weight (lbs)
IARU (13-IRIG)	16 16
Gimbal and star sensor assemblies - aluminum	36
- beryllium	25
Off-gimbal electronics	8 8
Totals	60 49

SIMS-D	Weight (lbs)
IARU (TGG)	25
IARU (13-IRIG)	15
Star sensor and electronics	5 5
Sun shield	1 1
Totals	31 21

* As modified by telephone calls to contractors during preparation of this report.

The estimate for SIMS-A is based on the assumption that no on-board IARU attitude algorithm is required. A space-qualified Control Data computer (Model 469) that will do the job weighs 2 lbs. The same assumption applies to SIMS-B, though in that case the attitude algorithm computation would be an additional requirement on a computer already available.

6.2.4 CRITERION 4 - POWER

In presenting estimates of power required it is believed desirable to provide some idea of how they were arrived at. This facilitates engineering evaluation of the validity of the estimates, and discloses special requirements that occur in one system but not in another, e.g., a very stable wheel-supply frequency in SIMS-A, or a space-qualified high voltage supply in SIMS-B. Therefore, the following power breakdown format was developed by the SIMS Study group to serve as a guide in assessing the overall requirement for each system.

IARU

Total input at 28V $\pm 2\%$ * - average and peak current

For each d.c. output specify:

nominal voltage and accuracy

average current

peak current, and conditions of occurrence

zero- to full-load regulation

line regulation*

noise over 0.01 Hz - 100 KHz

ripple

temperature range and sensitivity

destination(s)

For each a.c. output specify:

nominal voltage and accuracy

average current (and power factor, if applicable)

* Until more details are available on the spacecraft power supply the $\pm 2\%$ will be assumed to cover the effects of source impedance, high and low transients, coherent noise, broadband noise, temperature, etc.

peak current (and power factor, if applicable),
and conditions of occurrence
minimum- to full-load regulation
line regulation*
waveform and number of phases
frequency, including accuracy and stability
undesired harmonic content
temperature range and sensitivity
destination(s)

STAR SENSOR

Same as for IARU

SYSTEM

Total input at $28V \pm 2\%$ * - average and peak current
IARU - average and peak current
Star Sensor - average and peak current
Programmer (Computer for SIMS-B) - average current
Temperature Regulator - average and peak current
Interface electronics - average current

Although none of the SIMS candidates is at a stage of development that would support a complete response to the questions contained in this format, the information made available by Honeywell¹⁵³ and Kollsman provides a good basis for SIMS-A power estimates. The sources for SIMS-B star tracker power estimates are Reference 35, and a telecon between D. Kirby of TRW and M. Smith of CSDL on June 14. A SIMS-A type of IARU is assumed for SIMS-B. For SIMS-D, silicon-detector star mapper power estimates by both Honeywell and Kollsman, both of which are very similar (and yield about 5 watts** total), are used. For

* See footnote on previous page.

** Both contractors estimated approximately 3 watts of regulated power for their silicon-detector star mappers. The 5 watts is based on 60% conversion efficiency assumed by CSDL.

the SIMS-D IARU CSDL experience was applied to the proposed designs, one based on the TGG and the other on the 13-IRIG. The power requirements of the programmer (computer for SIMS-B), temperature regulator, and interface electronics were not estimated for any of the candidates because mission planning details were deemed inadequate for the pertinent design exercises. Overall power requirements summarized from detailed estimates given in Appendix A are presented below.

SIMS-A	Average Power (W)	
IARU (13-IRIG)	34	
Silicon-detector star mapper	5	
Total	39	
SIMS-B	Average Power (W)	
IARU (13-IRIG)	34	
Gimbal and star sensor assemblies	13	
Off-gimbal electronics	15*	
Total	62	
SIMS-D	Average Power (W)	
IARU (TGG)	50	
IARU (13-IRIG)	35	
silicon-detector star mapper	5	5
Totals	55	40

----- The estimate for SIMS-A is based on the assumption -----
that no on-board IARU attitude algorithm computer is required. A space-qualified Control Data computer (Model 469) that will do the job consumes about 10W average. The same assumption applies to SIMS-B, though in that case the attitude algorithm computation would be an additional requirement on a computer already available.

* This can be reduced to 3W by cycling.

6.2.5 CRITERION 5 - TELEMETRY REQUIREMENT

The telemetry estimates presented here make no allowances for non-nominal attitude rates as might be caused by orbit adjustments or momentum dumping. This should be of no consequence for SIMS-D, and perhaps only a minor problem for SIMS-B. For SIMS-A, with its long data smoothing segment, the omission may prove serious, so the impact of such rates should be assessed when sufficient information is available. Assumptions on which the estimates are based are:

$$\text{Orbital rate} = (104.6)^{-1} \text{ revolutions/min.} = 206.5''/\text{s}$$

$$\text{Attitude error rate} = 0.005^\circ/\text{s}(3\sigma) = 18''/\text{s}(3\sigma)$$

$$\text{Maximum time from clock reset} = 1 \text{ day} = 8.64 \times 10^4 \text{ s}$$

6.2.5.1 SIMS-A

The telemetry requirement for SIMS-A is essentially the same as for SIMS-D if the IARU attitude algorithm computation is performed on board the spacecraft.

The estimates recorded below are based on the assumption that the attitude algorithm is not done on board. Instead of computer-generated Euler angles or direction cosines, the incremental angles indicated in the pulse-count registers of the gyro-float rebalance electronics are telemetered. The lack of any on-board record of the total Euler angles (or equivalent) through which the instrument mounting structure has rotated from the time of initialization to any specified time in the data smoothing segment (about 8 orbit periods, or 14 hours) leads to two major differences in telemetry requirements compared to the case with on-board algorithm computation:

- (1) IARU sampling must at no time in a data smoothing segment be interrupted.

- (2) IARU registers must be sized to provide high assurance that the most extreme rate will not cause overflow.

The IARU registers will be sized for 10σ attitude error rates - 5σ to satisfy (2) and an additional factor of 2 to cover the possibility of an actual σ greater than the a priori value.

IARU

Whole words - 100 s sampling period

time: 25 bits - based on 1 or less days from clock reset

$$\text{LSB} = \frac{(206.5)^{\wedge} / \text{s}(8.64 \times 10^4) \text{s/day}}{2^{25} \text{ counts/day}} = 0.53^{\wedge}$$

$$\text{clock accuracy} = \frac{0.53}{\sqrt{6}} = 0.22^{\wedge}(1\sigma)$$

Incremental words - 0.1 s sampling period

pitch: 7 bits (6 bits plus sign) - based on 10σ attitude error rate and $0.50^{\wedge}/\text{count}$

$$\text{sample size} = \frac{[206.5 + \frac{10}{3}(18)]^{\wedge} / \text{s}(0.1) \text{s/sample}}{0.50^{\wedge}/\text{count}}$$

$$= 53 \text{ counts/sample} < 6 \text{ bits}$$

$$\text{sample accuracy} = \frac{0.50}{\sqrt{6}} = 0.20^{\wedge}(1\sigma)$$

roll: 5 bits (4 bits plus sign) - based on 10σ attitude error rate and $0.50^{\wedge}/\text{count}$

$$\text{sample size} = \frac{\frac{10}{3}(18)^{\hat{n}}/s(0.1) \text{ s/sample}}{0.50^{\hat{n}}/\text{count}}$$

$$= 12 \text{ counts/sample} < 4 \text{ bits}$$

$$\text{sample accuracy} = \frac{0.50}{\sqrt{6}} = 0.20^{\hat{n}}(1\sigma)$$

yaw: same as for roll

STAR MAPPER

Slit identification: 1 bit - to define slit set (3 slits per set)

Transit time: 16 bits - measured from beginning of 100 s data block

$$\text{LSB} = \frac{[206.5 + \frac{10}{3}(18)]^{\hat{n}}/s(100) \text{ s/sample}}{2^{16} \text{ counts/sample}} = 0.41^{\hat{n}}$$

$$\text{accuracy} = \frac{0.41}{\sqrt{6}} = 0.17^{\hat{n}}(1\sigma)$$

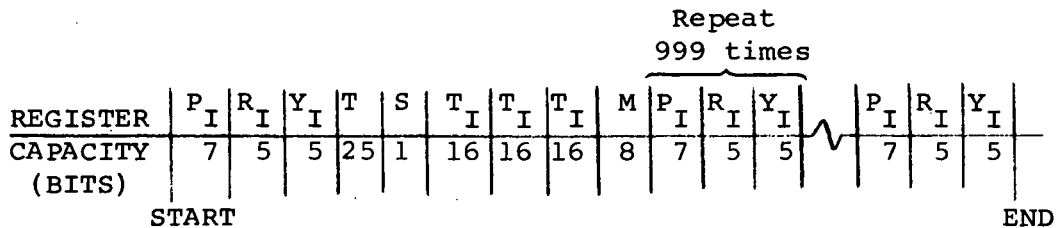
STATUS MONITOR

8 bits - any point encoded at 7 bits plus sign every 100 s

$$\text{LSB} = \frac{100\%}{2^7} = 0.78\%$$

$$\text{accuracy} = \frac{0.78}{\sqrt{6}} = 0.32\%(1\sigma)$$

DATA BLOCK



NOMENCLATURE: P - Pitch; R - Roll; Y - Yaw; T - Time;
S - Slit set; I - Incremental; M - Status
Monitor

The data block contains 17,082 bits covering 100 s of real time. The data is recorded continuously over a data smoothing segment (~14 hrs).

$$\frac{\text{bits}}{\text{revolution}} = \frac{104.6(60) \text{ s/rev}}{(100) \text{ s/block}} (17,082) \text{ bits/block} = \underline{1.1 \times 10^6 \text{ bits}}$$

6.2.5.2 SIMS-B

If the IARU attitude algorithm is not performed on board the spacecraft the telemetry requirement for SIMS-B is essentially the same as it is for SIMS-A in that case, i.e., continuous IARU sampling, and a data block of approximately 17,000 bits covering 100 s of real time (1.1×10^6 bits/revolution). Because of the fast settling time of SIMS-B the data smoothing segment will probably be much shorter than the 14 hours assumed for SIMS-A. This means that a loss of IARU data would not be as detrimental though it still would be much more so than for the case where the IARU attitude algorithm is performed on board.

If the IARU attitude algorithm is performed on board the spacecraft the telemetry requirement for SIMS-B is essentially the

same as for SIMS-D, i.e., IARU sampling only during payload operation and stellar data acquisition (less than 30% of the time), and a data block of approximately 15,000 bits covering 100 s of real time (2.8×10^5 bits/revolution).

The noise-equivalent-angle of the SIMS-B star tracker can be reduced by a divisor of \sqrt{n} where n is the number of sets of gimbal angles sampled per star. This does not have a major influence on the telemetry requirement.

6.2.5.3 SIMS-D

IARU

Whole words - 100 s sampling period

pitch: 22 bits - 21 bits over 360° plus sign

$$\text{LSB} = \frac{(360)^\circ (3600''/\circ)}{2^{21}} = 0.62''$$

$$\text{encoder accuracy} = \frac{0.62}{\sqrt{6}} = 0.25''(1\sigma)$$

roll: 16 bits - 15 bits over 5° plus sign

$$\text{LSB} = \frac{(5)^\circ (3600''/\circ)}{2^{15}} = 0.55''$$

$$\text{encoder accuracy} = \frac{0.55}{\sqrt{6}} = 0.22''(1\sigma)$$

yaw: same as for roll

time: 25 bits - based on 1 or less days from clock reset.

$$\text{LSB} = \frac{(206.5)''/\text{s}(8.64 \times 10^4) \text{ s/day}}{2^{25} \text{ counts/day}} = 0.53''$$

$$\text{clock accuracy} = \frac{0.53}{\sqrt{6}} = 0.22''(1\sigma)$$

Incremental words - 0.1 s sampling period

pitch: 7 bits (6 bits plus sign) - based on $6\sigma^*$
attitude error rate

$$\begin{aligned} \text{sample size} &= \frac{[206.5 + \frac{6}{3}(18)]''/\text{s}(0.1) \text{ s/sample}}{(0.62)''/\text{count}} \\ &= 39 \text{ counts/sample} < 6 \text{ bits} \end{aligned}$$

roll: 4 bits (3 bits plus sign) - based on 6σ
attitude error rate

$$\begin{aligned} \text{sample size} &= \frac{\frac{6}{3}(18)''/\text{s}(0.1) \text{ s/sample}}{(0.55'')''/\text{count}} \\ &= 6.5 \text{ counts/sample} < 3 \text{ bits} \end{aligned}$$

yaw: same as for roll

STAR MAPPER

Slit identification: 1 bit -- to define slit set (3 slits
per set)

Transit time: 16 bits - measured from beginning of 100 s
data block

* 3σ to keep the error rate low, and an additional factor of 2 to cover the possibility of an actual σ greater than the a priori value.

$$\text{LSB} = \frac{[206.5 + \frac{6}{3}(18)]^{\frac{1}{n}} / \text{s}(100) \text{s/sample}}{2^{16} \text{ counts/sample}} = 0.37^{\frac{1}{n}}$$

$$\text{accuracy} = \frac{0.37}{\sqrt{6}} = 0.15^{\frac{1}{n}}$$

STATUS MONITOR

8 bits - any point encoded at 7 bits plus sign every 100 s

$$\text{LSB} = \frac{100\%}{2^7} = 0.78\%$$

$$\text{accuracy} = \frac{0.78}{\sqrt{6}} = 0.32\%$$

DATA BLOCK

REGISTER CAPACITY (BITS)	P	R	Y	T	S	T _I	T _I	T _I	M	Repeat 999 times					
	22	16	16	25	1	16	16	16	8	P _I	R _I	Y _I	P _I	R _I	Y _I
	START														END

The data block contains 15,121 bits covering 100 s of real-time. It is assumed that the payload operates only during passage over the sun-illuminated part of the earth, and for not more than 60% of the time over that part.

$$\begin{aligned} \frac{\text{maximum number of bits}}{\text{revolution}} &= (0.3) \frac{104.6(60) \text{s/rev}}{(100) \text{s/block}} (15,121) \text{bits/block} \\ &= \underline{2.8 \times 10^5 \text{ bits}} \end{aligned}$$

6.2.6 CRITERION 6 - TOTAL UNOBSTRUCTED FIELD-OF-VIEW REQUIRED

The SIMS-A and -D star mapper, which is assumed here to be Honeywell Radiation Center's silicon-detector unit, has a 10° field-of-view (FOV) as measured between outer tips of collinear slit pairs. A sunshield is provided that allows normal operation as long as the optical axis remains at least thirty degrees from the direction to the sun, and from the direction of light from any highly reflective spacecraft surface illuminated by the sun or earth. It must also remain at least fifteen degrees from the direction of sunlight or earthlight scattered by spacecraft structure.

SIMS-A simulation results presented in subsection 5.4.2 show that when the star mapper optical axis is parallel to the spacecraft yaw axis (i.e., approximately toward the zenith), the attitude determination error is much larger in yaw than in roll and pitch. When the optical axis remains in the orbital plane but is directed substantially fore or aft of zenith the attitude determination uncertainty in both roll and yaw is large. This effect is due to the fact that, with the star mapper optical axis fixed with respect to the gyro axes, gyro drift rate biases are not all satisfactorily estimated. The effect is not observed in SIMS-D simulations because in that system gyro axes rotate continuously with respect to the star mapper optical axis.

The effect is of little consequence for the following set of conditions that would often obtain:

- 1) Removal of payload sensor errors caused by attitude errors and error rates is not greatly affected by yaw uncertainty.
- 2) Spacecraft mounting constraints, including those mentioned above in connection with reflected and

scattered sunlight and earthlight, do not disallow the optical axis of the star mapper from being parallel to the spacecraft yaw axis (i.e., approximately zenith-directed).

- 3) The zenith-directed optical axis remains at least 30° from the direction to the sun.

The first condition is satisfied by the thematic mapper in its normal data-taking orientation (i.e., optical axis parallel to the spacecraft yaw axis when at the center-scan position, and scan plane normal to the roll axis). The second condition can probably be satisfied if the sensor is located close to the outside end of the appropriate EOS instrument bay, and if proper attention is paid to optical properties of adjacent structure. Of the three EOS orbits, noon, 9:00AM and twilight, identified in the SIMS Study guidelines*, the latter two satisfy the third condition. Unfortunately, the noon orbit would necessitate a large displacement of the optical axis of the starmapper out of the orbit plane. When that is necessary, not only is the large attitude determination uncertainty shared by both pitch and yaw, but the swath of the celestial sphere covered is reduced.

For 9:00 AM and twilight orbits the optical axis of the SIMS-D star mapper can be located anywhere fore or aft of zenith that satisfies the FOV requirement and stray light constraints, since the only effect is to shift the time scale of the star sequence observed when the optical axis is zenith-directed. The reduction of the swath of the celestial sphere that results from the out-of-plane displacement of the optical axis of the star mapper in the noon orbit would probably be of little consequence for a SIMS-D because that system requires very few stars.

* See Appendix A -- "Excerpts from the Technical Proposal" in Reference 85.

The FOV of the SIMS-B star tracker as determined by the gimbal freedom is $90^{\circ} \times 30^{\circ}$. Although the instantaneous FOV is very small, taking advantage of the very low noise of the image dissector necessitates very good shielding against stray light. Hence the angle between the optical axis and the direction to the sun must not be less than 45° , and reflected or scattered sunlight and earthlight must be avoided. The mounting arrangement preferred by TRW is "an orientation of the star tracker FOV in the pitch-yaw plane with gimbal 0-0 at 15 degrees above the pitch axis. The 90° gimbal freedom is oriented horizontally".¹⁵⁴ This arrangement, if permissible within spacecraft mounting and stray light constraints, would avoid sun interference. Unfortunately, it was not known at CSDL to be preferred by TRW in time to impact the star availability studies and error simulations.

Although the FOV of the SIMS-B star tracker is far greater than that of the SIMS-A and -D star mapper, and thereby poses potentially more difficult spacecraft integration problems due to stray light and structural interference, to speak of reducing its FOV to that for a star mapper, as has been suggested,¹⁵⁴ misses the SIMS-B concept. The concept is that performance advantages offered by the large FOV and the operating principles of the SIMS-B tracker will offset spacecraft integration problems and the larger size, weight, power consumption, complexity, etc., of the tracker as compared with a star mapper. All of this is not to say that there should be no reduction in the FOV of the tracker. The error study results for SIMS-B reported in subsection 5.4.3 show that a substantial reduction would not seriously degrade the SIMS-B accuracy. This was found by TRW to be true also for the preferred mounting arrangement. An attractive feature of the SIMS-B tracker, arising from the fact that its large FOV is implemented by gimbaling a sensor with

a small instantaneous FOV, is that any field or fields within the $90^{\circ} \times 30^{\circ}$ can be selected merely by programming. This can be exploited in meeting spacecraft and mission interface constraints, in performance optimization, and in implementing special moding. An example of the latter is the random star acquisition scheme described in subsection 6.2.8.

6.2.7 CRITERION 7 - SIMPLICITY OF DESIGN, AND RELIABILITY

None of the SIMS candidates has reached the development status that will support a comprehensive, quantitative assessment of reliability. Although the objective of the SIMS Study would be met if the reliability of each of the three candidates could be assessed on a comparative basis without extensive quantitative information, it is probably unwise at this time to attempt even that. Accordingly, only an informal commentary is presented here. It may contain some useful facts and guidelines for future reliability efforts.

Simplicity

Implicit in the title of this criterion is the recognition that simplicity of design is the most important guideline for achieving high reliability. Also well-known, and among the reasons for the importance of this guideline, is that it usually has a more desirable influence on cost, weight, power consumption, availability, etc., than does design complexity.

Those engaged in systems design, motivated by a desire for technical challenges and high-level funding, will often opt for complexity, while those engaged in the planning and conduct of missions, seeking systems that stay within various constraints and enhance the probability of mission success, appreciate simplicity. The main SIMS concept is favorable to the latter group. NASA's requirement for precision attitude determination (an "after-the-fact" function) rather than precision attitude indication and control (real-time functions) allows for much simpler spaceborne instrumentation and control equipment. The only significant

penalty for that simplification is a requirement for 5% sidelap in ground swaths (100^{nm} for $\sim 11^\circ$ scan) of the thematic mapper. The sidelap prevents holidays from occurring in the data due to attitude variations (0.6° , 3σ) about the mean (0.5° max.).

Although the thematic mapper is the only EOS payload sensor requiring precision attitude information, a requirement for precision attitude indication could conceivably arise in the future. Attitude indication systems can be configured using any SIMS candidate as a starting point. Methods of doing this (see subsection 6.2.8), which still follow the design simplicity guideline, employ an optimum mix of on-board computation and ground control/command/data processing.

Among the important consequences of the main SIMS concept is that in all of the SIMS systems the star sensor and IARU operate independently of each other and in open loop fashion. That is, the data acquired by the star sensor and IARU is not processed on board the spacecraft nor on the ground to produce commands between or to the sensors. The risks inherent in such operations are thereby avoided.

Although the SIMS concept yields great simplification the three candidate realizations of it are of varying simplicity. If the IARU attitude algorithm computation is not done on board the spacecraft in SIMS-A, SIMS-A is simpler than SIMS-D: neither requires a computer; both employ the same type of star sensor; but mounting the gyros on the support structure is simpler than gimbaling them*. The requirement for precision torquing of

*Structure-mounting gyros usually poses special alignment and calibration problems but these are not believed likely to prove serious for SIMS-A or -B because of the calibration methods possible with stellar data.

structure-mounted gyros is offset by the requirement for precision gimbal-angle indication for gimballed gyros. If the algorithm is executed on board, then the SIMS-A IARU merely represents a shift from mechanical complexity of the SIMS-D IARU toward electronic complexity, and it is no longer obvious which of the two is the simpler. Except in a few instances, where it has specifically been treated as an unresolved design problem, the IARU attitude algorithm computation has been assumed in the SIMS Study to be a task for the ground-based data reduction center(s).

The question of whether the SIMS-A IARU algorithm should be done on board or on the ground is an interesting one in relation to the design simplicity guideline for achieving reliability. Omitting the algorithm computer from the spaceborne equipment complement would have a highly desirable impact on all factors affected by mechanization complexity, e.g., power, weight, reliability (in one sense). The sense in which reliability would be improved is that the requirement for a computer that can operate in space without uncorrected failure for 3 to 5 years would be avoided. However, reliability would be degraded in the sense that the complexity of the link between the pulse-count registers and the algorithm computer(s) — the latter being ground-based — would be greatly increased. Since the attitude data is in incremental form in the pulse-count registers the system becomes less fault-tolerant. On the other hand failures in a data link transmitting Euler angles (or their equivalent) are generally much easier both to detect and to correct. Moreover, when the failures are of limited duration their effect on accuracy can be severe for the incremental-angle transmission case while moderate for whole-angle transmission. This point is illustrated in connection with SIMS-A

telemetry requirements (see subsection 6.2.5). Defining the complications or risks associated with ground-based data reduction when the attitude data is incremental is beyond the scope of this study, but when defined, they too may be found to carry a significant reliability penalty.

Backup

A number of schemes that provide backup in the event of a SIMS failure are possible. Although most of them call for some advance planning in spaceborne equipment design and in command/control/data processing, the hardware and software demands are moderate. The backup schemes described here are not based on redundancy design techniques; they merely make use of what is assumed to remain functioning after a specified failure. Some of them are applicable to total failure of the SIMS, but are discussed below only in relation to failure separately of a star sensor or IARU. Moreover, no attempt is made in the discussion to accomodate particular failure modes for these two subsystems - their failures are assumed to be total. This is not a very practical assumption, but not to make it would open up more possibilities than can be covered in a brief treatment.

Failure of the Star Sensor -

The first recourse on failure of a star sensor would be to switch to a landmark-inertial measurement system (LIMS). The LIMS, which is described in subsection 6.2.8, would probably be at least as accurate as a SIMS. A possible drawback might be that it necessitates somewhat less desirable data processing procedures than a SIMS, but that would be a small complaint if the SIMS were to have failed.

If for some reason (such as a lack of satisfactory landmark data) the LIMS should not be a workable alternative, the horizon-inertial measurement system (HIMS) that provides EOS attitude indication for the attitude control system might be sufficiently accurate for some of the thematic mapper data. By using early SIMS data the HIMS can be very accurately calibrated relative to the SIMS reference block. Its performance as a backup would depend on the stability of the calibration. That too can be determined with early SIMS data.

Failure of the IARU -

The HIMS calibration using early SIMS data should be done in a manner that results in separate calibration of the HIMS gyros. Then, in the event of IARU failure, those gyros can be the IARU of a lower grade SIMS. Performance will not be highly dependent on calibration stability in that case since stellar data will be available.

The early SIMS data should also be applied to modeling the EOS attitude dynamics. In the absence of an IARU (or using the lower grade HIMS IARU) the model might prove effective in predicting attitude changes between star sightings.

The SIMS-B star tracker can under certain conditions provide an excellent backup in the event of IARU failure. If the payload is the thematic mapper currently proposed for EOS, its normal operating mode has the optical axis parallel to spacecraft yaw at the center-scan position, and the scan sector extends to $\pm 6^\circ$ about spacecraft roll from that position. Since the expected 0.1° attitude determination accuracy of the HIMS⁸⁹ (before calibration

by the SIMS) provides fairly good accuracy in yaw for the thematic mapper in this orientation, the star tracker only needs to provide precise pitch and roll data. For the twilight orbit the star tracker can be mounted so that when the gimbals are at their center positions the optical axis is parallel to spacecraft yaw; and the gimbal freedom can be chosen to allow continuous tracking of any star in the spherical rectangle defined by $\pm 45^\circ$ rotation about pitch and $\pm 15^\circ$ about roll. For the 9:00 AM orbit the 45° sun angle constraint necessitates the entire 30° roll freedom being oriented to one side of the orbit plane. Barring a redesign of the sunshield, the tracker would have to be inactive over a fairly long interval in the noon orbit. Although the accuracy of this backup, when the signal star is within 10° of zenith, is probably nearly as good as the SIMS itself, its actual performance should be evaluated by simulations. The HIMS gyros or the model of spacecraft dynamics might provide the attitude data needed during the change from one signal star to another.

Redundancy¹⁶⁶

Redundant design is the use of more components than necessary with the aim of increasing reliability.* Unfortunately, that aim is often pursued ineptly because of the difficulty of determining when and how to apply redundant design. While no attempt is made here to answer those questions as they apply to SIMS, some of the appertaining problems are identified in the hope of forestalling hard design decisions until sufficient information

*This is somewhat less technical, though more general, than the definition found in the literature. There, redundancy means the creation of new parallel paths in a system structure to improve the system reliability.

is available. A good starting point is a discussion of commonly used reliability formulas.

Reliability Formulas -

A set of commonly used reliability formulas is:

$$(1) \quad R(t) = e^{-\lambda t}$$

$$(2) \quad R_2(t) = 2e^{-\lambda t} - e^{-2\lambda t}$$

$$(3) \quad R_{2S}(t) = (1 + \lambda t)e^{-\lambda t}$$

$$(4) \quad R_{34}(t) = 4e^{-3\lambda t} - 3e^{-4\lambda t}$$

where:

$R(t)$ is the probability that the failure time (a random variable) of the item in question will exceed t .

λ is the hazard* of the item in question.

Subscript "2" denotes an item consisting of 2 of the type defined in (1) in parallel and both operating.

Subscript "2S" denotes an item consisting of 2 of the type defined in (1) in parallel, one on standby with an ideal switch.

Subscript "34" denotes an item consisting of 4 items of the type defined in (1), at least 3 of which must operate for success.

*Also called hazard rate, and failure rate.

The term "item" refers to a system, subsystem, part, component, etc.

A useful quantity is the expected time to failure, or mean time to failure (MTTF). It can be shown to equal the time integral of $R(t)$ from zero to infinity. For (1), (2), (3) and (4) it is λ^{-1} , $1.5\lambda^{-1}$, $2\lambda^{-1}$ and $(7/12)\lambda^{-1}$ respectively. Also, if the item (system) in (1) is composed of a number of items (subsystems) in series (i.e., system success depends on the success of all subsystems), the system hazard λ is composed of the sum of the subsystem hazards; and, by performing the above-mentioned integration, the MTTF is found to be the reciprocal of the sum of the subsystem hazards.

To facilitate discussing assumptions on which the foregoing formulas are based, they are applied to some IARU configurations employing redundancy.

IARU Configurations Employing Redundancy -

Four IARU configurations based on structure-mounted 13-IRIG gyros are as follows:

- 1) Three gyros with mutually orthogonal input axes, each with completely independent electronics, including power supplies, mounted on a common temperature-controlled structure.
- 2) Two of 1), both operating.
- 3) Two of 1), one on standby. Equipment for switching to the standby unit (which includes that for failure detection) is assumed to carry negligible risk of failure.

- 4) Same as 1) except that a fourth gyro and its own electronics are added. Its input axis is aligned with the diagonal from the cube corner defined by the input axes of the gyro triad. (It can serve in the event of failure of any one member of the triad.)

One might wish to see some gimbaled configurations included. However, to do so could lead unnecessarily to confusion about the reliability principles under discussion. The differences between IARUs employing structure-mounted gyros and those employing gimbaled gyros are so great that a unified treatment of the two would be labored and perhaps of doubtful comparative value. For example, drawing a line between the attitude algorithm computer and the structure-mounted gyros, as was done for the examples above, is simple; the corresponding line for the gimbaled IARU is not so easily defined. Also, loss of wheel sync, or of stability in the regulators of gyro or mounting structure temperature, to a degree that would be catastrophic for structure-mounted gyros, might have no significant effect on a gimbaled IARU. For these and other reasons different MTTFs would have to be defined for the same type of gyro in the two different IARUs; and, as is shown below, getting an MTTF for only one case is difficult.

The number for each of the four configurations is chosen to agree with that of the formula that applies. In configurations 2) and 3), when a gyro fails in one of the 2 IARUs, that entire IARU is useless — probably not a very practical assumption.

Although the advantages of standby configuration 3) are obvious, configuration 2) in which both IARUs operate at the same time also has attractive features. Not only do they facilitate catastrophic-failure detection, but they are also readily applicable to detection of marginal or intermittent failures, and to failure diagnosis.

Results of evaluating the formulas are presented in Table 6-2 where reference values for R and t are .90 and 4.0 years, respectively. For formulas (1) - (3) the reference value of λ is 0.088 years^{-1} , and for (4) it is 0.029 years^{-1} . A reliability of .90 was chosen because: failure of the SIMS IARU does not eliminate all sources of precision attitude data (see discussion of backups); the thematic mapper data would still be useful even without precision attitude; the thematic mapper is not a prime payload, i.e., if it fails the mission does not end, as would be the case, for example, if the HIMS failed. The 4 years chosen for t is based on the 3-5 years operating life called for in the SIMS work statement (see Appendix A of Reference 85). The hazards, 0.088 and 0.029 years^{-1} , are based on an MTTF of 300,000 hours (34 years) per gyro. That is the figure used by Honeywell Aerospace for its Air Force system employing 13-IRIGs*.

The figures in the table show that unless a compromise in the target, $R(4) = .90$, can be accepted, the SIMS-A IARU will have to include redundant gyros. This presumes, of course, the relevance of the formulas, and the validity of the hazard assumed.

*The information available to the SIMS Study group indicates that the stated MTTF pertains to the gyro plus electronics, essentially as described for configuration 1).

TABLE 6-2

Evaluation of Reliability Formulas for the SIMS-A IARU

Reference values for R and t are .90 and 4.0 years, respectively.
 Reference values for λ are 0.088 and 0.029 years⁻¹ for formulas
 (1)-(3) and (4), respectively,

Formula	R	t (years)	λ (years ⁻¹)	MTTF (years)
1	.70	4.0	0.088	11
2	.91	4.0	0.088	17
3	.95	4.0	0.088	23
4	.94	4.0	0.029*	20
1	.90	1.2	0.088	11
2	.90	4.3	0.088	17
3	.90	6.1	0.088	23
4	.90	5.2	0.029*	20
1	.90	4.0	0.026	37
2	.90	4.0	0.095	16
3	.90	4.0	0.133	15
4	.90	4.0	0.038*	15

* For 1 gyro.

Therefore, some of the assumptions underlying the formulas and their use are reviewed here.

Assumptions Underlying the Formulas -

Some of the assumptions on which the formulas and their use are based are:

- (a) All failures considered are catastrophic, i.e., when an item fails it is useless.
- (b) The hazard (failure rate) for any particular item i is a constant (λ_i).
- (c) For the theory to be applicable to an actual item i , λ_i must be known.
- (d) The subsystems of a series configuration are truly in series.
- (e) The subsystems of a series configuration are independent.

(a) Defining what is a catastrophic failure for a particular item is not always simple. To do so for SIMS would necessitate a thorough review of how SIMS data is to be used so that guidelines can be established that permit distinctions to be made between catastrophic failure and intermittent or marginal failure. The aforementioned Air Force system is to be used for guidance as well as in the orbital phase of the mission. Intermittent operation during guidance would almost certainly be a catastrophic failure, and marginal operation would probably be catastrophic for comparatively small departures from specified performance. A SIMS could tolerate some intermittent failures and a comparatively large amount of marginal failure. Therefore, assuming the same hazard

for the gyros in the SIMS-A IARU as for those in the Air Force system is probably quite pessimistic. The different operating environments (e.g., rotation, acceleration, vibration, thermal) should also be considered.

(b) Assuming that the hazard is constant, if in fact it is a function of time, could, depending on the nature of the function, make the exercise in reliability analysis on which Table 6-2 is based entirely irrelevant, and perhaps a cause of incorrect and very costly design decisions. Nonetheless, when the amount of test data available for a gyro type is not sufficient for defining the hazard, systems designers, trying to meet a quantitatively specified reliability, usually choose a priori a hazard of the simplest form, a constant. An attempt was made during the SIMS Study to find out if the data available to date on the 13-IRIG warrants the assumption of a constant hazard. A conversation between the writer and A. Lattanzi of the CSDL, a member of the Miniature Components Group which developed the 13-IRIG, revealed that: no inherent failure mechanism has been identified; a number of units have exceeded 10,000 hours operating time and show no performance degradation; failures that have occurred were traced to manufacturing defects. Although Mr. Lattanzi will not challenge the 34 years MTTF used by Honeywell, he does not have the data that would enable him to predict the 111 years MTTF per gyro indicated in the ninth line of figures in Table 6-2 as the target for the 13-IRIGs to be used in SIMS. Still, he is confident that the 13-IRIG (and any other well-made gyro) is just as reliable as other components of comparable complexity and precision (see, for example, the discussion below of the SIMS-A star mapper). Such confidence appears warranted by CSDL experience with ~~three 2PBG-6F gyros~~. According to ~~W. Brown~~ of the CSDL, they were used for a number of years in the early 'sixties before being installed in the inertial measurement unit of the

FAA's SEAL* system where they have since logged over 30,000 hours each with no failures. Thus, although the evidence is not sufficiently quantitative, $R(4) = .90$ appears to be a reasonable target for a SIMS-A IARU without redundancy. The implication in that assertion, if a claim of 111 years MTTF is to be avoided, is that the hazard cannot be constant. A likely alternative is the familiar "bathtub" curve, approximated by a linearly decreasing hazard, followed by a constant hazard, followed by a linearly increasing hazard. Mr. Lattanzi believes that the period of decreasing hazard would be less than a month, so it is possible to ignore that region by requiring a one-month "burn-in" for the gyros. This model allows one to assume a small enough hazard in the constant region to meet the reliability goal without implying a huge MTTF. Of course, it is essentially an a priori hazard function, but there appears to be a better basis for it than for the constant hazard, and it can hopefully forestall heroic redundancy measures in the absence of data to support them.

(c) Clearly, if the SIMS-A IARU is to be subjected to formal reliability analyses through which the need for redundant design can be tested, not only must the hazard function be reasonably well known, but so also must its parameter(s). That is, the a priori approach must be avoided for parameter evaluation as well as for hazard modeling. If the "bathtub" hypothesis is correct, 2 or 3 parameters are needed: the time at which "infant mortality" ceases; the gyro hazard (λ) in the region where it is constant; the time at which "wear-out" begins. Actually, the latter need only be shown to exceed 4 years. Also, since the time at which infant mortality ceases is probably less than a month it can be greatly overestimated without imposing a severe "burn-in" penalty. What is needed, then, is a life-test set-up

* Signal Evaluation Airborne Laboratory (SEAL) for basic flight inspection.

for λ (or the hazard function, if the tests show that it is not a constant) in which the SIMS-A IARU environment and modeling are simulated. It seems that the cost would be moderate compared to that which could result from failures or excessive design complications caused by ignorance. If the tests are begun soon, the results will be available in time to support the SIMS design for the EOS.

(d) Implicit in the way all three of the reliability formulas have been used up to this point is the assumption that the gyros in each triad (IARU) are truly in series. In fact, if in configuration 1) only one gyro fails, what remains of the IARU is still useful. If the gyro that fails is the yaw gyro, and the payload is the thematic mapper (see discussion of backups), what remains is by far the most important part of the IARU. Configurations 2) and 3) provide a more dramatic example of the series assumption. They make very inefficient use of the potential for improved system reliability offered by the extra gyros. The series assumption was made simply to provide examples to which formulas (2) and (3) are applicable.

(e) Another assumption, also made so that the configurations provide examples to which the formulas apply, is that the subsystems in series are independent. Gyros of the same design, assembled by the same people in the same facility, and that kind of sameness applying to the parts used in the gyro assembly and electronics, would seem to make the probability that one gyro fails, given that one or more of the others failed, non-zero. This is not to say that measures should be taken to assure independence just to make the simplest form of reliability analysis applicable - it is merely a caution against overreliance on the theory. For example, the assumption for configuration 1) that each gyro has completely independent electronics, including power supplies, is not intended as a practical recommendation;

when all factors are considered, a common power supply (i.e., system of converters, inverters and regulators) may appear a better alternative.

Star Sensors

The star mapper is extremely reliable, primarily because of its simplicity, but also because of its extra slits. By using separate electronics for each slit (of which there usually are 2 sets of 3), a slit set with one slit failed is essentially as good as a full set; and complete failure of a set only halves the effective field-of-view of the sensor. For its silicon-detector star mapper, which takes advantage of these opportunities for redundancy Honeywell estimates a reliability of .9990 for 2 years.*

Reliability figures were not obtained for the SIMS-B star tracker, but some life-test data was provided in a letter¹⁵⁴ from D. Kirby of TRW. It states that "TRW has conducted a life test of the star tracker gimbal which simulated 5 years of vacuum operation with no measurable wear and no change in lubrication properties."

*Based on a telecon between D. Paulson of Honeywell Aerospace and M. Smith of the CSDL. Honeywell uses a hazard, λ , per slit channel of 7.38×10^{-7} hours⁻¹. The reliability formula for a slit set has the same form as (4) except that here success depends on "2 out of 3" rather than "3 out of 4", i.e.,
 $R_{23} = 3e^{-2\lambda t} - 2e^{-3\lambda t}$. The reliability of the sensor is $(R_{23})^2$ since there are 2 slit sets. Apparently, Honeywell considers the detectors and their electronics to be the dominant sources of risk.

6.2.8 CRITERION 8 - MODULARITY OF DESIGN, AND GROWTH POTENTIAL

The two major subsystems, the IARU and star sensor, operate independently on board the spacecraft. This aspect of modularity, which holds for all of the SIMS configurations, facilitates implementation of a number of the growth features discussed below.

A thorough treatment of the subject of growth potential is not attempted here because of its enormous scope. Moreover, because the SIMS work statement does not identify growth objectives, no attempt is made to assess quantitatively those growth features that are identified. A hierarchy of SIMS growth categories, assumed in this discussion to be listed in order of decreasing importance, is as follows:

- 1) Capability for increased function in the EOS mission.
- 2) Adaptability to alternative system configurations for EOS.
- 3) Capacity for improved performance.
- 4) Ability to meet requirements of new EOS missions.
- 5) Ability to meet requirements of other NASA programs.
- 6) Adaptability to subsystems changes.

1) Increased Function

Attitude Indication -

The extended SIMS functional capability most likely to be called for in the future is attitude indication, i.e., attitude information provided sufficiently close to real time as to

be suitable for control purposes such as payload sensor pointing or spacecraft attitude control. In support of this claim, in the "Excerpts from Unpublished Draft, Phase A Report, ' EOS System Definition Studies'"⁸⁹ it is stated that "a natural evolution of a precision attitude determination system (SIMS) would be a precision attitude control system to orient a high resolution sensor or sensors in real time". An accuracy goal of 0.01° is defined.

To outline in general terms how a SIMS would be modified to provide attitude indication some assumptions are made about what is given and what is desired. It is assumed first that attitude with respect to the local orbital frame is desired. That frame has its origin at the terminus of the geocentric position vector \bar{r} of the spacecraft, its z-axis (yaw) along $-\bar{r}$ and its y-axis (pitch) along $\bar{v} \times \bar{r}$, where \bar{v} is the spacecraft velocity vector. The x-axis (roll) completes the right-handed x-y-z triad. Since SIMS-derived data only pertains to inertial attitude, it is further assumed that \bar{r} and \bar{v} (or quantities derived from them) are available to an on-board computer. \bar{r} and \bar{v} are determined either from ground-based radar tracking data; or from ground-based processing of EOS payload imagery and SIMS (or SIMS-like) data [see discussion under item 2) below].

With the foregoing assumptions, the SIMS modifications required for attitude indication can be shown to be essentially the introduction of an on-board computer, or the expanded capability of an already-available computer in the case of SIMS-B and possibly in the case of SIMS-A. The question of interest is: how much of a computer? For SIMS-A and -B the answer is: probably a very complex one. For SIMS-D the answer is: probably a very simple one. The bases for these assertions are perhaps best explained by reference to the more important coordinate transformation matrices pertaining to attitude indication.*

* The discussion presented here in terms of coordinate transformation matrices was adapted from a discussion of a similar problem in section 7 of Reference 162. The latter contains useful supplementary information.

Referring to a coordinate frame by a lower case letter, e.g., u; and denoting the frame v to frame u transformation matrix by M_{uv} :

$$M_{om} = M_{or} M_{rq} M_{qm}, \quad \text{with}$$

o — local orbital frame

m — frame imbedded in instrument mounting structure

r — reference inertial frame

q — quasi-inertial frame.

The elements of M_{om} implicitly contain (or, as in most practical cases, explicitly are) the computed Euler angles defining the orientation of the instrument mounting structure relative to the local orbital frame. Therefore, the attitude indication problem is essentially solved when the pertinent elements of M_{om} are determined. The attitude angles are, of course, time varying quantities, and the time scale on which they are indicated must be close enough to real time so that the impact of the time lag error on the attitude control error is tolerable.

The case for SIMS-D is taken up first since it is the easiest to treat. q is imbedded in the stable member of the IARU. Its axes and those of m coincide with the gimbal axes at the time when the latter are uncaged from their 0-0-0 orientations. Thus, the elements of M_{qm} are simply trigonometric functions of the gimbal angles (or approximately the angles themselves, when small). The elements of M_{rq} are derived from M_{qm} and star mapper data. Although the derivation entails extensive computations, if the r frame is chosen to be initially (when the gimbals are uncaged) coincident (or nearly so) with

with the q frame, the elements of M_{rq} will be small and almost constant. They will reflect instrument calibrations and gyro drift rate biases, and should be representable by polynomials in time which are of low degree. Since the coefficients of those polynomials will probably remain constant for several orbital periods, the extensive computations mentioned above can be executed at a ground-based data processing center. That center can periodically provide coefficient changes to be uplinked. The elements of M_{or} can be computed from \bar{r} and \bar{v} and are therefore highly predictable. If the r frame is chosen to be initially coincident (or nearly so) with the o frame, the elements of M_{or} need reflect little more than the almost constant rotation rate of the o frame about its pitch axis. The reason for the "or nearly so" within parentheses is that this is one of two constraints placed on the r frame and both of them are not always consistent. The main rotation angle of the o frame can be represented by a simple polynomial in time, probably of second degree. Thus, with the elements of M_{rq} small, almost constant, and predictable over several orbital periods, and with the elements of M_{or} also highly predictable over long periods and having simply describable elements, coefficients in polynomials for the elements of a composite matrix M_{oq} could be uplinked to the spacecraft every revolution or so. The on-board computations would then consist of taking the sine and cosine of the pitch gimbal angle and forming the elements of M_{qm} ; updating the polynomial elements of M_{oq} and taking the sine and cosine of the main angle; and partially pre-multiplying M_{qm} by M_{oq} . The reason for only partially multiplying the latter two matrices is that the Euler attitude angles are small enough so that the elements of M_{om} are, to within an error of less than 1° , equal to the angles, thus necessitating computation of only three elements of M_{om} as well as avoiding the need for trigonometric inversion. This is true even for the current EOS attitude control specification

(0.5° bias plus 0.6° , 3σ). The small angle (i.e., less than 1°) assumption is also implicit in the identification of computations for M_{qm} where sines and cosines of roll and yaw gimbal angles were assumed unnecessary. Although the foregoing computations are straightforward and fairly simple, what little complexity is present is associated with removing the effects of orbital rate via the $M_{Oq} M_{qm}$ product. Since that rate is highly predictable and almost constant, it would seem that some simple artifice (such as applying a fixed pulse rate to the pitch gimbal angle encoder register) could be found that would eliminate the need for sine and cosine computations. If that were accomplished, the computer requirement for an attitude indication system based on SIMS-D would be trivial. In any case, attitude indication using SIMS-D warrants a good deal of further study.

For both SIMS-A and -B, q coincides with m at the beginning of the data smoothing interval. It is subsequently defined by M_{qm} whose elements are derived by an on-board IARU attitude algorithm computer operating on incremental angles sampled from the gyro pulse-count registers. The need to perform the algorithm computations on board the spacecraft arises from the fact that the attitude error rates are essentially unpredictable and relatively large (even if reduced an order of magnitude from the current $6^\circ/\text{s}$, 1σ EOS specification). Fortunately, with initialization at about 0.1° , and rotation of the orbit plane by probably less than 1° , the algorithm needs cope with a large angle about only one axis. This remains true even if the 0.01° control specification applies only during payload operation, with 1° being allowed the rest of the time* to provide relief to the control actuators. Nonetheless, on-board IARU attitude algorithm computations constitute a major computer requirement for SIMS-A

*The 1° figure may be somewhat optimistic in the case where sensor orientation is to be accomplished by gimbaling rather than by spacecraft attitude control.

and -B that is not shared by SIMS-D. Another major computer requirement arises from the long intervals - perhaps several orbital periods - over which the system must operate without ground assistance. Factors that determine the unaided operating period are uplink and downlink opportunities, time lags in ground-based data processing, and hand-off constraints. Since it seems reasonable to expect that simulations will show that the maximum unaided IARU attitude algorithm operating period, if dictated by these factors, would lead to intolerable algorithm errors, it is likely that a major part of the stellar correction and calibration of the IARU (computation of the elements of M_{rq}) will have to be done on board the spacecraft. On-board stellar correction may also be found necessary by a lack of stability in the coefficients employed in computing the elements of M_{rq} . This is more likely to be the case for SIMS-A because of the many sources of error rate uncertainty and the difficulty of estimating some error rate biases. Besides the additional computation burden imposed by on-board estimation of the elements of M_{rq} , the estimation accuracy may suffer, the elegant schemes feasible for ground-based data processing not being permissible. The loss of estimation accuracy would not be as serious a disadvantage for SIMS-B as for SIMS-A because the former is less dependent on data smoothing. On the other hand, methods of estimating slowly-changing components of elements of M_{rq} at a ground-based data processing center may moderate the accuracy problem for SIMS-A.

While the discussion above leaves many questions open it does seem to support the claim that attitude indication with a SIMS-D imposes a computation requirement that is moderate compared to that for SIMS-A or -B. The actual requirements and performance limitations should be investigated in depth if and when attitude indication becomes a definite objective.

Orbit Estimation -

If acquisition of a sufficient number of well-spaced landmarks in the payload imagery could be relied upon, the primary orbit estimation system, which is based on a transponder-aided ground-based radar tracking network, could be replaced by one based on the SIMS and landmark data. Motives for adopting such a landmark-stellar-inertial measurement system (LSIMS) might be reduced cost or improved performance.

The reduced cost would obtain by eliminating the space-borne transponder and the services of the tracking net. The only penalty would be increased data processing, much if not all of which would be automatic.

It is not yet possible to say whether improved performance would result from the use of landmarks - major questions remain unanswered. Among them are:

1. What performance improvements are desired?
2. Can "acquisition of a sufficient number of well-spaced landmarks in the payload imagery" be relied upon?

The first question breaks down into a number of smaller questions: What accuracy is sought? In relation to what frame? Does the error specification apply only where the payload operates? Is short (one orbital period) setting time desired? This last question is concerned with the possible need for attitude indication. The next-to-last suggests that a hybrid landmark-radar system might be of use. Such a system is alluded to in "Excerpts from Unpublished Draft, Phase A report, 'EOS System Definition Studies'"⁸⁹, where it is stated that "the gyro portion of the precision attitude determination system (SIMS) can also be used in conjunction with landmark techniques to greatly reduce the frequency of landmarks required".

The second major question was identified in the SIMS pre-proposal (Appendix B of the first Interim Technical Report⁸⁵) as the object of two tasks. They are reproduced below.

Task 2. Landmark Study (2 man-months)

Define a landmark study that will eventually lead to:

- a) image analysis techniques applicable to observation vector* determination;
- b) a data file of recognizable and surveyed landmarks;
- c) a computer program of landmark availability, including statistical estimation of cloud cover effects, for mission simulations;
- d) contributions by EOS and other earth observation programs to the data file and cloud cover model.

Task 7. System Employing Landmarks (1 man-month)

Using results of tasks 2, 4, 5 and 6 define future studies in relation to landmark-inertial and landmark-stellar-inertial systems for attitude determination and observation vector determination. (Tasks 4, 5, and 6 comprise essentially what subsequently became the SIMS Trade Study.)

Even though these tasks were merely to define landmark studies, not to execute them, it seems in retrospect that the

*The "observation vector" was defined in the aforementioned Appendix B as having its origin at the vertex of the objective of the payload sensor, being parallel to the optical axis there, and terminating at the surface of the earth.

number of man-months assigned to them was optimistic. The fact that they did not become a part of the SIMS Trade Study (because of funding limitations) makes comparing the capabilities of the three SIMS systems for orbit estimation impractical at this time. However, it does seem that if their capabilities are found to differ greatly, SIMS-D will be favored.

2) Alternative System Configurations

Landmark-Inertial System -

The star sensor could be omitted from a SIMS, and landmarks could be employed instead of stars for attitude determination. The resulting landmark-inertial measurement system (LIMS) would use a satellite-to-landmark line in the same way that a SIMS employs a starline. Coordinates of one point on the landmark line would be the satellite position as derived by the orbit estimation system. Coordinates of the other point would be derived from payload imagery.

Among the possible motives for adopting a LIMS are: elimination of a major SIMS subsystem, the star sensor, or providing a backup technique in the event of its failure or unanticipated inadequacies; improved observation vector determination.

Since SIMS is itself a subsystem of the observation vector determination system, if the LIMS supports better observation vector accuracy, ~~it is more desirable from an overall~~ accuracy standpoint. The ground-based radar tracking system determines the origin of the observation vector. Its terminus is determined, in the SIMS case, from star sensor, IARU and imager^{*} data; and, in the LIMS case, from IARU, imager and tracking system data. Hence, observation vector determination

* It should be noted, however, that SIMS is applicable to observation vector determination for a sensor that does not acquire known and/or surveyed landmarks, e.g., an ocean surface temperature mapper, or an earth limb radiometer. (The definition of "observation vector" for the latter case is, of course, different than as given here.)

employing a SIMS as against a LIMS involves an additional subsystem (the star sensor) and its errors, so the LIMS gains an advantage in accuracy. Another feature of the LIMS that should prove advantageous from an accuracy standpoint is that its landmark data is acquired in just those parts of the orbit where good attitude information is desired, i.e., during acquisition of imagery. Whether or not these accuracy advantages are realizable depends on the outcome of landmark availability studies of the type to have been defined by Tasks 2 and 7 discussed above in connection with an LSIMS.

A LIMS-D (i.e., a LIMS based on the SIMS-D IARU) which employs TGGs would probably need no more than 2 landmark lines per orbital revolution having suitable angular separation, say, greater than 40° acute angle. On the other hand, a LIMS-A or -B would require a good deal more than 2 landmark lines per orbital revolution, and, unless those lines occurred at regular intervals, such systems would probably be infeasible.

Self-Contained Landmark-Inertial System -

A self-contained LIMS (SLIMS) is a system that provides both attitude determination and orbit estimation using data from the IARU and payload imagery only. That is, it does not rely on ground-based tracking nor on stellar data. Motives for adopting a SLIMS could be any of those given above for an LSIMS or a LIMS. However, contrary to the case for an LSIMS and a LIMS, it cannot be stated categorically, given any number of well-spaced landmarks, that a SLIMS is technically possible. It is not known whether the defining equations are well-conditioned, and, though some believe they are and some believe they are not, the controversy will probably not be resolved until some computer simulations are carried out. If such simulations should prove that a SLIMS is possible, and if landmark studies

indicate that it is feasible, a SLIMS-D will probably be the only practicable implementation. The bases for this assertion are in the argument above for a LIMS-D, and in the recognition that a SLIMS requires many more landmarks than a LIMS.

3) Improved Performance

Adoption of a LIMS or SLIMS should have a beneficial impact on every SIMS trade criterion, except possibly ground data processing, that pertains directly or indirectly to performance, i.e., weight, power, accuracy, telemetry, reliability and field-of-view. The impact on cost and availability should also prove beneficial. However, the question to be considered here in relation to each of the three SIMS configurations is: What improvements are possible in the SIMS system as such?

Gyro Redundancy -

SIMS-A and -B reliability improvements through gyro redundancy are achievable with much greater efficiency than for SIMS-D. For example, by adding a fourth gyro to the SIMS-A or -B IARU, and aligning its input axis with the diagonal from the cube corner defined by the input axes of the gyro triad, it can serve in the event of failure of any one member of the triad. Although such an arrangement can be implemented with only a moderate penalty in weight and cost, and almost none in power, ascertaining the extent of the improvement in reliability would necessitate a careful study of failure modes and their probabilities, with special regard to shared circuitry. More elegant, high-efficiency arrangements using more than one additional gyro are possible. However, need rather than efficiency should be the motive for redundancy. In that regard it should be noted that SIMS is not a primary spacecraft subsystem; a SIMS failure does not jeopardize the entire EOS mission.

Star Mapper Redundancy -

Because of the comparative simplicity of the star mapper, two units could be employed in SIMS-A or -D as a low-penalty method of increasing both accuracy and reliability. This option would probably not be exercised for SIMS-D because it is not star-poor, and it has LIMS as a back-up in the event of star mapper failure.

Photomultiplier for Star Mapper -

The star mapper in SIMS-A and -D is based on a silicon detector. It seems that a star mapper employing the photomultiplier tube (pmt) for detection might be superior to those based on solid-state detectors. Unfortunately, there is no pmt candidate with accuracy in the neighborhood of the SIMS specification, so this expectation cannot easily be tested.

The reasons for the decision to employ solid-state detectors in SPARS are given in reference 15: "Since the Air Force had expressed a desire for a solid-state device and since solid-state devices tend to have greater growth potential than do vacuum tubes, the decision was made to go to solid state". The basis for the Air Force's "desire for a solid-state device" is not given and is therefore not subject to comment. However, the claim that "solid-state devices tend to have greater growth potential than vacuum tubes", even if true when a pmt is considered to be a vacuum tube, is hardly a compelling argument for ignoring the pmt. The actual status of each type of detector in relation to desired performance characteristics should have been considered the key concern of a technical trade study. Moreover, "vacuum tube" calls to mind a thermionic device*.

* Webster's New World Dictionary and the American College Dictionary both give two definitions for "vacuum tube"; the first refers to thermionic devices and the second to gas discharge devices.

Although typical thermionic tubes have notoriously short lifetimes and should not be considered for long space missions, pmt lifetimes consistent with the EOS goal have already been demonstrated in space.

For the reasons stated here, a star mapper trade study that includes a unit employing a pmt is recommended for SIMS-A and -D. Such a study would have to be preceded by a pmt star mapper design exercise and probably some pre-prototype development.

Random Acquisition with a SIMS-B Tracker -

Early in the SIMS Trade Study the possibility of operating the SIMS-B star tracker in a random acquisition mode was investigated. Based on a review of technical literature covering the tracker, and conversations with cognizant TRW engineers, CSDL personnel concluded that the scan rate required for complete examination of a sufficiently large part of the celestial sphere was too fast for the sensor. Recently that conclusion was found to be incorrect.* The tracker could, for example, completely examine the 30° swath of the celestial sphere bisected by the orbit plane for stars of magnitude 3.5 and brighter. The only change required is a doubling of the aperture in front of the electron multiplier section of the image dissector.

The most important advantage of a random acquisition mode is that it eliminates the only requirement in SIMS-B for an on-board computer (assuming that the IARU attitude algorithm is not done on board). In the currently-proposed configuration the tracker optical axis is directed to within acquisition range of a preselected star by applying computer-selected command angles to the tracker gimbals. This mode would also impose the only requirement for uplinking data, if future studies should

*Telecon between R. Gates of TRW and M. Smith of the CSDL on May 23.

indicate that a star catalog for the entire celestial sphere, and associated acquisition timing problems over 3 - 5 years, would call for too large a storage capacity.

To make sure that any two stars acquired successively have adequate angular separation for a complete IARU alinement, the actual scan pattern might be centered alternately at 30° to either side of the orbit plane. In other words, the tracker optical axis would be articulated back and forth between 45° and 15° from zenith in the plane normal to the orbit plane until a star is acquired. It would then enter the track mode and remain in that mode until the gimbal angles were sampled. After that, the optical axis would be commanded to the other side of the orbit plane where the same type of acquisition scan would be conducted. Thus, any two stars acquired successively would be separated by at least 30° .

For the random acquisition parameters (30° scan and ≤ 3.5 star magnitude) considered here the SIMS-B star availability study indicates that a typical time between star acquisitions would be a few minutes and it would rarely exceed ten minutes. The actual figures would of course be the object of star availability studies if random acquisition were adopted.

Elimination of a Star Tracker Gimbal -

One of the gimbals of the SIMS-B star tracker could be eliminated. Assuming, for explanation purposes, that when the gimbals are centered the axis about which $\pm 45^\circ$ of rotational freedom is provided is spacecraft roll, and the other axis, about which is $\pm 15^\circ$ of rotational freedom is provided is spacecraft pitch, the gimbal providing pitch freedom could be omitted. With the resulting configuration, when a star is acquired in the 0.5° raster scan the roll track-mode is entered, and readout is triggered when orbital rate brings the star to the optical axis.

In the case of random acquisition the scan rate would have to be increased to insure that the star would not have passed the midpoint of the electronic scan line when acquired. In the case of computer-controlled acquisition there would be no need to increase the search rate because the search angle is too small for such a problem to arise. However, in both cases, only one gimbal angle reading would be obtained for each star. One of the advantages of the tracker as currently configured is that a number of gimbal angle sets can be obtained for each star that is tracked, thus allowing for averaging to reduce the noise-equivalent angle. To keep this advantage, instead of eliminating the "pitch" gimbal it could be retained but with only about 1° of freedom. This would also avoid the need for a higher scan rate in the random acquisition mode.

Reducing to 1° the angular freedom of the gimbal that now has 30° should reduce the geometrical errors for both gimbals and the angle readout error for the one with 1° of freedom, and it would simplify design of the gimbal, servo and angle indicator for the 1° axis at least.

3-Axis Readout for the SIMS-D IARU -

The number of contributors to gimbal geometry errors is known to be large⁷⁹, and, though calibration of the SIMS-D IARU gimbal angle indicators both before and during the mission will help to inhibit them, it would be desirable to avoid them altogether if possible. A method of accomplishing that objective is to construct the gimbals in a manner that makes the gyro-stabilized member directly accessible from the IARU case, and to employ a readout (3-axis) that indicates the orientation of the stable member with respect to the case directly by taking advantage of the direct access to the stable member. A readout of this type is employed in the Draper Laboratory's Flmbal^{80,81}. Although

the units so far developed for that system are not accurate enough for a SIMS, the fact that a SIMS incurs very little rotation about roll and yaw greatly increases the likelihood that a Flimbal-type readout could be developed for it.

The single 3-axis readout is not being recommended here for SIMS-D. Since fabrication of a conventional gimbal system employing shaft-by-shaft indication of the orientation of the stable member with respect to the IARU case and meeting the SIMS IARU performance goals appears feasible, the conventional system is recommended for the first SIMS-D model. The single 3-axis readout should be developed for possible use on a later model of a SIMS-D IARU, and as a technique for any gimballed instrument whose precise orientation is needed. It seems likely that NASA will have use for many such instruments in the future.

4) New EOS Missions

Geostationary EOS -

Among the more obvious applications of a geostationary EOS are: detection and tracking of large-scale weather phenomena, fires, floods, icebergs, tsunamis, ocean currents, and air and water pollutants; survey and seasonal monitoring of plant life such as crops, forests, grass, and brush, and associated soils and hydrological conditions; measurement of secular changes in polar ice caps, global pollutants, sea levels, global temperatures and heat balance; resource surveys for water, minerals, timber, fossil fuels, and geothermal power; discovery or detection of geologic phenomena such as fault lines, earthquakes and volcanoes.

The kinds of sensors employed will be mostly radiometric, spectrometric, or spectroradiometric. Many operate outside the visual spectrum and many do not produce imagery as the final output. Some of those that produce imagery are not applicable

to a LIMS because of the part of the spectrum chosen or the regions of the earth observed. Hence, some observation vector determination (or indication) systems for a geostationary EOS will employ a horizon-inertial measurement system (HIMS) and/or a SIMS. The angular accuracy of a HIMS should be better for a geostationary orbit than for a low-altitude orbit because: the limb altitude uncertainty subtends a smaller angle; the coordinates of the sensed part of the limb can be chosen fixed relative to the earth; the horizon sensors can operate at very low noise bandwidth. Still, it is unlikely that a HIMS would have accuracy comparable to a properly-configured SIMS, so it is appropriate to consider a SIMS for a geostationary orbit.

To facilitate comparing the SIMS configurations an imaging payload sensor with operating characteristics similar to a thematic mapper is assumed. It is of course implicit in the comparison that the imagery is not suitable for a LIMS. The three main determinants of accuracy for observation vector determination are payload-sensor spatial resolution, orbit estimation accuracy, and SIMS accuracy. The three, when expressed as angles, are more or less equal for the 500 nm polar orbit currently planned for EOS, although SIMS accuracy appears to be the pacer. For a geostationary orbit a marked improvement in estimating the elements should be possible, and, because of the extremely low payload sensor noise-bandwidth permissible, a very small angular resolution would be feasible even without enlarging the optics. Therefore, the SIMS accuracy desired would be at least as good as the current SIMS specification.

To avoid having to cope with the problem of sun - star sensor aspect, it is assumed that if necessary an additional star sensor would be employed. Although a proper comparison of the three SIMS configurations for a geostationary orbit would include error simulations based on star availability, a cursory review of the star distributions published in Appendix C of the

second Interim Technical Report¹⁴¹ suggests that a SIMS-B or -D would be applicable, and a SIMS-A would probably not be applicable. The SIMS-B tracker with its wide coverage of the celestial sphere and its small instantaneous field-of-view, could, without interference from "noise stars", acquire two stars of sufficient angular separation for IARU frame identification at any time. For SIMS-D, to avoid the long delay (about 3 hours) in acquiring two stars of suitable angular separation, two star mappers with optical axes separated by about 60° would be needed. The low noise-bandwidth associated with the lower orbital rate permits detection of higher magnitude stars. This and the fairly good distribution of stars accessible to a star mapper in an equatorial satellite indicate that SIMS-D would not have to operate without full stellar correction for more than one hour.

Stratospheric Temperature Monitor -

Atmospheric scientists have indicated concern at various times during the past few decades about the effects of increases in CO₂ concentration caused by fossil fuel consumption. During the sixties, when work in the environmental sciences accelerated, a number of studies dealing with CO₂ pollution were published. The main effect predicted is an increase in surface temperature. It will be accompanied by a reduction of temperature in the stratosphere many times larger. For this reason a panel of the President's Science Advisory Committee (PSAC) recommended in a report¹⁶⁷ in 1965 that stratospheric temperature be monitored as part of a study of the overall CO₂ pollution problem. The recommendation was taken as the motivation for an orbital measurement program that was suggested in a CSDL study³⁷ in 1969. The suggestion contained a loosely-defined proposal for the measurement system, and a derivation of the system accuracy requirements. The latter were refined in subsequent correspondence and

conversations with atmospheric specialists. The proposed system and the accuracy sought constitute an interesting example of a non-imaging payload — an infrared radiometer — requiring observation vector* determination at an accuracy level only an EOS with a SIMS could provide.

The increased CO₂ concentration and the resulting reduction in stratospheric temperature will cause a shifting of the coordinates of the 15μ CO₂ limb-radiance profile** at a rate predictable from the theory of atmospheric radiation. The aim of the proposed system was to monitor that shifting over the remainder of the century. The proposed spacecraft instrumentation included an uprated version of the infrared radiometer^{163,164} developed at the CSDL for Project PROFILE³⁸, and a stellar-inertial attitude determination system of the type that today would be considered a SIMS. Together with the ground-based radar tracking net, and the radiometer scan-angle indicator, the SIMS would provide the data for observation vector determination. The overall error was apportioned equally (based on RSS) to orbit estimation, attitude determination, and radiometer noise. The resulting goal for the SIMS was a few arcseconds, i.e., very close to the .001° (1σ) set for the SIMS Study. The goal for satellite lifetime was set at a minimum of two years in order to assure that the indicated limb shift would be distinctly observable with each instrument package, and to facilitate progressive averaging of the data.

SIMS-A would be marginal for this application, and, since potential for improvement relative to the current SIMS

* Defined in this application as: originating at the vertex of the radiometer objective, being parallel to the optical axis there, and terminating at the intersection of the optical axis with the geocentric line normal to it.

** The limb-radiance profile is the radiance observed from space along a line parallel to a tangent as a function of distance above the tangent (i.e., altitude above the earth's surface). Correlation distances at constant altitude are great enough that the effects of scanning through an angle introduce negligible error, and the effects of satellite motion are removable.

accuracy goal is highly desirable, it would be a poor choice. Although SIMS-B or -D would be applicable, a trade study to determine which is more desirable would emphasize potential for improved accuracy.

5) Other NASA Programs

High-Eccentricity Orbits -

Among the non-observatory applications of a planet-oriented satellite are mapping charged particle belts, magnetic fields, and influx of extra-planetary radiation. The former two would probably be accomplished with high-eccentricity orbits to achieve a very large sample space. While all of the SIMS configurations would be applicable to such orbits, it should be noted that the "adaptive pulse-torquing loop" proposed in Appendix A of the second Interim Technical Report ¹⁴¹ as a way to overcome torquing problems in a SIMS-A that arise from the relatively high orbital rate would probably be inapplicable. The average-rate computer would actually see a rate changing continuously, and the required number of rate bias settings might prove prohibitively large. When the planet is earth, for which the orbital elements of the satellite are precisely known a priori, the possibility of applying a function with slightly adaptive parameters, rather than adaptive bias levels, does not seem practical either. If the function generator did not prove unacceptably complicated, the concept itself might prove incompatible with the objectives of a stable torquing mechanization.

Interplanetary Missions -

For interplanetary missions, none of the SIMS configurations appears to offer a very good means of attitude determination (or indication). Both SIMS-A and -D would be ruled out by lack of a turning rate suitable for star mapper operation during planetary transfer.

The deficiencies of SIMS-B are not as severe as for -A and -D, and are most evident when attitude indication is desired (which will probably be almost always). Round-trip communication time lags alone could be several minutes even for the nearest planet, so unless extremely low or highly predictable attitude rates obtain during planetary transfer and encounter (including, in some cases, orbiting the planet in a plane that prevents communication part of the time), all of which seems quite unlikely, the IARU attitude algorithm would have to be done on board. When an attitude algorithm computer must be included with a structure-mounted IARU no major advantages over a gimballed IARU can be claimed in advance of mission-oriented design and trade studies. However, a gimballed IARU can claim a distinct advantage if operation over several hours at SIMS accuracy levels is required or desired, and, since missions to other planets have already been successfully conducted, it is assumed here that accuracy would be the principal reason for adopting a SIMS in any future mission. Hence the SIMS-D1-B⁸⁵ would warrant consideration for interplanetary missions.

A configuration trade study for the Grand Tour guidance, navigation and control system was conducted in 1968-69 at the CSDL. The candidate selected for the stellar-inertial subsystem was of the same configuration as the SIMS-D1-B, and the IARU was very similar to the two being proposed for SIMS-D. That is, similar accuracy was sought, and designs were exercised for both the 13-IRIG and the TGG (referred to at that time as the 50 Series Gyro.)

Inertial Attitude -

For an artificial satellite whose attitude is to remain fixed with respect to an inertial frame, SIMS-B, programmed for attitude indication, is highly desirable. SIMS-A and -D are not applicable because of the absence of spacecraft rotation

essential to star mapper operation. In this particular instance SIMS-B is superior even to a SIMS-D1-B - provided that the attitude control actuators can stabilize the spacecraft in a linear control mode to a level of error rate comparable to that which can be indicated. In that case, the gyros are in the kind of environment (inertially non-rotating) that they try to create for themselves when on the stable member of a gimballed system. Hence the gimbals of a SIMS-D IARU would only be in the way.

Programming SIMS-B for inertial attitude indication ought to be possible without an on-board computer, if the IARU is of high quality. This implies, of course, that computer-controlled star acquisition is unnecessary. However, it is not unlikely that a system design study would indicate an optimum mix of on-board and ground-based computations. Such a study might also lead to addition of a second star tracker, and the OAO type of moding that would then be possible.

6) Subsystem Changes

In the foregoing discussion of growth potential each of the SIMS candidates is shown to have outstanding advantages for some applications. The subsections treating other trade criterions also show that each candidate stands out in its turn. It is therefore fortunate that the two key subsystems of both SIMS-A and -B and one of the two in SIMS-D either exist or are under development. These are: the star mapper for SIMS-A and -D; the IARU for SIMS-A and -B; and the star tracker for SIMS-B. If a gimballed IARU is developed, the key subsystems for all three of the SIMS candidates will be available, and will include those of SIMS-D1-B (i.e., a gimballed IARU and a gimballed star tracker⁸⁵). Moreover, a number of subsystems of each type are likely to be available eventually; three types of star mapper already exist at varying stages of development, and another (employing a pmt

detector) has been suggested by the CSDL. Therefore, subsystems integration schemes conducive to configuration changes through the use of different subsystem types and to upgrading through advances in sensor technology should be devised. The potential for modularity inherent in the independent operation of the SIMS IARU and star sensor should be exploited in such schemes. For example, those two subsystems should have entirely separate electronics assemblies.

6.2.9 CRITERION 9 - COST OF GROUND SUPPORT EQUIPMENT

The fact that NASA wants the cost of GSE to be dealt with as a separate trade criterion even though it is just a part of the overall cost (treated in subsection 6.2.1) suggests that in NASA's experience it has often proved to be quite significant and perhaps somewhat underestimated.

In its attempt to evaluate GSE costs for the SIMS candidates the SIMS Study group set up certain guidelines. The cost of GSE was assumed to include not only that of the equipment but also of operating, maintaining, housing, and transporting it. Locations of preflight GSE were assumed to be every facility the SIMS system arrives at, after leaving that of the subsystems integration manufacturer, enroute to and including the spacecraft at the point of launch. Examples might be a spacecraft subsystems integration facility, a launch area hangar, and a launch vehicle subsystems integration facility. GSE for mission support will consist of equipment, personnel, and space required for monitoring, control, and data processing at NASA ground stations; and the facilities maintained by the SIMS contractor(s) for simulation or diagnostic purposes in support of the missions.

Since none of the SIMS candidates has flown, nor even approached flight-worthy status, assessments of actual GSE costs would be tenuous at best. Fortunately, for trade purposes comparative estimates are adequate. Within the context of GSE cost factors as defined above, it is the consensus of the SIMS Study group that no outstanding differences among the three candidates are apparent.

6.2.10 CRITERION 10 - COMPLEXITY OF GROUND CONTROL/COMMAND/ DATA PROCESSING OPERATIONS

In all of the SIMS systems the star sensor and IARU operate independently of each other and in open loop fashion. That is, the data acquired by the star sensor and IARU is not processed on board the spacecraft or on the ground to produce commands between or to the sensors. Therefore, no ground control/command or uplink is required. However, when further systems studies are conducted, a moderate ground control/command capability may be found desirable for mode control, reliability management, efficient use of power, etc.

The various possible data processing operations are too ramified to be fully defined without a much more extensive interface between NASA and the CSDL than was possible within SIMS time and funding limitations. Also, the period in which the SIMS Study was conducted probably occurred too early in relation to EOS planning for such an interface to be fruitful. The two most important uses of SIMS data (together with orbit estimation data) are image rectification and image location. Image rectification is correction of image data so that points in the imagery have the same relative locations as in the scene. Image location is the determination of the locations of those points in an earth-fixed reference frame, and the appropriate annotation of the imagery. The detailed operations leading to image rectification and image location, and wide-ranging schemes for utilization of landmark data, have been subjects of discussion in various CSDL publications, but the only studies actually carried out at the CSDL are for reducing the SIMS data to smoothed estimates of inertial

attitude. Based on those studies -- which assume no on-board IARU attitude algorithm computation and no use of landmarks -- data processing requirements for each of the SIMS candidates differ significantly, but are probably moderate compared to those of the EOS payload.

6.2.11 CRITERION 11 - SYSTEM AVAILABILITY

A system containing the essential components of the SIMS-A candidate is being built by Honeywell Aerospace for the Air Force^{153,165}. The flight system is scheduled for completion by 5/1/73. It will employ the Honeywell Radiation Center's silicon-detector starmapper, and an inertial measurement unit (IMU) with three accelerometers and four 13-IRIGs. To make the IMU suitable for a SIMS IARU Honeywell proposes to reduce the Air Force system to a gyro triad by deleting a redundant gyro and its electronics, 3 accelerometers and their electronics, and a redundant power supply. The starmapper random error specification for the Air Force system is $8''$, and the bias error (due to shifts during launch in alignment of the slits relative to a reference surface on the exterior of the housing) is $4''$. Based on its experience with SPARS, Honeywell believes it can meet $2''$ for each of these errors. Therefore, should a SIMS-A be chosen for EOS, it will probably meet any reasonable delivery schedule, and most non-recurring costs will have been paid by the Air Force.

It is assumed here that the SIMS-B IARU would also be a 13-IRIG triad. In that case, only the availability of the star tracker needs to be assessed. The first prototype, which is gimbaled in 2 axes, is described in two AIAA papers^{33,35} presented in August 1971. A second prototype having only one axis of mechanical freedom is currently under development. In December 1970 TRW submitted a formal quote to GSFC (to the attention of T. Huber) for a 2-axis flight-worthy instrument to be available 12-13 months after receipt of an order. Therefore, any reasonable

EOS delivery schedule would probably be met by a SIMS-B, and a large part of the non-recurring costs of the IARU and star tracker will have been paid by the Air Force and NASA respectively.

Since it is assumed in this study that the SIMS-D star mapper will be the one Honeywell is developing for the aforementioned Air Force system, the availability of a SIMS-D rests on that of its IARU. Unfortunately, that IARU exists as no more than a preliminary design concept. Although the SIMS IARU Studies Task Group estimates that a flight-worthy system could be produced two years after contract initiation, that estimate is not the result of a proposal effort. Even if such an effort were to produce such an estimate there ought to be some concern about the lack of prototype development experience extending over many years, as has been enjoyed by the key subsystems of SIMS-A and -B.

The instrument mounting structure, temperature regulator, programmer (or computer), and interface electronics are not believed to be pacing items in relation to availability of any of the SIMS candidates.

6.3 RECOMMENDATIONS

SIMS Follow-on Studies —

Recommendations for advancing SIMS technology were stated or implied in subsection 6.2 and elsewhere in this report. They are repeated below for convenient reference.

1. Continue SIMS error studies:
 - a) Incorporate the most comprehensive and up-to-date error models and design parameters.
 - b) Simulate the rotational environment to the fullest extent practicable.
 - c) Simulate the attitude algorithm computation for SIMS-A and -B.
 - d) Investigate digital filtering as a way of smoothing SIMS-D IARU gimbal angle data, and the corresponding data derived by the attitude algorithm operating on SIMS-A or -B angle increments.
 - e) Evaluate the effects of noise stars on SIMS-A and -D starmapper data.
2. Expand the analytical studies to show how SIMS, thematic mapper, and radar-tracking data are combined to rectify and annotate imagery.
3. Conduct a trade study of gyro candidates, and perform tests required to model uncertainties and biases in drift rate, input axis misalignment and torquing scale factor (the latter two only if the IARU is to

be structure-mounted).

4. Conduct a trade study of star sensor candidates, and develop error models.
5. If a starmapper is to be employed in a selected SIMS, carry out the design and development of a unit employing a photomultiplier as the detector.
6. Determine whether the attitude algorithm computation for a structure-mounted IARU should be done on board the spacecraft, or at the ground-based data reduction center(s). Coordinate this effort with that of task 1. c) above.
7. Perform studies and tests required to assess the merits of the various SIMS backup schemes identified in subsection 6.2.7.
8. If growth potential is to be weighed heavily in selecting the SIMS candidate, proceed with SIMS-D IARU development.

Geometric Systems Studies —

In connection with growth potential (see subsection 6.2.8), a number of systems concepts making use of SIMS-type subsystems were identified, e.g., LSIMS, SLIMS, LIMS. As in the case for SIMS, their application is to observation vector determination, indication, and/or control. In previous CSDL publications^{37,5,61}, recommending that these systems be studied, they are said to belong to the "technology of dynamic geometry", a phrase that characterizes most of the work done at the CSDL. Accordingly, they have come to be called geometric

systems. It is recommended here also, that these systems be studied. However, the potential scope of such studies is so broad that a prior study should probably be conducted for the purpose of further defining the geometric systems and the problems associated with each. Priorities could then be established in accordance with EOS objectives.

APPENDIX A

TRADE CRITERION INFORMATION SUMMARY

A.1 INTRODUCTION

It was intended that this appendix would provide an organized and uniformly-thorough presentation of information on each of the candidates of the SIMS Trade Study, from the separate standpoints of each of the trade criteria in each case. While the organizational objective has been achieved, the uniformity of thoroughness has not. The treatment, due to the time constraint and to the variations in individual approach to and emphasis on the execution of this appendix, ranges from no information at all in some cases to relatively exhaustive treatment in others. The value of the appendix, in terms of its facilitating a point-by-point comparison, is therefore diminished. However, the value of the material compiled is, itself, sufficient to warrant inclusion of the appendix as planned*. References to supplementary material to be found elsewhere in this and other documents are included wherever possible, particularly in those tabular entries where information presented in this appendix is limited.

A.2 INDEX

Figure A-1 provides a quick-reference key to the location of specific information to be found in this appendix. Page numbers of Appendix A listed in the figure denote the pages on which each individual subject begins - or is treated entirely.

* In some cases, material originally submitted for Appendix A has been included in the report text; it is omitted here and reference is made to the text.

Note that for criteria 5, 6 and 8, the single presentation for each candidate is at system* level. For the other criteria, presentations at principal subsystem levels** as well as at system level are included.

A.3 FORMAT

Each presentation in this Appendix is preceded and identified by a heading of standard form designed to provide information on the subject of the presentation that follows it. The format identifies the candidate (SIMS-A, SIMS-B, or SIMS-D), the criterion to be discussed, and the scope of the discussion (IARU, SSA, or SYSTEM). Examples are:

<u>SIMS-B (SSA)</u>	<u>POWER</u>
<u>SIMS-A (SYSTEM)</u>	<u>COST OF GSE</u>
<u>SIMS-D (IARU)</u>	<u>COMPLEXITY OF COMMAND/CONTROL/ DATA PROCESSING OPERATIONS</u>

The technical content of Appendix A begins on page A-4.


* Criterion 6 is developed at SSA level, but treated as System level, and is supplemented by System level discussion in subsection 6.2.6

** "Principal subsystems" refers to:

IARU - Inertial Attitude Reference Unit

SSA - Star Sensor Assembly

Figure A-1 Index to Contents of Appendix A

CRITERIONS	SEE APPENDIX A PAGE NO. <div></div>	SIMS-A				SIMS-B				SIMS-D							
		I A R U		S S A		S Y S T E M		I A R U		S S A		I A R U		S S A		S Y S T E M	
1. COST		4	5	8	8	9	9	9	9	10	10	10	10				
2. ACCURACY		10	11	13	16	16	17	19	20	20	20	20					
3. WEIGHT		22	22	26	26	26	27	28	28	28	28						
4. POWER		28	29	31	31	32	32	32	32	32	33						
5. TELEMETRY REQUIREMENT		33				33				33							
6. TOTAL UNOBSTRUCTED FOV REQUIREMENT		33				36				36							
7. SIMPLICITY OF DESIGN, AND RELIABILITY		37	38	40	40	40	40	40	41	41	41	41					
8. MODULARITY OF DESIGN, AND GROWTH POTENTIAL		41				41				42							
9. COST OF GSE		42	42	42	42	42	43	43	43	43	43						
10. COMPLEXITY OF GROUND CONTROL/ COMMAND/DATA PROCESSING OPERATIONS		43	44	44	44	44	45	45	45	45	46						
11. AVAILABILITY		46	46	47	47	47	47	47	47	48	48						

SIMS-A (IARU) COST* **

1) Engineering Prototype (Qualified)	274K
2) Three Flight Systems (Initial)	707K
3) Laboratory Test Facility	400K
4) Engineering Support	133K
Non-Recurring Cost of Prototype and 3 Flight Systems	1514K
Per Unit (Recurring) Cost Thereafter	186K

Notes

*This IARU contains 3 13-IRIG gyros, power supplies and the interface and test unit.

**Honeywell data, supplied by D. Paulson (HI) to J.D. Coccoli (MIT/CSDL), in telecon on 5/24/72 (documented in Attachment C of Ref. 146). Cost data were derived from current firm, fixed-price USAF contract, and are expected to be relevant for several years.

SIMS-A (SSA) COST

SIMS-A-C

<u>ITEM</u>	<u>STAR SENSOR ASSEMBLY</u>	<u>SUNSHIELD</u>
• Fabrication Prototype	51K	34K
• Qual. Testing	26K	15K
• Three Flight Systems	163K	22K
• Cost/Unit Thereafter	54K	7K
• Lab. Test Facilities - Owner* Precision Rate Table - HA 24 Star Simulators - AF Calib. Equip for Star Simu's. - AF Detector Cell Tester - AF Star Sensor Tester - AF Computer and Accessories - HA Software - HA Misc. Hardware - AF	(See SIMS-A/IARU Cost Criterion) 170K 150K 40K 50K (" " " " " (" " " " "	(" " " " " (" " " " "

NOTE

*Owner - HA (Honeywell Aerospace); AF (Air Force).

(Continued)

SIMS-A (SSA) COST (Continued)

SIMS-A-C (Continued)

<u>ITEM</u>	<u>STAR SENSOR ASSEMBLY</u>	<u>SUNSHIELD</u>
<ul style="list-style-type: none"> • Acceptance Tests (3 Units) • Product Quality Assurance, Material Supply, Lab Modifications, System Test. 	38K <div style="position: absolute; left: 380px; top: 400px; font-size: 3em;">}</div> (See SIMS-A/IARU Cost Criterion)**	12K
Totals (Excluding Cost/Unit Thereafter and IARU-Shared Expenses)	688K	83K

(Continued)

NOTE

**These items were common to the IARU and SSA or to the SYSTEM, and are reported on one sheet to avoid the confusion of duplication.

SIMS-A (SSA) COST (Continued)

SIMS-A-HR

The contractor declined to provide cost data, on grounds that it might compromise a competitive advantage on several proposal efforts. The contractor indicated that cost information might be available by July 1, 1972, pending resolution of the competitive issues.

HA (Paulson) indicated that the SIMS-A-HR costing would be fairly well represented by the SIMS-A-C cost information. Therefore, see preceding information on SIMS-A-C star sensor cost.

SIMS-A-KI

The contractor indicated a per unit cost of \$30,000 and a non-recurring cost of \$300,000, subject to change with a more definite statement of work. Based on the above statement and the SIMS-A-C star sensor cost breakdown, MIT/CSDL offers an estimate in the table below:

<u>ITEM</u>	<u>SSA</u>	<u>SUNSHIELD</u>
• Fab. Prototype	30K	34K
• Qual. Testing	26K	15K
• Three Flight Systems	100K	22K
• Cost/Unit Thereafter	30K	7K

(Continued)

SIMS-A (SSA) COST (Continued)

SIMS-A-KI (Continued)

<u>ITEM</u>	<u>SSA</u>	<u>SUNSHIELD</u>
• Lab Test Facil:	410K	(See SIMS-A-C/Star Sensor and SIMS-A/IARU Cost Criteria)
• Acceptance Tests (3 Units)	38K	12K
• Product Qual. Assurance, etc.	(See SIMS-A-C/Star Sensor Cost Criterion)	
Totals (Excluding Cost/Unit Thereafter and IARU-Shared Costs for Lab Facilities and System)	604K	83K

SIMS-A (SYSTEM) COST

Refer to subsection 6.2.1.

SIMS-B (IARU) COST

The contractor declined to provide cost data to avoid compromising a competitive advantage, primarily for a subcontractor. NASA GSFC has detailed cost breakdowns for the contractor's PADS systems for the ATS satellites.

SIMS-B (SSA) COST

(See SIMS-B IARU Cost Criterion.)

SIMS-B (SYSTEM) COST

(See SIMS-B IARU Cost Criterion.)

SIMS-D (IARU) COST*

	<u>13-IRIG** VERSION</u>	<u>TGG*** VERSION</u>
1) Engineering Prototype (Qualified)	360K	690K
2) Three Flight Systems (Initial)	825K	1470K
3) Laboratory Test Facility	375K	375K
4) Engineering Support****	<u>830K</u>	<u>830K</u>
Non-Recurring Cost of Prototype and 3 Flight Systems	2390K	3365K
Per Unit (Recurring) Cost Thereafter	210K	380K

Notes

*MIT/CSDL Estimates (23I) based on a 15-instrument purchase, 5 for Prototype and spares, 10 for three Flight Systems and spare.

**Assumes 25K per 13-IRIG instrument.

***Assumes 90K per TGG instrument.

****Includes limited documentation.

SIMS-D (SSA) COST

SIMS-D-HR

The contractor declined to provide cost data, on grounds that it might compromise a competitive advantage on several proposal efforts. The contractor indicated that cost information might be available by July 1, 1972. Pending resolution of the competitive issues.

However, SIMS-A-HR/Star Sensor/Cost criterion is representative.

SIMS-D (SYSTEM) COST

Refer to subsection 6.2.1.

SIMS-A (IARU) ACCURACY (Uses GG-334 Gyros)

<u>ERROR SOURCE</u>	<u>MAGNITUDE (1σ)</u>
Gyro Bias Drift Rate Uncertainty	0.15 deg/hr
Gyro Random Drift Rate (White Noise)	0.01 deg/hr
Gyro Constant Angle Noise (Quantization, etc.) . . .	0.1 arcsec
Gyro Scale Factor Bias Uncertainty	10 PPM
Gyro Scale Factor Noise.	5 PPM
Gyro Input Axis Misalignment Bias Uncertainty. . . .	10 arcsec
Gyro Input Axis Misalignment Noise	5 arcsec

NOTE: The bias errors are assumed to be constant over the SIMS data processing interval but their values have the above initial uncertainties.

SIMS-A (SSA) ACCURACY

SIMS-A-C (CdS Type)

<u>CONTRIBUTOR</u>	<u>ERROR</u>
Attitude Rate Error.	$0.1^{\hat{n}}$ (1σ)
Edge Roughness	$0.02^{\hat{n}}$ (1σ)
Edge Waviness.	$0.6^{\hat{n}}$ (1σ)
Optics Blur Variation With Spectral Class.	$0.2^{\hat{n}}$ (1σ)
CdS Time Constant Per 1% Stability	$0.3^{\hat{n}}$ (1σ)
Noise-Equivalent Angle (at 3.9^M) (Lacking $1/f$ Noise Information).	$1.3^{\hat{n}}$ (1σ)
Uniform Temperature Change From Nominal by $4^{\circ}F$	$0.2^{\hat{n}}$ (Bias)
Temperature Gradient:	
Mounting Flange Located at Meniscus.	$0.3^{\hat{n}}/^{\circ}F$ (Bias)
Mounting Flange Located at Mirror.	$0.07^{\hat{n}}/^{\circ}F$ (Bias)
30° Canted Slit Bias Lag	$0.5^{\hat{n}}$ (Fixed Bias)

RSS of 1σ contributors at 3.9^M with 1% time constant stability
 $1.5^{\hat{n}}$ (1σ).

SIMS-A-HR (Silicon Type)

<u>CONTRIBUTOR</u>	<u>ERROR</u>
Attitude Rate Error.	$0.2^{\hat{n}}$ (1σ)
Edge Roughness	$0.01^{\hat{n}}$ (1σ)
Edge Waviness.	$0.30^{\hat{n}}$ (1σ)
Slit Straightness.	$1.50^{\hat{n}}$ (3σ)

(Continued)

SIMS-A (SSA) ACCURACY (Continued)

SIMS-A-HR (Silicon Type) (Continued)

Optics.	TBD (Assign $0.5''$ (1σ) Unsubstantiated)
Electronic Stability Per $1\% \tau$	$0.01''$
Noise-Equivalent Angle (At 3.5^M)	$0.5''$ (1σ)
Temperature Effects	$0.01''/^{\circ}F$ (MIT, Bias Estimate)
Symmetry Error.	$< 1.0''$ (Fixed Bias)
30° Canted Slit Bias Lag.	$0.8''$ (Fixed Bias)
<hr/>	
RSS of 1σ Contributors at 3.5^M with 1% Time Constant Stability	
$\approx 0.9''$ (1σ)	

SIMS-A-KI (Silicon Type)

<u>CONTRIBUTOR</u>	<u>ERROR</u>
Attitude Rate Error.	$0.2''$ (1σ)
Edge Roughness	$0.01''$ (1σ)
Edge Waviness.	$0.2''$ (1σ)
Slit Straightness.	$1.0''$ (3σ)
Electronic Stability Per $1\% \tau$	$0.01''$ (1σ)
Optics	TBD (Assign $0.5''$, 1σ Unsubstantiated)
Noise-Equivalent Angle (At 3.3^M)	$0.3''$ (1σ)
Temperature Effects.	TBD

(Continued)

SIMS-A (SSA) ACCURACY (Continued)

SIMS-A-KI (Silicon Type) (Continued)

Symmetry Error. $0.4''$ (Bias Variable Over
Range of Stellar Magnitudes)
 30° Canted Slit Bias Lag. $0.2''$ (Fixed Bias)

RSS of 1σ contributors at 3.3^M with 1% time constant stability
and including symmetry error $\cong 0.8''$ (1σ)

SIMS-A (SYSTEM) ACCURACY

The nominal values of the error sources and parameters
used to generate the SIMS-A attitude accuracy results are:

Initial State Uncertainties

Pitch, Roll, Yaw..... 60 arcsec (1σ)
Gyro Bias Drift 0.15 deg/hr (1σ)

Star Mapper

Field of View. 4 degrees

Pointing Direction zenith

Measurement Error:

CDS Star Mapper . . . 1.6 arcsec (1σ)

SIL Star Mapper . . . 1.1 arcsec (1σ)

SIMS-A (SYSTEM) ACCURACY (Continued)

Star Distributions are those identified as typical
for CDS and SIL in subsection 5.2.5.

Detector Magnitude Thresholds:

CDS Star Mapper . . . 4.0

SIL Star Mapper . . . 3.6

Star measurement technique is Original Technique,
identified in subsection 5.3.2.2.1.

IARU (using 3 gyros-type GG334A)

Gyro Random Drift Rate

(White Noise) 0.01 deg/hr (1σ)

Gyro Constant Angle Noise. 0.1 arcsec (1σ)

SIMS-A (SYSTEM) ACCURACY (Continued)

ACCURACY OF ATTITUDE DETERMINATION FOR SIMS-A AND
SENSITIVITY TO VARIATION IN CERTAIN QUANTITIES

Quantity Changed	Extent of Changes	Star Mapper	Data Interval (Orbits)	Attitude Accuracy(1 σ) - arcsec		
				Pitch	Roll	Yaw
Data Interval	1-16 Orbits	SIL	—	0.3	0.5	7.5-2
		CDS	—	0.3	1.6-0.6	15.5-3.9
Mapper Error (1 σ)	0.5 $^{\circ}$ -2.1 $^{\circ}$	SIL	8	0.2-0.4 ↓	0.3-0.8	1.4-5.3
			16		0.3-0.7	1.0-3.8
	0.8 $^{\circ}$ -3.2 $^{\circ}$	CDS	8		0.4-1.0	2.8-10.8
			16		0.4-0.9	2.0-7.8
Mapper FOV	4 $^{\circ}$ -10 $^{\circ}$	SIL	8 ↓	0.3 ↓	0.5	2.7-0.9
		CDS			0.6	5.5-1.5
Magnitude Threshold	3.2 -4.0	SIL			0.5	1.6-1
	3.25-4.75	CDS			0.8-0.6	5.9-3.9
Gyro Random Drift (1 σ)	0.01-0.3 deg/hr	SIL		0.3-0.8	0.5-1.1	2.7-4.1
Gyro Constant Angle Noise (1 σ)	0.01 $^{\circ}$ -0.3 $^{\circ}$	SIL		0.1-0.5	0.3-0.8	2.6-3.0

- Notes: - Performance results taken from subsection 5.4.2.
- Nominal values of error sources and parameters shown on preceeding page and in subsection 5.4.2.

SIMS-B (IARU) ACCURACY (Uses GI-K7G Gyros)

<u>ERROR SOURCE</u>	<u>MAGNITUDE (1σ)</u>
Gyro Bias Drift Rate Uncertainty.	0.15 deg/hr
Gyro Random Drift Rate (White Noise).	0.002 deg/hr
Gyro Constant Angle Noise (Quantization, etc.)	0.1 arcsec
Gyro Scale Factor Bias Uncertainty.	10 PPM
Gyro Scale Factor Noise	5 PPM
Gyro Input Axis Misalignment Bias Uncertainty	10 arcsec
Gyro Input Axis Misalignment Noise.	5 arcsec

NOTE: The bias errors are assumed to be constant over the SIMS data processing interval but their values have the above initial uncertainties.

SIMS-B (SSA) ACCURACY

Star Sensor Unit Bias Uncertainty:	$< 1.5^{\circ}$ (1 σ)
Electronic Noise-Equivalent Angle: [at 3.5 ^M (S-20)]	$< 1.5^{\circ}$ (1 σ)
Gimbal Thermo-Mechanical Stability:	
Outer Gimbal	$< 0.5^{\circ}$ (1 σ)
Inner Gimbal	$< 0.5^{\circ}$ (1 σ)
Gimbal Encoder Uncertainty:	
Outer Gimbal	$< 1.0^{\circ}$ (1 σ)
Inner Gimbal	$< 1.0^{\circ}$ (1 σ)
RSS:	$< 2.4^{\circ}$ (1 σ)/Axis

SIMS-B (SYSTEM) ACCURACY

The nominal values of the error sources and parameters used to generate the SIMS-B attitude accuracy results are:

Initial State Uncertainties

Pitch, Roll, Yaw	60 arcsec (1σ)
Gyro Bias Drift.	0.15 deg/hr (1σ)

Star Tracker

Gimbal Angle Limits:

Outer (Roll)	± 45 degrees
Inner (Pitch)	± 15 degrees
Zero Gimbal Pointing Direction . .	Zenith

Measurement Error:

Outer Gimbal.	1.2 arcsec (1σ)
Inner Gimbal.	1.2 " "
Alpha Angle	1.5 " "
Beta Angle.	1.5 " "

Star Distribution — star selected every 20 degrees
of orbital motion for orbit of 7/1/72

Detector Magnitude Threshold . . . 3.5

(S-20)

IARU (using 3 gyros-type GI-K7G)

Gyro Random Drift (White Noise) . .	0.002 deg/hr (1σ)
Gyro Constant Angle Noise.	0.1 arcsec (1σ)

SIMS-B (SYSTEM) ACCURACY (Continued)

ACCURACY OF ATTITUDE DETERMINATION FOR SIMS-B
AND SENSITIVITY TO VARIATION IN CERTAIN QUANTITIES.

Quantity Changed	Extent of Change	Data Interval (Orbits)	Attitude Accuracy(1 σ) -arcsec		
			Pitch	Roll	Yaw
Data Interval	1-12 orbits	—	0.6-0.3	0.7-0.4	1.0-0.4
Star Update Interval	8°-40°	8	0.3-0.4	0.4	0.4-0.5
Star Tracker Error (1 σ) (See Notes)	0.25-2.0 (Relative to Nominal)	8	0.2-0.5	0.2-0.6	0.2-0.8
Tracker Outer Gimbal Limit	$\pm 15^\circ$ - $\pm 45^\circ$	8	0.3	0.4	0.9-0.4
Gyro Random Drift (1 σ)	0.002-0.3 deg/hr	4	0.4-1.3	0.4-1.2	0.5-1.4
Gyro Constant Angle Noise (1 σ)	0.01" - 0.4"	8	0.2-0.7	0.2-0.7	0.3-0.8

- Notes:
- Performance results taken from subsection 5.4.3
 - Nominal values of error sources and parameters shown on preceding page and in subsection 5.4.3
 - Above results for tracker error are for simultaneous variation in one sigma values of all four tracker measurement errors.

SIMS-D (IARU) ACCURACY

GYRO (Type TGG)*:

	<u>MAGNITUDE (1σ)</u>
Bias Drift Rate Uncertainty**	0.03 deg/hr
Random Drift Rate (2 noise models presently assumed)	
- One model produces the following angle error where t is time	$10^{-5}t$ arcsec
- The other model is a white noise.	0.00015 deg/hr
Constant Angle Noise	0.01 arcsec

GIMBALS:

	<u>MAGNITUDE (1σ) - arcsec</u>		
	<u>IGA</u>	<u>MGA</u>	<u>OGA</u>
Servo Error (Noise)	0.85	0.85	0.85
Readout Error Over 360 $^{\circ}$ (Noise)	2.0	--	--
Readout Error Over $\pm 5^{\circ}$ (Noise)	--	1.0	1.0
IGA to MGA Orthogonality Uncertainty**	--	1.0	1.0
MGA to OGA Orthogonality Uncertainty**	--	--	1.0

* No equivalent error model information available for the 13-IRIG at time of publication.

** The gyro bias drift rate is assumed to be constant over the SIMS data processing interval but its value has the above initial uncertainty. The uncertainties in gimbal orthogonality are those after system flight calibration.

SIMS-D (SSA) ACCURACY

Use SIMS-A-HR. [See SIMS-A (SSA) ACCURACY.]

SIMS-D (SYSTEM) ACCURACY

The nominal values of the error sources and parameters used to generate the SIMS-D attitude accuracy results are:

Initial State Uncertainties

Pitch, Roll, Yaw.	60 arcsec (1σ)
Gyro Bias Drift	0.03 deg/hr (1σ)

SIL Star Mapper

Field-Of-View	4 degrees
Pointing Direction.	Zenith
Measurement Error	1.1 arcsec (1σ)
Star Distribution is that identified as typical for SIL in subsection 5.2.5	
Detector Magnitude Threshold. .	3.6
Star Measurement Technique is Original Technique identified in subsection 5.3.4.2.1	

IARU (using 3 gyros-type TGG)

Gyro Random Drift is modeled so that resulting variance in angle is $10^{-10} t^2 \text{ arcsec}^2$.	
Gyro Constant Angle Noise . . .	0.01 arcsec (1σ)
Random Error of IARU Gimbals:	
Middle, Outer.	1.3 arcsec (1σ)
Inner.	2.2 arcsec (1σ)

(Continued)

SIMS-D (SYSTEM) ACCURACY (Continued)

ACCURACY OF ATTITUDE DETERMINATION FOR SIMS-D
AND SENSITIVITY TO VARIATION IN CERTAIN QUANTITIES

Quantity Changed	Extent of Change	Attitude Accuracy(1 σ)-arcsec		
		Pitch	Roll	Yaw
Data Interval	1-16 orbits	0.4-0.1	1.3-0.3	1.3-0.3
Mapper Error (1 σ)	0.5 $^{\circ}$ -2.1 $^{\circ}$	0.2	0.6-0.8	0.6-0.8
Mapper FOV	4 $^{\circ}$ -10 $^{\circ}$	0.2-0.1	0.7-0.4	0.7-0.4
Magnitude Threshold	3.2-4.0	0.2	0.8-0.5	0.7-0.5
Gyro Random Drift (As Modeled for TGG)	1-150 times nominal sigma	0.2-0.7	0.7-1.3	0.7-1.4
Gyro Random Drift (1 σ) (White Noise Model)	0.01-0.3 deg/hr	0.2-1.0	0.7-1.8	0.7-2.2
Gyro Constant Angle Noise (1 σ)	0.01 $^{\circ}$ -0.3 $^{\circ}$	0.2-0.6	0.7-1.2	0.7-1.2
IARU Gimbal Error (1 σ) (See Notes)	0.5-2.0 (Relative to Nominal)	0.1-0.4	0.4-1.2	0.4-1.2

Notes:

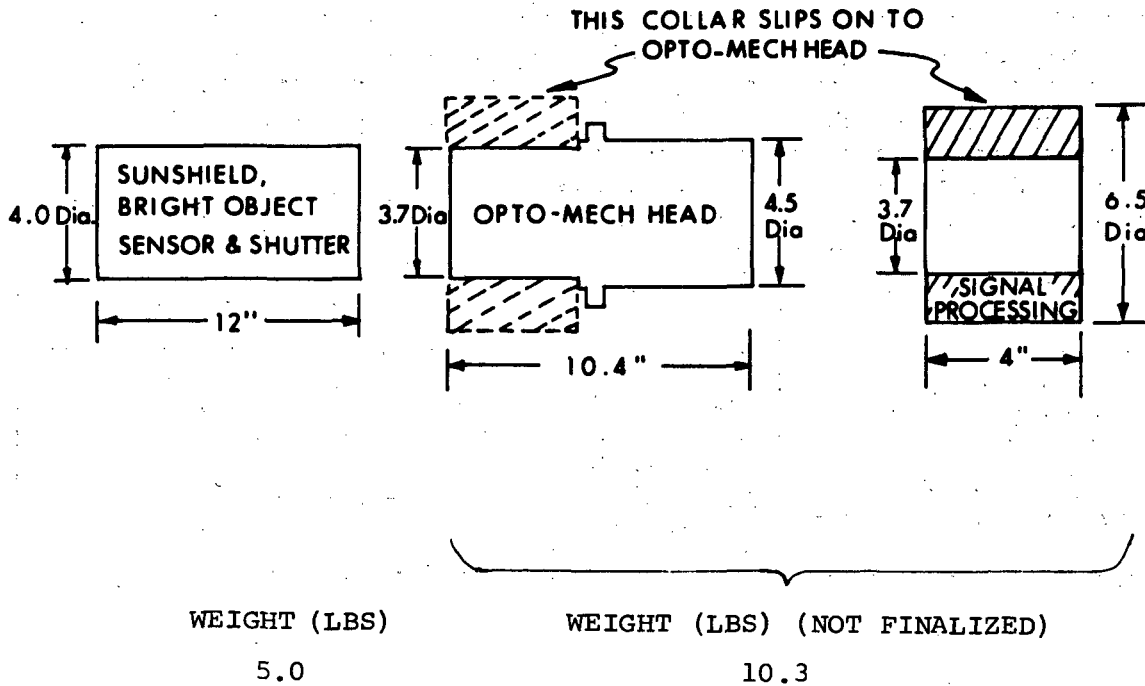
- Performance results taken from subsection 5.4.4
- Nominal values of error sources and parameters shown on preceding page and in subsection 5.4.4
- Above results for IARU gimbal error are for simultaneous variation in one sigma values of all three gimbal angle errors.
- Unless otherwise indicated the above results are for a data interval of 4 orbits.

SIMS-A (IARU) WEIGHT

16 lbs for IARU with 3 13-IRIGs (Letter Data)

SIMS-A (SSA) WEIGHT

Earlier SPARS-like Star Mapper (SPARS PHASE IB) with
4° Field-Of-View; CdS Photodetector



TOTALS: 15 LBS

365 CUBIC INCHES

NOT FINALIZED BY HA

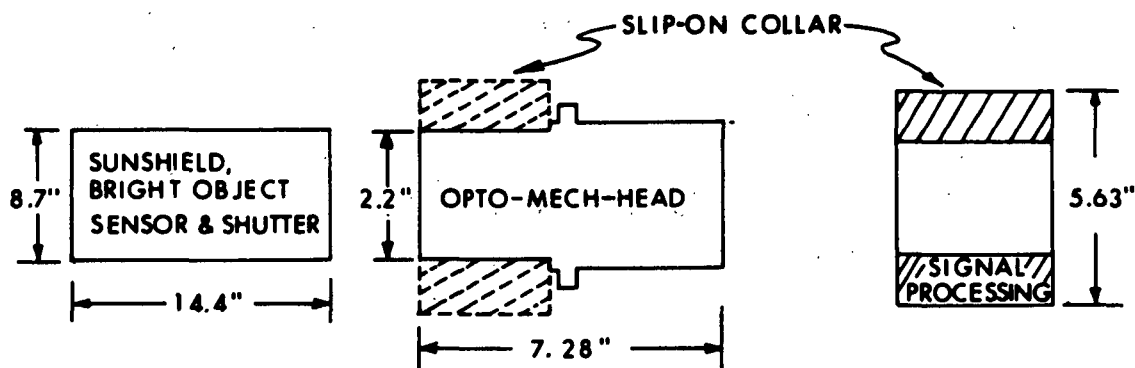
This was a
laboratory
item only.

(Continued)

SIMS-A (SSA) WEIGHT (Continued)

Latest SPARS-like Star Mapper (PARS) with 10° Field-Of-View; CdS Photodetector.

SIMS-A-C



WEIGHT (LBS)	WEIGHT (LBS)	WEIGHT (LBS)
2.74 SUNSHIELD	4.0	
.97 BRIGHT OBJECT SENSOR, SOLENOID, FLAPPER VALVE AND MISC. HDWARE		

TOTALS: 7.7 POUNDS

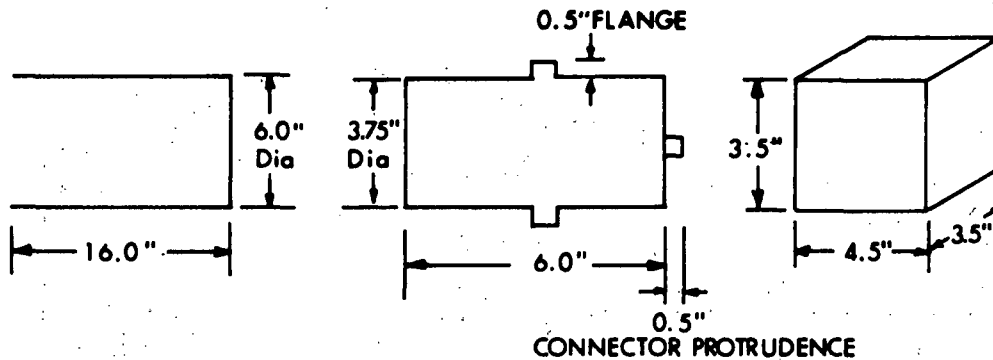
940. CUBIC INCHES

(MIT/CSDL
Estimate)

(Continued)

SIMS-A (SSA) WEIGHT (Continued)

SIMS-A-HR (Silicon Star Mapper for PARS)



WEIGHT (LBS)

1.25

WEIGHT (LBS)

3.0

WEIGHT (LBS)

0.6 ELECTRONICS

~1.0 *HOUSING AND
CONNECTORS

TOTALS: ~5.9 LBS

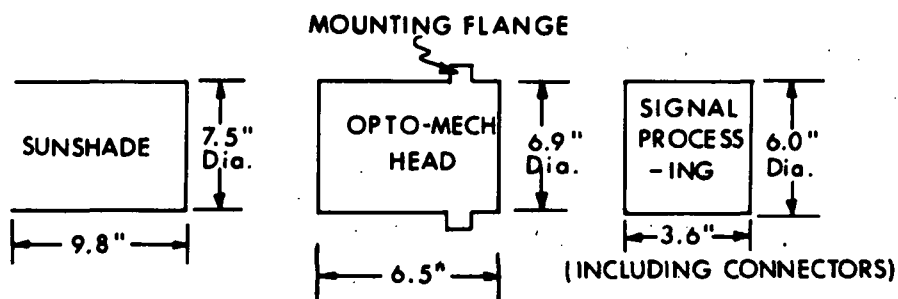
574 CUBIC INCHES*

(Continued)

* Data not available, therefore MIT estimate.

SIMS-A (SSA) WEIGHT (Continued)

SIMS-A-KI (Silicon Star Mapper)



WEIGHT (LBS)

1.4

WEIGHT (LBS)

2.32 Front Lens
 1.97 Mangin Mirror
 .06 Corrector Lens
 .30 Tube (Be)
 2.18 Detector Supp.
 Ass'y
 1.87 Corrector Supp.
 Ass'y

WEIGHT (LBS)

1.1 Electronics
 1.2 End Cover and
 Connectors

1.4

8.70

2.3

Sub-Totals: 11.0 LBS

375 CUBIC INCHES

Totals: 12.4 LBS

810.0 CUBIC INCHES

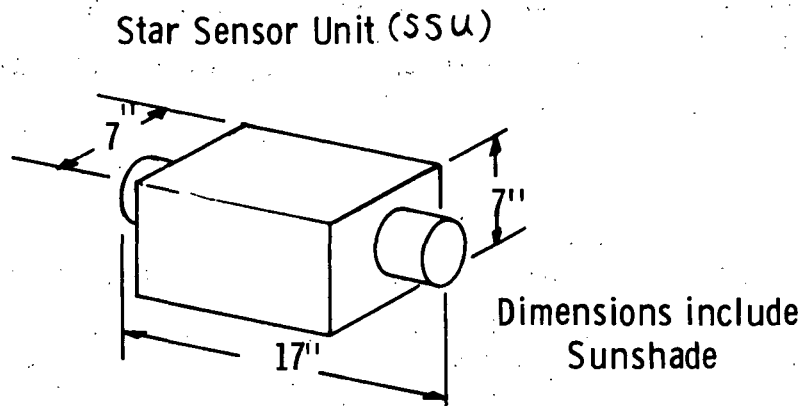
SIMS-A (SYSTEM) WEIGHT

Refer to subsection 6.2.3 and to preceding data on sub-system weights.

SIMS-B (IARU) WEIGHT

No information available.

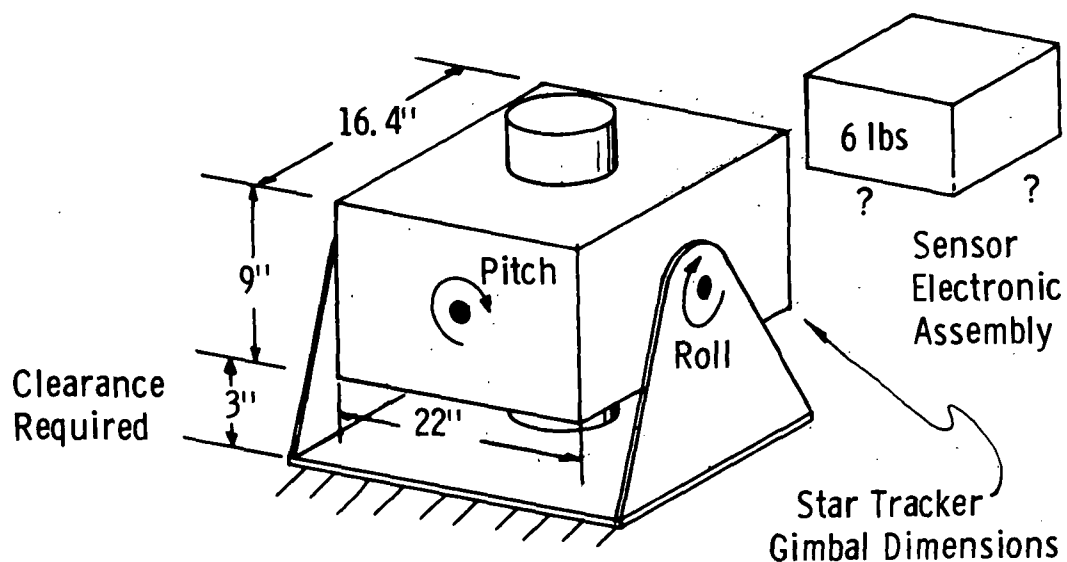
SIMS-B (SSA) WEIGHT



WEIGHT: 16 LBS (Includes Sunshade)

(Continued)

SIMS-B (SSA) WEIGHT (Continued)



WEIGHT: 25 LBS

TOTAL SSA WEIGHT: SEA + STG + SSU = 47 LBS

SIMS-B (SYSTEM) WEIGHT

Refer to subsection 6.2.3 and to preceding data on subsystem weights.

SIMS-D (IARU) WEIGHT

Approximately 15 lbs (13-IRIG Version).

SIMS-D (SSA) WEIGHT

Refer to SIMS-A-HR [See SIMS-A (SSA) WEIGHT]

SIMS-D (SYSTEM) WEIGHT

Refer to subsection 6.2.3 and to preceding data on subsystem weights.

SIMS-A (IARU) POWER (and Size)

Power

IARU (Including ITU) - 35 Watts* from S/C 28V (3 13-IRIGs)

Size

MIT/DL Estimates IARU as 6 inch cube ($\approx 220 \text{ in}^3$) (3 13-IRIGs)

Notes

Source - Letter data (see ref. 153)

* Assume operation in stable ambient temperature environment.

SIMS-A (SSA) POWER

SIMS-A-C

Latest SPARS-like Star Mapper (PARS) with 10° FOV CdS Photodetector

<u>+15 \pm 0.5 VDC</u>	1.65 WATTS
<u>-15 \pm 0.5 VDC</u>	1.28 WATTS
<u>+ 5 \pm 0.25 VDC</u>	0.37 WATTS

SUBTOTAL	3.30 WATTS
----------	------------

+28 \pm 0.5 VDC

Sunshutter Actuation for 400 Milliseconds	10.00 WATTS
---	-------------

Sunshutter Holding	3.00 WATTS
-----------------------	------------

SIMS-A-HR

+15 \pm 0.5 VDC

Into Opto-Mech Head	0.15 WATT
Into Electronic Processing	1.08 WATTS
	<u>1.23 WATTS</u>

SIMS-A (SSA) POWER (Continued)

SIMS-A-HR (Continued)

-15 ± 0.5 VDC

Into Opto-Mech Head	0.15 WATT
Into Electronic Processing	1.35 WATTS
	<u>1.50 WATTS</u>

+ 5 ± 0.25 VDC

Electronic Processing	0.30 WATT
-----------------------	-----------

Total Power* 3.03 WATTS

*Qualification: Output sufficient to drive three low-powered TTL inputs. Output not quite sufficient to drive one high-powered TTL input. Need to add:

+15 ± 0.5 VDC	0.00 WATT
-15 ± 0.5 VDC	0.45 WATT
+ 5 ± 0.25 VDC	0.09 WATT
	<u>0.54 WATT</u>

Therefore:

3.03 + 0.54 = 3.57 watts with high-powered TTL.

SIMS-A-KI

+15 ± 0.5 VDC

Preamplifiers	.054 WATT
Postamplifiers - Threshold Detectors	.029 WATT
	<u>.083 WATT</u>

SIMS-A (SSA) POWER (Continued)

SIMS-A-KI (Continued)

-15 \pm 0.5 VDC

Preamplifiers	.054 WATT
Postamplifiers -	
Threshold Detectors	.058 WATT
	<u>.112 WATT</u>

+ 5 \pm 0.5 VDC

Postamplifiers -	
Threshold Detectors	.150 WATT
Logic	2.610 WATTS
	<u>2.760 WATTS</u>

Total Power Dissipation 2.96 WATTS

Electrical Interface

+15 VDC	+5 VDC
-15 VDC	5 VDC RETURN
-15 VDC RETURN	CHASSIS GROUND

SIMS-A (SYSTEM) POWER

Refer to subsection 6.2.4 and to preceding data on sub-system power.

SIMS-B (IARU) POWER

No information available.

SIMS-B (SSA) POWER

Star Tracker Gimbals:		<u>Interface</u>
Preamps	1.4 WATTS	} +15 v -15 v + 5 v GND
Encoders (and thermal simulators)	16.0 WATTS	
Motors (1.5 watts nominal each)	6.0 WATTS	
		-20 v
Star Sensor Unit	3.0 WATTS	} +15 \pm 1% v -15 \pm 1% v + 5 \pm 5% v
SEA	Included in STG and SSU	
TOTAL		<u>26.4 WATTS</u>

SIMS-B (SYSTEM) POWER

Refer to subsection 6.2.4 and to preceding data on sub-system power.

SIMS-D (IARU) POWER

3-TGGs: Refer to Figs. 3-6 and 3-7, and to Table 3-7, in Ref. 141.

3 13-IRIGs: Refer to Figs. 3-3 and 3-4, and to Table 3-2, in this report.

SIMS-D (SSA) POWER

Refer to SIMS-A-HR candidate, under SIMS-A (SSA) Power Criterion.

SIMS-D (SYSTEM) POWER

Refer to subsection 6.2.4, and to preceding data on sub-system power.

SIMS-A (SYSTEM) TELEMETRY REQUIREMENT

Refer to subsection 6.2.5.1.

SIMS-B (SYSTEM) TELEMETRY REQUIREMENT

Refer to subsection 6.2.5.2.

SIMS-D (SYSTEM) TELEMETRY REQUIREMENT

Refer to subsection 6.2.5.3.

SIMS-A (SYSTEM)* TOTAL UNOBSTRUCTED FIELD-OF-VIEW REQUIREMENT

SIMS-A-C

Total Unobstructed FOV	10°	Swath Width ⁽¹⁾
Sunshield Design Angle	30°	Cone Half Angle ⁽²⁾
Earth Horizon and Spacecraft Structure Limitations (i.e., primarily reflected and scattered sunlight)	15°	Cone Half Angle (Can be zenith-mounted on the aft bay or tower)

NOTES

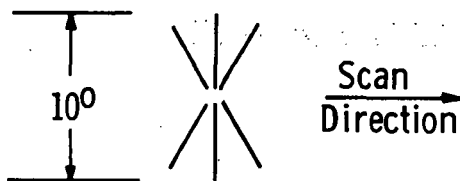
- (1) The central photodetector slits extend a total of 10° and scan out a swath of the celestial sphere of

(Continued)

* Actually, SSA. The single presentation is listed as at System level. Additional discussion at System level is found in subsection 6.2.6, as indicated on Page A-2.

SIMS-A-C (Continued)NOTES (Continued)

$10^\circ \times 360^\circ \cos$ (Orbital Offset Angle) due to the spacecraft orbital pitch rate.



- (2) Can mount on sensor bay pointing at zenith for 9:00 AM and twilight orbits; although an offset from the orbit plane of 10° or 15° opposite the sun will provide added insurance against sun scatter, it must be determined from system simulations how this affects the third axis accuracy problem. For a noon orbit, one sensor can either be mounted on the sensor bay offset 36° from the orbit plane, or two sensors used in the orbit plane, one zenith-pointing and the other depressed 70° aft.

SIMS-A-HR

Total Unobstructed FOV	10° Swath Width ⁽¹⁾
Sunshield Design Angle	30° Cone Half Angle ⁽²⁾

NOTES

- (1) Same as for SIMS-A-C, Note (1).
(2) Same as for SIMS-A-C, Note (2).

SIMS-A (SYSTEM)TOTAL UNOBSTRUCTED FIELD-OF-VIEW
REQUIREMENT (Continued)SIMS-A-HR (Continued)

Earth Horizon and Spacecraft
Structure Limitations (i.e.,
primarily reflected and
scattered sunlight)

15° Cone Half Angle
(Can be zenith-
mounted on the
aft bay or tower)

SIMS-A-KI

Total Unobstructed FOV

6° Swath Width⁽¹⁾

Sunshield Design Angle

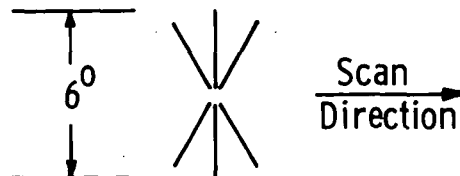
30° Cone Half Angle⁽²⁾

Earth Horizon and Spacecraft
Structure Limitations (i.e.,
primarily reflected and
scattered sunlight)

15° Cone Half Angle
(Can be zenith-
mounted on the aft
bay or tower)

NOTES

- (1) The central photodetector slits extend a total of 6° and scan out a swath of the celestial sphere of 6° X 360° cos(Orbital Offset Angle) due to the spacecraft orbital pitch rate.



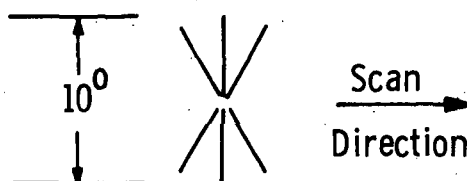
- (2) Same as for SIMS-A-C, Note (2).

SIMS-B (SYSTEM) TOTAL UNOBSTRUCTED FIELD-OF-VIEW REQUIREMENT

$\pm 45^{\circ}$ ROLL (Outer Gimbal)

$\pm 15^{\circ}$ PITCH (Inner Gimbal)

No spacecraft interference if mounted on top of aft sensor bay with nominal boresight pitched 15° aft.



Sunshield Design Angle: 45°

Earth Limb: 15°

Bright Object: 15°

SIMS-D (SYSTEM) TOTAL UNOBSTRUCTED FIELD-OF-VIEW REQUIREMENT

Refer to SIMS-A-HR candidate, under SIMS-A (SYSTEM) Total Unobstructed Field-Of-View Criterion.

SIMS-A (IARU) SIMPLICITY OF DESIGN, AND RELIABILITY

GENERAL

- 1) The only severe mechanical build requirements are relative alignment and orthogonality of gyro axes.
- 2) The strapdown mechanization is more amenable to various redundancy requirements to attain the desired system reliability.

PRESENT SPARS TECHNOLOGY PERFORMANCE REQUIREMENTS

Orbital Constraints:

Rate	155 to 260 Deg./Hr.
Coord. Frame	Local Vertical
Vehicle Attitude	± 1 Deg. Per Axis
Inclination	All Angles

Warmup and Acquisition:

Warmup	30 Minutes
Acquisition	One Orbit After Initiation (Reqd.)
	$\frac{1}{2}$ Orbit After Initiation (Goal)

Orbital Performance: (30°F to 100°F)

Three Axis Error	N.A.	See pp. A-10 to A-14 for error models used in simulations.
Star Detection	N.A.	
Over Celestial Sphere	450 Stars Min.	
Over Any Orbital Revolution	8 Stars Min.	

Reliability: 0.9526 for 30-Day Mission.

SIMS-A (SSA) SIMPLICITY OF DESIGN, AND RELIABILITY

SIMS-A-C

1. No moving parts, therefore mechanically much greater reliability than a tracker.
2. No high voltage requiring special fabrication and insulation.
3. More sensitive to external electromagnetic interference at pre-amp input than a PMT tracker.
4. Less sensitive to static external electric and magnetic fields than a PMT tracker.
5. Curved focal plane and low f/No. impose more severe tolerances on fabrication and structural support relative to HR and KI mapper optics.
6. Probability of success = 0.999998/slit for a 2-year mission, according to HA.
7. No special search and acquisition modes.
8. Signal processing less complex than for a tracker, and comparable to other star mappers examined (i.e., HR and KI).

SIMS-A-HR

1. Same comments as for SIMS-A-C, Note 1.
2. " " " " " " , Note 2.

SIMS-A (SSA) SIMPLICITY OF DESIGN, AND RELIABILITY (Continued)

SIMS-A-HR (Continued)

3. Same comments as for SIMS-A-C, Note 3.
4. " " " " " " ", Note 4.
5. Optics theoretically the most stable, mechanically and thermally, per pound of supporting structure, of any of the mapper optics examined. A single solid quartz element contains all of the optical power.
6. Estimate probability of success = 0.99 per any four slits for 3 years.
7. Same comments as for SIMS-A-C, Note 7.
8. " " " " " " ", Note 8.

SIMS-A-KI

1. Same comments as for SIMS-A-C, Note 1.
2. " " " " " " ", Note 2.
3. " " " " " " ", Note 3.
4. " " " " " " ", Note 4.
5. Optics mechanical and thermal stability judged intermediate between the HR and HA mapper optics.
6. KI estimates a failure rate of 4.493 failures per 10^6 hours

SIMS-A (SSA) SIMPLICITY OF DESIGN, AND RELIABILITY (Continued)

SIMS-A-KI (Continued)

7. Same comments as for SIMS-A-C, Note 7.

8. " " " " " " , Note 8.

SIMS-A (SYSTEM) SIMPLICITY OF DESIGN, AND RELIABILITY

Refer to subsection 6.2.7.

SIMS-B (IARU) SIMPLICITY OF DESIGN, AND RELIABILITY

Comments included under SIMS-A (IARU) for this criterion are generally applicable here.

SIMS-B (SSA) SIMPLICITY OF DESIGN, AND RELIABILITY

The star Tracker Assembly is a state-of-the-art system; its design is not overly-conservative requiring the utmost in mechanical and thermal stability. It is probably as simple and reliable a tracker as can be achieved with these severe accuracy and stability requirements.

SIMS-B (SYSTEM) SIMPLICITY OF DESIGN, AND RELIABILITY

Refer to subsection 6.2.7.

SIMS-D (IARU) SIMPLICITY OF DESIGN, AND RELIABILITY

GENERAL

1. Years of experience in this technology.
2. No special alignment requirements for sensors, and prelaunch sensor calibrations are readily available.
3. Gyro design . . . The 13-IRIG was specifically designed with simplicity and reliability as the driving criteria.

SIMS-D (SSA) SIMPLICITY OF DESIGN, AND RELIABILITY

SIMS-D-HR

Same comments apply as for SIMS-A-HR SSA, for this criterion.

SIMS-D (SYSTEM) SIMPLICITY OF DESIGN, AND RELIABILITY

Refer to subsection 6.2.7.

SIMS-A (SYSTEM) MODULARITY OF DESIGN, AND GROWTH POTENTIAL

Refer to subsection 6.2.8.

SIMS-B (SYSTEM) MODULARITY OF DESIGN, AND GROWTH POTENTIAL

Refer to subsection 6.2.8.

SIMS-D (SYSTEM) MODULARITY OF DESIGN, AND GROWTH POTENTIAL

Refer to subsection 6.2.8.

SIMS-A (IARU) COST OF GSE

Laboratory Test Facility 400K [from SIMS-A (IARU) Cost Criterion]

SIMS-A (SSA) COST OF GSE

SIMS-A-C

No launch pad GSE required, except for a theodolite for alignment during mounting on spacecraft.

SIMS-A-HR

(Same as for SIMS-A-C)

SIMS-A-KI

(Same as for SIMS-A-C)

SIMS-A (SYSTEM) COST OF GSE

Refer to subsection 6.2.9.

SIMS-B (IARU) COST OF GSE

Same as for SIMS-A. [Refer to SIMS-A (IARU) COST OF GSE]

SIMS-B (SSA) COST OF GSE

[Refer to SIMS-B (SSA) COST]

SIMS-B (SYSTEM) COST OF GSE

Refer to subsection 6.2.9.

SIMS-D (IARU) COST OF GSE

Position Table and Theodolites for Alignment and Orthogonality Calibration	25K
Mini-Computer for Instrument Calibrations	150K
Miscellaneous	130K
Total	305 K

SIMS-D (SSA) COST OF GSE

[Refer to SIMS-A (SSA) COST OF GSE; same as for SIMS-A-C]

SIMS-D (SYSTEM) COST OF GSE

Refer to subsection 6.2.9.

SIMS-A (IARU) COMPLEXITY OF GROUND CONTROL/COMMAND/DATA
PROCESSING OPERATIONS

Possible IARU Interface Requirement:

- A) Individual instrument on/off switch
- B) Individual wheel synch detectors
- C) Commandable back up power control
- D) Individual instrument $\Delta\theta$ accumulator register
output interface

SIMS-A-(IARU) COMPLEXITY OF GROUND CONTROL/COMMAND/DATA
PROCESSING OPERATIONS (Continued)

Possible IARU Interface Requirement (Continued):

- E) Boost/orbit moding capability
- *F) Star sensor test signals

SIMS-A (SSA) COMPLEXITY OF GROUND CONTROL/COMMAND/DATA
PROCESSING OPERATIONS

SIMS-A {
 -C
 -HR
 -KI

No Ground Control/Command required. Could include an SSA Power ON/OFF command, but no on-board computer required for SSA data processing operations.

SIMS-A (SYSTEM) COMPLEXITY OF GROUND CONTROL/COMMAND/DATA
PROCESSING OPERATIONS

Refer to subsection 6.2.10.

SIMS-B (IARU) COMPLEXITY OF GROUND CONTROL/COMMAND/DATA
PROCESSING OPERATIONS

No information available

* ITU (for entire SIMS-A) is part of the IARU package.

Letter data, see ref 153.

No ground control/command required. Could include an IARU Power ON/OFF Command, but no on-board computer required for IARU data processing operations. (Assumes attitude algorithm is updated on ground.)

SIMS-B (SSA) COMPLEXITY OF GROUND CONTROL/COMMAND/DATA
PROCESSING OPERATIONS

No information available.

SIMS-B (SYSTEM) COMPLEXITY OF GROUND CONTROL/COMMAND/DATA
PROCESSING OPERATIONS

Refer to subsection 6.2.10.

SIMS-D (IARU) COMPLEXITY OF GROUND CONTROL/COMMAND/DATA
PROCESSING OPERATIONS

Uplink

- (1) power on/off
- (2) power high-low
- (3) Re-initial (cage)/uncage
- (4) spares (5 signals)

Downlink

- (1) 3-axis Digitized Resolver Readouts
 - (2) 3-axis Analog Resolver Outputs
 - (3) 4 temperature readouts
 - (4) 6 miscellaneous electronic readouts
 - (5) 1 alarm/fail indication signal
-

Processing

All on the ground

SIMS-D (SSA) COMPLEXITY OF GROUND CONTROL/COMMAND/DATA
PROCESSING OPERATIONS

Same as for SIMS-A. [Refer to SIMS-A (SSA) COMPLEXITY
OF. . . etc.]

SIMS-D (SYSTEM)

COMPLEXITY OF GROUND CONTROL/COMMAND/DATA
PROCESSING OPERATIONS

Refer to subsection 6.2.10.

SIMS-A (IARU)

AVAILABILITY

Estimated time for build of the engineering prototype and the first three flight IARU models is 20 months from go-ahead.

Letter Data, ref 153.

13 IRIGs are in production

Electronic designs require modifications

SIMS-A (SSA)

AVAILABILITY

SIMS-A-C

10° FOV CdS SSA will be fabricated and flown by 5/1/73.

SIMS-A-(SPARS-LIKE)

4° FOV CdS SSA is fabricated, has completed lab testing, and will be flown in 2nd quarter of 1972.

SIMS-A-HR

10° FOV Silicon SSA will be fabricated by 12/72.

SIMS-A (SSA) AVAILABILITY (Continued)

SIMS-A-KI

To be determined

SIMS-A (SYSTEM) AVAILABILITY

Refer to subsection 6.2.11.

SIMS-B (IARU) AVAILABILITY

No information available.

SIMS-B (SSA) AVAILABILITY

Engineering model now in final assembly, and will be tested by July 1, 1972. Flight hardware can be available in 12 to 15 months after receipt of order.

SIMS-B (SYSTEM) AVAILABILITY

Refer to subsection 6.2.11.

SIMS-D (IARU) AVAILABILITY

First flight system two years from go-ahead.

SIMS-D (SSA) AVAILABILITY

SIMS-D-HR

Same as for SIMS-A-HR. [Refer to SIMS-A (SSA) AVAILABILITY,
under SIMS-A-HR.]

SIMS-D (SYSTEM) AVAILABILITY

Refer to subsection 6.2.11.

APPENDIX B*

REVISED CATALOG OF STARS OF MAGNITUDE 4.0 OR BRIGHTER AS SEEN BY ONE OR MORE DETECTORS

COLUMN HEADING	DESCRIPTION
YBS#	The Yale Bright Star Catalog number. A "D" following the number indicates that the star is a component of a double and satisfies the double-star criterion.
NAME	Generally the Bayer or Flamsteed designation taken from the Yale Bright Star Catalog. A numeral following a Greek letter is a superscript.
RA	The right ascension for 1975, interpolated linearly from the values given for the years 1900 and 2000 in the Y.B.S. Catalog.
DEC	The declination for 1975, interpolated as above.
S20	The S-20 detector magnitude
CdS	The cadmium sulfide detector magnitude.
SIL	The silicon detector magnitude
S	Source. If S=0, detector magnitudes are computed from the color index versus spectral type function =1, det. mags. are computed from UBVRIJKL photometry 2, det mags. are computed from 13-color photometry
VIS	Visual magnitude
SP.TYPE	Spectral type, taken from the Y.B.S. catalog

* This appendix supersedes Appendix B of Ref. 141.

YBS#	NAME	RA	DEC	S20	CDS	SIL	S	VIS	SP.TYPE
15D	ALF AND	0.12	28.95	1.80	1.87	2.07	2	2.07	R8 III
21D	BET CAS	0.13	59.01	2.54	2.53	2.08	2	2.27	F2 IV
25	EPS PHE	0.14	-45.89	4.69	4.64	3.38	2	3.88	K0 III
39	GAM PEG	0.20	15.05	2.27	2.40	2.85	2	2.83	B2 IV
45	CHI PEG	0.22	20.06	5.76	5.78	3.49	2	4.81	M2 III
46D		0.22	-7.92	5.95	6.06	3.27	0	5.13	M3 III
48	7 CET	0.22	-19.07	5.46	5.50	3.16	2	4.49	M1 III
74	IOT CET	0.30	-8.97	4.46	4.41	2.93	2	3.56	K2 III
77	ZET TUC	0.31	-65.03	4.64	4.65	3.89	2	4.23	G2 V
85	T CET	0.34	-20.20	5.63	5.82	2.61	0	5.00	M5 II
98	BET HYI	0.41	-77.39	3.27	3.26	2.48	2	2.80	G2 IV
100	KAP PHE	0.42	-43.82	4.12	4.11	3.88	2	3.94	A7 V
103	47 PSC	0.45	17.75	5.52	5.63	2.84	0	4.70	M3 III
105	ETA SCL	0.44	-33.15	5.75	5.81	3.22	2	4.81	M4 III
130	KAP CAS	0.53	62.80	3.95	4.06	4.07	2	4.17	B1 I
153	ZET CAS	0.59	53.76	3.20	3.32	3.73	2	3.71	B2 V
163	EPS AND	0.62	29.18	5.01	4.98	3.86	2	4.35	G8 III
165D	DEL AND	0.63	30.73	4.24	4.20	2.59	2	3.30	K3 III
168D	ALF CAS	0.65	56.40	3.13	3.08	1.67	2	2.24	K0 II
188	BET CET	0.71	-18.12	2.90	2.85	1.56	2	2.09	K1 III
211	57 PSC	0.75	15.35	6.09	6.24	3.24	0	5.36	M4
215D	ZET AND	0.77	24.13	4.97	4.94	3.50	2	4.14	K1 II
219D	ETA CAS	0.79	57.68	3.82	3.82	3.10	2	3.44	G0 V
224	DEL PSC	0.79	7.45	5.44	5.44	3.48	2	4.47	K5 III
248	20 CET	0.86	-1.27	5.75	5.76	3.71	2	4.77	M0 III
257		0.88	-63.00	6.27	6.46	3.25	0	5.64	M5
259		0.90	24.43	6.53	6.82	3.22	0	6.19	M7
264D	GAM CAS	0.92	60.58	1.72	1.88	2.15	2	2.27	R0 IV
269D	MU AND	0.92	38.36	4.01	3.99	3.83	2	3.88	A5 V
271	ETA AND	0.93	23.28	5.12	5.08	3.92	2	4.40	G8 III
280	ALF SCL	0.96	-29.50	3.96	4.03	4.26	1	4.32	B8 III
285		1.09	86.12	5.16	5.10	3.60	2	4.24	K2 III
294	EPS PSC	1.03	7.75	5.02	4.98	3.74	2	4.28	K0 III
334	ETA CET	1.12	-10.32	4.34	4.29	2.85	2	3.46	K3 III
337D	BET AND	1.14	35.48	3.07	3.09	0.91	2	2.10	M0 III
338D	ZET PHE	1.12	-55.38	3.97	3.94	3.97	1	4.09	B6 V
352	TAU PSC	1.17	29.97	5.35	5.30	3.95	2	4.51	K0 III
402D	THE CET	1.38	-8.31	4.47	4.42	3.10	2	3.65	K0 III
403	DEL CAS	1.40	60.10	2.79	2.77	2.59	2	2.65	A5 V
424D	ALF UMI	2.23	89.13	2.45	2.42	1.67	2	1.96	F8 I
429	GAM PHE	1.45	-43.45	4.42	4.43	2.37	2	3.41	K5 II
434	MU PSC	1.48	6.02	5.81	5.79	4.00	2	4.86	K4 III
437D	ETA PSC	1.50	15.22	4.37	4.33	3.14	2	3.62	G8 III
440	DEL PHE	1.50	-49.21	4.71	4.67	3.44	2	3.95	K0 III
458	UPS AND	1.59	41.27	4.45	4.45	3.80	2	4.08	F8 V
464	51 AND	1.61	48.49	4.52	4.48	2.89	2	3.59	K3 III
472	ALF ERI	1.61	-57.37	0.12	0.21	0.51	2	0.48	B5 IV
489	NU PSC	1.67	5.36	5.41	5.38	3.64	2	4.46	K3 III
496	PHI PER	1.70	50.56	3.65	3.79	3.95	2	4.09	B1 III
509	TAU CET	1.72	-16.07	4.06	4.05	3.12	2	3.53	G8 V

YBS#	NAME	RA	DEC	S20	CDS	SIL	S	VIS	SP.TYPE
510	OMI PSC	1.73	9.02	5.01	4.96	3.77	2	4.26	G8 III
519		1.75	-50.94	6.30	6.41	3.62	0	5.48	M3 III
539	ZET CET	1.84	-10.46	4.57	4.52	3.14	2	3.71	K2 III
542	EPS CAS	1.88	63.56	3.02	3.10	3.38	2	3.37	R3 IV
544	ALF TRI	1.86	29.46	3.76	3.76	3.16	2	3.41	F6 IV
551		1.89	40.56	5.20	5.15	3.71	0	4.32	K2
553	BET ARI	1.89	20.68	2.80	2.79	2.63	2	2.67	A5 V
555	PSI PHE	1.88	-46.44	5.29	5.37	2.66	2	4.41	M4 III
566D	CHI ERI	1.92	-51.72	4.35	4.33	3.24	2	3.69	G5 IV
580	50 CAS	2.02	72.30	3.97	3.97	3.94	2	3.95	A1 V
583	57 CET	1.98	-20.95	6.34	6.39	3.98	0	5.41	M1
585	UPS CET	1.98	-21.20	5.00	5.01	2.90	2	4.01	M1 III
587		1.99	- 8.64	6.13	6.32	3.11	0	5.50	M5
591	ALF HYI	1.97	-61.69	3.15	3.14	2.76	2	2.87	F0 V
602	CHI PHE	2.01	-44.84	6.10	6.13	3.89	0	5.14	K5
603D	GAM1 AND	2.04	42.21	2.86	2.85	1.37	1	2.10	K3 II
617	ALF ARI	2.10	23.33	2.89	2.84	1.40	2	2.03	K2 III
622	BET TRI	2.13	34.87	3.17	3.16	2.96	2	3.03	A5 III
631	15 ARI	2.15	19.38	6.58	6.69	3.90	0	5.76	M3
649	XI1 CET	2.19	8.73	5.06	5.03	3.91	2	4.37	G8 II
674D	PHI ERI	2.26	-51.63	3.36	3.41	3.60	2	3.57	R8 V
681D	OMI CET	2.30	- 3.10	3.75	3.98	0.48	2	3.21	M6
689	69 CET	2.34	0.27	6.15	6.23	3.64	0	5.27	M2
699	65 AND	2.40	50.17	5.74	5.74	3.74	2	4.75	K4 III
750	15 TRI	2.57	34.57	6.27	6.38	3.59	0	5.45	M3
758	R TRI	2.59	34.16	6.03	6.18	3.18	0	5.30	M4
779	DEL CET	2.64	0.22	3.53	3.66	4.12	2	4.10	R2 IV
794	IOT ERI	2.66	-39.96	4.89	4.85	3.56	2	4.11	K0 III
799D	THE PER	2.71	49.11	4.45	4.46	3.86	2	4.12	F7 V
804D	GAM CET	2.70	3.13	3.56	3.56	3.43	2	3.48	A2 V
811	PI CET	2.72	-13.97	3.99	4.06	4.27	2	4.25	P7 V
824	39 ARI	2.77	29.15	5.38	5.33	3.94	2	4.52	K1 III
834D	ETA PER	2.81	55.80	4.84	4.85	2.82	2	3.82	K3 I
838D	41 ARI	2.81	27.16	3.43	3.48	3.65	2	3.63	R8 V
841	BET FOR	2.80	-32.52	5.23	5.19	3.96	2	4.46	G6 III
843	17 PER	2.83	34.96	5.55	5.56	3.46	2	4.58	K5 III
854D	TAU PER	2.87	52.66	4.55	4.51	3.53	2	3.95	G5 III
867	45 ARI	2.91	18.23	6.44	6.67	3.26	0	5.94	M6 III
868	R HOR	2.88	-50.00	4.34	4.63	1.03	0	4.00	M7
874	ETA ERI	2.92	- 9.00	4.72	4.68	3.32	2	3.89	K1 III
911	ALF CET	3.02	4.00	3.52	3.55	1.23	2	2.56	M2 III
915D	GAM PER	3.05	53.40	3.49	3.46	2.51	2	2.92	G8 III
921	RHO PER	3.06	38.74	4.28	4.38	1.46	2	3.45	M4 II
935D		3.09	- 6.20	6.08	6.19	3.40	0	5.26	M3
936D	BET PER	3.11	40.85	1.97	2.02	2.10	2	2.15	R8 V
937	IOT PER	3.12	49.52	4.46	4.46	3.72	2	4.03	G0 V
941D	KAP PER	3.13	44.77	4.57	4.52	3.30	2	3.80	K0 III
951	DEL ARI	3.17	19.64	5.16	5.11	3.83	2	4.35	K2 III
963D	ALF FOR	3.18	-29.08	4.17	4.18	3.58	2	3.85	F8 IV
999		3.31	28.96	5.49	5.50	3.50	2	4.49	K4 III

YBS#	NAME	RA	DEC	S20	CDS	SIL	S	VIS	SP.TYPE
1003D	TAU4 ERI	3.31	-21.84	4.59	4.65	2.03	2	3.70	M3
1004		3.31	-24.21	6.48	6.56	3.97	0	5.60	M2
1008		3.32	-43.16	4.81	4.79	3.90	2	4.27	G5 V
1009		3.37	64.50	6.19	6.22	3.98	0	5.23	M0 II
1017	ALF PER	3.38	49.76	2.23	2.20	1.53	2	1.80	F5 I
1030	OMI TAU	3.39	8.95	4.31	4.27	3.16	2	3.61	G8 III
1035D		3.45	59.86	4.50	4.54	3.99	2	4.28	B9 I
1038	XI TAU	3.43	9.65	3.59	3.64	3.75	2	3.76	B8
1052	SIG PER	3.48	47.91	5.33	5.30	3.57	2	4.37	K3 III
1066	5 TAU	3.49	12.86	4.99	4.94	3.59	2	4.13	K0 II
1084	EPS ERI	3.53	-9.55	4.39	4.35	3.21	2	3.71	K2 V
1087	PS1 PER	3.58	48.12	3.95	4.03	4.18	2	4.24	B5
1122	DEL PER	3.69	47.70	2.74	2.82	3.05	2	3.04	B5 III
1131D	OMI PER	3.71	32.20	3.57	3.67	3.77	2	3.84	B1 III
1135D	NU PER	3.72	42.50	4.13	4.11	3.53	2	3.77	F5 II
1136	DEL ERI	3.70	-9.85	4.23	4.19	3.06	2	3.53	K0 IV
1142	17 TAU	3.72	24.04	3.48	3.54	3.71	2	3.72	B6 III
1143D		3.70	-37.40	5.47	5.43	3.96	2	4.59	K2
1149	20 TAU	3.74	24.29	3.67	3.73	3.85	2	3.88	B7 III
1155		3.79	65.45	5.44	5.54	2.75	2	4.48	M1 III
1156	23 TAU	3.75	23.87	3.98	4.04	4.14	2	4.18	B6 IV
1162	PI ERI	3.75	-12.18	5.44	5.46	3.23	2	4.47	M2
1165D	ETA TAU	3.77	24.04	2.66	2.72	2.86	2	2.88	B7 III
1175	BET RET	3.73	-64.88	4.72	4.68	3.24	2	3.85	K0 IV
1178D	27 TAU	3.79	23.97	3.43	3.49	3.62	2	3.64	B8 III
1195		3.81	-36.27	4.89	4.85	3.72	2	4.17	G5 III
1203D	ZET PER	3.88	31.81	2.66	2.77	2.77	2	2.88	B1 I
1208	GAM HYI	3.79	-74.32	4.22	4.25	2.00	2	3.25	M0 III
1220D	EPS PER	3.94	39.93	2.32	2.47	2.90	2	2.90	B0.5 V
1228	XI PER	3.96	35.71	3.66	3.79	3.94	2	4.03	B7
1231D	GAM ERI	3.95	-13.59	3.94	3.95	1.81	2	2.96	M0 III
1239	LAM TAU	3.99	12.41	3.10	3.18	3.43	2	3.44	B3 V
1247	DEL RET	3.97	-61.47	5.53	5.56	3.34	2	4.55	M2 III
1251	NU TAU	4.03	5.93	3.89	3.89	3.86	2	3.87	A1 V
1256	37 TAU	4.05	22.02	5.20	5.15	3.81	2	4.36	K0 III
1264	GAM RET	4.01	-62.22	5.40	5.48	2.76	2	4.50	M5
1273	48 PER	4.11	47.65	3.83	3.91	4.02	2	4.07	B3 V
1298	OMI1 ERI	4.18	-6.90	4.34	4.32	3.90	2	4.06	F2 III
1303D	MU PER	4.22	48.34	4.89	4.86	3.63	2	4.16	G0 I
1325D	OMI2 ERI	4.24	-7.70	5.03	5.01	3.96	2	4.41	K1 V
1326	ALF HOR	4.22	-42.35	4.70	4.66	3.32	2	3.86	K1 III
1336D	ALF RET	4.23	-62.53	4.08	4.03	2.93	2	3.35	G6 II
1345		4.29	-20.78	6.73	6.88	3.88	0	6.00	M4
1346	GAM TAU	4.31	15.56	4.40	4.35	3.14	2	3.63	K0 III
1355D	EPS RET	4.27	-59.37	5.32	5.27	3.83	0	4.44	K2 IV
1373	DEL TAU	4.36	17.47	4.53	4.48	3.27	2	3.76	K0 III
1393	43 ERI	4.38	-34.07	4.94	4.93	3.05	2	3.96	M1 III
1409	EPS TAU	4.45	19.13	4.34	4.28	3.04	2	3.53	K0 III
1411	THE1 TAU	4.45	15.90	4.61	4.56	3.37	2	3.85	K0 III
1412	THE2 TAU	4.45	15.81	3.58	3.57	3.33	2	3.43	A7 III

YBS#	NAME	RA	DEC	S20	CDS	SIL	S	VIS	SP.TYPE
1451	47 ERI	4.55	- 8.27	5.92	6.03	3.24	0	5.10	M3
1453	UPS1 ERI	4.54	-29.82	5.18	5.15	3.98	1	4.50	G6 III
1454	58 PER	4.58	41.22	5.09	5.07	3.53	2	4.22	G5 I
1457D	ALF TAU	4.57	16.45	1.89	1.90	-0.19	2	0.92	K5 III
1463	NU ERI	4.58	- 3.40	3.40	3.53	3.96	2	3.94	R2 III
1464	UPS2 ERI	4.58	-30.62	4.56	4.52	3.36	2	3.82	K0 III
1465D	ALF DOR	4.56	-55.10	3.06	3.11	3.28	2	3.27	A0
1481D	53 ERI	4.62	-14.35	4.68	4.63	3.26	2	3.85	K2 III
1492D	R DOR	4.61	-62.12	4.48	5.05	-0.09	2	4.50	M7
1497	TAU TAU	4.68	22.92	3.96	4.04	4.30	2	4.29	R3 V
1520	MU ERI	4.74	- 3.30	3.66	3.75	4.03	2	4.02	B5 IV
1527		4.83	63.46	6.49	6.57	3.98	0	5.61	M2
1542	ALF CAM	4.86	66.29	3.94	4.07	4.21	2	4.31	O9.5 I
1543	PI3 ORI	4.81	6.91	3.49	3.49	2.95	2	3.18	F6 V
1552	PI4 ORI	4.83	5.56	3.20	3.32	3.69	2	3.69	B2 III
1556	OMI1 ORI	4.85	14.21	5.54	5.65	2.86	0	4.72	M3
1562	5 ORI	4.87	2.47	6.25	6.30	3.89	0	5.32	M1
1567	PI5 ORI	4.88	2.41	3.24	3.36	3.75	2	3.74	B2 III
1577	IOT AUR	4.92	33.11	3.72	3.71	1.85	2	2.72	K3 II
1580D	OMI2 ORI	4.92	13.46	4.99	4.95	3.48	2	4.12	K2 III
1601	PI6 ORI	4.95	1.68	5.46	5.43	3.72	2	4.48	K2 II
1603D	BET CAM	5.02	60.41	4.74	4.70	3.59	2	4.03	G0 I
1605D	EPS AUR	5.00	43.80	3.42	3.40	2.64	2	2.99	A8 I
1612	ZET AUR	4.99	41.02	4.54	4.57	2.81	2	3.77	K5 III
1641	ETA AUR	5.08	41.20	2.76	2.86	3.19	2	3.17	R3 V
1652D	GAM CAE	5.06	-35.52	5.43	5.39	3.91	2	4.55	K3
1654	EPS LEP	5.07	-22.40	4.16	4.14	2.34	2	3.19	K5 III
1663	ETA2 PIC	5.07	-49.62	5.88	5.96	3.37	0	5.00	M2 III
1666	BET ERI	5.11	- 5.12	2.90	2.89	2.72	1	2.81	A3 III
1679	LAM ERI	5.13	- 8.78	3.73	3.86	4.28	2	4.27	B2 IV
1693		5.17	-11.88	6.18	6.41	3.00	0	5.68	M6
1695		5.12	-63.43	5.83	5.98	2.98	0	5.10	M4
1698D	RHO ORI	5.20	2.84	5.34	5.29	3.83	2	4.45	K3 III
1702	MU LEP	5.20	-16.23	3.04	3.10	3.29	2	3.28	B9 III
1707D	R AUR	5.25	53.55	6.84	7.13	3.53	0	6.50	M7
1708D	ALF AUR	5.25	45.97	0.67	0.63	-0.36	2	0.04	G8 III
1713D	BET ORI	5.22	- 8.23	-0.14	-0.04	0.11	2	0.16	B8 I
1722		5.27	42.77	6.36	6.51	3.51	0	5.63	M4
1726D	16 AUR	5.28	33.34	5.34	5.32	3.78	1	4.54	K3 III
1735D	TAU ORI	5.27	- 6.87	3.31	3.37	3.60	2	3.59	B5 III
1756	LAM LEP	5.31	-13.21	3.63	3.78	4.32	2	4.30	B0.5 IV
1784	29 ORI	5.38	- 7.82	4.86	4.82	3.62	2	4.13	G8 III
1790	GAM ORI	5.40	6.33	1.06	1.19	1.66	2	1.64	B2 III
1791	BET TAU	5.41	28.58	1.38	1.45	1.69	2	1.68	B7 III
1829D	BET LEP	5.45	-20.77	3.44	3.41	2.42	2	2.83	G5 III
1845	119 TAU	5.51	18.57	5.36	5.50	2.62	2	4.41	M2 I
1852D	DEL ORI	5.51	- 0.32	1.57	1.72	2.24	2	2.23	O9.5 II
1855	UPS ORI	5.51	- 7.33	3.93	4.09	4.64	2	4.62	B0 V
1862	EPS COL	5.51	-35.50	4.74	4.69	3.32	2	3.87	K1
1865D	ALF LEP	5.53	-17.85	2.80	2.77	2.44	2	2.57	F0 I

YBS#	NAME	RA	DEC	S20	CDS	SIL	S	VIS	SP.TYPE
1876	PHI1 ORI	5.56	9.47	3.86	4.01	4.40	2	4.40	B0 IV
1879D	LAM ORI	5.56	9.92	2.79	2.94	3.38	2	3.40	B8
1899D	IOT ORI	5.57	- 5.93	2.12	2.28	2.81	2	2.80	B9 III
1903	EPS ORI	5.58	- 1.22	1.12	1.27	1.71	2	1.72	B0 I
1907	PHI2 ORI	5.59	9.27	4.81	4.78	3.56	2	4.09	G8 III
1910	ZET TAU	5.60	21.13	2.51	2.62	2.98	2	2.98	B2 IV
1922	BET DOR	5.56	-62.50	3.29	3.41	3.81	1	3.73	F8 I
1931D	SIG ORI	5.62	- 2.61	3.13	3.28	3.75	2	3.76	B9.5 V
1948D	ZET ORI	5.66	- 1.96	1.13	1.29	1.76	2	1.77	B9.5 I
1956D	ALF COL	5.65	-34.10	2.38	2.45	2.64	2	2.64	B8 V
1964		5.59	-73.75	6.51	6.66	3.66	0	5.78	M4
1983D	GAM LEP	5.72	-22.46	3.94	3.94	3.35	2	3.60	F6 V
1998	ZET LEP	5.76	-14.84	3.63	3.63	3.50	1	3.56	A3 V
2004	KAP ORI	5.78	- 9.67	1.54	1.68	2.06	2	2.08	B0.5 I
2011	UPS AUR	5.82	37.31	5.77	5.80	3.56	2	4.80	M1
2012D	NU AUR	5.83	39.14	4.85	4.80	3.42	2	4.00	K0 III
2020	BET PIC	5.78	-51.07	4.01	4.01	3.78	2	3.85	A3 V
2035	DEL LEP	5.84	-20.87	4.52	4.48	3.24	2	3.79	G8 III
2040	BET COL	5.83	-35.77	3.99	3.94	2.56	2	3.12	K2 III
2042	GAM PIC	5.82	-56.16	5.35	5.30	3.90	0	4.50	K1 III
2061D	ALF ORI	5.90	7.40	1.36	1.45	-1.19	2	0.39	M2 I
2063	U ORI	5.91	20.15	5.57	5.91	2.14	0	5.40	M8
2077	DEL AUR	5.96	54.28	4.51	4.46	3.23	2	3.72	K0 III
2085	ETA LEP	5.92	-14.17	3.97	3.97	3.59	2	3.74	F0 V
2088D	BET AUR	5.96	44.95	1.97	1.96	1.91	2	1.92	A2 V
2091	PI AUR	5.97	45.95	5.28	5.38	2.59	2	4.39	M3 II
2095D	THE AUR	5.97	37.20	2.51	2.53	2.61	1	2.58	B9.5 V
2113		5.98	- 3.08	5.43	5.39	3.83	2	4.54	K2 III
2120	ETA COL	5.97	-42.82	4.84	4.80	3.41	2	3.96	K0 III
2156	S LEP	6.08	-24.20	6.50	6.73	3.32	0	6.00	M6
2168	19 LEP	6.11	-19.16	6.19	6.27	3.68	0	5.31	M2
2215	1 LYN	6.26	61.52	5.72	5.83	3.04	0	4.90	M3
2216D	ETA GEM	6.22	22.51	4.16	4.21	1.69	2	3.25	M3 III
2219	KAP AUR	6.23	29.51	5.09	5.05	3.76	2	4.31	G8 III
2227D	GAM MON	6.23	- 6.27	4.92	4.88	3.25	2	3.98	K3 III
2245	ETA2 DOR	6.19	-65.58	5.83	5.94	3.15	0	5.01	M3
2256	KAP COL	6.26	-35.12	5.11	5.08	3.80	0	4.36	G8 III
2273	7 MON	6.31	- 7.82	3.90	4.00	4.23	0	4.25	B2 V
2275		6.31	- 2.94	5.82	5.87	3.46	0	4.89	M1
2282	ZET CMA	6.32	-30.05	2.57	2.68	3.06	2	3.02	B2.5 V
2286D	MU GEM	6.36	22.53	3.89	3.95	1.35	2	2.98	M3 III
2289	PSI1 AUR	6.38	49.30	5.96	5.99	3.75	0	5.00	M0 I
2294	BET CMA	6.36	-17.94	1.38	1.52	2.01	2	2.00	B1 II
2296	DEL COL	6.35	-33.42	4.45	4.41	3.36	2	3.79	G4
2326	ALF CAR	6.39	-52.67	-0.59	-0.61	-0.88	2	-0.77	F0 I
2343D	NU GEM	6.46	20.23	3.89	3.96	4.18	2	4.17	B7 IV
2387D	XI1 CMA	6.51	-23.40	3.82	3.94	4.36	1	4.35	B0.5 IV
2421	GAM GEM	6.60	16.42	1.98	1.97	1.94	2	1.95	A0 IV
2429	NU2 CMA	6.59	-19.23	4.79	4.74	3.44	2	3.97	K1 IV
2443	NU3 CMA	6.61	-18.21	5.31	5.26	3.86	2	4.45	K1 II

YBS#	NAME		RA	DEC	S20	CDS	SIL	S	VIS	SP.TYPE	
2450			6.64	-14.11	5.85	5.83	4.00	2	4.85	K3	III
2451	NU	PUP	6.62	-43.16	2.94	3.00	3.17	2	3.17	B8	III
2469			6.68	- 9.14	6.14	6.17	3.93	0	5.18	M0	
2473D	EPS	GEM	6.71	25.16	4.02	3.98	2.36	2	3.04	G8	I
2478D	30	GEM	6.71	13.26	5.40	5.36	3.89	2	4.52	K1	III
2484	XI	GEM	6.73	12.92	3.74	3.74	3.20	2	3.43	F5	IV
2491D	ALF	CMA	6.73	-16.68	-1.45	-1.45	-1.41	2	-1.42	A1	V
2506	18	MON	6.78	2.43	5.34	5.28	3.92	2	4.48	K0	III
2508			6.77	- 8.97	5.99	6.04	3.63	0	5.06	M1	II
2527			6.94	77.00	5.54	5.51	3.77	2	4.59	K4	III
2538	KAP	CMA	6.81	-32.49	3.21	3.39	3.73	2	3.99	R2	V
2540D	THE	GEM	6.85	34.00	3.76	3.75	3.58	2	3.64	A3	III
2550	ALF	PIC	6.80	-61.91	3.47	3.45	3.17	2	3.28	A5	V
2553	TAU	PUP	6.82	-50.59	3.81	3.76	2.30	2	2.92	K0	III
2554			6.82	-53.59	4.98	4.96	3.93	0	4.39	G3	
2574	THE	CMA	6.88	-12.02	5.06	5.04	3.21	2	4.10	K4	III
2580	OMI1	CMA	6.88	-24.17	4.85	4.85	2.97	1	3.92	K3	I
2608			6.93	-48.68	5.76	5.87	3.08	0	4.94	M1	
2609			7.48	87.06	5.95	6.03	3.44	0	5.07	M2	
2618D	EPS	CMA	6.96	-28.93	0.87	1.02	1.50	2	1.50	B2	II
2639			7.01	- 5.70	6.08	6.16	3.57	0	5.20	M2	
2646D	SIG	CMA	7.01	-27.90	4.51	4.54	2.33	2	3.50	M0	I
2650D	ZET	GEM	7.04	20.60	4.36	4.33	3.40	2	3.76	F7	I
2652			7.00	-51.38	5.73	5.78	3.37	0	4.80	M1	
2653	OMI2	CMA	7.03	-23.80	2.54	2.66	2.97	2	3.01	R3	I
2657	GAM	CMA	7.04	-15.60	3.84	3.91	4.12	2	4.12	B8	II
2693	DEL	CMA	7.12	-26.36	2.39	2.35	1.55	2	1.84	F8	I
2697D	TAU	GEM	7.16	30.29	5.33	5.28	3.73	2	4.40	K2	III
2703			7.19	51.47	6.34	6.45	3.66	0	5.52	M3	
2717	51	GEM	7.20	16.21	5.73	5.88	2.88	0	5.00	M4	III
2742			7.43	82.45	5.63	5.78	2.78	0	4.90	M4	
2747			7.24	8.04	6.53	6.68	3.68	0	5.80	M4	
2748D			7.21	-44.61	5.76	5.97	1.05	2	5.08	M5	
2749	OMG	CMA	7.23	-26.72	3.48	3.59	3.86	2	3.92	B3	IV
2763D	LAM	GEM	7.28	16.58	3.69	3.67	3.54	2	3.58	A3	V
2764D			7.26	-23.27	5.67	5.68	3.65	1	4.78	M0	
2766			7.26	-27.84	5.40	5.45	3.13	1	4.60	M3	
2773	PI	PUP	7.27	-37.05	3.67	3.69	1.66	2	2.70	K5	III
2777D	DEL	GEM	7.31	22.03	3.77	3.76	3.34	1	3.53	F0	IV
2782D	TAU	CMA	7.29	-24.90	3.82	3.96	4.37	2	4.39	O9	III
2795D	56	GEM	7.34	20.50	6.06	6.09	3.85	0	5.10	M0	
2802			7.33	-25.84	6.60	6.75	3.75	0	5.87	M4	
2803	DEL	VOL	7.28	-67.90	4.61	4.57	3.61	2	3.99	F8	II
2821	IOT	GEM	7.40	27.85	4.59	4.54	3.28	2	3.81	K0	III
2827	ETA	CMA	7.38	-29.25	2.08	2.19	2.39	2	2.43	B5	I
2845	BET	CMI	7.43	8.33	2.71	2.74	2.89	2	2.89	B7	V
2854D	GAM	CMI	7.45	8.98	5.28	5.27	3.43	2	4.32	K3	III
2864	6	CMI	7.47	12.07	5.49	5.44	3.88	2	4.55	K2	III
2878D	SIG	PUP	7.47	-43.25	4.26	4.27	2.26	2	3.30	K5	III
2902			7.54	-14.46	5.87	5.95	3.36	0	4.99	M2	I

YBS#	NAME		RA	DEC	S20	CDS	SIL	S	VIS	SP.TYPE	
2905	UPS	GEM	7.57	26.95	5.06	5.06	3.00	2	4.08	M0	III
2938	74	GEM	7.63	17.72	6.01	6.04	3.80	0	5.05	M0	
2943D	ALF	CMI	7.63	5.30	0.64	0.64	0.12	2	0.34	F5	IV
2970	ALF	MON	7.67	-9.49	4.75	4.70	3.44	2	3.95	K0	III
2973	SIG	GEM	7.70	28.95	5.02	4.99	3.62	1	4.28	K1	III
2985D	KAP	GEM	7.72	24.46	4.32	4.28	3.13	2	3.60	G8	III
2990D	BET	GEM	7.73	28.08	1.92	1.87	0.62	2	1.14	K0	III
2993D	1	PUP	7.71	-28.34	5.62	5.64	3.47	2	4.64	K5	
2996	3	PUP	7.71	-28.89	4.11	4.12	3.83	2	3.99	A3	II
2999			7.75	37.58	6.00	6.11	3.32	0	5.18	M3	
3003	81	GEM	7.74	18.56	5.87	5.86	3.94	2	4.92	K5	III
3013D	PI	GEM	7.77	33.48	6.10	6.13	3.89	0	5.14	M0	
3017			7.74	-37.92	4.62	4.66	2.45	2	3.63	K	
3024D	ZET	VOL	7.70	-72.54	4.77	4.72	3.43	2	3.99	K0	III
3045D	XI	PUP	7.80	-24.80	4.25	4.20	2.75	2	3.34	G3	I
3055D			7.81	-46.30	3.69	3.81	4.07	0	4.10	R0.5	III
3080			7.86	-40.52	4.50	4.45	3.15	2	3.71	G5	III
3090			7.88	-48.05	3.84	3.95	4.20	0	4.23	R1	I
3102	11	PUP	7.93	-22.82	4.72	4.70	3.82	1	4.20	F8	II
3117	CHI	CAR	7.94	-52.92	3.03	3.13	3.47	2	3.46	B2	IV
3129D	V	PUP	7.96	-49.17	3.80	3.95	4.38	2	4.39	R2	
3141	28	MON	8.00	-1.33	5.69	5.67	3.77	2	4.71	K4	III
3145			8.02	2.42	5.32	5.28	3.68	2	4.41	K2	III
3153			7.99	-60.53	6.12	6.15	3.91	0	5.16	M0	II
3159			8.00	-63.50	1.65	1.78	2.22	1	4.83	B3	IV
3165	ZET	PUP	8.05	-39.93	1.54	1.71	2.26	2	2.27	O5	
3170			8.05	-32.61	5.93	5.98	3.57	0	5.00	M1	
3185D	RHO	PUP	8.11	-24.23	3.12	3.09	2.56	2	2.76	F6	II
3187			8.10	-45.18	6.00	6.03	3.79	0	5.04	M0	
3188D	ZET	MON	8.12	-2.91	5.10	5.06	3.88	2	4.35	G2	I
3207D	GAM	VEL	8.15	-47.27	1.20	1.34	1.76	2	1.76	C7	
3225			8.17	-39.54	5.26	5.21	3.86	0	4.44	K	
3243D			8.22	-40.27	5.31	5.26	3.82	0	4.43	K0	
3248	R	CNC	8.25	11.81	6.34	6.63	3.03	0	6.00	M7	
3249D	BET	CNC	8.25	9.27	4.54	4.52	2.65	2	3.55	K4	III
3275	31	LYN	8.35	43.28	5.27	5.27	3.28	2	4.28	K5	III
3282			8.34	-32.97	5.78	5.81	3.57	0	4.82	K1	III
3307	EPS	CAR	8.37	-59.42	2.64	2.68	0.95	2	1.88	K0	II
3314			8.41	-3.83	3.89	3.90	3.91	2	3.91	A0	V
3318	ALF	CHA	8.32	-76.84	4.37	4.37	3.87	2	4.09	F6	IV
3319	27	CNC	8.42	12.73	6.32	6.43	3.64	0	5.50	M3	
3323D	OMI	UMA	8.47	60.80	4.04	4.01	2.95	2	3.39	G5	III
3340D	THE	CHA	8.36	-77.40	5.16	5.11	3.76	0	4.34	K0	III
3347	BET	VOL	8.42	-66.05	4.63	4.58	3.13	2	3.78	K2	III
3403	PI2	UMA	8.63	64.42	5.51	5.46	3.99	2	4.63	K2	III
3418	SIG	HYA	8.62	3.44	5.36	5.30	3.82	2	4.44	K2	III
3438D	BET	PYX	8.65	-35.21	4.65	4.61	3.48	2	3.93	G4	III
3445D			8.66	-46.56	4.40	4.37	3.32	2	3.82	F2	I
3447	OMI	VEL	8.66	-52.83	3.19	3.29	3.62	2	3.60	B3	III
3454	ETA	HYA	8.70	3.47	3.86	3.96	4.34	2	4.31	B3	V

YBS#	NAME		RA	DEC	S20	CDS	SIL	S	VIS	SP.TYPE	
3461D	DEL	CNC	8.72	18.24	4.80	4.75	3.40	2	3.97	K0	III
3468	ALF	PYX	8.71	-33.11	3.19	3.32	3.72	2	3.71	B2	III
3475D	IOT	CNC	8.75	28.86	4.73	4.69	3.51	1	4.02	G8	II
3477D			8.73	-42.56	4.71	4.69	3.55	0	4.06	G5	
3484D	12	HYA	8.75	-13.46	5.02	4.98	3.86	2	4.32	G8	III
3485D	DEL	VEL	8.73	-54.62	2.00	2.00	1.93	1	1.93	A0	V
3487			8.75	-45.96	3.96	3.96	3.89	2	3.93	A0	III
3518	GAM	PYX	8.82	-27.61	4.81	4.78	3.27	1	4.00	K4	III
3547	ZET	HYA	8.90	6.05	3.92	3.87	2.64	2	3.14	K0	II
3569D	IOT	UMA	8.96	48.13	3.34	3.33	3.07	2	3.17	A7	V
3571D			8.91	-60.55	3.66	3.72	3.90	2	3.89	B8	II
3574D			8.93	-52.62	5.55	5.59	3.32	1	4.69	B5	V
3576	RHO	UMA	9.00	67.73	5.74	5.76	3.41	2	4.80	M3	III
3614			9.05	-47.00	4.64	4.60	3.13	2	3.77	K2	III
3628D	KAP	PYX	9.12	-25.75	5.43	5.44	3.49	1	4.56	M0	
3634D	LAM	VEL	9.12	-43.33	3.22	3.24	1.03	2	2.21	K5	I
3639	RS	CNC	9.15	31.08	6.35	6.58	3.17	0	5.85	M6	
3659	A	CAR	9.17	-58.86	3.14	3.23	3.54	2	3.50	B2	IV
3663			9.18	-62.21	3.80	3.81	3.87	1	4.02	B3	IV
3665D	THE	HYA	9.22	2.42	3.83	3.85	3.93	2	3.92	B9.5	V
3685	BET	CAR	9.22	-69.61	1.73	1.73	1.69	2	1.72	A1	IV
3690D	38	LYN	9.29	36.92	3.91	3.90	3.80	2	3.84	A3	V
3696			9.26	-57.43	5.28	5.25	3.61	0	4.33	K5	
3698			9.33	56.82	6.50	6.65	3.65	0	5.77	M4	
3699	IOT	CAR	9.27	-59.16	2.58	2.55	2.22	2	2.35	F0	I
3705	ALF	LYN	9.33	34.50	4.14	4.15	2.10	2	3.16	M0	III
3718	THE	PYX	9.34	-25.86	5.56	5.59	3.43	1	4.72	M1	III
3726			9.35	-42.09	6.39	6.50	3.71	0	5.57	M3	I
3731D	KAP	LEO	9.39	26.29	5.34	5.30	3.75	2	4.45	K2	III
3734	KAP	VEL	9.36	-54.91	2.11	2.22	2.57	2	2.55	B2	IV
3748	ALF	HYA	9.44	-8.56	3.00	2.97	1.20	2	2.02	K4	III
3751			9.56	81.43	5.28	5.26	3.45	2	4.29	K3	III
3757D	23	UMA	9.49	63.17	3.92	3.91	3.47	2	3.66	F0	IV
3765	EPS	ANT	9.47	-35.84	5.46	5.49	3.25	0	4.50	K4	III
3769	8	LMI	9.50	35.21	6.30	6.35	3.94	0	5.37	M1	
3773	LAM	LEO	9.50	-23.09	5.33	5.33	3.30	2	4.35	K5	III
3775D	THE	UMA	9.52	51.80	3.52	3.52	2.93	2	3.19	F6	IV
3803	N	VEL	9.51	-56.92	4.18	4.18	2.16	2	3.20	K5	III
3816D	R	CAR	9.53	-62.69	6.10	6.30	3.10	2	5.83	M5	
3820			9.59	31.28	6.44	6.52	3.93	0	5.56	M2	
3825			9.56	-59.12	5.50	5.48	3.86	1	4.10	B5	II
3834			9.62	4.76	5.63	5.60	3.91	2	4.69	K3	III
3845	IOT	HYA	9.64	-1.02	4.85	4.81	3.17	2	3.91	K3	III
3852D	OMI	LEO	9.66	10.01	3.94	3.92	3.32	2	3.54	A2	
3866	PSI	LEO	9.71	14.15	6.29	6.37	3.78	0	5.41	M2	
3870			9.75	57.23	6.02	6.13	3.34	0	5.20	M3	
3873	EPS	LEO	9.74	23.88	3.62	3.58	2.59	2	2.99	G0	II
3882	R	LEO	9.77	11.55	4.57	4.91	1.14	0	4.40	M8	
3884	L	CAR	9.74	-62.40	5.09	5.07	3.37	2	4.09	G2	
3888D	UPS	UMA	9.82	59.17	4.00	3.99	3.61	2	3.77	F2	IV

YBS#	NAME		RA	DEC	S20	CDS	SIL	S	VIS	SP.TYPE	
3890D	UPS	CAR	9.77	-64.95	3.22	3.20	2.77	2	2.98	A9	II
3903	UPS1	HYA	9.84	-14.73	4.85	4.80	3.66	2	4.12	G8	III
3905	MU	LEO	9.86	26.13	4.82	4.77	3.26	2	3.91	K2	III
3923			9.89	-18.88	5.87	5.92	3.51	0	4.94	M1	III
3940D	PHI	VEL	9.93	-54.46	3.23	3.31	3.53	2	3.56	B5	II
3950	PI	LEO	9.98	8.15	5.69	5.72	3.43	2	4.72	M2	III
3975	ETA	LEO	10.10	16.89	3.41	3.45	3.48	2	3.53	A0	I
3980D	31	LEO	10.11	10.12	5.35	5.33	3.48	2	4.37	K4	III
3982D	ALF	LEO	10.12	12.09	1.17	1.22	1.41	2	1.40	B7	V
3990			10.13	-51.68	4.31	4.28	3.10	1	4.87	B2	V
3994D	LAM	HYA	10.16	-12.24	4.40	4.35	3.11	2	3.60	K0	III
4023			10.23	-42.01	3.90	3.89	3.82	2	3.84	A2	V
4031	ZET	LEO	10.26	23.54	3.72	3.70	3.26	2	3.44	F0	III
4033	LAM	UMA	10.26	43.04	3.48	3.47	3.42	2	3.44	A2	IV
4037	OMG	CAR	10.22	-69.91	3.17	3.21	3.32	2	3.33	B7	IV
4045			10.26	-51.07	6.92	7.11	3.90	0	6.29	M5	
4050			10.27	-61.21	4.40	4.39	2.52	2	3.40	K5	I
4063			10.31	-54.91	5.38	5.33	3.98	0	4.56	K	
4069	MU	UMA	10.35	41.62	4.06	4.07	1.96	2	3.09	M0	III
4088	44	LEO	10.40	8.91	6.43	6.54	3.75	0	5.61	M3	
4094	MU	HYA	10.41	-16.72	4.79	4.78	2.87	2	3.81	K4	III
4100D	BET	LMI	10.44	36.83	4.89	4.85	3.71	2	4.17	G8	III
4102			10.40	-73.90	4.27	4.27	3.83	2	4.02	F3	IV
4104	ALF	ANT	10.43	-30.95	5.20	5.23	2.99	0	4.24	M0	III
4114			10.45	-58.62	4.13	4.11	3.65	2	3.84	F0	II
4127	46	LEO	10.51	14.26	6.42	6.50	3.91	0	5.54	M2	
4133	RHO	LEO	10.52	9.43	3.30	3.44	3.82	2	3.83	B1	I
4140			10.52	-61.55	2.95	3.05	3.23	2	3.32	B5	V
4159			10.58	-57.42	5.35	5.30	3.80	0	4.44	K3	
4162			10.60	-27.29	5.76	5.84	3.25	0	4.88	M2	
4163	U	HYA	10.61	-13.25	5.98	6.17	3.38	2	4.99	C73	
4174	GAM	CHA	10.59	-78.47	5.18	5.19	3.08	2	4.20	M0	III
4180D			10.64	-55.47	4.82	4.80	3.83	0	4.26	G2	II
4184			10.68	31.83	6.79	6.98	3.77	0	6.16	M5	
4199	THE	CAR	10.70	-64.25	2.20	2.35	2.84	2	2.83	09.5	V
4200			10.71	-60.44	5.38	5.33	3.98	0	4.56	K	
4216D	MU	VEL	10.76	-49.30	3.40	3.36	2.24	2	2.70	G5	III
4222			10.77	-64.25	3.90	3.87	2.41	1	4.91	B3	IV
4232	NU	HYA	10.81	-16.05	4.03	3.99	2.46	2	3.13	K3	III
4234	DEL2	CHA	10.76	-80.42	4.53	4.50	3.23	1	4.48	B3	V
4247	46	LMI	10.87	34.35	4.61	4.57	3.26	2	3.81	K0	III
4257			10.87	-58.72	4.51	4.47	3.29	2	3.80	K0	III
4267	56	LEO	10.91	6.32	6.44	6.63	3.42	0	5.81	M5	III
4287	ALF	CRT	10.98	-18.17	4.92	4.87	3.53	2	4.09	K0	III
4295	BET	UMA	11.01	56.52	2.36	2.36	2.37	2	2.37	A1	V
4299	61	LEO	11.01	-2.35	5.75	5.76	3.61	2	4.76	K5	III
4301D	ALF	UMA	11.04	61.88	2.63	2.58	1.25	2	1.81	K0	II
4333			11.13	36.44	6.52	6.65	3.75	0	5.74	M3.5	
4335	PSI	UMA	11.14	44.62	3.90	3.85	2.44	2	3.03	K1	III
4337			11.13	-58.85	4.88	4.85	3.33	2	3.99	G0	I

YBS#	NAME		RA	DEC	S20	CDS	SIL	S	VIS	SP.TYPE	
4357	DEL	LEO	11.21	20.65	2.71	2.69	2.51	2	2.58	A4	V
4359	THE	LEO	11.22	15.57	3.35	3.35	3.31	2	3.34	A2	V
4362	72	LEO	11.23	23.22	5.59	5.64	3.15	2	4.66	M3	III
4377D	NU	UMA	11.29	33.22	4.45	4.42	2.69	2	3.49	K3	III
4382	DEL	CRT	11.30	-14.63	4.44	4.39	3.02	2	3.60	G8	III
4386	SIG	LEO	11.33	6.17	4.00	4.02	4.08	2	4.08	B9	V
4399D	IOT	LEO	11.38	10.67	4.24	4.24	3.73	2	3.93	F2	IV
4434	LAM	DRA	11.50	69.47	4.84	4.86	2.70	2	3.86	M0	III
4449			11.53	-30.95	5.97	6.05	3.46	0	5.09	M2	III
4450D	XI	HYA	11.53	-31.71	4.30	4.26	3.09	2	3.57	G7	III
4463D			11.57	-47.23	6.52	6.63	3.84	0	5.70	M3	III
4467D	LAM	CEN	11.58	-62.88	3.08	3.10	3.15	2	3.16	B9	II
4471	UPS	LEO	11.59	-0.68	5.08	5.03	3.81	2	4.32	G9	III
4483	OMG	VIR	11.62	8.27	6.07	6.22	3.22	0	5.34	M4	III
4517	NU	VIR	11.74	6.66	5.02	5.02	2.92	2	4.05	M1	III
4518	CHI	UMA	11.75	47.92	4.59	4.54	3.06	2	3.71	K0	III
4520D	LAM	MUS	11.74	-66.58	3.82	3.81	3.61	2	3.69	A7	II
4522			11.75	-61.03	4.69	4.67	3.64	0	4.10	G3	III
4532			11.79	-26.61	5.84	5.99	2.99	0	5.11	M4	III
4534D	BET	LEO	11.80	14.71	2.21	2.20	2.09	2	2.11	A3	V
4537			11.81	-63.65	3.98	3.97	3.32	1	4.38	B3	V
4540	BET	VIR	11.82	1.91	3.96	3.96	3.27	2	3.56	F8	V
4546			11.83	-45.03	5.38	5.34	3.78	0	4.45	K4	III
4554	GAM	UMA	11.88	53.84	2.43	2.42	2.43	2	2.42	A0	V
4603	THE2	CRU	12.05	-63.03	4.78	4.76	3.60	1	4.73	R3	IV
4608	OMI	VIR	12.07	8.87	4.86	4.82	3.63	2	4.12	G8	III
4621D	DEL	CEN	12.12	-50.58	2.03	2.15	2.44	2	2.51	B2	V
4623	ALF	CRV	12.12	-24.58	4.22	4.22	3.83	1	4.00	F2	V
4630	EPS	CRV	12.15	-22.48	3.98	3.94	2.30	2	3.03	K3	III
4638	RHO	CEN	12.17	-52.23	3.66	3.73	3.99	1	4.01	B4	V
4656	DEL	CRU	12.23	-58.61	2.31	2.44	2.90	2	2.88	B2	IV
4660	DEL	UMA	12.24	57.17	3.41	3.40	3.30	2	3.32	A3	V
4662	GAM	CRV	12.24	-17.40	2.38	2.43	2.60	2	2.59	B8	III
4671	EPS	MUS	12.27	-67.81	4.76	4.95	1.74	0	4.13	M5	III
4679D	ZET	CRU	12.28	-63.86	3.93	3.92	3.87	1	4.07	B3	IV
4682D			12.29	-55.00	5.82	5.93	3.14	0	5.00	M3	
4689	ETA	VIR	12.31	-0.53	3.92	3.92	3.89	2	3.88	A2	V
4700	EPS	CRU	12.33	-60.26	4.59	4.57	2.82	2	3.64	K3	
4726	71	UMA	12.40	56.92	6.63	6.74	3.95	0	5.81	M3	
4737	GAM	COM	12.43	28.40	5.21	5.15	3.78	2	4.34	K1	III
4739			12.44	-58.85	6.23	6.38	3.38	0	5.50	M4	
4743	SIG	CEN	12.44	-50.10	3.52	3.61	3.94	1	3.92	B2	V
4745	73	UMA	12.44	55.85	6.49	6.57	3.98	0	5.61	M2	
4755			12.48	-41.60	6.75	6.90	3.90	0	6.02	M4	
4757D	DEL	CRV	12.48	-16.38	2.90	2.91	2.98	2	2.96	B9.5	V
4763D	GAM	CRU	12.50	-56.97	2.61	2.68	0.05	2	1.73	M3	II
4765	4	DRA	12.48	69.34	5.73	5.88	2.88	0	5.00	M4	
4773	GAM	MUS	12.52	-72.00	3.50	3.60	3.92	2	3.91	B5	V
4785	BET	CVN	12.54	41.49	4.66	4.66	3.96	2	4.26	G0	V
4786	BET	CRV	12.55	-23.26	3.34	3.30	2.20	2	2.65	G5	III

YBS#	NAME	RA	DEC	S20	CDS	SIL	S	VIS	SP.TYPE
4787	KAP DRA	12.54	69.92	3.53	3.61	3.85	2	3.87	B7
4798D	ALF MUS	12.59	-69.00	2.16	2.29	2.73	2	2.71	B3 IV
4800	T UMA	12.59	59.62	6.23	6.38	3.38	0	5.50	M4
4802	TAU CEN	12.61	-48.40	3.93	3.93	3.86	2	3.90	A2 V
4807		12.62	1.99	6.53	6.64	3.85	0	5.71	M3
4823		12.67	-59.55	2.97	2.97	2.57	1	4.96	B7 IV
4846	Y CVN	12.73	45.57	6.30	6.53	3.53	2	5.30	C54
4853D	BET CRU	12.77	-59.56	0.68	0.83	1.32	2	1.31	B0.5 IV
4888		12.86	-48.81	5.26	5.23	3.59	0	4.31	K2
4898D	MU1 CRU	12.89	-57.05	3.67	3.75	4.09	1	4.07	B3 IV
4902	PSI VIR	12.88	- 9.41	5.67	5.73	3.23	2	4.77	M3 III
4905	EPS UMA	12.88	56.09	1.77	1.77	1.77	2	1.78	A0
4909		12.90	47.34	6.46	6.65	3.44	0	5.83	M5 III
4910	DEL VIR	12.91	3.52	4.31	4.36	1.84	2	3.41	M3 III
4915D	ALF2 CVN	12.91	38.45	2.74	2.79	2.96	2	2.94	B9.5
4920	36 COM	12.96	17.55	5.76	5.77	3.64	2	4.79	M0 III
4923	DEL MUS	13.01	-71.42	4.53	4.48	2.99	2	3.66	K2 III
4932	EPS VIR	13.02	11.10	3.59	3.54	2.39	2	2.85	G9 II
4942D	XI2 CEN	13.09	-49.77	3.88	3.97	4.29	1	4.28	B2 V
4949	40 COM	13.09	22.75	6.25	6.44	3.23	0	5.62	M5 III
4954	41 COM	13.10	27.77	5.80	5.79	3.83	2	4.82	K5 III
4983	BET COM	13.18	28.01	4.62	4.62	3.92	2	4.21	G0
5015	SIG VIR	13.27	5.60	5.67	5.75	3.16	0	4.79	M2
5020	GAM HYA	13.29	-23.05	3.69	3.64	2.51	2	2.98	G8 III
5028	IOT CEN	13.32	-36.58	2.79	2.79	2.73	2	2.75	A2 V
5035D		13.35	-60.85	2.28	2.28	2.25	1	4.53	B5 V
5056	ALF VIR	13.40	-11.02	0.38	0.52	1.00	2	0.98	B1 V
5062	80 UMA	13.40	55.13	4.14	4.12	3.92	2	3.99	A5 V
5064	68 VIR	13.42	-12.57	6.19	6.22	3.98	0	5.23	M0 III
5080D	R HYA	13.47	-23.15	8.19	8.89	3.18	2	8.42	M7
5095	74 VIR	13.51	- 6.12	5.70	5.74	3.41	2	4.74	M2 III
5101	S VIR	13.53	- 7.07	6.34	6.63	3.03	0	6.00	M7
5107	ZET VIR	13.56	- 0.47	3.46	3.45	3.34	2	3.35	A3 V
5132D	EPS CEN	13.64	-53.34	1.77	1.91	2.37	2	2.35	B1 V
5134		13.64	-49.82	6.17	6.51	2.74	0	6.00	M8 III
5150	82 VIR	13.67	- 8.57	5.88	5.96	3.37	0	5.00	M2 III
5154	83 UMA	13.66	54.81	5.64	5.67	3.36	2	4.67	M2 III
5190	NU CEN	13.80	-41.56	2.85	2.98	3.45	2	3.42	B2 IV
5191	ETA UMA	13.78	49.44	1.46	1.56	1.90	2	1.87	B3 V
5192	2 CEN	13.80	-34.32	4.70	4.88	1.71	1	4.21	M4 III
5193D	MU CEN	13.80	-42.36	2.94	3.06	3.47	2	3.46	B2 V
5200	UPS BOO	13.80	15.92	5.03	5.03	3.03	2	4.06	K5 III
5219		13.84	34.56	5.71	5.77	3.25	2	4.78	K5 III
5226D	10 DRA	13.85	64.84	5.51	5.56	2.99	2	4.61	M3
5228		13.88	-28.46	5.37	5.32	3.97	0	4.55	K0
5231	ZET CEN	13.90	-47.17	1.98	2.11	2.59	2	2.56	B2 IV
5235	ETA BOO	13.89	18.52	3.10	3.08	2.37	2	2.65	G0 IV
5248	PHI CEN	13.95	-41.98	3.40	3.50	3.86	1	3.86	B2 IV
5249	UPS1 CEN	13.95	-44.68	3.46	3.55	3.91	1	3.83	B2 V
5261	THE APS	14.05	-76.68	6.23	6.38	3.38	0	5.50	M4

YBS#	NAME	RA	DEC	S20	CDS	SIL	S	VIS	SP.TYPE
5267D	BET CEN	14.03	-60.25	-0.00	0.14	0.64	2	0.63	B1 II
5285	CHI CEN	14.08	-41.06	3.97	4.06	4.39	1	4.33	B3 V
5287	PI HYA	14.08	-26.56	4.08	4.03	2.62	2	3.23	K2 III
5288	THE CEN	14.09	-36.26	3.35	3.30	2.03	2	2.57	K0 III
5291	ALF DRA	14.06	64.49	3.58	3.59	3.67	2	3.65	A0 III
5299		14.12	43.97	6.03	6.16	3.05	2	5.27	M4 III
5300	13 BOO	14.12	49.58	6.13	6.21	3.62	0	5.25	M2
5301		14.16	-16.18	5.70	5.81	3.02	0	4.88	M3
5315	KAP VIR	14.19	-10.17	5.14	5.10	3.41	2	4.20	K3 III
5326D	R CEN	14.25	-59.80	6.03	6.18	3.18	0	5.30	M4
5334		14.19	69.55	6.12	6.20	3.61	0	5.24	M2
5338	IOT VIR	14.25	-5.88	4.43	4.43	3.79	2	4.07	F7 IV
5339	DEL OCT	14.38	-83.55	5.16	5.11	3.71	0	4.31	K1
5340	ALF BOO	14.24	19.31	0.83	0.79	-0.81	2	-0.07	K2 III
5352		14.27	15.38	6.68	6.79	4.00	0	5.86	M3
5354	IOT LUP	14.30	-45.95	3.10	3.21	3.57	2	3.55	B3 IV
5367D	PSI CEN	14.32	-37.78	4.03	4.04	3.98	0	4.04	A0 IV
5404	THE BOO	14.41	51.97	4.38	4.38	3.80	2	4.03	F7 V
5429D	RHO BOO	14.51	30.49	4.53	4.49	2.88	2	3.60	K3 III
5430D	5 UMI	14.46	75.80	5.23	5.20	3.44	2	4.25	K4 III
5435D	GAM BOO	14.52	38.42	3.24	3.22	2.99	2	3.05	A7 III
5440D	ETA CEN	14.57	-42.04	1.85	1.98	2.39	2	2.38	B1.5 V
5453	RHO LUP	14.60	-49.31	3.82	3.88	4.02	0	4.04	B5 V
5459D	ALF CEN	14.63	-60.73	0.28	0.25	-0.65	2	-0.28	G2 V
5463D	ALF CIR	14.67	-64.86	3.39	3.38	3.08	2	3.19	F0 V
5469D	ALF LUP	14.67	-47.29	1.80	1.93	2.37	2	2.36	B2 II
5470	ALF APS	14.75	-78.93	4.85	4.82	3.08	2	3.87	K5 III
5471		14.67	-37.69	3.56	3.66	4.01	2	3.99	B3 V
5485		14.70	-35.07	4.99	4.96	3.32	0	4.04	K5 III
5487	MU VIR	14.70	-5.54	4.12	4.12	3.64	2	3.85	F3 IV
5490	34 BOO	14.71	26.62	5.74	5.79	3.31	2	4.80	M3
5511	109 VIR	14.75	2.00	3.71	3.71	3.72	2	3.72	A0 V
5512		14.75	15.24	6.45	6.64	3.43	0	5.82	M5
5526	58 HYA	14.81	-27.86	5.24	5.23	3.55	1	4.41	K4
5531D	ALF2 LIB	14.82	-15.95	2.90	2.89	2.71	2	2.76	A
5540	R APS	14.92	-76.55	5.96	5.99	3.75	0	5.00	M0
5563	BET UMI	14.85	74.25	3.08	3.06	1.22	2	2.10	K4 III
5571	BET LUP	14.95	-43.03	2.15	2.28	2.72	2	2.70	B2 IV
5576D	KAP CEN	14.96	-42.00	2.64	2.75	3.16	2	3.14	B2 V
5589		14.95	66.03	5.50	5.62	2.58	2	4.73	M5 III
5600	OMG BOO	15.02	25.10	5.80	5.79	3.84	2	4.82	K4 III
5601	110 VIR	15.03	2.18	5.14	5.09	3.79	2	4.34	K0 III
5602	BET BOO	15.02	40.48	4.24	4.20	3.03	2	3.50	G8 III
5603	SIG LIB	15.04	-25.18	4.23	4.29	1.71	2	3.31	M4 III
5616	PSI BOO	15.06	27.05	5.43	5.38	3.84	2	4.51	K2 III
5646D	KAP LUP	15.17	-48.64	3.66	3.68	3.66	0	3.71	B9 V
5649D	ZET LUP	15.17	-52.00	4.10	4.05	2.92	2	3.39	G8 III
5654		15.18	19.06	6.51	6.66	3.66	0	5.78	M4
5670	BET CIR	15.26	-58.71	4.15	4.15	3.98	0	4.06	A3 V
5671	GAM TRA	15.28	-68.59	2.93	2.94	2.88	2	2.91	A1 V

YBS#	NAME	RA	DEC	S20	CDS	SIL	S	VIS	SP.TYPE
5681D	DEL BOO	15.24	33.41	4.24	4.19	2.99	2	3.50	G8 III
5685	BET LIB	15.26	-9.29	2.40	2.45	2.62	2	2.62	R8 V
5686	2 LUP	15.27	-30.06	5.06	5.03	3.74	1	4.32	K0
5695	DEL LUP	15.33	-40.56	2.68	2.81	3.27	2	3.25	B2 IV
5705D	PHI1 LUP	15.34	-36.17	4.56	4.56	2.57	2	3.59	K5 III
5735	GAM UMI	15.35	71.92	3.10	3.10	2.97	2	3.04	A3 II
5739	TAU1 SER	15.41	15.52	6.10	6.15	3.74	0	5.17	M1 III
5744	IDT DRA	15.41	59.05	4.19	4.14	2.70	2	3.31	K2 III
5747	BET CRB	15.45	29.19	3.91	3.89	3.62	2	3.66	F0 III
5763	NU1 BOO	15.50	40.92	6.06	6.07	4.00	2	5.07	K5 III
5771D	EPS TRA	15.57	-66.23	4.92	4.87	3.52	0	4.10	K0 III
5778	THE CRB	15.53	31.45	3.85	3.93	4.19	2	4.16	R7
5787D	GAM LIB	15.57	-14.70	4.66	4.62	3.37	2	3.90	G8 III
5793	ALF CRB	15.56	26.80	2.19	2.20	2.23	2	2.22	A0 V
5794D	UPS LIB	15.59	-28.05	4.51	4.49	2.76	2	3.56	K5 III
5797D	OMG LUP	15.61	-42.48	5.28	5.31	3.07	0	4.32	M0 III
5800	MU CRB	15.57	39.10	6.01	6.09	3.50	0	5.13	M2
5806		15.61	-23.07	6.53	6.89	2.68	2	5.89	K0
5812	TAU LIB	15.62	-29.70	3.21	3.31	3.67	2	3.64	B2.5 V
5838	KAP LIB	15.68	-19.59	5.75	5.76	3.66	2	4.78	K5 III
5849D	GAM CRB	15.69	26.38	3.83	3.83	3.84	2	3.83	A0 IV
5854D	ALF SER	15.72	6.50	3.53	3.48	2.05	2	2.64	K2 III
5867D	BET SER	15.75	15.50	3.76	3.74	3.66	2	3.67	A2 IV
5879	KAP SER	15.79	18.21	5.09	5.11	2.92	2	4.11	M1 III
5881	MU SER	15.81	-3.34	3.50	3.52	3.57	2	3.56	A0 V
5883	CHI LUP	15.82	-33.54	3.89	3.90	3.96	1	4.02	A0 III
5892	EPS SER	15.83	4.56	3.86	3.85	3.69	2	3.72	A
5894	R SER	15.83	15.21	5.94	6.23	2.63	0	5.60	M7
5897	BET TRA	15.88	-63.35	3.03	3.02	2.66	2	2.81	F2 IV
5899	RHO SER	15.84	21.06	5.74	5.74	3.74	2	4.76	K5 III
5908	THE LIB	15.87	-16.66	4.90	4.86	3.58	2	4.11	K0 III
5928D	RHO SCO	15.92	-29.14	3.35	3.47	3.88	2	3.86	B2 V
5932	2 HER	15.90	43.22	6.17	6.28	3.49	0	5.35	M3 III
5933	GAM SER	15.92	15.73	4.15	4.15	3.56	2	3.83	F6 IV
5944D	PI SCO	15.96	-26.05	2.40	2.53	2.94	2	2.93	B1 V
5947D	EPS CRB	15.94	26.95	5.05	5.01	3.48	2	4.15	K3 III
5948D	ETA LUP	15.97	-38.33	2.84	2.97	3.43	2	3.40	B2 V
5953	DEL SCO	15.98	-22.55	1.83	1.97	2.30	2	2.33	R0 V
5984D	BET1 SCO	16.07	-19.73	2.11	2.23	2.52	2	2.53	R0.5 V
5986	THE DRA	16.02	58.63	4.38	4.37	3.74	2	4.00	F8 IV
5987	THE LUP	16.08	-36.73	3.88	3.96	4.26	1	4.32	B2 V
5993	OMG1 SCO	16.09	-20.60	3.58	3.70	3.94	2	3.96	B1 V
5997	OMG2 SCO	16.10	-20.80	4.95	4.92	3.90	2	4.30	G2
6001		16.11	-26.27	6.27	6.35	3.76	0	5.39	M2
6010	47 SER	16.12	8.60	6.54	6.65	3.86	0	5.72	M3
6020D	DEL1 APS	16.28	-78.64	5.46	5.61	2.61	0	4.73	M4 III
6027D	NU SCO	16.18	-19.40	3.76	3.85	3.91	2	3.99	R2 IV
6030D	DEL TRA	16.22	-63.62	4.65	4.60	3.28	2	3.82	G2 II
6039	10 HER	16.18	23.55	6.69	6.84	3.84	0	5.96	M4
6055		16.25	-53.75	6.18	6.26	3.67	0	5.30	M2

YBS#	NAME		RA	DEC	S20	CDS	SIL	S	VIS	SP.TYPE	
6056	DEL	OPH	16.22	- 3.62	3.71	3.73	1.54	2	2.74	M1	III
6072D	GAM2	NOR	16.30	-50.10	4.76	4.73	3.45	0	4.01	G8	III
6075	EPS	OPH	16.28	- 4.64	3.98	3.94	2.72	2	3.23	G9	III
6081	OMI	SCO	16.32	-24.11	5.15	5.13	3.82	1	4.51	A5	II
6084D	SIG	SCO	16.33	-25.52	2.70	2.79	2.72	2	2.87	B1	III
6086			16.28	59.81	6.24	6.39	3.39	0	5.51	M4	
6092D	TAU	HER	16.32	46.37	3.57	3.65	3.94	2	3.92	B5	IV
6095D	GAM	HER	16.35	19.21	4.01	3.98	3.60	2	3.75	A9	III
6102	GAM	APS	16.49	-78.83	4.57	4.52	3.39	2	3.86	K0	IV
6107	NU1	CRB	16.36	33.86	6.08	6.16	3.57	0	5.20	M2	
6119	U	HER	16.41	18.94	7.04	7.33	3.73	0	6.70	M7	
6128			16.44	- 7.54	6.12	6.20	3.61	0	5.24	M2	III
6132D	ETA	DRA	16.39	61.56	3.44	3.40	2.29	2	2.73	G8	III
6134D	ALF	SCO	16.46	-26.38	1.93	2.03	-0.60	2	1.00	M1	I
6143			16.50	-34.65	3.85	3.94	4.24	1	4.35	B2	IV
6146	30	HER	16.46	41.94	5.55	5.84	1.99	2	5.06	M6	III
6147D	PHI	OPH	16.50	-16.56	4.98	4.93	3.85	2	4.25	G8	III
6148	BET	HER	16.49	21.54	3.51	3.46	2.34	2	2.78	G8	III
6149D	LAM	OPH	16.49	2.04	3.84	3.83	3.79	2	3.81	A1	V
6159	29	HER	16.52	11.54	5.82	5.82	3.88	2	4.85	K4	III
6163D	BET	APS	16.66	-77.46	5.05	5.00	3.65	0	4.23	K0	III
6165	TAU	SCO	16.57	-28.17	2.18	2.33	2.85	2	2.81	B0	V
6166			16.58	-35.20	5.12	5.09	3.37	0	4.15	K6	
6175	ZET	OPH	16.60	-10.52	2.21	2.34	2.52	2	2.57	O9.5	V
6200D	42	HER	16.63	48.97	5.78	5.86	3.27	0	4.90	M2	
6212D	ZET	HER	16.67	31.65	3.24	3.23	2.44	2	2.77	G0	IV
6217	ALF	TRA	16.77	-68.99	2.92	2.89	1.15	2	1.93	K4	III
6220	ETA	HER	16.70	38.98	4.21	4.17	3.05	2	3.51	G7	III
6227			16.74	15.80	6.46	6.57	3.78	0	5.64	M3	
6229D	ETA	ARA	16.79	-59.00	4.75	4.76	2.68	2	3.78	K5	III
6241	EPS	SCO	16.81	-34.25	3.17	3.12	1.73	2	2.29	K2	III
6242			16.78	42.28	6.71	6.86	3.86	0	5.98	M4	
6247D	MU1	SCO	16.84	-38.01	2.49	2.62	3.02	2	3.02	B1.5	V
6252D	MU2	SCO	16.84	-37.97	3.06	3.19	3.62	2	3.61	R2	IV
6257			16.87	-43.01	6.40	6.55	3.55	0	5.67	M4	
6271	ZET	SCO	16.88	-42.31	4.60	4.57	2.81	2	3.64	K5	III
6285	ZET	ARA	16.94	-55.95	4.14	4.15	2.13	2	3.14	K5	III
6295	EPS1	ARA	16.96	-53.11	4.96	4.91	3.41	0	4.05	K3	III
6299	KAP	OPH	16.94	9.42	4.08	4.03	2.60	2	3.21	K2	III
6308			16.97	-25.05	6.68	6.79	4.00	0	5.86	M3	
6322D	EPS	UMI	16.81	82.07	4.89	4.85	3.75	2	4.20	G5	III
6324	EPS	HER	16.99	30.95	3.88	3.89	3.93	2	3.93	A0	V
6337			17.03	14.12	5.94	5.99	3.52	2	5.02	M3	III
6380	ETA	SCO	17.17	-43.20	3.67	3.66	3.15	2	3.34	F0	IV
6393D	37	OPH	17.19	10.61	6.21	6.29	3.70	0	5.33	M2	
6396	ZET	DRA	17.15	65.75	2.92	2.99	3.19	2	3.19	B6	III
6406D	ALF1	HER	17.23	14.41	3.72	3.92	0.49	2	3.14	M5	II
6410D	DEL	HER	17.23	24.86	3.21	3.21	3.08	2	3.13	A3	IV
6418	PI	HER	17.24	36.83	4.16	4.13	2.38	2	3.18	K3	II
6452			17.32	18.09	5.88	5.96	3.37	0	5.00	M2	

YBS#	NAME	RA	DEC	S20	CDS	SIL	S	VIS	SP.TYPE
6453	THE OPH	17.34	-24.97	2.75	2.87	3.29	2	3.26	R2 IV
6461	BET ARA	17.39	-55.51	3.85	3.82	2.06	2	2.84	K3 I
6462D	GAM ARA	17.39	-56.36	2.81	2.95	3.32	2	3.34	R1 III
6498	SIG OPH	17.42	4.17	5.35	5.33	3.50	2	4.35	K3 II
6500D	DEL ARA	17.48	-60.66	3.44	3.50	3.66	2	3.73	B8 V
6508	UPS SCO	17.48	-37.28	2.16	2.28	2.72	2	2.68	R3 I
6510D	ALF ARA	17.50	-49.86	2.41	2.53	2.76	2	2.86	R2.5 V
6526	LAM HER	17.50	26.12	5.41	5.38	3.62	2	4.43	K4 III
6527	LAM SCO	17.53	-37.08	1.08	1.21	1.67	2	1.63	B1 V
6536D	BET DRA	17.50	52.33	3.53	3.49	2.33	2	2.80	G2 II
6546		17.58	-38.62	5.10	5.05	3.70	0	4.28	K0 III
6553	THE SCO	17.59	-42.98	2.17	2.15	1.62	2	1.83	F0 I
6556	ALF OPH	17.56	12.58	2.24	2.23	2.03	2	2.09	A5 III
6561D	XI SER	17.60	-15.38	3.76	3.74	3.40	2	3.53	F0 IV
6580	KAP SCO	17.68	-39.02	1.85	1.98	2.45	2	2.41	B2 IV
6582	ETA PAV	17.72	-64.72	4.47	4.42	2.98	2	3.58	K1 III
6588	IOT HER	17.65	46.03	3.39	3.49	3.84	2	3.83	R3 V
6603	BET OPH	17.70	4.58	3.66	3.61	2.17	2	2.78	K2 III
6615D	IOT1 SCO	17.76	-40.11	3.49	3.45	2.75	2	3.02	F2 I
6623D	MU HER	17.76	27.75	4.00	3.96	3.07	2	3.43	G5 IV
6629	GAM OPH	17.78	2.72	3.78	3.78	3.74	2	3.75	A0 V
6630		17.80	-37.04	4.06	4.02	2.53	2	3.18	K1 III
6688	XI DRA	17.88	56.87	4.63	4.58	3.11	2	3.75	K2 III
6693D		17.96	-30.26	6.15	6.23	3.64	0	5.27	M2 I
6695	THE HER	17.92	37.25	4.83	4.79	3.22	2	3.86	K1 II
6698	NU OPH	17.96	-9.78	4.11	4.05	2.85	2	3.32	G9 III
6702		17.93	45.35	6.72	6.95	3.54	0	6.22	M6
6703	XI HER	17.95	29.25	4.45	4.40	3.24	2	3.72	G9 III
6705D	GAM DRA	17.93	51.49	3.24	3.24	1.26	2	2.26	K5 III
6714D	67 OPH	17.99	2.93	3.75	3.84	3.92	2	3.97	B5 I
6743	THE ARA	18.08	-50.10	3.23	3.36	3.65	2	3.66	B0.5 II
6746	GAM SGR	18.07	-30.43	3.81	3.76	2.49	2	2.99	K0 III
6765	98 HER	18.08	22.23	5.94	6.02	3.43	0	5.06	M2
6771D	72 OPH	18.10	9.56	3.87	3.85	3.69	2	3.74	A4 V
6779	OMI HER	18.11	28.76	3.79	3.80	3.81	2	3.83	B9 V
6787D	102 HER	18.13	20.81	3.90	4.02	4.39	2	4.38	B2 V
6812D	MU SGR	18.20	-21.06	3.93	3.97	3.68	2	3.86	B8 I
6815	104 HER	18.18	31.40	5.79	5.90	3.11	0	4.97	M3
6832D	ETA SGR	18.27	-36.77	4.02	4.06	1.59	2	3.11	M3 II
6834		18.25	2.37	6.73	6.88	3.88	0	6.00	M4
6842		18.27	-27.06	5.52	5.53	3.57	1	4.63	K5
6855D	XI PAV	18.35	-61.50	5.24	5.19	3.75	0	4.36	K2 III
6859D	DEL SGR	18.32	-29.83	3.69	3.65	1.98	2	2.70	K2 III
6861		18.33	-24.93	6.88	7.07	3.86	0	6.25	M5
6868	106 HER	18.32	21.95	5.91	5.94	3.73	2	4.94	M0 III
6869	ETA SER	18.33	-2.89	3.95	3.91	2.72	2	3.23	K0 IV
6872	KAP LYR	18.32	36.05	5.23	5.18	3.74	2	4.35	K2 III
6879D	EPS SGR	18.38	-34.40	1.81	1.82	1.84	2	1.85	B9 IV
6891		18.35	49.10	5.93	6.01	3.42	0	5.05	M2
6895	109 HER	18.38	21.75	4.72	4.68	3.20	2	3.84	K2 III

YBS#	NAME		RA	DEC	S20	CDS	SIL	S	VIS	SP.TYPE	
6896D	21	SGR	18.40	-20.56	5.68	5.67	3.91	2	4.79	K2	II
6897	ALF	TEL	18.42	-45.98	3.13	3.23	3.56	2	3.55	R3	III
6905	ZET	TEL	18.45	-49.08	4.88	4.83	3.57	2	4.13	K0	
6913	LAM	SGR	18.44	-25.45	3.65	3.59	2.30	2	2.81	K2	III
6973	ALF	SCT	18.56	- 8.27	4.80	4.77	3.11	2	3.86	K3	III
6982D	ZET	PAV	18.67	-71.45	4.87	4.83	3.39	2	4.01	K2	III
6991			18.63	-43.20	6.18	6.26	3.67	0	5.30	M2	
7001D	ALF	LYR	18.60	38.76	0.05	0.05	0.04	2	0.04	A0	V
7009	XY	LYR	18.62	39.65	6.53	6.68	3.68	0	5.80	M4	
7039	PHI	SGR	18.74	-27.02	2.95	3.01	3.18	2	3.16	B8	III
7061D	110	HER	18.74	20.52	4.50	4.50	3.97	2	4.19	F6	V
7063	BET	SCT	18.76	- 4.77	5.03	4.99	3.59	2	4.21	G5	II
7074D	LAM	PAV	18.83	-62.21	3.26	3.32	3.35	1	4.33	R1	V
7106D	BET	LYR	18.82	33.34	3.12	3.21	3.29	2	3.37	R7	V
7107	KAP	PAV	18.91	-67.28	4.28	4.26	3.68	0	3.90	F5	
7121	SIG	SGR	18.90	-26.33	1.59	1.69	2.08	2	2.03	B2	V
7139D	DEL2	LYR	18.89	36.87	5.06	5.18	2.19	2	4.25	M4	II
7150	XI2	SGR	18.94	-21.13	4.38	4.33	2.88	2	3.49	K1	III
7157	13	LYR	18.91	43.92	4.82	5.00	1.62	2	4.14	M5	III
7176	EPS	AQL	18.97	15.03	4.88	4.83	3.52	2	4.05	K2	III
7178D	GAM	LYR	18.97	32.65	3.17	3.19	3.23	2	3.24	B9	III
7193	12	AQL	19.01	- 5.78	4.86	4.81	3.47	2	4.03	K1	III
7217D	OMI	SGR	19.05	-21.77	4.53	4.49	3.21	2	3.75	G8	
7234	TAU	SGR	19.09	-27.70	4.20	4.15	2.70	2	3.31	K1	III
7235D	ZET	AQL	19.07	13.83	2.99	2.99	2.97	2	2.98	A0	V
7236	LAM	AQL	19.08	- 4.92	3.28	3.31	3.46	2	3.44	B9	V
7242	DEL	CRA	19.11	-40.54	5.43	5.38	3.98	0	4.58	K1	
7243	R	AQL	19.09	8.20	5.84	6.13	2.53	0	5.50	M7	
7259	BET	CRA	19.14	-39.37	5.01	4.96	3.53	2	4.11	G3	
7310	DEL	DRA	19.21	67.62	3.85	3.81	2.58	2	3.08	G9	III
7314	JHE	LYR	19.26	38.09	5.26	5.21	3.70	2	4.34	K0	II
7328	KAP	CYG	19.28	53.32	4.51	4.47	3.30	2	3.77	K0	III
7337D	BET1	SGR	19.35	-44.51	3.92	3.95	3.97	0	4.01	R8	V
7340	RHO1	SGR	19.34	-17.90	4.11	4.09	3.80	2	3.91	F0	IV
7348	ALF	SGR	19.37	-40.66	3.91	3.93	3.91	0	3.96	B9	III
7352	TAU	DRA	19.27	73.30	5.39	5.34	3.80	2	4.46	K3	III
7377	DEL	AQL	19.40	3.07	3.58	3.57	3.20	2	3.35	F0	IV
7405	ALF	VUL	19.46	24.62	5.43	5.43	3.34	2	4.48	M0	III
7414	36	AQL	19.49	- 2.84	5.95	6.00	3.59	0	5.02	M1	III
7417D	BET	CYG	19.50	27.91	3.87	3.86	2.39	2	3.09	K5	II
7420	IOT	CYG	19.48	51.68	3.93	3.92	3.72	2	3.79	A5	V
7429D	MU	AQL	19.55	7.33	5.34	5.29	3.84	2	4.46	K3	III
7442			19.55	49.20	6.79	6.94	3.94	0	6.06	M4	
7488	BET	SGE	19.67	17.42	5.21	5.16	3.90	2	4.40	G8	II
7509			19.69	55.39	5.98	6.17	2.96	0	5.35	M5	
7525	GAM	AQL	19.75	10.55	3.75	3.73	1.89	2	2.75	K3	II
7528D	DEL	CYG	19.74	45.07	2.84	2.85	2.89	2	2.90	B9.5	III
7536	DEL	SGE	19.77	18.47	4.70	4.75	2.37	2	3.87	M2	II
7557D	ALF	AQL	19.83	8.80	0.92	0.91	0.65	2	0.74	A7	V
7564	CHI	CYG	19.83	32.85	7.88	8.71	3.03	2	8.40	S71	

YBS#	NAME	RA	DEC	S20	CDS	SIL	S	VIS	SP.TYPE
7566D	19 CYG	19.83	38.65	6.08	6.16	3.57	0	5.20	M2
7570	ETA AQL	19.85	0.94	4.52	4.48	3.38	2	3.81	F6 I
7581	IOT SGR	19.89	-41.93	4.95	4.92	3.56	2	4.12	K0 III
7582D	EPS DRA	19.80	70.20	4.54	4.50	3.41	2	3.86	G8 III
7590	EPS PAV	19.96	-72.97	3.93	3.94	3.95	2	3.95	A0 V
7602D	BET AQL	19.90	6.34	4.37	4.34	3.29	2	3.73	G8 IV
7604	59 SGR	19.92	-27.23	5.37	5.35	3.69	1	4.50	K3
7615D	ETA CYG	19.96	35.02	4.69	4.64	3.38	2	3.90	K0 III
7625		19.99	-59.45	5.50	5.73	2.32	0	5.00	M6
7635	GAM SGE	19.96	19.42	4.54	4.55	2.49	2	3.56	K5 III
7645D	13 SGE	19.98	17.45	6.12	6.27	3.27	0	5.39	M4
7650	62 SGR	20.02	-27.77	5.46	5.54	2.77	2	4.59	M4 III
7652		20.03	-38.00	5.74	5.72	3.96	2	4.77	K5
7665	DEL PAV	20.10	-66.25	4.18	4.14	3.22	2	3.56	G8 V
7673	XI TEL	20.09	-52.95	5.92	5.93	3.78	2	4.93	M2 III
7676	64 DRA	20.02	64.75	6.20	6.25	3.84	0	5.27	M1 III
7680D		20.07	15.43	6.26	6.34	3.75	0	5.38	M2 III
7685	RHD DRA	20.05	67.80	5.48	5.44	3.83	2	4.53	K3 III
7704		20.08	67.95	6.32	6.37	3.96	0	5.39	M1
7710	THE AQL	20.17	-0.89	3.09	3.11	3.20	2	3.19	B9.5 III
7735D	OMI1 CYG	20.21	46.66	4.61	4.62	2.98	2	3.80	K2 II
7744	23 VUL	20.25	27.72	5.41	5.39	3.76	2	4.52	K3 III
7747D	ALF1 CAP	20.27	-12.58	5.04	5.00	3.72	2	4.24	G3 I
7751	OMI2 CYG	20.24	47.62	4.96	4.99	2.97	2	4.04	K3 I
7754D	ALF2 CAP	20.28	-12.61	4.31	4.27	3.11	2	3.59	G9 III
7776D	BET CAP	20.33	-14.86	3.66	3.64	2.62	2	3.08	F8 V
7790	ALF PAV	20.39	-56.81	1.52	1.63	1.99	2	1.94	B3 IV
7796D	GAM CYG	20.36	40.17	2.80	2.75	1.92	2	2.22	F8 I
7804		20.33	68.80	6.62	6.81	3.60	0	5.99	M5
7806	39 CYG	20.38	32.10	5.38	5.35	3.65	2	4.44	K3 III
7834	41 CYG	20.47	30.28	4.36	4.33	3.78	2	3.99	F5 II
7851	OMG2 CYG	20.51	49.13	6.30	6.38	3.79	0	5.42	M2
7852	EPS DEL	20.53	11.22	3.74	3.81	4.05	2	4.04	B6 III
7866	47 CYG	20.55	35.16	5.55	5.60	3.49	2	4.64	K2 I
7869D	ALF IND	20.60	-47.37	3.90	3.86	2.63	2	3.11	K0 III
7884D	71 AQL	20.62	-1.19	5.04	4.99	3.81	2	4.31	G8 III
7886		20.61	18.18	6.77	7.00	3.59	0	6.27	M6
7900	UPS CAP	20.64	-18.22	5.98	6.06	3.47	0	5.10	M2 III
7906D	ALF DEL	20.64	15.83	3.65	3.68	3.77	2	3.77	B9 V
7913	BET PAV	20.71	-66.29	3.62	3.60	3.36	2	3.42	A5 IV
7924D	ALF CYG	20.68	45.18	1.25	1.28	1.18	2	1.28	A2 I
7936	PSI CAP	20.74	-25.36	4.43	4.43	3.92	2	4.13	F5 V
7941	U DEL	20.74	18.01	6.23	6.42	3.21	0	5.60	M5 II
7942D	52 CYG	20.74	30.62	5.00	4.95	3.66	2	4.20	K0 III
7949D	EPS CYG	20.75	33.87	3.24	3.19	1.92	2	2.46	K0 III
7950	EPS AQR	20.77	-9.59	3.79	3.79	3.76	2	3.78	A1 V
7951	3 AQR	20.77	-5.12	5.43	5.49	2.92	2	4.51	M3 III
7957D	ETA CEP	20.75	61.74	4.12	4.08	2.90	2	3.41	K0 IV
7980	OMG CAP	20.84	-27.02	5.11	5.14	3.02	2	4.12	K5 III
7986	BET IND	20.88	-58.55	4.59	4.55	3.06	2	3.65	K0 III

YBS#	NAME		RA	DEC	S20	CDS	SIL	S	VIS	SP.TYPE	
8028	NU	CYG	20.94	41.07	3.96	3.96	3.93	2	3.97	A0	V
8044			20.99	19.22	6.55	6.66	3.87	0	5.73	M3	
8079	XI	CYG	21.07	43.83	4.72	4.74	2.67	2	3.72	K5	I
8080D	24	CAP	21.09	-25.10	5.49	5.51	3.34	2	4.49	M1	III
8089D	63	CYG	21.10	47.55	5.58	5.57	3.62	2	4.57	K4	II
8092	OMI	PAV	21.18	-70.23	5.89	5.97	3.38	0	5.01	M2	III
8113	T	CEP	21.15	68.38	5.54	5.83	2.23	0	5.20	M7	
8115	ZET	CYG	21.20	30.13	4.00	3.95	2.77	2	3.22	G8	II
8128	29	CAP	21.24	-15.27	6.10	6.21	3.42	0	5.28	M3	
8130D	TAU	CYG	21.23	37.94	4.04	4.04	3.54	2	3.74	F0	IV
8131	ALF	EQU	21.24	5.15	4.32	4.29	3.59	2	3.89	G0	III
8146D	UPS	CYG	21.28	34.80	3.95	4.07	4.31	2	4.38	R2	V
8162D	ALF	CEP	21.30	62.48	2.64	2.63	2.35	2	2.45	A7	IV
8167	IOT	CAP	21.35	-16.94	4.96	4.92	3.83	2	4.27	G8	III
8173D	1	PEG	21.35	19.71	4.92	4.87	3.50	2	4.08	K1	III
8181	GAM	PAV	21.41	-65.48	4.54	4.55	3.93	2	4.22	F8	V
8196	SX	PAV	21.44	-69.61	5.54	5.83	2.23	0	5.20	M7	
8204D	ZET	CAP	21.42	-22.52	4.52	4.47	3.33	2	3.74	G4	I
8223			21.46	22.07	6.66	6.81	3.81	0	5.93	M4	
8225D	2	PEG	21.48	23.52	5.52	5.54	3.36	2	4.55	M1	III
8232D	BET	AQR	21.50	-5.69	3.55	3.51	2.49	2	2.89	G0	I
8238D	BET	CEP	21.47	70.44	2.61	2.76	3.28	2	3.24	R2	III
8252	RHO	CYG	21.55	45.49	4.66	4.63	3.48	2	3.98	G8	III
8262	W	CYG	21.58	45.27	5.91	6.25	2.18	2	5.46	M4	
8278	GAM	CAP	21.64	-16.78	3.97	3.94	3.56	2	3.68	A	
8284D	75	CYG	21.65	43.15	6.03	6.08	3.67	0	5.10	M1	III
8289	7	PEG	21.68	5.55	6.22	6.30	3.71	0	5.34	M2	
8306			21.70	41.04	6.27	6.35	3.76	0	5.39	M2	
8308D	EPS	PEG	21.72	9.77	3.43	3.42	1.60	2	2.42	K2	I
8313	9	PEG	21.72	17.23	5.14	5.10	3.72	2	4.29	G5	I
8316D	MU	CEP	21.71	58.67	4.95	5.19	1.81	2	4.10	M2	I
8317	11	CEP	21.69	71.20	5.39	5.33	3.98	2	4.53	K0	III
8322D	DEL	CAP	21.76	-16.25	3.11	3.11	2.72	2	2.86	A	
8334	NU	CEP	21.75	61.02	4.67	4.67	3.94	2	4.29	A2	I
8335	PI2	CYG	21.76	49.20	3.85	3.95	4.24	2	4.24	B3	III
8353	GAM	GRU	21.87	-37.48	2.81	2.87	3.04	2	3.01	B8	III
8383	VV	CEP	21.93	63.51	5.60	5.71	3.17	1	4.90	M2	I
8411	LAM	GRU	22.08	-39.67	5.31	5.28	3.64	1	4.46	K2	III
8413	NU	PEG	22.07	4.93	5.85	5.83	4.00	2	4.88	K4	III
8414	ALF	AQR	22.07	-0.44	3.71	3.67	2.50	2	2.95	G2	I
8416	18	CEP	22.05	63.00	5.91	6.10	2.89	0	5.28	M5	
8421			22.07	46.63	6.29	6.63	2.86	0	6.12	M8	
8425D	ALF	GRU	22.11	-47.09	1.47	1.54	1.76	2	1.74	R5	V
8430	IOT	PEG	22.10	25.21	4.05	4.05	3.50	2	3.75	F5	
8433	UPS	PSA	22.12	-34.17	5.92	5.97	3.56	0	4.99	M1	
8450	THE	PEG	22.15	6.07	3.62	3.61	3.51	2	3.53	A2	V
8465	ZET	CEP	22.17	58.07	4.39	4.37	2.54	2	3.37	K1	I
8481	EPS	OCT	22.29	-80.56	5.59	5.82	2.41	0	5.09	M6	III
8483			22.19	63.17	6.67	6.78	3.99	0	5.85	M3	
8485D			22.21	39.59	5.45	5.42	3.68	2	4.49	K3	III

YBS#	NAME	RA	DEC	S20	CDS	SIL	S	VIS	SP.TYPE
8498	1 LAC	22.25	37.62	5.11	5.08	3.34	2	4.12	K3 II
8499	THE AQR	22.26	- 7.91	4.93	4.88	3.68	2	4.16	G8 III
8518D	GAM AQR	22.34	- 1.51	3.78	3.80	3.86	2	3.86	B9 III
8521D		22.35	-46.07	7.28	7.59	3.57	2	6.62	S47
8538	BET LAC	22.38	52.11	5.18	5.14	3.86	2	4.41	G9 III
8556	DEL1 GRU	22.46	-43.61	4.79	4.74	3.50	2	3.97	G5
8560D	DEL2 GRU	22.47	-43.88	5.00	5.07	2.39	2	4.11	M4.5 III
8571D	DEL CEP	22.47	58.29	4.93	4.89	3.83	2	4.25	F5 I
8572	5 LAC	22.47	47.59	5.32	5.38	3.09	2	4.38	M0 I
8582	NU TUC	22.52	-62.11	5.67	5.76	2.95	2	4.80	M4
8585D	ALF LAC	22.50	50.15	3.75	3.75	3.75	2	3.75	A2 V
8597	ETA AQR	22.57	- 0.25	3.87	3.91	4.04	2	4.04	B8 V
8621D		22.63	56.67	5.82	5.97	2.97	0	5.09	M4
8628	EPS PSA	22.65	-27.18	3.98	4.01	4.18	1	4.19	B8 V
8632	11 LAC	22.66	44.14	5.42	5.38	3.73	2	4.49	K3 III
8634D	ZET PEG	22.67	10.70	3.24	3.28	3.42	2	3.42	B8 V
8636	BET GRU	22.69	-47.01	2.95	3.06	0.16	2	2.11	M3 II
8637	19 PSA	22.68	-29.50	6.80	6.99	3.78	0	6.17	M5
8649	66 AQR	22.70	-18.96	5.62	5.60	3.86	2	4.67	K4 III
8650D	ETA PEG	22.70	30.09	3.59	3.55	2.49	2	2.92	G8 II
8665D	XI PEG	22.76	12.05	4.51	4.51	3.89	2	4.17	F7 V
8667	LAM PEG	22.76	23.43	4.76	4.71	3.42	2	3.94	G8 II
8675	EPS GRU	22.78	-51.45	3.59	3.58	3.45	2	3.48	A2 V
8679	TAU AQR	22.80	-13.72	5.02	5.03	2.94	2	4.04	M0 III
8684	MU PEG	22.81	24.47	4.23	4.19	3.02	2	3.51	G8 III
8694	IOT CEP	22.81	66.07	4.29	4.24	2.94	2	3.48	K1 III
8698	LAM AQR	22.86	- 7.72	4.69	4.74	2.34	2	3.74	M2 III
8699D	15 LAC	22.85	43.18	5.90	5.93	3.69	0	4.94	M0
8709	DEL AQR	22.89	-15.95	3.34	3.33	3.23	2	3.26	A3 V
8720D	DEL PSA	22.91	-32.67	4.96	4.92	3.74	2	4.21	G8
8726		22.92	49.60	5.83	5.86	3.71	1	4.94	K5 I
8728	ALF PSA	22.94	-29.75	1.26	1.25	1.15	2	1.15	A3 V
8747	ZET GRU	22.99	-52.88	4.86	4.82	3.58	2	4.11	G5 III
8748		22.91	84.22	5.65	5.62	3.83	2	4.67	K4 III
8752		22.98	56.82	5.96	5.98	3.97	2	4.99	G0 I
8762	OMI AND	23.01	42.18	3.33	3.41	3.62	2	3.64	B6
8775D	BET PEG	23.04	27.95	3.42	3.48	0.89	2	2.49	M2 II
8781	ALF PEG	23.06	15.07	2.47	2.47	2.50	2	2.50	B9.5 III
8789D	86 AQR	23.09	-23.88	5.11	5.08	3.99	1	4.46	G9
8795	55 PEG	23.10	9.27	5.53	5.55	3.37	2	4.57	M2 III
8812	88 AQR	23.14	-21.30	4.56	4.51	3.03	2	3.64	K0 III
8815D	57 PEG	23.14	8.55	5.87	6.02	3.02	0	5.14	M4
8819D	PI CEP	23.12	75.25	5.02	4.98	3.98	2	4.39	G2 III
8820	IOT GRU	23.15	-45.38	4.71	4.66	3.43	2	3.90	K0 III
8834	PHI AQR	23.22	- 6.18	5.19	5.21	2.98	2	4.24	M2 III
8841D	PSI1 AQR	23.24	- 9.22	5.08	5.03	3.66	2	4.24	K0 III
8848	GAM TUC	23.27	-58.37	4.28	4.28	3.81	2	3.99	F0 III
8850	CHI AQR	23.26	- 7.85	5.66	5.85	2.64	0	5.03	M5
8852	GAM PSC	23.26	3.15	4.39	4.36	3.19	2	3.69	G7 III
8860D	8 AND	23.28	48.88	5.80	5.84	3.41	2	4.85	M2

YBS#	NAME	RA	DEC	S20	CDS	SIL	S	VIS	SP.TYPE
8863	GAM SCL	23.29	-32.67	5.28	5.23	3.86	2	4.41	G8 III
8892	98 AQR	23.36	-20.24	4.80	4.76	3.38	2	3.96	K0 III
8904	4 CAS	23.40	62.15	5.90	5.95	3.54	0	4.97	M1 III
8906	99 AQR	23.41	-20.77	5.40	5.39	3.49	2	4.42	K5 III
8916	THE PSC	23.44	6.25	5.11	5.06	3.73	2	4.28	K1 III
8940	71 PEG	23.54	22.36	5.97	6.16	2.95	0	5.34	M5
8961	LAM AND	23.61	46.33	4.47	4.44	3.13	2	3.73	G8 III
8969	IOT PSC	23.64	5.50	4.45	4.45	3.84	2	4.10	F7 V
8974	GAM CEP	23.64	77.48	4.02	3.96	2.68	2	3.22	K1 IV
8991	77 PEG	23.70	10.20	5.94	6.02	3.43	0	5.06	M2
8992	R AQR	23.71	-15.42	6.14	6.43	2.83	0	5.80	M7
9030	80 PEG	23.83	9.18	6.61	6.72	3.93	0	5.79	M3
9036	PHI PEG	23.85	18.98	5.93	6.01	3.42	0	5.05	M2
9045	RHO CAS	23.89	57.36	5.38	5.35	3.88	2	4.52	F8 I
9047		23.89	- 0.04	6.24	6.43	3.22	0	5.61	M5
9064	PSI PEG	23.94	25.00	5.57	5.63	3.09	2	4.67	M3 III
9072	OMG PSC	23.97	6.73	4.31	4.31	3.79	2	4.01	F4 IV
9089	30 PSC	0.01	- 6.15	5.37	5.44	2.77	2	4.47	M3 IV

APPENDIX C *

STAR DISTRIBUTION RESULTS

The plots of star distributions resulting from the Star Availability Studies described in subsection 5.2 are presented in this Appendix. Refer to subsection 5.2.3 and 5.2.4 for explanation of the plots and their symbology. (Note that Table 5-2 applies both star mapper and star tracker plots.) Following is a guide to the location of the individual plots:

STAR MAPPER RESULTS

<u>Detector</u>	<u>Minimum Usable Magnitude</u>	<u>FOV (deg)</u>	<u>Page</u>
Csd	3.25	4	C-2
"	4.75	4	C-3
Si	3.20	4	C-4
"	3.20	6	C-5
"	3.20	8	C-6
"	4.00	4	C-7
"	4.00	6	C-8
"	4.00	8	C-9

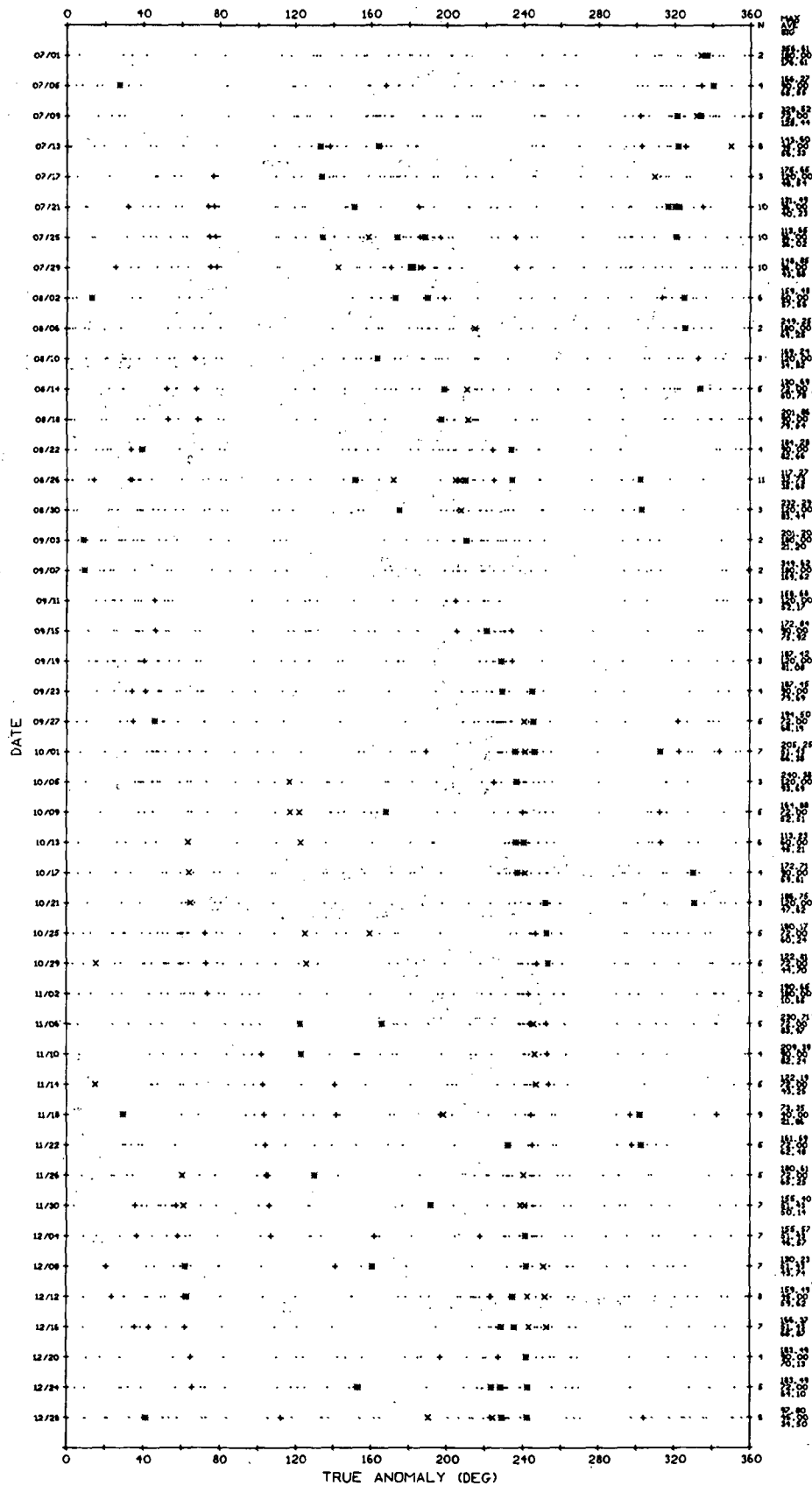
STAR TRACKER RESULTS (S-20)

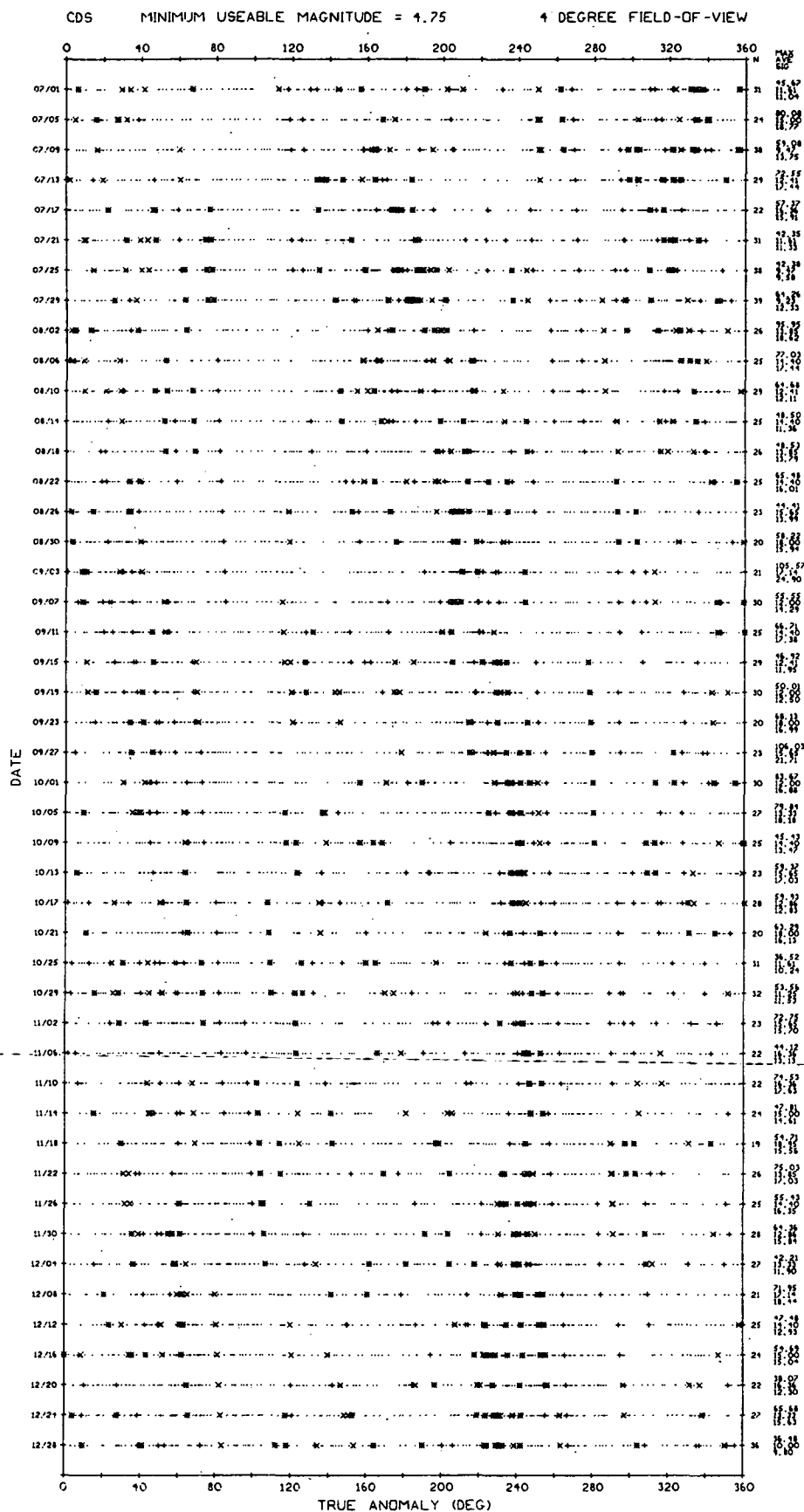
(Star Plots are for Orbit at 7/1/72)

<u>Measurement Interval (Deg)</u>	<u>Maximum Out-of-Plane Angle (Deg)</u>	<u>Page</u>
8	30	C-10
16	30	C-11
20	30	C-12
40	30	C-13
8	15	C-14
16	15	C-15
20	15	C-16
40	15	C-17

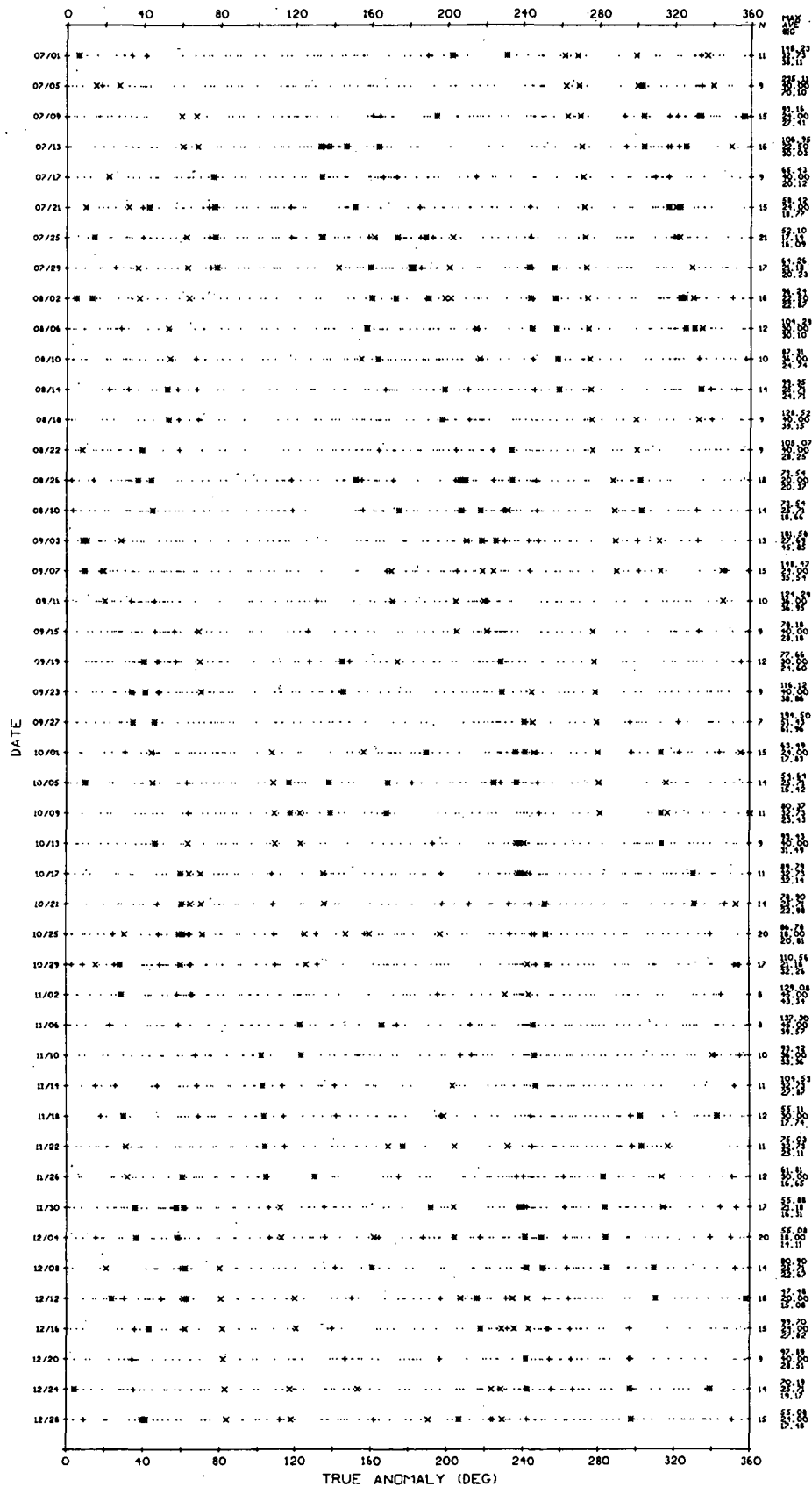
*This appendix supplements Appendix C of Ref. 141.

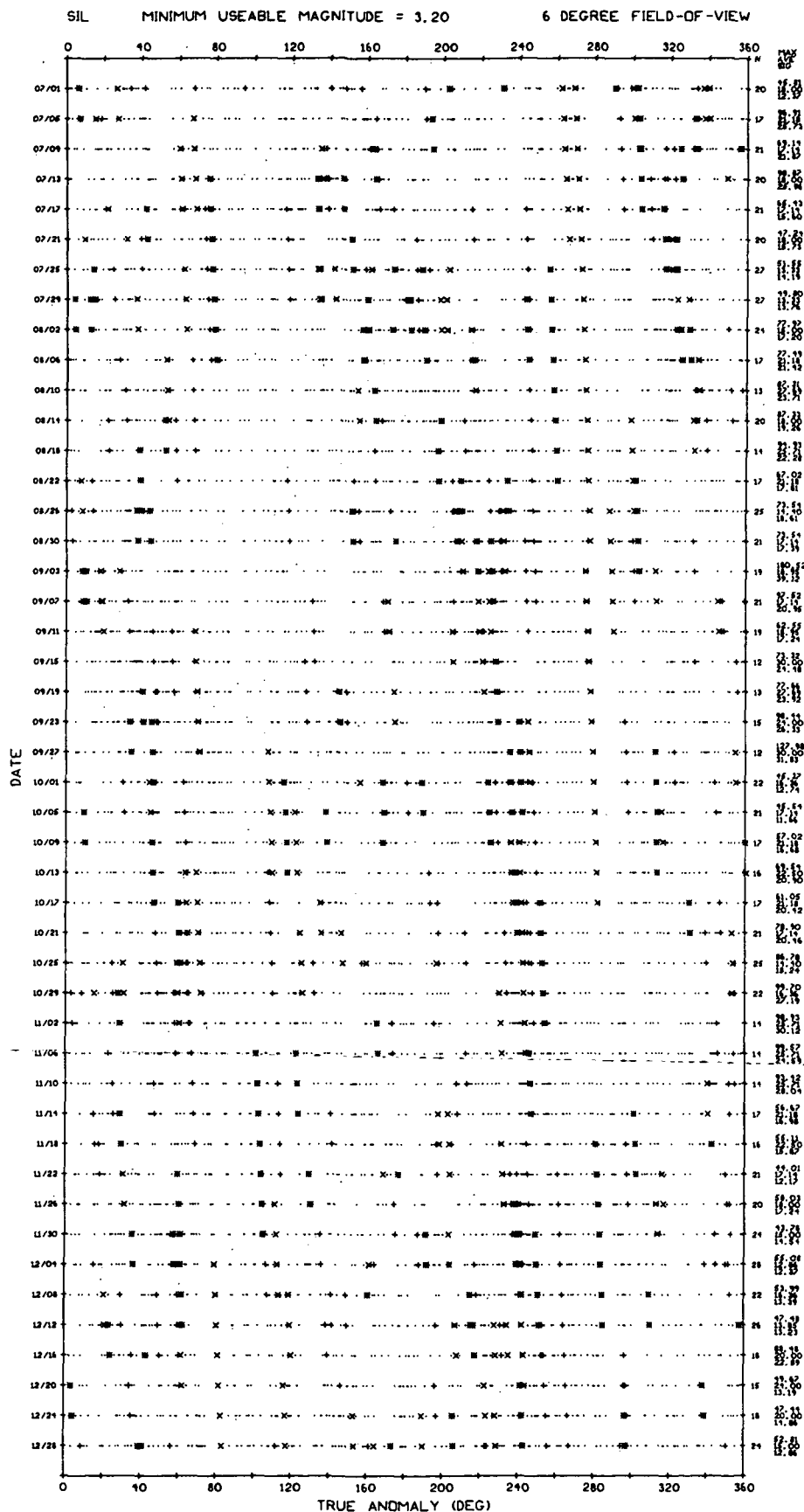
CDS MINIMUM USEABLE MAGNITUDE = 3.25 4 DEGREE FIELD-OF-VIEW



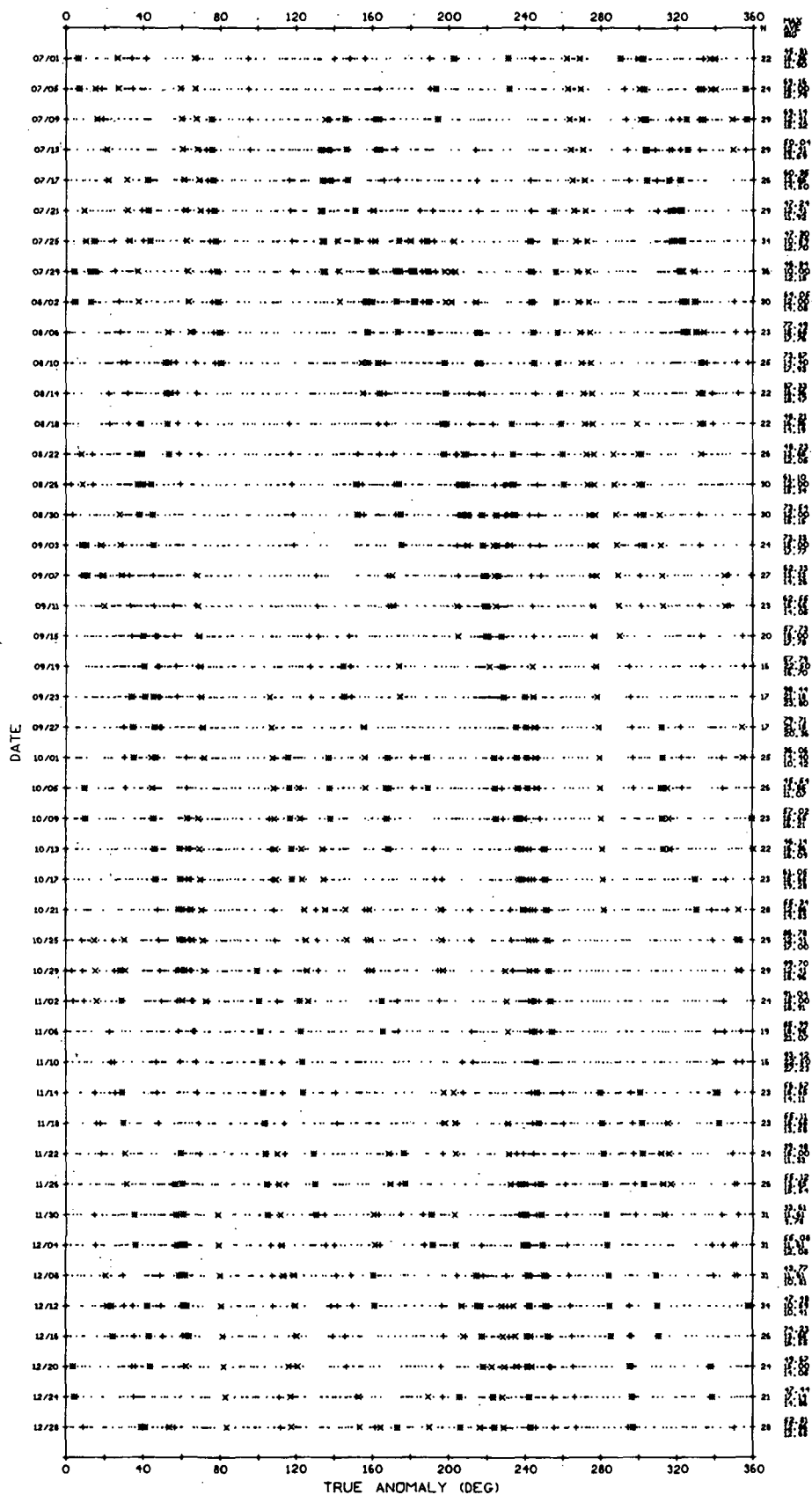


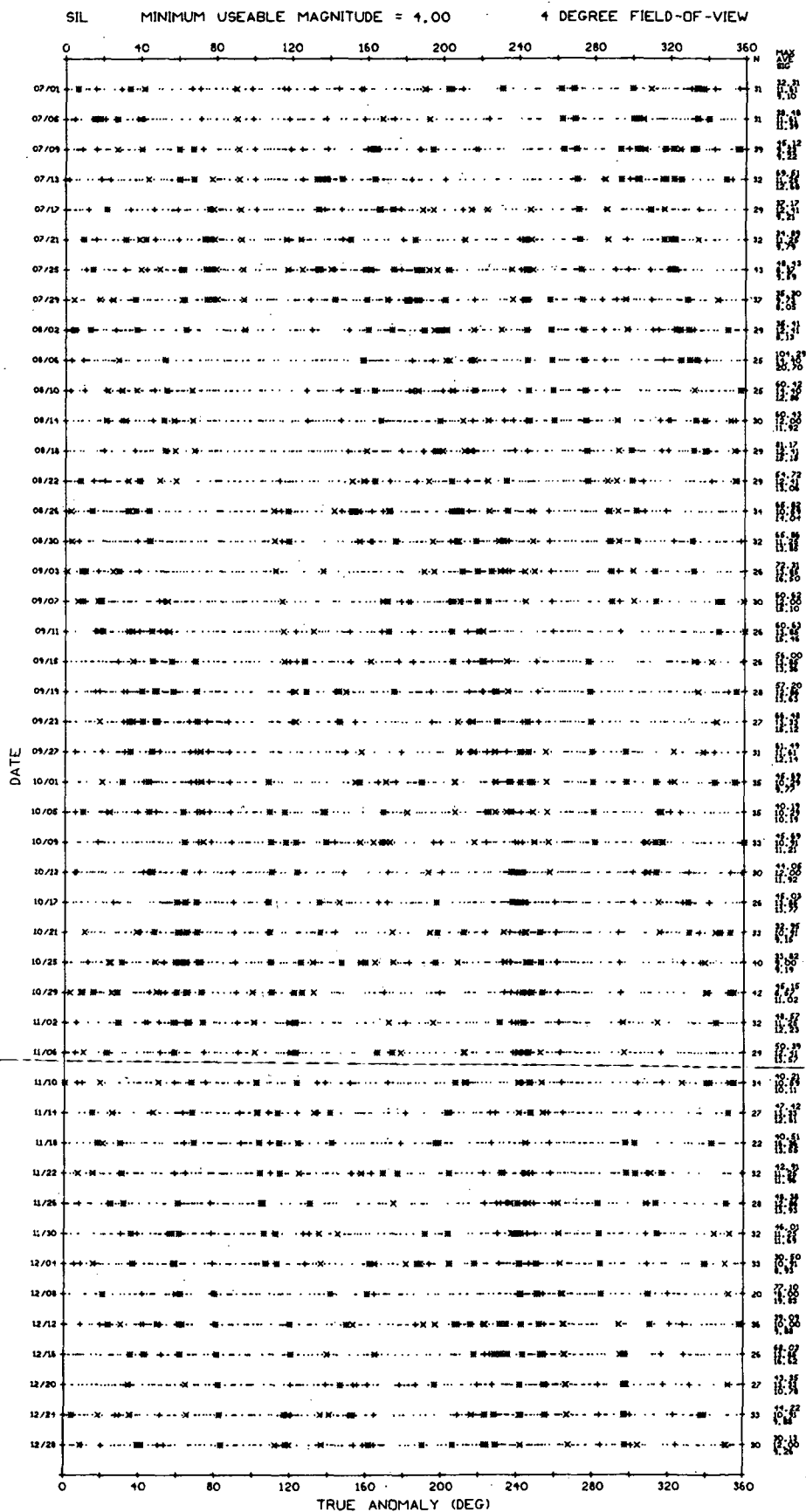
SIL MINIMUM USEABLE MAGNITUDE = 3.20 4 DEGREE FIELD-OF-VIEW

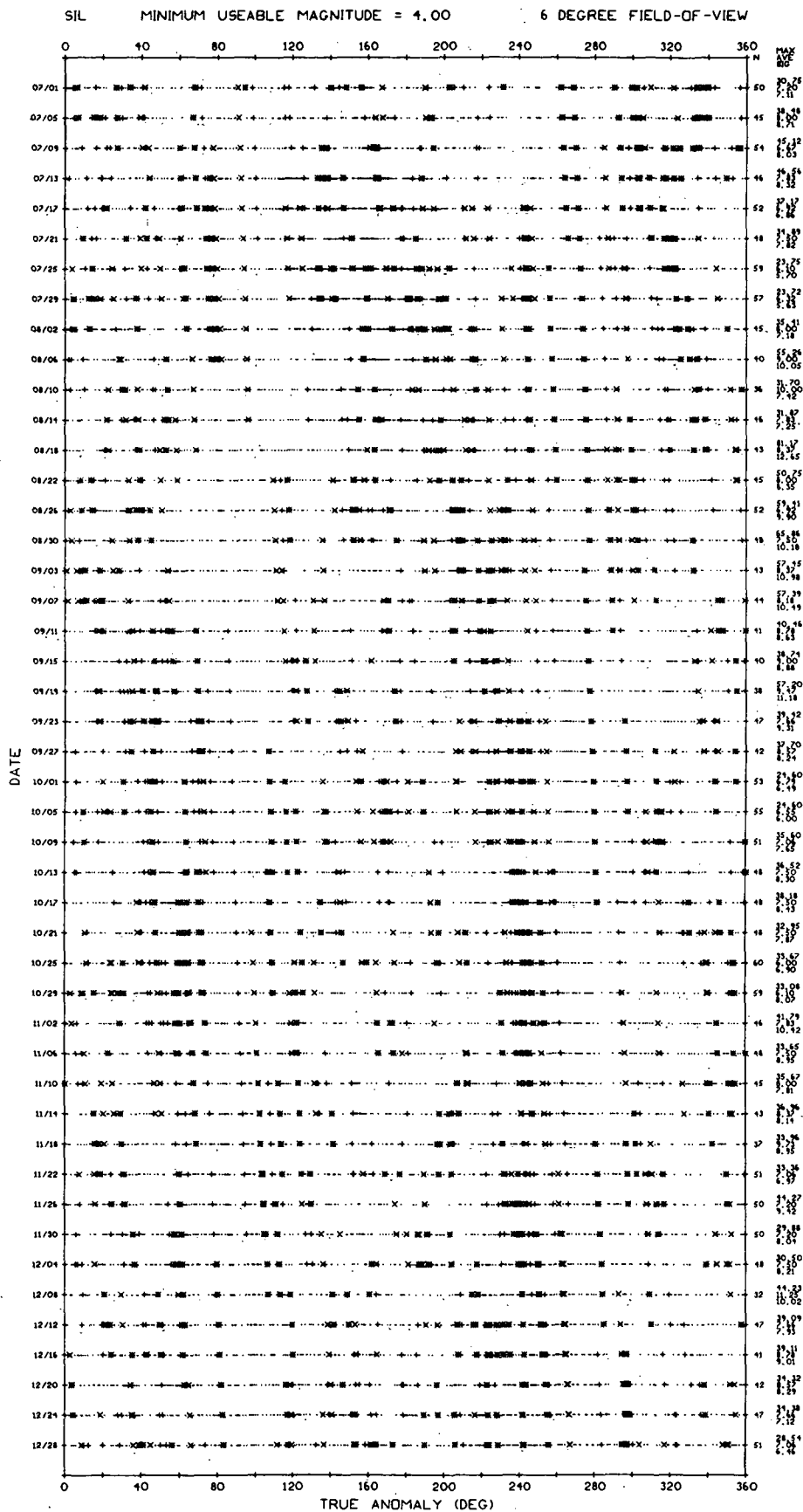


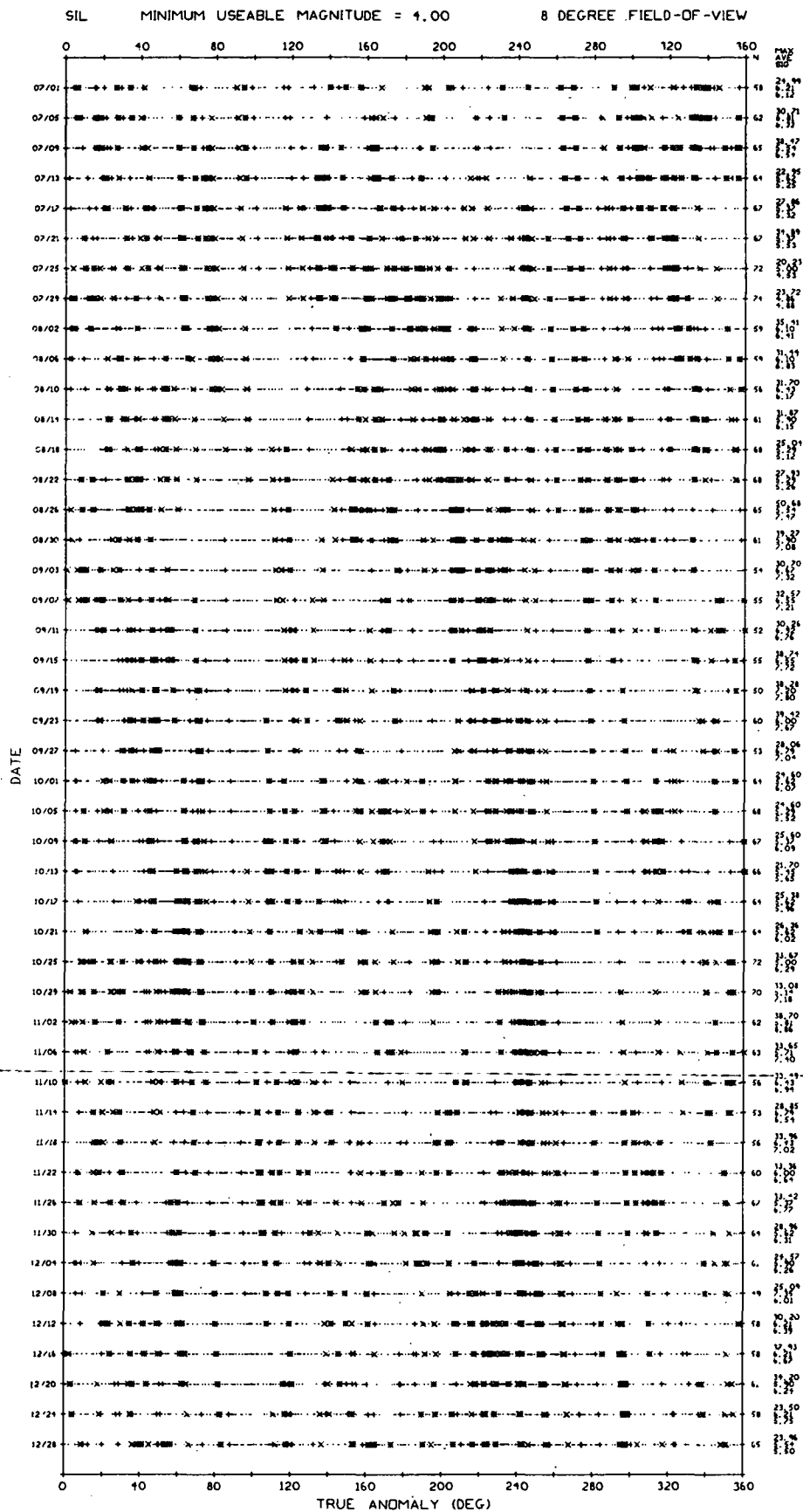


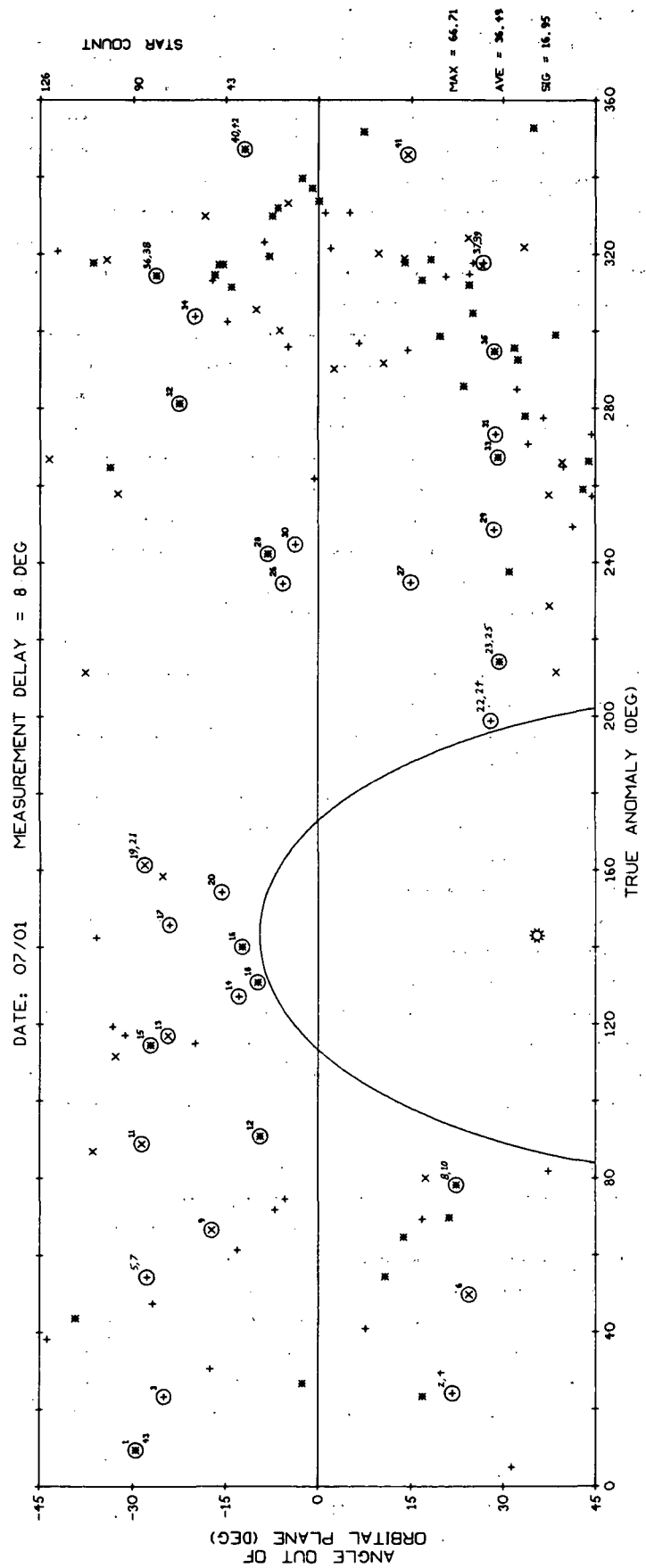
SIL MINIMUM USEABLE MAGNITUDE = 3.20 8 DEGREE FIELD-OF-VIEW

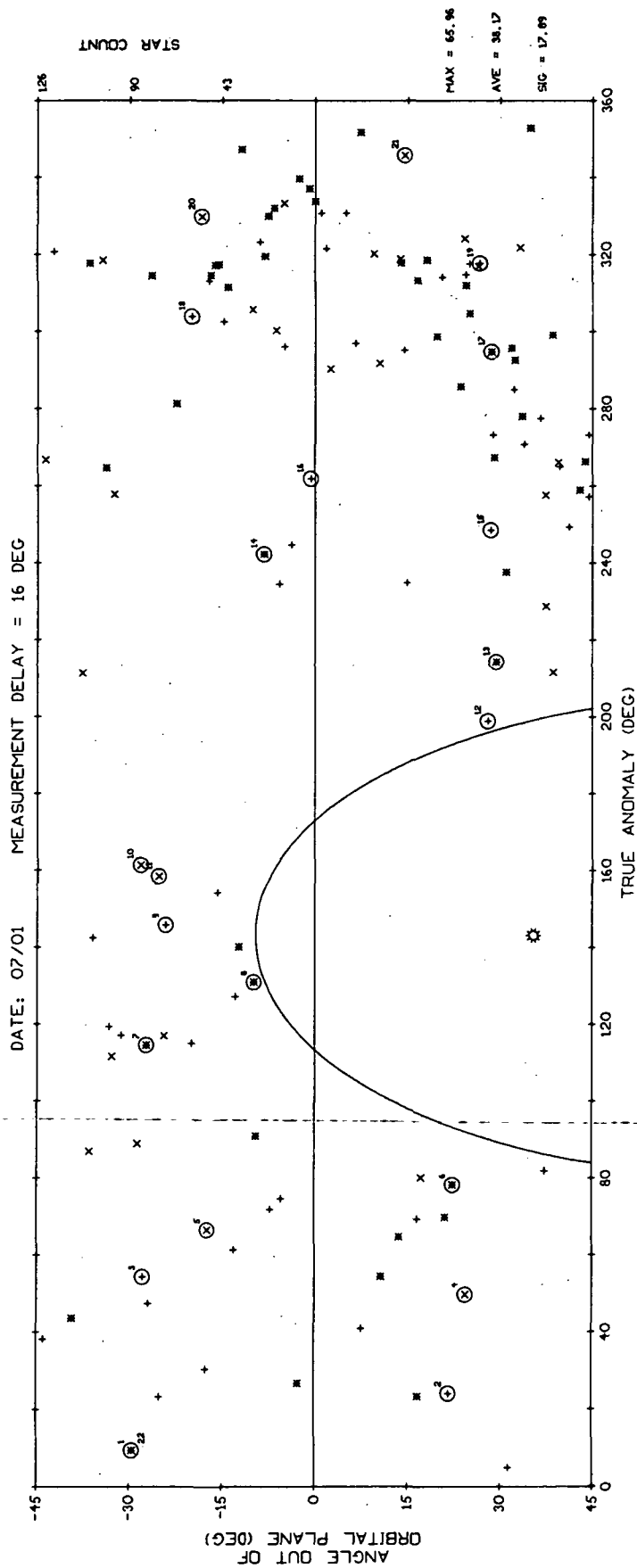


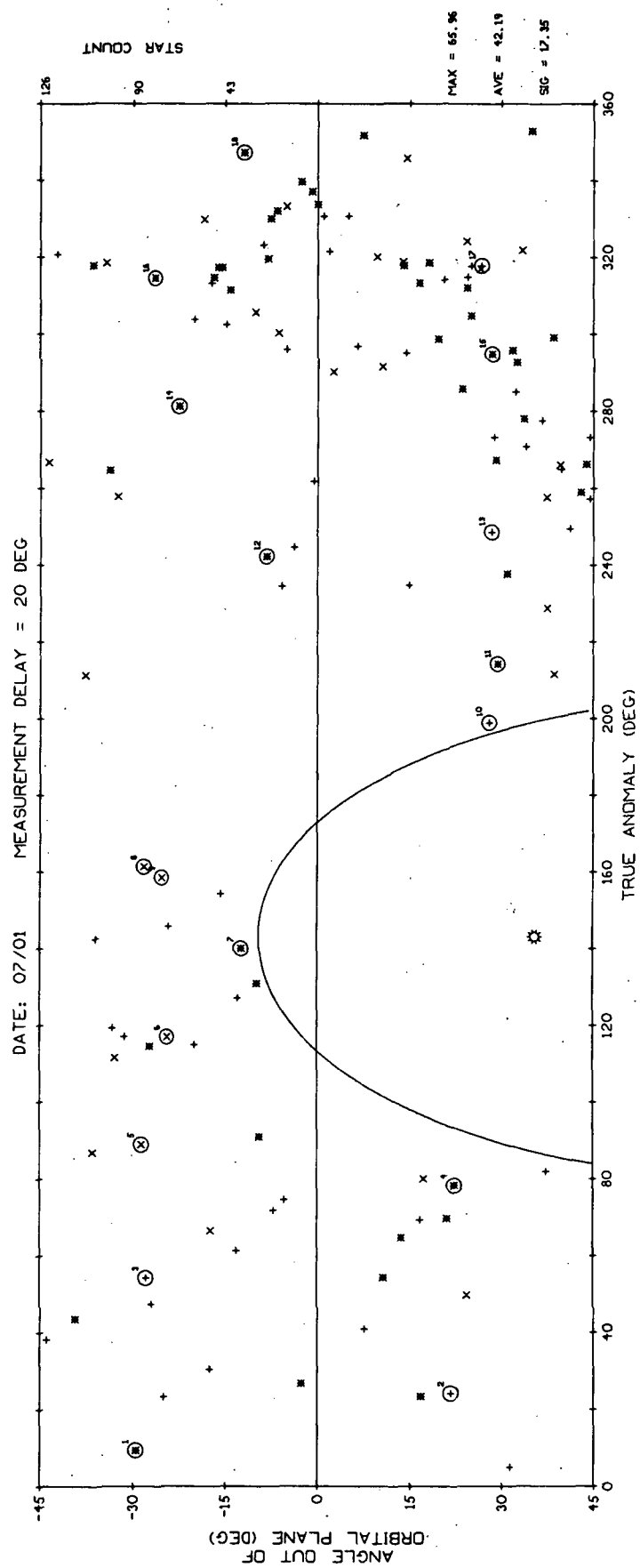


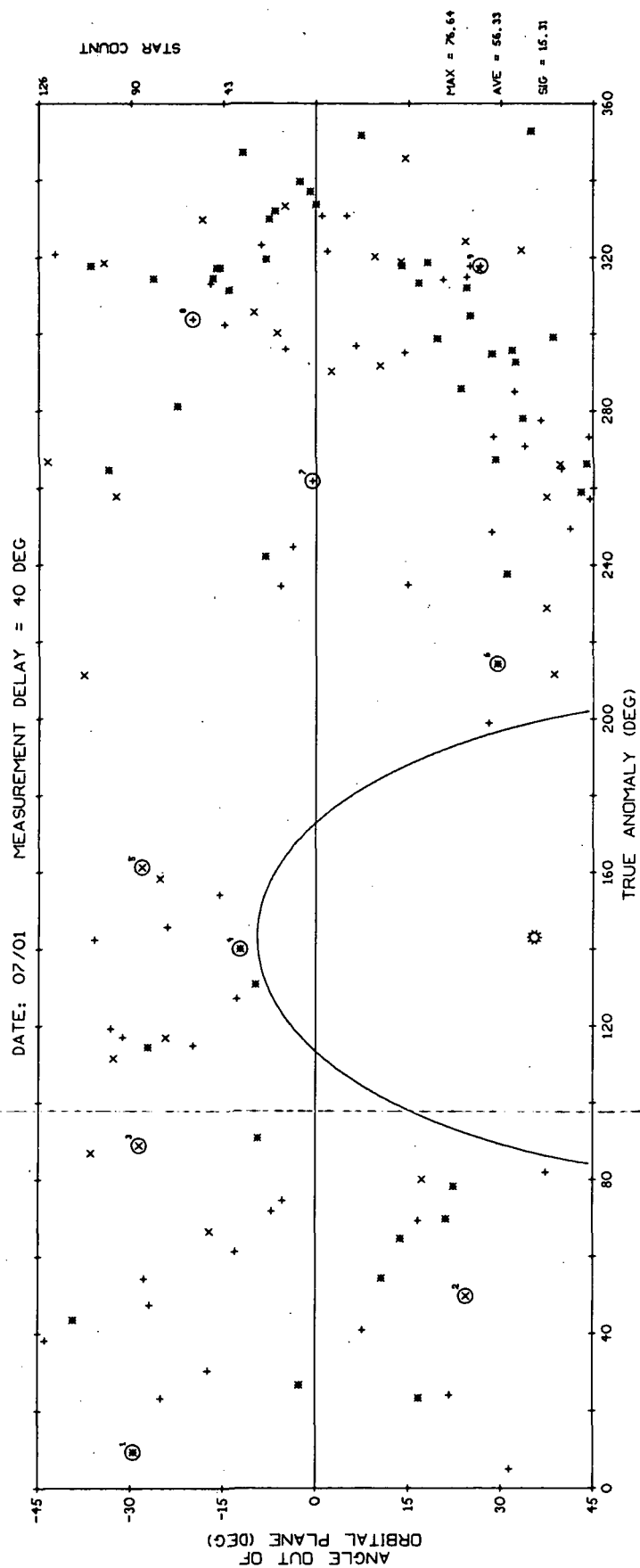


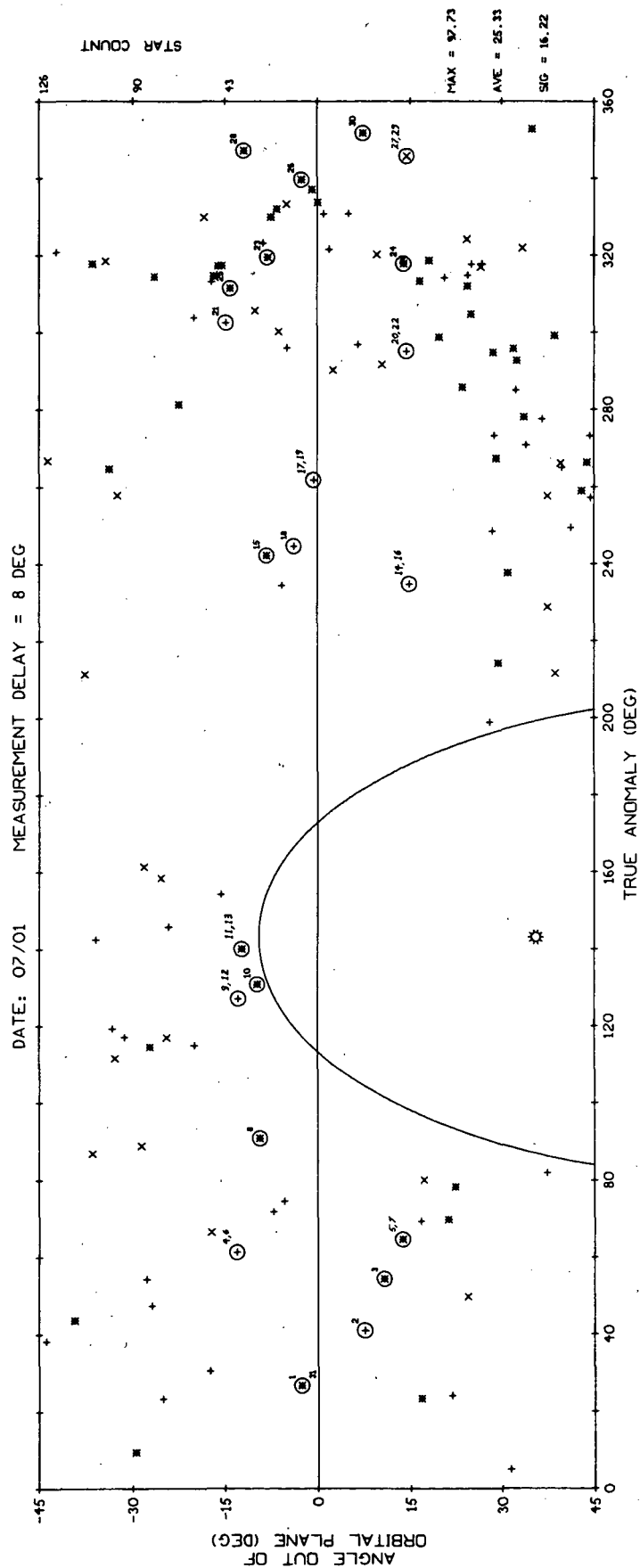


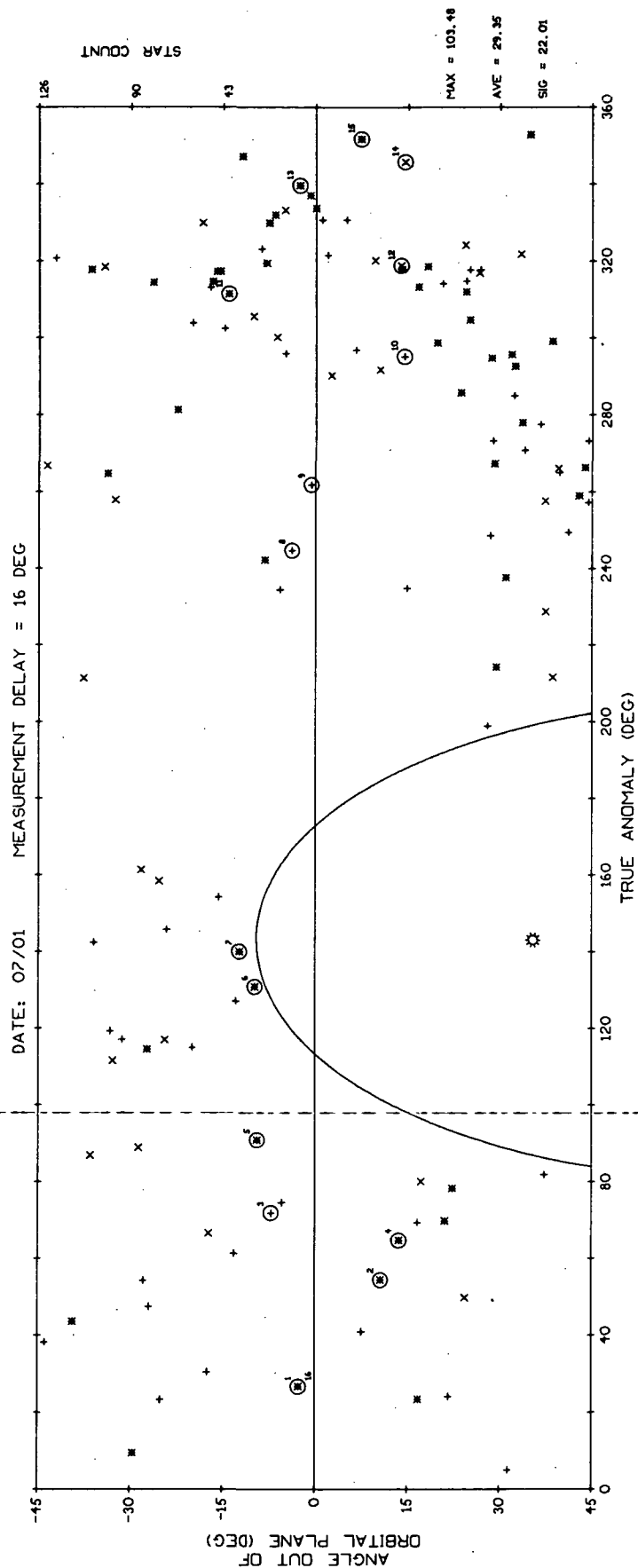


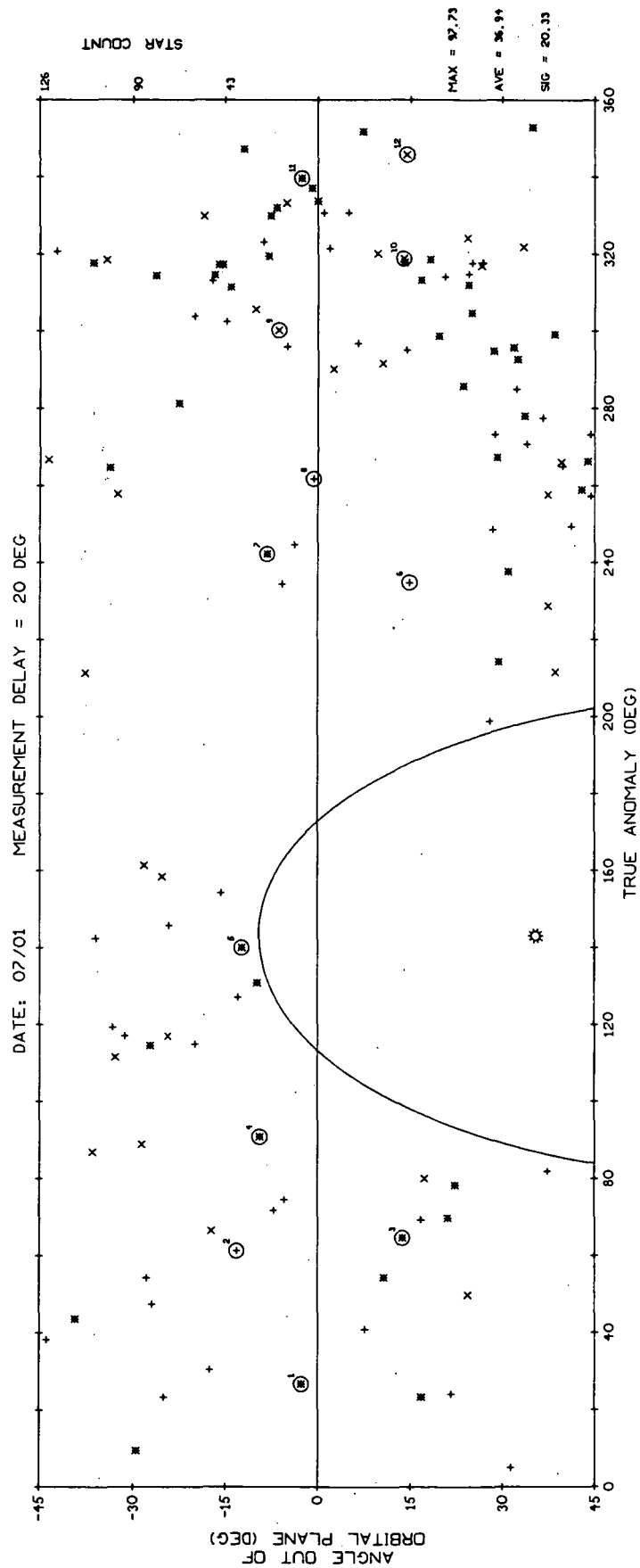


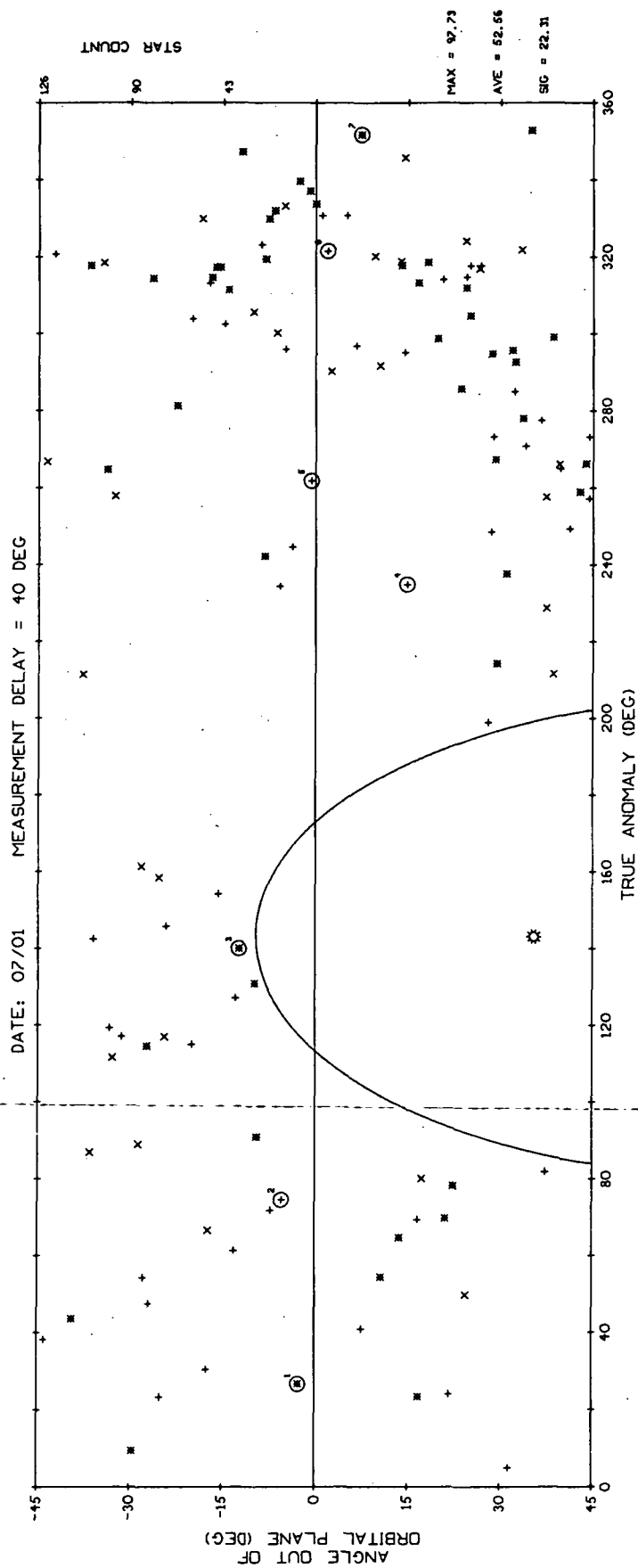












APPENDIX D

COMPARISON OF MIT/CSDL AND HONEYWELL TECHNIQUES OF STAR MAPPER MEASUREMENT

The purpose of this appendix is to compare the original technique of star mapper measurement used by MIT/CSDL in SIMS-A with that used by Honeywell in SPARS. The two techniques are essentially the same except for differences in the definition of the orbit-oriented coordinate system and the attitude angles. In this comparison, use is made of the SPARS equations given in the symposium paper, "SPARS Algorithms and Simulation Results" by D. C. Paulson, D. B. Jackson, and C. D. Brown of Honeywell (Reference 16).

Both MIT/CSDL and Honeywell use the same definition for the body-fixed coordinate system whose axes for the nominal orientation of the vehicle are as follows:

X_B - is along the projection of the spacecraft velocity vector onto the local horizontal plane

Y_B - is normal to the orbital plane

Z_B - is along the local nadir

Although not indicated in Reference 16, it is assumed that Honeywell uses the same standard basic inertial coordinate system as MIT/CSDL where the axes X_I and Y_I both lie in the equatorial plane with X_I pointing towards the vernal equinox, and Z_I is positive northerly.

To transform vectors from basic inertial to body-fixed coordinates use is made of the following matrix:

$$T_{BI} = T_{BO} T_{OI} \quad (D-1)$$

where the subscript 0 denotes the orbit-oriented coordinate system. For MIT/DL the matrix T_{OI} is

$$T_{OI} = \begin{bmatrix} 1 & 0 & 0 \\ 0 & ci & si \\ 0 & -si & ci \end{bmatrix} \begin{bmatrix} c\Omega & s\Omega & 0 \\ -s\Omega & c\Omega & 0 \\ 0 & 0 & 1 \end{bmatrix} = \begin{bmatrix} i \end{bmatrix}_x \begin{bmatrix} \Omega \end{bmatrix}_z \quad (D-2)$$

where Ω is the right ascension of the orbit ascending node and i is the orbit inclination. For Honeywell the matrix T'_{OI} (where a prime is used to denote Honeywell) is:

$$T'_{OI} = \begin{bmatrix} 0 & 1 & 0 \\ 0 & 0 & -1 \\ -1 & 0 & 0 \end{bmatrix} \begin{bmatrix} i \end{bmatrix}_x \begin{bmatrix} \Omega \end{bmatrix}_z \quad (D-3)$$

$$T'_{OI} = \begin{bmatrix} -cis\Omega & cic\Omega & si \\ -sis\Omega & sic\Omega & -ci \\ -c\Omega & -s\Omega & 0 \end{bmatrix} \quad (D-4)$$

where the expression in Equation D-4 agrees with Equation 7 of Reference 16. From the above it is seen that the difference between the two orbit-oriented coordinate systems is simply an interchange of axes due to the use of a 'switching' matrix in Equation D-3.

Since T_{OI} and T'_{OI} are different, T_{BO} and T'_{BO} will also be different. For MIT/DL the matrix T_{BO} is:

$$T_{BO} = \begin{bmatrix} 0 & 1 & 0 \\ 0 & 0 & -1 \\ -1 & 0 & 0 \end{bmatrix} \begin{bmatrix} \psi \end{bmatrix}_x \begin{bmatrix} \phi \end{bmatrix}_y \begin{bmatrix} \theta \end{bmatrix}_z \quad (D-5)$$

$$T_{BO} = \begin{bmatrix} -c\psi s\theta & c\psi c\theta & s\psi c\phi \\ +s\psi s\phi c\theta & +s\psi s\theta s\phi & \\ -s\psi s\theta & s\psi c\theta & -c\psi c\phi \\ -c\psi s\phi c\theta & -c\psi s\theta s\phi & \\ -c\phi c\theta & -c\phi s\theta & s\phi \end{bmatrix} \quad (D-6)$$

For Honeywell the matrix T'_{BO} is:

$$T'_{BO} = \begin{bmatrix} \psi \end{bmatrix}_z \begin{bmatrix} \phi \end{bmatrix}_x \begin{bmatrix} \theta \end{bmatrix}_y \quad (D-7)$$

$$T'_{BO} = \begin{bmatrix} c\psi c\theta & s\psi c\phi & -c\psi s\theta \\ +s\psi s\theta s\phi & & +s\psi s\phi c\theta \\ -s\psi c\theta & c\psi c\theta & s\psi s\theta \\ +c\psi s\theta s\phi & & +c\psi s\phi c\theta \\ c\phi s\theta & -s\phi & c\phi c\theta \end{bmatrix} \quad (D-8)$$

where the expression in Equation D-8 agrees with the matrix in Equation 21 of Reference 16. Note that the matrix in Equation D-8 can be changed to that in Equation D-6 by shifting the columns of the matrix and reversing the signs of the second and third rows.

In both techniques the elements of the geometry matrix are computed as follows (see Appendix A of Reference 16 and Section 5.3.2.2.1 of this report):

$$H_x = \frac{\partial}{\partial x} \text{ (DOT)} \quad x = (\theta, \phi, \psi, \dots) \quad (D-9)$$

where

$$\text{DOT} = \underline{n}_B \cdot \begin{bmatrix} T_{BO} & T_{OI} & \underline{s}_I \end{bmatrix} \quad (D-10)$$

Since only T_{BO} in Equation D-10 is a function of the presently used state elements (i.e., $\theta, \phi, \psi, \dots$) we have:

$$H_x = \underline{n}_B \cdot \left\{ \frac{\partial}{\partial x} [T_{BO}] T_{OI} \underline{s}_I \right\} \quad x = (\theta, \phi, \psi, \dots) \quad (D-11)$$

For Honeywell the expressions for H_x are:

$$H'_\theta = \underline{n}_B \cdot \begin{bmatrix} -c\psi s\theta & 0 & -c\psi c\theta \\ +s\psi c\theta s\phi & & -s\psi s\phi s\theta \\ s\psi s\theta & 0 & c\theta s\psi \\ +c\psi c\theta s\phi & & -c\psi s\phi s\theta \\ c\phi c\theta & 0 & -c\phi s\theta \end{bmatrix} T'_{OI} \underline{s}_I \quad (D-12)$$

$$H'_\phi = \underline{n}_B \cdot \begin{bmatrix} s\psi s\theta c\phi & -s\psi s\phi & s\psi c\phi c\theta \\ c\psi s\theta c\phi & -c\psi s\phi & c\psi c\phi c\theta \\ -s\phi s\theta & -c\phi & -s\phi c\theta \end{bmatrix} T'_{OI} \underline{s}_I \quad (D-13)$$

$$H'_\psi = \underline{n}_B \cdot \begin{bmatrix} -s\psi c\theta & c\psi c\phi & s\psi s\theta \\ +c\psi s\theta s\phi & & +c\psi s\phi c\theta \\ -c\psi c\theta & -s\psi c\phi & s\theta c\psi \\ -s\psi s\theta s\phi & & -s\psi s\phi s\theta \\ 0 & 0 & 0 \end{bmatrix} T'_{OI} \underline{s}_I \quad (D-14)$$

$$H'_{B_x} = H'_{B_y} = H'_{B_z} = 0 \quad (D-15)$$

In Appendix A of Reference 16, the matrices G_θ , G_ϕ , and G_ψ are the same as the large matrices on the right of Equations D-12 through D-14 except for the use of direction cosines. The direction cosines for SPARS are identified as the following elements of the matrix T'_{BO} in Equation D-8:

$$T'_{BO} = \begin{bmatrix} \lambda_1 & \lambda_2 & \lambda_3 \\ \mu_1 & \mu_2 & \mu_3 \\ \nu_1 & \nu_1 & \nu_1 \end{bmatrix} \quad (D-16)$$

Substitution of the corresponding expressions for λ , μ , and ν into G_θ , G_ϕ , and G_ψ will yield the large matrices on the right of Equations D-12 through D-14.

For MIT/CSDL the expressions for H_x are given in Equations 5-11 through 5-14.

Since the CSDL is presently using the smoother formulation to analyze SIMS-A for only a nominal attitude history (i.e., $\phi = \psi = 0$), the expressions for H_θ , H_ϕ , and H_ψ were simplified to those given in Equations 5-15 through 5-17. This same simplification could have been made in the SPARS equations for a nominal attitude history and the results would have been the following:

$$H'_\theta = \underline{n}_B \cdot \begin{bmatrix} -s\theta & 0 & -c\theta \\ 0 & 0 & 0 \\ c\theta & 0 & -s\theta \end{bmatrix} \underline{s}'_O \quad (D-17)$$

$$H'_\phi = \underline{n}_B \cdot \begin{bmatrix} 0 & 0 & 0 \\ s\theta & 0 & c\theta \\ 0 & -1 & 0 \end{bmatrix} \underline{s}'_O \quad (D-18)$$

$$H'_\psi = \underline{n}_B \cdot \begin{bmatrix} 0 & 1 & 0 \\ -c\theta & 0 & s\theta \\ 0 & 0 & 0 \end{bmatrix} \underline{s}'_O \quad (D-19)$$

where \underline{s}'_O is $T'_{OI} \underline{s}_I$.

APPENDIX E

EXCERPTS FROM THE TECHNICAL PROPOSAL COVERING EXPANSIONS OF TASKS 4 AND 6 OF THE ORIGINAL STATEMENT OF WORK

Following are pages 4, 5, 6 and 9 of MIT/CSDL Proposal No. 72-176 (reference 146), which constitute the Technical Section thereof. The tasks are essentially as presented by NASA in reference 168. The schedule reflects the work plan.

This appendix is a self-contained section of the present report. Its paragraph and figure numbering do not correlate with the rest of this report.

CSDL Proposal No. 72-176

TECHNICAL SECTION

I. CONTRACTOR ACCEPTANCE OF STATEMENT OF WORK

This proposal is submitted in response to NASA MSC letter BC25-72/0683-A17 dated 27 April 1972, N.J. Beauregard to J. Nelson of MIT/CSDL, "Proposed Supplemental Agreement Number 105S to Contract NAS 9-4065". This proposed Supplemental Agreement is intended by NASA to modify Task Order No. 42 to Contract NAS 9-4065. Task modifications were to be as set forth in subsection II. 1 of this Technical Section; additional funds therefore were provided, as indicated in the attached NASA Form 633-4; and the period of contract performance was extended, as shown in subsection III of this Technical Section.

The Draper Laboratory accepts the amendments to the original Task Order Tasks 4 and 6, and will comply with the schedule as revised herein in accordance with the proposed extended period of performance. The effort proposed herein is responsive within estimated budgetary constraints to the technical requirements of the proposed Supplemental Agreement Number 105S to Contract NAS 9-4065 (T.O. 42).

II. STATEMENT OF WORK

Subsections I, II and III of the Technical Section of Enclosure "A" to MIT/CSDL Proposal No. 71-173, dated 14 June 1971, are incorporated herein by reference, to be modified as hereinafter set forth.

II. 1 TASK DESCRIPTIONS (MODIFIED)

Task 4 - Develop adequate error models and perform an error analysis demonstrating the accuracy of configuration D. Repeat the error analysis for other configurations using available data.

Perform a more detailed error simulation of SIMS-A to establish a lower accuracy bound on the SIMS implementation.

Task 6 - Perform a preliminary reliability analysis of the configurations.

Include consideration of the use of payload sensor imagery to update the gyros in the cases of configurations A and B.

III. SCHEDULE

Subsection IV of the Technical Section of enclosure "A" to MIT/CSDL Proposal No. 71-173, dated 14 June 1971, is superseded by this subsection. It reflects both the no-cost extensions to the original contract period of performance and the funded extension that is the principal subject of the present proposal.

III.1 INCORPORATION OF NO-COST EXTENSIONS

By mutual consent among MIT/CSDL, NASA/MSC and NASA/GSFC, the period of performance of the original Task Order No. 42 to Contract NAS9-4065 was extended from eight months ending 29 February 1972, to nine months ending 31 March 1972, and then to eleven months ending 31 May 1972, in each instance to improve the scope and quality of documentation of results. The no-cost extension of the Task Order through 31 May 1972, is incorporated herein, and in the revised schedules shown hereinafter, by reference.

III.2 REVISED STUDY SCHEDULE

Figure 1 presents the proposed schedule for the accomplishment of the tasks of this study, as modified including extension of the contract period through 30 September 1972, including presentation and documentation of results achieved.

TASK	1971												1972											
	J	A	S	O	N	D	J	F	M	A	M	J	J	A	S									
Block Diagram			1	c																				
Spacecraft Interfaces			1	-c-	-																			
Configuration Design			1	-c-	-																			
Error Analysis, Including Special SIMS-A Study																								
Sensitivity Analysis																								
Reliability, Including Consid. of Payload Sensor Imagery in SIMS A & B																								
Configuration Comparisons																								
Letter Reports		c	c	c	c	c	c	c	c	c	x	x	x	x	x									
Interim Technical Reports					c			c																
Technical Review Meetings					c			c																
Final Report																								

Major Effort
 - - - - Minor or Extended Effort
 c Completed
 1 ; x Planned Completion

APPENDIX E

Figure 1 Schedule

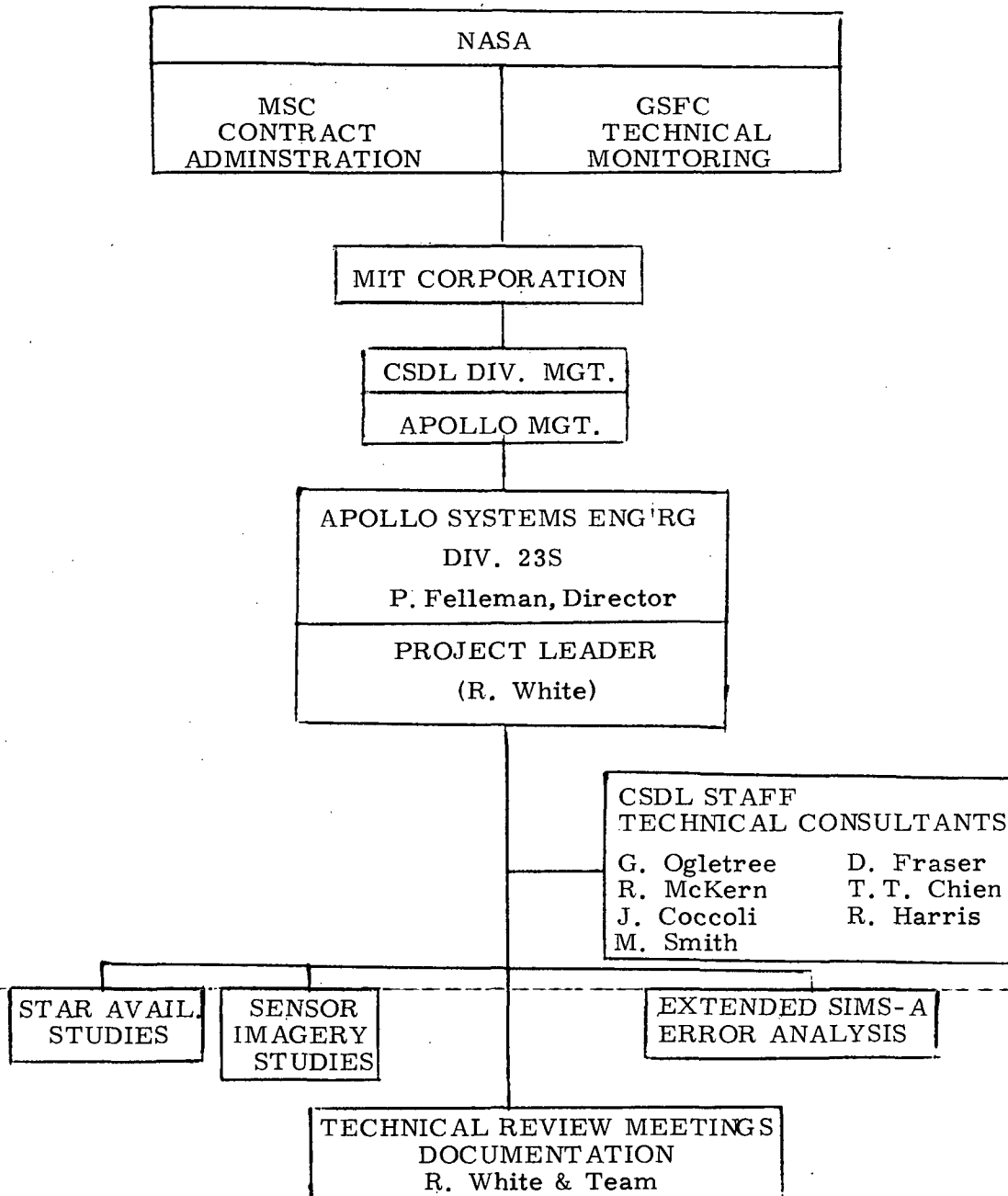


Figure 2 Project Organization

APPENDIX F

POST SCRIPT

- A telephone conversation between J. Coccoli, MIT/CSDL, and D. Paulson, Honeywell Aerospace Division, on June 23, 1972, confirmed the fact that the silicon star mapper developed by Honeywell Radiation Center has been chosen as the SSA for PARS*, an applications outgrowth of SPARS technology. Selection decisions among the star mappers of HR, KI, and CDC for other SPARS study and application programs are still pending as of this date.
- The electronics in the HR star mapper does not require a delay to establish and set a threshold. Therefore, the speculative functional block diagram indicated in Figure 4-7 is inappropriate. While detail is still not available, we know that HR uses three fixed threshold levels. Logic is used to process only the highest threshold crossed. The threshold is sensed at both the leading and trailing edge. A method of integrating timing signals is initiated at the leading edge threshold, and the integration rate back-down at trailing edge threshold is at a doubled rate. The signal processing is analog rather than digital.

- - - - -

The remaining pages of this appendix are a document received from Honeywell Aerospace Division at release of this report to publication. It is included herein, as received, with permission of D.C. Paulson of Honeywell, and without MIT/CSDL review or comment.

* See page 4-1

26 JUNE 1972

STAR SENSOR TRADEOFF

FOR PARS - HL

PREPARED BY:

D.C. PAULSON

GUIDANCE AND CONTROL DEPARTMENT
HONEYWELL AEROSPACE DIVISION
13350 U.S. HIGHWAY 19
ST. PETERSBURG, FLORIDA 33733

STAR SENSOR TRADEOFF FOR PARS - H4

Summary

A tradeoff study was conducted to select a star sensor (and associated supplier) for the PARS-H4 system being developed for an Air Force program. Two candidates were considered: a sensor provided by Control Data Corporation (CDC) using a Cadmium Sulfide detector, and one provided by Honeywell Radiation Center (HRC) which uses a Silicon detector. The result of this tradeoff was the selection of the HRC Silicon approach on the basis of superior performance potential, lower weight and parts count, and operational advantages.

Trade-off Details

Table 1 summarizes the set of performance requirements to which the two candidates were designed. Also listed are the predicted performance of each of the two candidates by the respective suppliers. Table 2 summarizes the major differences, including physical characteristics, of the two approaches. Table 3 presents further information that includes development status.

From these data, the HRC approach is seen to have a greater performance potential, particularly in the area of uniformity, and has operational advantages of no sun

shutter and a smaller sun shield. However, much of the initial performance prediction data provided by HRC for the Silicon approach were based on computations or extrapolation of very limited tests as compared to the considerable test data available on CdS sensors. Accordingly, additional tests were conducted to increase confidence in the HRC predictions. These tests utilized a sensor consisting of a brassboard optomechanical assembly (very close to final design and construction of the PARS H-4 sensor) and breadboard electronics.

The tests conducted, their objectives and results are given in Table 4. Results indicated that the Silicon approach exceeds the requirements in all areas except worst case sensitivity (sensitivity at least sensitive position along slit). Uniformity was not as good as predicted by HRC, but the random error was better than predicted. It is felt that uniformity will likely improve during the PARS-H₄ development program, when many detectors will be built and tested and selection can be made from a larger sample.

On the basis of potentially superior uniformity, lower parts count, operational advantages of the Silicon approach, HRC was selected as the star sensor supplier for the PARS-H₄ program.

TABLE 1

PARS H-4 Star Sensor
Performance Specification

	<u>Required</u>	<u>CDC Prediction</u>	<u>HRC Prediction</u>
<u>FIELD OF VIEW</u>	10°	Comply	Comply
<u>TRANSIT ACCURACY</u>			
Random (1 σ)	8 $\widehat{\text{sec}}$	8 $\widehat{\text{sec}}$	4 $\widehat{\text{sec}}$
Systematic (1 σ)	4 $\widehat{\text{sec}}$	4 $\widehat{\text{sec}}$	4 $\widehat{\text{sec}}$
<u>NUMBER OF STARS DETECTED</u>			
Minimum	460	Comply	Comply
Maximum	560	Comply	Comply
<u>PROBABILITY OF DETECTION (≥ 380 STARS)</u>	0.90	> 0.90 (4.1 M _{Cds})	> 0.90 (3.6 M _{Si})
<u>DETECTOR UNIFORMITY</u>	$\pm 30\%$ Max.	Comply	$\pm 5\%$
<u>S/N MINIMUM (> 380 Stars)</u>	10:1	Comply	Comply
<u>MIN. TIME BETWEEN FALSE ALARMS</u>	1 x 10 ⁴ sec	Comply	Comply
<u>SUN IN FIELD OF VIEW</u>	Survive, But Not Operate	Comply, But Requires Sun Shutter	Comply With No Sun Shutter

TABLE 2

PARS H-4 SSA Configuration Comparison

	<u>CDC</u>	<u>HRC</u>
<u>Detector</u>	Cadmium Sulfide (CdS)	Silicon (Si)
<u>Optical System</u>		
Optical System	Concentric Catadioptric	Solid Catadioptric
Relative Aperture	f/1.14	f/1.40
Entrance Aperture	2.1 Inches	2.7 Inches
Effective Aperture	1.7 Inches	2.5 Inches
<u>Signal Processing</u>	Peak Detection	Edge Detection
<u>Sun Shutter</u>	Required	Not Required
<u>Size</u>		
OD	5.625 Inches	3.75 Inches
Length	7.28 Inches	6.0 Inches
	Including Electronics	(Less Flange) Not In- cluding 35 in ³ Elec- tronics
<u>Weight</u>		
SSA + Electronics	3.9 lb.	3.6 lb.
Sun Shield	<u>1.3 lb.</u>	<u>1.3 lb.</u>
	5.2 lb.	4.9 lb.
<u>Power</u>	3.3w Continuous Plus 3.0w For Sun Shutter	3.0w Continuous
<u>No. of Electronics Parts</u>	805	500

TABLE 3

PARS H-4 Star Sensor
Additional Tradeoff Data

<u>DETECTOR</u>	<u>CDC</u>	<u>HRC</u>
History	4 Years Experience On SPARS	Dev. Models + 2 Years AAF Tests
Material	Build Process Produces Random Results	Build Process Is Predictable
Sensitivity	Extensive Data - Is Higher Than Si	Limited Data, Better Dim Star Rejection
Uniformity	±30%	±5%
Environments	Humidity Protection Required	Humidity Protection Not Required
Background Lumination	Required	Not Required (Can Withstand Higher Background)
<u>OPTICAL SYSTEM</u>		
Off-Axis Image Degradation	No Problem	Potential Problem
Detector Shape	Curved	Flat
Alignment Stability Of Principal Optics	Difficult To Maintain	Inherently Stable
<u>SENSOR BUILD EXPERIENCE</u>	3 Phase IB Prototypes Built On SPARS	1 Four-Inch Development Model
	1 Mod II Flight Type In Qual Test	1 3.2-Inch Brassboard
	2 Mod II Flightworthy Models In Fab	

TABLE 4

HRC Star Sensor Test Results

<u>TEST</u>	<u>OBJECTIVE</u>	<u>REQUIREMENT</u>	<u>RESULT</u>
Outdoor At HRC	Establish Sensitivity	S/N > 10:1 On 3.6 M _{Si} A ₀ Star	14:1 Nominal 8.8:1 Worst Case } After Correction For Atmos- pheric Attenuation
On Lab Star At Honeywell, Mpls.	Establish Uniformity	±30%	±17%
	Establish Random Error	8 sec (1σ)	2 sec (1σ)
On Electronics At HRC	Establish Color Insensi- tivity	< 1 sec Shifts	< 1 sec
	Establish Magnitude Insensitivity	< 1 sec Shift	< 1 sec
<u>Test Apparatus</u>			
Sensor Field of View	7.6°	(detector smaller than would be used in PARS-H4)	
f/No	2.0		
Effective Aperture	2.5"	(above test results corrected to PARS-H4 design)	

SECTION 7

REFERENCES

1. through 84. (These are the references contained in reference 85.)

NOTE - CORRECTION Ref. 15 should have been as follows:

15. William R. Davis, Lockheed MSC, and Joseph A. Miller, Honeywell Aerospace Division, "SPARS - a Completely Strapdown Concept for Precise Determination of Satellite Vehicle Attitude".*

85. (Included here for convenience.) G. Ogletree with J. Coccoli, R. McKern, M. Smith, R. White, "Interim Technical Report No. 1, Candidate Configuration Trade Study, Stellar-Inertial Measurement System (SIMS) for an Earth Observation Satellite (EOS)," Report E-2616, MIT/CSDL, 5 November 1971.

85. through 140. (These are the references contained in reference 141.)

141. G. Ogletree, J. Coccoli, R. McKern, M. Smith and R. White, ~~"Interim Technical Report No. 2, Candidate Configuration~~ Trade Study, Stellar-Inertial Measurement System (SIMS) for an Earth Observation Satellite (EOS)," Report E-2630, MIT/CSDL, 31 January 1972.

* Proceedings of the Symposium on Spacecraft Attitude Determination, held at Aerospace Corporation, El Segundo, CA, Sept 30, Oct 1-2, 1969, Co-Sponsored by USAF Space and Missile Systems Organization and Aerospace Corporation.

142. MIT/CSDL Letter Report, 72-392L-2, G. Ogletree to Hollie R. Hodges, NASA/MSC, "NAS9-4065, T.O. 42 (SIMS Configuration Trade Study)," (Seventh) Monthly Letter Report, 7 February 1972.
143. MIT/CSDL Letter Report, 72-392L-3, G. Ogletree to Hollie R. Hodges, NASA/MSC, "NAS9-4065, T.O. 42 (SIMS Configuration Trade Study)," (Eighth) Monthly Letter Report, 15 March 1972.
144. MIT/CSDL Letter Report, 72-392L-4, G. Ogletree to Hollie R. Hodges, NASA/MSC, "NAS9-4065, T.O. 42 (SIMS Configuration Trade Study)," (Ninth) Monthly Letter Report, 12 April 1972.
145. MIT/CSDL Letter Report, 72-392L-5, G. Ogletree to Martin L. Hooper, NASA/MSC, "NAS9-4065, T.O. 42 (SIMS Configuration Trade Study)," (Tenth) Monthly Letter Report, 12 May 1972.
146. MIT/CSDL Letter Report, 72-392L-6, G. Ogletree to Martin L. Hooper, NASA/MSC, "NAS9-4065, T.O. 42 (SIMS Configuration Trade Study)," (Eleventh) Monthly Letter Report, 7 June 1972.
147. MIT/CSDL Proposal 72-176 to NASA Manned Spacecraft Center (acting as procurement agency for NASA/GSFC), 9 May 1972, "Modification of Candidate Configuration Trade Study, Stellar-Inertial Measurement System for a Proposed Earth Observation Satellite," transmitted by letter, 16 May 1971, D.C. Driscoll to M.L. Hooper/BC25, NASA/MSC. (See Appendix E of this report for Technical Section).

148. Ronald A. Harris, "Use of the IRU(OAO) in the Stellar-Inertial Measurement System (SIMS) for an Earth Observational Satellite (EOS), MIT/CSDL Skipper B Group Operational Systems Section Memorandum No. SOS-SYS-72130, 7 June 1972.
149. NASA/GSFC Letter, Dr. A. Guha to G. Ogletree, MIT/CSDL, 28 February 1972 (on SIMS-A Measurement Equations and Simulations).
150. MIT/CSDL Letter, R. White to Dr. A. Guha, NASA/GSFC, 24 March 1972, (23S Memo 72-22), in Response to Ref. 149.
151. MIT/CSDL Letter, G. Ogletree to Dr. A.K. Guha of NASA/GSFC, 26 April 1972, (Response to Ref. 149).
152. Hughes Aircraft Company Letter, B. Klestadt and G.R. Telle to G. Ogletree, MIT/CSDL, 24 March 1972 (on Applicability of the Hughes STARS Concept to the EOS/SIMS Application), Included as Attachment C to Ref. 144.
153. Honeywell Letter, D.C. Paulson to G. Ogletree, MIT/CSDL, 20 April 1972, Honeywell Aerospace Division Letter (File #440.3).
-
154. TRW Letter, D.K. Kirby to G. Ogletree, MIT/CSDL, 24 April 1972, TRW Systems Group Letter.
155. Northrop Northronics Letter and Attachments, J.C. Dieselman to R. McKern, MIT/CSDL, 16 February 1972, Northrop Northronics Letter.
156. H. McQuat, "A Proposition for Redundant IMU's," MIT/CSDL Internal Memo 23S#72-40, 5 June 1972.

157. "Advanced Star Sensor - Final Technical Report," prepared by Kollsman Instrument Corporation for Air Force Systems Command, Aeronautical Systems Division, WPAFB, under Contract No. F33615-71-c-1159, 28 May 1971.
158. Kollsman Letter, J.J. Connors Jr., to J. David Coccoli, MIT/CSDL, 22 March 1972, Including Enclosure of Curves by Texas Instruments of the Relative Response of Several Specific Silicon Detectors.
159. E.J. Farrell, C.D. Zimmerman, D.F. Nickel, and R.C. Borden, "A Theoretical Investigation of Information Limits of Scanning Optical Systems," NASA-CR-672, prepared by Control Data Corporation for Langley Research Center under Contract No. NAS1-4646, January 1967.
160. Telephone Conversation between Mr. Joseph Miller of Honeywell Aerospace Division and J. David Coccoli of MIT/CSDL SIMS Study Team, 19 May 1972.
161. Telephone Conversation between Mr. R.F. Gates of TRW Systems Group and Mark Smith of MIT/CSDL SIMS Study Team, 25 May 1972.
162. G. Ogletree, L. Johnson, L. Yorgy, G. Karthas, W. Tanner, M. Smith, "-SKYLOTS- Skylab-B Observation Telescope System (A Conceptual Design Definition), Final Report," Report R-675, MIT/CSDL, October 1970.
163. Mark A. Smith, "Infrared Radiometer Development Second Milestone Report," Report R-630, MIT/CSDL, October 1970.
164. H.K. Smithson, ARO, Inc., and W.A. Drohan, MIT/CSDL, "Testing of the SAMSO/MIT Radiometer in Simulated Orbital

Temperature and Pressure Environments," Report AEDC-TR-72-28, Von Kármán Gas Dynamics Facility, AEDC, AFSC, Arnold Air Force Station, Tennessee, March 1972.

- 165. D. Paulson, HI, to D. Coccoli, MIT, "SIMS-A Costs," Honeywell Aerospace Division Informal Memorandum Documenting Telecon, Paulson to Coccoli, 24 May 1972, Included in Ref. 146 as Attachment C thereto.
- 166. Martin L. Shooman, Probabalistic Reliability: An Engineering Approach, McGraw-Hill, 1968.
- 167. "Restoring the Quality of Our Environment," report by the Environmental Pollution Panel — President's Science Advisory Committee, November 1965.
- 168. NASA/MSX TWX, BC25-72-T0700-A17, Normand J. Beauregard to John Nelson (MIT/CSDL), dated 1 May 1972 (including RFP on Proposed Supplemental Agreement No. 1055 to Contract NAS9-4065).

E-2651

SECTION 8

DISTRIBUTION

EXTERNAL

NASA (MSC) Library (3)
NASA (GSFC) Library (3)
NASA (Hq) Library (3)
NASA/MSC (M.L. Hooper) (5 + 1R)
NASA/GSFC (J.W. Kelly) (20 + 1R)
USAF/SAMSO (Maj. H.A. Briesacher, SYGS) (2)

INTERNAL

MIT/CSDL

Apollo Central Files (2)	B. Dane
Apollo Library (2)	W. Denhard
Technical Documentation Center (10)	E. DeSimone
R. Battin	C. Draper
P. Bowditch	W. Drohan
A. Boyce	R. Duffy
J. Coccoli	J. B. Feldman
R. Cooper	Julius Feldman
D. Cox	P. Felleman
B. Cuevas	K. Fertig
R. Cushing	K. Fox

D. Fraser	G. Mayo
J. Gilmore	R. McKern
F. Grant	H. McOuat
G. Grover	E. Mechler
Edw. Hall	H. Musoff
Eldon Hall	J. Nelson
J. Harper	J. Nugent
R. Harris	G. Ogletree
S. Helfant	J. Parr
E. Hickey	R. Ragan
F. Houston	G. Quinn
B. Hildebrant	M. Sappupo
D. Hoag	L. Schnee
A. Hoch	N. Sears
J. Hursh	M. Smith
R. Hutchinson	G. Stubbs
G. Karthas	G. Suntheimer
J. Kirk	K. Tompkins
M. Landey	M. Trageser
H. Laning	P. Vernam
L. E. Larson	R. White
J. Lawrence	R. Woodbury
C. Lory	W. Wrigley
R. Marshall	L. Yorgy
P. Matthews	

MIT

Charles Hayden Library (3)

Engineering Library (3)

Aeronautics and Astronautics Library (3)

Professor Rene Miller

Arthur Smith (Patent Office)

Robert Byers

ILO Files (2)